LEABHARLANN CHOLÁISTE NA TRÍONÓIDE, BAILE ÁTHA CLIATH | TRINITY COLLEGE LIBRARY DUBLIN
Ollscoil Átha Cliath | The University of Dublin

Terms and Conditions of Use of Digitised Theses from Trinity College Library Dublin

Copyright statement

All material supplied by Trinity College Library is protected by copyright (under the Copyright and Related Rights Act, 2000 as amended) and other relevant Intellectual Property Rights. By accessing and using a Digitised Thesis from Trinity College Library you acknowledge that all Intellectual Property Rights in any Works supplied are the sole and exclusive property of the copyright and/or other IPR holder. Specific copyright holders may not be explicitly identified. Use of materials from other sources within a thesis should not be construed as a claim over them.

A non-exclusive, non-transferable licence is hereby granted to those using or reproducing, in whole or in part, the material for valid purposes, providing the copyright owners are acknowledged using the normal conventions. Where specific permission to use material is required, this is identified and such permission must be sought from the copyright holder or agency cited.

Liability statement

By using a Digitised Thesis, I accept that Trinity College Dublin bears no legal responsibility for the accuracy, legality or comprehensiveness of materials contained within the thesis, and that Trinity College Dublin accepts no liability for indirect, consequential, or incidental, damages or losses arising from use of the thesis for whatever reason. Information located in a thesis may be subject to specific use constraints, details of which may not be explicitly described. It is the responsibility of potential and actual users to be aware of such constraints and to abide by them. By making use of material from a digitised thesis, you accept these copyright and disclaimer provisions. Where it is brought to the attention of Trinity College Library that there may be a breach of copyright or other restraint, it is the policy to withdraw or take down access to a thesis while the issue is being resolved.

Access Agreement

By using a Digitised Thesis from Trinity College Library you are bound by the following Terms & Conditions. Please read them carefully.

I have read and I understand the following statement: All material supplied via a Digitised Thesis from Trinity College Library is protected by copyright and other intellectual property rights, and duplication or sale of all or part of any of a thesis is not permitted, except that material may be duplicated by you for your research use or for educational purposes in electronic or print form providing the copyright owners are acknowledged using the normal conventions. You must obtain permission for any other use. Electronic or print copies may not be offered, whether for sale or otherwise to anyone. This copy has been supplied on the understanding that it is copyright material and that no quotation from the thesis may be published without proper acknowledgement.

The Cellular Transducer in Damage-Stimulated Bone Remodelling

Jan Geert Hazenberg

A thesis submitted to the University of Dublin in partial fulfilment of the requirements for the degree of

Doctor of Philosophy

Department of Mechanical and Manufacturing Engineering
Trinity College Dublin
&
Department of Anatomy
Royal College of Surgeons in Ireland

Tuesday, 30 March 2004

Supervised by Prof. D. Taylor

TRINITY COLLEGE
14 OCT 2004
LIBRARY DUBLIN
THOS.S
7424

t Hogelaand

t Is de lucht achter Oethoezen,
t Is t torentje van Spiek,
t Is de weg van Lains noar Klooster,
En deur Westpolder langs de diek.

t Binnen de meulens en de moaren,
t Binnen de kerken en de börgen,
t Is t laand woar ik as kind,
Nog niks begreep van pien of zörgen.

Dat is mien laand, mien Hogelaand...

t Is n doevetil, n dörpsstroat,
t Is n olde bakkerij
t Binnen de grote boerenploatsen,
Van Waarvum Oskerd, zo noar Mij.

t Is de waait, t is de hoaver,
t Is t koolzoad in de blui,
t Is de horizon bie Roanum,
Vlak noa n dunderbui
Dat is mien laand, mien Hogelaand...

t Is n mooie oavend in maai,
n Kou houst doeknekt in t gruinlaand,
Ik heb veur d'eerste moal verkeren,
En vuil de vonken van dien haand.

De wilde plannen dij ik haar,
Komt sikkom niks meer van terecht,
Totdat de nacht van t Hogelaand,
n Donker klaid over ons legt,
Dat is mien laand, mien Hogelaand...

Ede Staal

Table of Contents

Table of Contents III

List of Figures VI

List of Tables X

Publications XI

Acknowledgements XII

Declaration XIV

Summary XV

Nomenclature XVII

Chapter 1 Introduction to Bone 1

1.1 Introduction 1
1.2 Bone shape and function 2
1.3 Composition of bone 4
1.4 Organisation of bone 5
1.5 Bone cells 7
1.6 The development of bone 8
1.7 Bone adaptation 10
1.7.1 Cell signalling and cellular transducers 14
1.7.2 Experimental studies 16
1.7.3 Theoretical studies 22
1.8 Mechanical properties of bone 23
1.9 Microcracks 25
1.10 Clinical relevance 29
1.11 Aims and objectives 32

Chapter 2 Fracture Mechanics 34

2.1 Introduction 34
2.2 Fracture Mechanics concepts 34
2.3 Linear elastic fracture mechanics (LEFM) 35
2.3.1 Griffith energy balance 35
2.3.2 Energy release rate 36
2.3.3 The stress intensity factor 37

2.3.3.1 Crack shape analysis 38
2.3.4 Relationship between K and G 43
2.3.5 Crack tip plasticity 43
2.3.5.1 The Irwin approach 44
2.3.5.2 The Dugdale model (strip yield model) 45
2.3.6 Plane stress and plane strain 46
2.3.7 Crack opening displacements 46
2.3.8 Mixed mode fracture and kinked cracks 48
2.4 Elastic-Plastic Fracture Mechanics (EPFM) 53
2.4.1 Crack Tip Opening Displacement (CTOD) 53
2.4.2 J-integral 54
2.4.3 Relation between CTOD, G, K and J 55
2.5 Fatigue Crack Growth 56
2.5.1 Short crack problems 58
2.6 Fracture in composites 59
2.7 Fracture Mechanics applied to Bone 61

Chapter 3 A Theoretical Model of the Cellular Transducer 71

3.1 Introduction 71
3.1.1 Aims and objectives 74
3.2 Crack growth and shape development model 76
3.2.1 The input parameters 77
3.2.1.1 Estimating the threshold values 80
3.2.2 Predicting crack shapes 82
3.3 Establishing the rules for bone repair and adaptation 89
3.3.1 Crack lengths related to repair and adaptation 90
3.4 The source of the signal 91
3.4.1 Rupturing of Cells 91
3.4.1.1 Failure criteria and material strength 92
3.4.1.2 Estimating crack-face displacements. 93
3.4.1.3 Predicting the number of ruptured osteocyte processes. 100
3.4.1.4 Rupture of cells ahead of the crack. 103
3.4.2 Strain sensing by cells 103
3.5 Discussion 106
3.6 Conclusions 110

Chapter 4 Experimental Validation of the Theoretical Model 111

4.1 Introduction 111
4.1.1 Visualisation of cell-processes 111
4.1.1.1 Antibody staining 113
4.1.2 Linear elastic fracture mechanics 115
4.1.3 Aims and objectives 116
4.2 Materials and methods 117
4.2.1 Design of the rig and specimens 117
4.2.2 Testing procedure 120
4.2.3 Image analysis from microscopy 123
4.2.4 Protocol for staining cellular material 124

4.3 Results 127
4.3.1 Specimen analysis 127
4.3.1.1 Force measurements 127
4.3.1.2 Crack growth observations 130
4.3.1.3 Crack growth angle 135
4.3.1.3 Crack displacements due to angle 136
4.3.1.4 Crack growth rate during testing 138
4.3.2 Ruptured cell processes 143
4.3.3 Theoretical analysis 146
4.3.3.1 Stress intensity analyses 147
4.3.3.2 Crack displacement analysis of tested specimens 151
4.3.3.2.1 Analytical estimation 152
4.3.3.2.2 Finite element analysis estimation 155
4.3.3.3 Assessment of applicability of LEFM 157
4.3.3.3.1 Effect of the material properties 158
4.3.3.3.2 Effect of crack growth and kink-angle on COD and CSD 163
4.3.3.3.3 Effect of plastic zone 165
4.3.4 Comparing methods 167
4.4 Discussion 175
4.5 Conclusions 180

Chapter 5 General Discussion 182

5.1 The cellular transducer 182
5.1.1 Rupturing cell processes 182
5.1.2 Strain sensing 184
5.1.3 Crack growth and shape 185
5.2 Is there a need for mechanotransduction? 186
5.3 Implementation of proposed models in FEA 190
5.4 Limitations 193

Chapter 6 General Conclusions and Future Work 195

6.1 Future work 196

Chapter 7 References 198

Chapter 8 Appendices 231

List of Figures

Fig. 1-1 Loading modes of bone (Snijders *et al.*, 1995) 3
Fig. 1-2 Different types of bone (Dandy, 2003) 3
Fig. 1-3 Hierarchical structural organization of bone (Rho *et al.*, 1998) 5
Fig. 1-4 Long bones and their microstructure (Hayes, 1991) 6
Fig. 1-5 Osteocytes and canaliculi (Villee *et al.*, 1989) 8
Fig. 1-6 Endochondral ossification; from mesenchymal cells to bone (Atkinson *et al.*, 2003) 10
Fig. 1-7 Schematic diagram of a BMU (Martin *et al.*, 1998) 12
Fig. 1-8 Schematic depiction of the relationship between remodelling activity and osteoporotic fracture risk (solid line) (Heaney, 2003) 14
Fig. 1-9 Theoretical net rate of apposition/resorption as a function of mechanical loading (Carter, 1982) 17
Fig. 1-10 Stain gauge implanted on the dorsal surface of the 2nd metatarsus (Milgrom *et al.*, 2000a) 18
Fig. 1-11 Schematics of two different *in vivo* bone stimulation models by Mosley and Lanyon (1998) (left) and Qin *et al.* (2003) (right). 19
Fig. 1-12 Definition of stress components and stiffness matrix 24
Fig. 1-13 Microcrack labelled with calcein (green) (Lee *et al.*, 2000) 26
Fig. 1-14 Diffuse damage in bovine tibia (Reilly and Currey, 2000) 26
Fig. 1-15 A microcrack entrapped between two osteons (Martin *et al.*, 1998) 27
Fig. 1-16 Microdamage accumulation during testing (O'Brien *et al.*, 2003) 28
Fig. 2-1 Centre cracks and edge cracks (Ewalds and Wanhill, 1989) 38
Fig. 2-2 Modes of failure (Ansys) 38
Fig. 2-3 Rectangular notch developing into an ellipse during fatigue testing (Miranda *et al.*, 2002) 40
Fig. 2-4 Major and minor axis of an elliptical crack 40
Fig. 2-5 Comparing the complete integral with an approximation method 41
Fig. 2-6 Correction factors for an elliptical flaw in a solid body (Anderson, 1995) 42
Fig. 2-7 The crack tip plastic zone according to Irwin (Janssen *et al.*, 2002) 44
Fig. 2-8 Size of the plastic zone according to Dugdale (Janssen *et al.*, 2002) 45
Fig. 2-9 Definition of crack-face displacement (Ewalds and Wanhill, 1989) 47
Fig. 2-10 Crack tip opening displacement according to Irwin (Janssen *et al.*, 2002) 47
Fig. 2-11 Definition of crack angle β (Anderson, 1995) 48
Fig. 2-12 Pre-existing crack PP' and a 'secondary' kinked crack PQ (Horri and Nemat-Nassar, 1986) 49
Fig. 2-13 Kinked crack (Denda and Dong, 1999) 52
Fig. 2-14 Kinked crack (Chen, 1999) 52
Fig. 2-15 Crack blunting as a result of plastic deformation (Anderson, 1995) 54
Fig. 2-16 Definition of the path 'S' around the crack tip 55

Fig. 2-17 Schematic of constant amplitude load cycles ____ 57
Fig. 2-18 Schematic of typical fatigue crack growth (FCG) data (Newman, 2000). ____ 58
Fig. 2-19 Schematic of competition between intrinsic and extrinsic mechanisms (Ritchie, 1999) ____ 61
Fig. 2-20 S-N curve of human femoral bone (Zioupos *et al.*, 1996). ____ 63
Fig. 2-21 Schematic of toughness testing specimens for mode I and II redrawn from Yeni and Norman (2000). ____ 64
Fig. 2-22 Pattern of fracture (Dandy, 2003) ____ 65
Fig. 2-23 Predicted crack growth rate with constant repair rate (Taylor, 1997) ____ 69
Fig. 3-1 Input variables for crack growth and shape development model ____ 77
Fig. 3-2 Geometry and orientation of an elliptical crack in cortical bone. ____ 78
Fig. 3-3 Microcracks and cortical bone regions (Martin *et al.*, 1998) ____ 80
Fig. 3-4 Flow chart used for the computer model (variables crack angle, osteon spacing and threshold values). ____ 83
Fig. 3-5 Shape development for a crack trapped between two osteons. ____ 84
Fig. 3-6 Change in stress intensity factor due to a change in crack shape ____ 85
Fig. 3-7 Transverse length versus longitudinal length. Solid lines represent predicted threshold values at various angles, red dots are experimental data form O'Brien *et al.* (2000) ____ 86
Fig. 3-8 Sensitivity analysis for different stress levels and varying crack angles ____ 87
Fig. 3-9 Experimental data (O'Brien (2000)) versus predicted crack lengths and shapes. ____ 89
Fig. 3-10 Cell processes spanning a crack subjected to tensile and compressive loading. ____ 93
Fig. 3-11 Axis definition for an elliptical crack ____ 94
Fig. 3-12 Effect of axis ratio on crack opening displacement ____ 96
Fig. 3-13 Comparing the calculated values with the FEA results ____ 98
Fig. 3-14 Comparing calculated CSD using equations 3-12 & 2-14 with FEA. ____ 99
Fig. 3-15 Comparing calculated COD using equations 3-13 & 3-15 with FEA. ____ 100
Fig. 3-16 Maximum COD and CSD due to shear and tension, assuming isotropic and orthotropic elastic properties. ____ 101
Fig. 3-17 Predicted number of cell-processes that failed, using high and low osteocyte densities for three different crack lengths. ____ 102
Fig. 3-18 Predicted number of cells experiencing more than 4000 με, using two osteocyte densities: high (20,000 osteocytes/mm^3) and low (5,000 osteocytes/mm^3) ____ 106
Fig. 3-19 Comparison of the signals from the high-strain zone and from ruptured cell processes, for a typical crack of length 2a= 100 μm at different applied stresses. ____ 108
Fig. 4-1 Scanning electron micrograph of a resin-impregnated section of human cortical bone (Currey, 2002) ____ 112
Fig. 4-2 Primary-secondary antibody staining schematic (van der Loos, 1999) ____ 115

Fig. 4-3 Microscope: space between stage (1) and lenses (2). 117
Fig. 4-4 Test rig used for crack growth analysis 118
Fig. 4-5 Grip used in test rig 119
Fig. 4-6 Milled slot (red arrow) in frame of test rig 119
Fig. 4-7 Crack growth in bone sample D8s3 (scale bar = 50 μm) 120
Fig. 4-8 Osteon orientation for specimens 121
Fig. 4-9 Adjusting the grips to the right position 122
Fig. 4-10 Rig under microscope 122
Fig. 4-11 Illustration on measurements taken for COD and CSD 124
Fig. 4-12 Readings from loadcell for longitudinal notches 128
Fig. 4-13 Readings from loadcell for transverse notches 128
Fig. 4-14 Testing un-notched specimens with and without cling film 129
Fig. 4-15 Examples of sub-stages in specimens D6s4, D3s7 and D9s2 130
Fig. 4-16 Example of crack initiated from notch (taken from specimen D8s2) 131
Fig. 4-17 Diverted crack near the tip of specimen D9s7 132
Fig. 4-18 Crack path crosses an osteocyte lacunae (specimen D8s2) 133
Fig. 4-19 Influence of the microstructure on the crack face displacements (specimen D8s2) 134
Fig. 4-20 Terraces near the crack tip of specimen D8s3 135
Fig. 4-21 Crack angle with respect to the longitudinal axis of the bone 136
Fig. 4-22 Maximum crack displacement as a result of crack angle 137
Fig. 4-23 Specimen D4s2, high COD and CSD values at 90° crack angle 138
Fig. 4-24 Crack length versus time 138
Fig. 4-25 Typical behaviour of crack growth during testing 139
Fig. 4-26 A crack crossing Volkmann's canals (specimen D10s4) 140
Fig. 4-27 Crack growth rate specimen d10s4, showing location of features 140
Fig. 4-28 Changes in crack growth rate as a result of changes in crack displacements (specimen D10s4) 141
Fig. 4-29 Mean crack growth rate versus applied average stress 142
Fig. 4-30 Crack angle versus mean crack growth rate 143
Fig. 4-31 SEM image of the specimen D5s6 at the crack tip (x2000 mag.) 144
Fig. 4-32 Osteocyte stained with Alizarin 145
Fig. 4-33 Ruptured cell-processes (scale bar 20 μm) 145
Fig. 4-34 Ruptured cell processes between the notch and the centre of the crack (scale bar 50 μm) 146
Fig. 4-35 Stress intensity factors during crack growth using standard fracture mechanics and crack displacements 150
Fig. 4-36 Changes in stress intensity factor over time 151
Fig. 4-37 Comparing the measured crack opening and shear displacement with analytical predictions in specimens with longitudinal notches (solid lines: mean and S.D.) 153
Fig. 4-38 Comparing the measured crack opening and shear displacement with analytical predictions in specimens with transverse notches (solid lines: mean and S.D.) 154
Fig. 4-39 Comparing the FEA results with the measured values for specimens with longitudinal notches 155
Fig. 4-40 Comparing the FEA results with the measured values for specimens with transverse notches 156

Fig. 4-41 Comparing crack displacements predicted by the FE-analysis with analytical solutions ____ 157
Fig. 4-42 Fibre orientation and axis definitions ____ 159
Fig. 4-43 The 'x-y' and '1-2' coordinate system ____ 159
Fig. 4-44 Crack displacements for cracks from longitudinal notches, using Chen's method. ____ 161
Fig. 4-45 Crack displacements for cracks from transverse notches, using Chen's method. ____ 161
Fig. 4-46 Crack displacements for cracks from longitudinal notches, using Denda's method. ____ 162
Fig. 4-47 Crack displacements for kinked cracks from transverse notches, using Denda's method. ____ 163
Fig. 4-48 Error calculated in COD and CSD due to crack growth rate ____ 164
Fig. 4-49 Error calculated in COD and CSD due to kink angle ____ 165
Fig. 4-50 Example 'Bland and Altman plot' comparing COD with the predicted COD using FEA ____ 170
Fig. 4-51 COD limits of agreement for longitudinal notches ____ 171
Fig. 4-52 CSD limits of agreement for longitudinal notches ____ 172
Fig. 4-53 COD limits of agreement for transverse notches ____ 173
Fig. 4-54 CSD limits of agreement for transverse notches ____ 174
Fig. 4-55 Crack propagation velocity in (a) human bone, (b) bovine bone (Vashishth *et al.*, 2000a) ____ 177
Fig. 5-1 Stretched cell processes by pure opening displacement (A) and by opening and shear displacements ____ 184
Fig. 5-2 Remodelling routine incorporating the cellular transducer ____ 191

List of Tables

Table 1-1 The anisotropic material properties of bone ____ 25
Table 1-2 Microcrack lengths found in bones of various species ____ 29
Table 2-1 Fracture toughness of cortical bone (Feng *et al.*, 2000) ____ 65
Table 3-1 Total stress intensity factor calculations for minor *a* and major *b* axis of an ellipse (Pickard, 1985) ____ 78
Table 3-2 Calculated stress intensity values for the nine cracks found by O'Brien (2000) ____ 81
Table 3-3 Experimental data from O'Brien *et al.* (2000) and calculated results ____ 86
Table 3-4 Crack opening calculated for nine different cracks using FEA ____ 95
Table 3-5 Results for the final corrections including major axis and axis ratio ____ 97
Table 4-1 Analysis of the readings from the loadcell ____ 129
Table 4-2 Crack growth angles (β) ____ 136
Table 4-3 Distance between feature 1 to 5 (specimens d10s4) ____ 141
Table 4-4 Stress intensity factors at crack initiation ____ 148
Table 4-5 Stresses and stress intensity factors during testing ____ 148
Table 4-6 Constant used in analytical methods ____ 153
Table 4-7 Plastic zone and CTOD estimation ____ 166
Table 4-8 Results for notches with the grain ____ 171
Table 4-9 Results for transverse notches ____ 173

Publications

Work presented in this thesis has appeared in the following publications:

Hazenberg, J. G., O'Brien, F. J., Lee, T. C. and Taylor, D. (2002) Microcrack growth and shape development in compact bone. In: Computer Methods in Biomechanics and Biomedical Engineering (Eds, Middleton, N. G., Shrive and Jones, M. L.) Gordon & Breach, Amsterdam, 410-415.

Hazenberg, J. G. and Taylor, D. (2002) Do micro-cracks disturb the cell-processes in cortical bone, In: Proceedings of Bioengineering in Ireland (8) and the 16th meeting of the Northern Ireland Biomedical Engineering Society, (Eds, Fitzpatrick, D. P., McCormack, B. A. O. and Dickson, G. R.) Department of Mechanical engineering, Sligo, Ireland, 24

Hazenberg, J. G., Taylor, D. and Lee, T. C. (2003) Microcrack behaviour and a possible link to bone remodelling, In: Bioengineering in Ireland (9); Proceedings of the ninth annual conference of the section of bioengineering of the royal academy of medicine in Ireland, (Eds, Fitzpatrick, D. P., McCormack, B. A. O. and McCormack, D.) Department of Mechanical engineering, Cavan, Ireland, 76

Taylor, D., Hazenberg, J. G. and Lee, T. C. (2003) The cellular transducer in damage-stimulated bone remodelling: a theoretical investigation using fracture mechanics, J Theoretical Biology, 225, 65-75.

Hazenberg, J. G., Taylor, D. and Lee, T. C. (2004a) Crack displacements cause damage to cell processes: is this the cellular transducer?, In: Bioengineering in Ireland (10):Proceedings of the tenth annual conference of the section of bioengineering of the royal academy of medicine in Ireland, (Eds, Fitzpatrick, D. P., McCormack, B. A. O. and McGloughlin, T.) Department of Mechanical engineering, Limerick, Ireland, 63

Hazenberg, J. G., Taylor, D. and Lee, T. C. (2004b) Crack opening and shear displacements cause damage to cell processes: is this the cellular transducer? In: ESB 2004, 's-Hertogenbosch, the Netherlands

O'Brien, F. J., Hardiman, D. A., Hazenberg, J. G., Mercy, M. V., Mohsin, S., Taylor, D. and Lee, T. C. (2004) The behaviour of microcracks in compact bone, In: ESB 2004, 's-Hertogenbosch, the Netherlands

O'Brien, F. J., Hardiman, D. A., Hazenberg, J. G., Mercy, M. V., Mohsin, S., Taylor, D. and Lee, T. C. (2004) The behaviour of microcracks in compact bone, European Journal of Morphology, In press.

Acknowledgements

Who could have thought that when I swapped Dublin for Groningen that this day would ever come. It would not have been possible without the help of a number of people. First and foremost I would like to thank David Taylor. Throughout the project you always supported and inspired me. You're a genius and a great supervisor to have!

Secondly, I would like to thank Clive Lee. Thanks for your suggestions, checking of all the equations (you know what I mean) and support.

Paddy, thanks for your constructive criticism and providing the funding for this project.

Various people in the anatomy department have been a great help in the project. I would like to thank Dave, Paul, Oran, Orlaith, Peter S., Peter K., John, Fergal, Vincent, Maeve, Stanley, Lorraine, Sinead and Alec.

A special thanks to the people in the biochemistry department, who tried to turn me in a 'cell-loving-engineer'. Without your help, cell staining might not even have appeared in my thesis, especially the help of Michael, Eilis, Francis, Aideen, Heidi and David was much appreciated.

Although I spend the majority of my time in the Royal Collage of Surgeons, without the help of various people in Trinity it would have been much more difficult to complete the work. Especially Garry Lyons and Craig Meskel for their technical support, Kevin for his suggestions and Peter O'Reilly and Gabriel for their help in constructing the test rig.

Besides the time I spent on my project, I am happy that Terry, Jimmy and Frank gave me the opportunity to do the goalkeeper training for the Trinity soccer team. Besides the training staff, I would like to thank the goalkeepers Dave, Sean, Joe, James, Paddy, Ikaros and Sam for their enthusiasm and efforts on and off the pitch. A special thanks to Tony Carrey, it was a pleasure to do the coaching of the second team with you, even when it rained!

Besides the people with who I had the pleasure of working, I have been extremely lucky to have good housemates. Especially Susanne and Wendy who have been a huge support.

A group of special friends which I have had the pleasure of meeting (sober or drunk) during my stay, which I hope stay friends with even when we are miles apart are Clair & Dave, Dawn & Michael, Paul Keogh, Francis and Heidi. Besides the people in Dublin, my friends back in Groningen have shown what friendship means. Especially Ronnie & Erica, Joost & Marijke, Johan, Michel, Dennis and Menja.

Geert, Alie en Janet, bedankt voor jullie steun ook in tijden als het minder goed ging.

Finally, I would like to thank Dave Hardiman, Ronnie Gankema en Joost Fokkelman. True friends throughout my time in Ireland in good and bad times. You have been a good boost for moral and have proven to be people that I can rely on. Thanks.

I gratefully acknowledge the financial support of the Higher Educational authority of Ireland under the PRTLI programme for their sponsorship through the Medilink and the Bone for Life projects.

Declaration

I declare that I am the sole author of this thesis and that all the work presented in it, unless otherwise referenced, is my own. I also declare that this work has not been submitted, in whole or in part, as an exercise for a degree or qualification at any other University.

I agree that the library of the University of Dublin may lend or copy this thesis upon request.

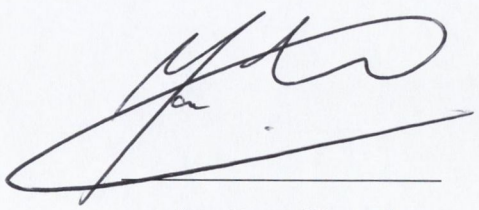

Jan Geert Hazenberg

Tuesday, 30 March 2004

Summary

People with osteoporosis, osteopenia or weight baring joint replacement, due to an altered loading configuration, are more susceptible to microdamage accumulation than normal human beings as are athletes who undertake strenuous exercise. Experimental evidence has linked bone adaptation to microdamage, and to increased cell activity. In this work, a theoretical investigation, using fracture mechanics, was used to assess which mechanisms might be present in bone to detect microcracks and to initiate an adequate response to prevent total fracture of bone. Two mechanisms were investigated: I) detection by rupturing of the cellular material itself and, II) strain detection by the osteocytes. Rupturing of cell processes due to crack opening and shear displacements was found to provide a feasible mechanism by which bone can detect and estimate the size of a microcrack. Analytical and numerical methods were developed to predict these crack face displacements and validated experimentally. Failure criteria were set based on the dimensions of an individual cell or cell process. Using these criteria, it was predicted that cracks slightly longer than those normally found in bone under normal physiological loads would cause ruptured cell processes. Smaller cracks, even under severe loading conditions would not be capable of doing so. For cracks which were several times longer than the typical length, even a moderate loading level would result in ruptured cell processes. Experimental work carried out using cell staining confirmed that crack displacements are capable of tearing cell processes. Rupturing of osteocytes near the crack tip was predicted to be very unlikely since strain levels are less than the fatigue failure strain of the material.

Strain detection by the osteocytes is a second potential mechanism for microdamage detection. Due to the stress concentrations near the crack, osteocytes are subjected to a high strain zone. The strain levels at osteocytes near small cracks under normal physiological loads are not unusually high, making the crack 'invisible' to bone.

Larger cracks, several times larger than normal, can stimulate large numbers of osteocytes even at low stress levels. Typical crack lengths subjected to stresses slightly higher than physiological, stimulate numerous osteocytes. Experimental validation for this mechanism was beyond the scope of the project. This requires the analysis of osteocyte cell cultures subjected to a local stress concentrator.

Both mechanisms, rupture of cellular material and strain detection, could provide a possible mechanism by which a crack can be detected, remodelled and the deposition of new bone regulated. Whether this decision is regulated by the number of broken cell processes or by the number of strain stimulated osteocytes requires further study.

Nomenclature

β	[deg.]	Crack angle
γ_c	[J/mm^2]	Surface energy
γ_p	[J/mm^2]	Work plastic strain
δ	[μm]	Crack opening displacement
Δa_n		Notional crack increment (Dugdale)
$\Delta K_{th,\ cement\ line}$	[MPa√m]	Stress intensity threshold range for the cement line
$\Delta K_{th,\ interstitial}$	[MPa√m]	Stress intensity threshold range for interstitial bone
$\Delta K_{th,\ intraosteonal}$	[MPa√m]	Stress intensity threshold range for intraosteonal bone
δ_t	[μm]	Crack tip opening displacement
ε_f		Failure strain
θ	[deg.]	Kink crack angle
μ		Shear modulus / friction coefficient
μm	[1x10^{-6} m]	Micrometer
με		Micro-strain
σ	[MPa]	Stress
σ_c	[MPa]	Gross failure stress
σ_y	[MPa]	Yield stress
τ	[MPa]	Shear stress
υ		Poisson's ratio
$2\delta S$	[μm]	Total crack shear displacement due to shear
$2\delta T$	[μm]	Total crack opening displacement due to tension
a_0	[mm]	Size of damaged zone ahead of the crack
d	[μm]	Spacing between the osteons
D_{cp}	#/mm^2	Damaged cell procesess
E	[MPa]	Young's modulus
F		Geometrical correction factor
f_c		Failure criteria
G	[J/mm^2]	Energy release rate
K_I, K_{II}, K_{III}	[MPa√m]	Mode I, II, and III stress intensity factor
R	[MPa√m]	Crack growth resistance
r_y		Radius of plastic zone (Irwin)
U	[J]	Elastic energy
CDM		Continuum Damage Mechanics
COD	[μm]	Total crack opening displacement, 2δ
CSD	[μm]	Total crack shear displacement
DEXA		Dual energy x-ray absorptiometry
EPFM		Elastic Plastic Fracture Mechanics
FCG		Fatigue crack growth
LEFM		Linear Elastic Fracture Mechanics
MSC		Microstructurally short crack
PSC		Physically small crack

Chapter 1 Introduction to Bone

1.1 Introduction

The skeleton is one of the eleven organ systems in the human body. It is mainly a mechanical organ, with its primary function being force transmission. It has been observed that living systems (humans, animals and tissue) respond to environmental changes by adapting and maintaining body equilibrium (homeostasis). This ability also applies to bone. Due to the dynamic nature of bone tissue, it is able to adjust to physiological and mechanical demands placed on it by the processes of growth and self-repair throughout life.

Historically, of all the systems in the human body, the skeleton has been the primary interest of engineers, due to its resemblance with man-made constructions. The idea that the external shape and the internal structure of bone adapts to mechanical loading conditions dates back to 1638, when Galileo (1638) suggested that the shape of bones was related to the mechanical loading. In 1892, Julius Wolff proposed a correlation between bone architecture and mechanical loading. He suggested that the trabecular architecture found in the proximal femur is orientated in the same direction as the stress trajectories which occur there. A contemporary of Wolff, Roux (1881) suggested that the bone adaptation was a self regulating mechanism, by which bone attempts to obtain maximum strength with minimum weight. By changing the shape of a bone and organising its internal structure, the amount of tissue required for bones to perform their function can be minimized.

The process of bone adaptation has been widely discussed in the literature, for example bone loss has been observed during long periods of bed rest (Inoue et al., 2000) and immobilisation of the lower and upper extremities (Rubin et al., 2001). On the other hand, bone can be gained via exercise e.g. tennis (Haapasalo et al., 2000)

and running (Bennell et al., 1998). Besides mechanical loading, other factors such as nutrition, disease, trauma, use and disuse, may affect bone quality and quantity (Frost, 1998).

Although exercise can increase bone mass, long periods of repetitive loading cause formation of microcracks. This is not necessarily problematic, since bone is able to repair itself. As long as the repair rate of bone is higher than the accumulation rate of these microcracks, fracture will, in general, not occur. The formation of microdamage, as a result of fatigue loading, results in a deduction in strength and decrease in stiffness, especially prior to failure (Hoshaw et al., 1997). Although the majority of these microcracks become dormant, some may grow to form macrocracks, resulting in fracture (Taylor and Lee, 2003). It is therefore of great importance that the most dangerous cracks are removed in order to maintain the structural intergrity.

1.2 Bone shape and function

Individual bones, or groups of bones, provide attachments for muscles, permitting the organism to move effectively and maintain posture by bearing loads during daily activities. This requires the interaction of over 206 different bones, approximately 700 muscles, tendons and ligaments. As a result, bones are subjected to various loading conditions during daily activities. In general, these loads result in tension, compression and torsion or a combination, depending on the type of activity (Fig. 1-1).

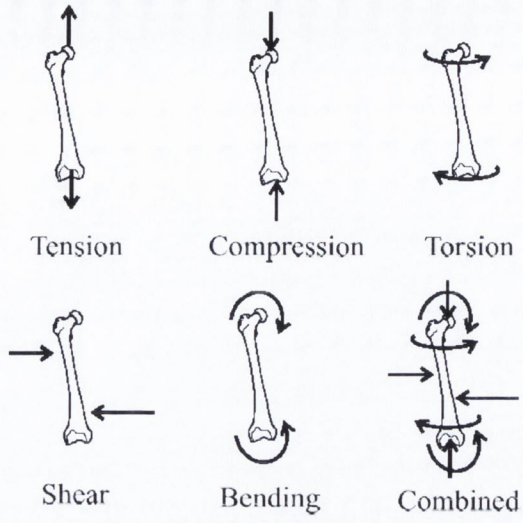

Fig. 1-1 Loading modes of bone (Snijders *et al.*, 1995)

Depending on their location and function, bones adapt their shape. These bones are classically divided in six broad groups: long- (Fig. 1-2a), short (Fig. 1-2d, e), flat- (Fig. 1-2b, c), irregular shaped-, sesamoid- and sutural bones.

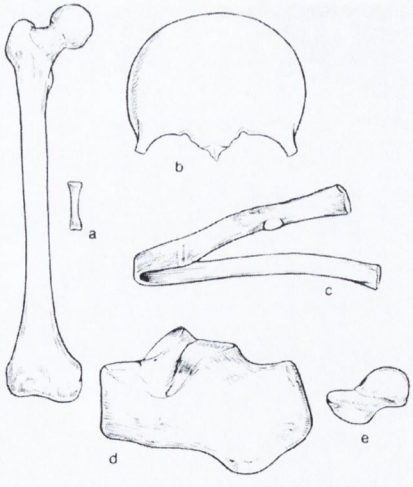

Fig. 1-2 Different types of bone (Dandy, 2003)

Besides its mechanical function, bone acts as a calcium reservoir and protects vital organs like the brain, heart and lungs. In the medullary cavities, yellow and red bone

marrow can be found which respectively provide storage for energy in the form of lipids, and produce red and white blood cells.

1.3 Composition of bone

Bone is a connective tissue consisting of cells embedded in a highly mineralised extracellular matrix. This extracellular matrix of bone consists of organic and inorganic components. The organic components can be further divided into fibres and ground substance. Fibres account for approximately 90% of the organic portion of the matrix or osteoid[1], serving as the framework for mineral deposition. The fibrous scaffold is mainly composed of type I collagen. Ground substance on the other hand is comprised of small proteoglycans, glycoproteins and water. The inorganic matrix is mainly comprised of hydroxyapatite, a mineral which is present in the form of hydroxylated calcium phosphate crystals [$Ca_{10}(PO4)]6(OH)_2$]. Other minerals which can be found are calcium phosphate, calcium carbonate, with lesser quantities of magnesium, hydroxyl, chloride, fluoride, citrate and sodium (Burkitt *et al.*, 2000).

The stiffness caused by the mineral phase provides resistance to compressive stresses, while the collagen provides bone with toughness and resistance to tensile stresses. Consequently, when these components are combined, bone is able to withstand the majority of bending stresses imposed during life.

[1] Osteoid is the organic phase of the extra-cellular matrix in bone.

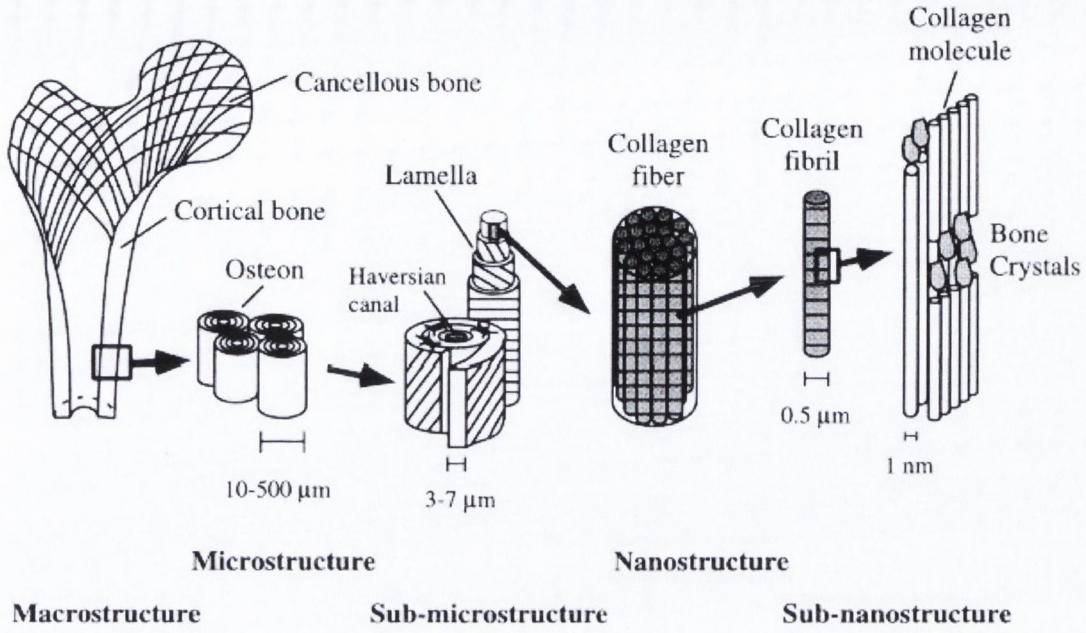

Fig. 1-3 Hierarchical structural organization of bone (Rho *et al.*, 1998)

1.4 Organisation of bone

Bone exists in two macroscopic arrangements based on its degree of porosity: compact (cortical) bone or trabecular (cancellous, spongy) bone. In compact bone, the microscopic units (see Fig. 1-3) are arranged in tightly packed parallel columns (> 0.7 g/cm^3) (Gibson and Ashby, 1988), creating a solid mass of bone that forms the outer shell of all skeletal elements and is often referred to as cortical bone. Cortical bone (see Fig. 1-4) provides the majority of the strength to resist weight-bearing forces in long bones. In contrast, trabecular bone (see Fig. 1-4) is composed of irregularly branching trabeculae (struts or plates) creating an open lightweight network (<0.7 g/cm^3) (Gibson and Ashby, 1988) in which bone marrow can be found. Spongy bone is located in the epiphyses of long bones and can also predominate in many short and irregular bones of the skeleton. The open network of trabeculae serves to distribute forces from the joint surface to the diaphyseal cortex and permits a degree of deformation for shock absorption.

Primary bone is produced *de novo* by intramembranous or endochondral ossification (see section 1.6). Secondary bone is formed following the removal of primary bone, as part of the remodelling cycle (see also section 1.7). It is a highly organized type of lamellar bone. Woven bone is rapidly formed and has a highly irregular arrangement of matrix. The collagen framework and mineralised matrix are arranged in lamellae or layers. The collagen fibres of each lamella run in opposite helical directions to those in adjacent lamellae, thereby increasing the strength of the microscopic unit (Ascenzi *et al.*, 1967).

Lamellar bone exists in three forms: osteonal, circumferential, and interstitial. Osteonal lamellar bone contains cylindrical units with an approximate diameter of 200 μm (called osteons) comprised of 15-20 circumferential lamellae surrounding a 50 μm neurovascular canal called a Haversian canal, covered by a thin endosteum layer. The tangential canals which join Haversian canals are called Volkmann's canals. In long bones, osteons tend to run approximately parallel to the long axis of the bone and Volkmann's canals run in a radial direction with respect to the osteons.

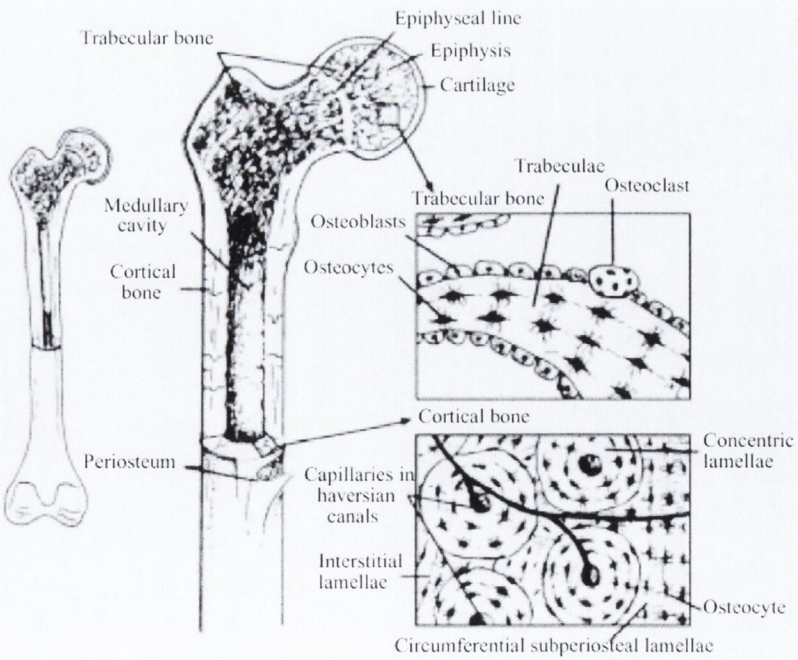

Fig. 1-4 Long bones and their microstructure (Hayes, 1991)

The remnants of old Haversian systems that have been cut by remodelling units are called interstitial lamellar bone (see Fig. 1-7). Circumferential lamellae encircle the marrow cavity or the external surface of a bone.

The fibrous layer covering all outer surfaces of bone is called the periosteum. This membrane covers the entire bone except the joint surfaces, which are covered with articular cartilage. Blood vessels and nerve fibres that pass into the bone via Volkmann's canals permeate the periosteum. A cellular layer covering the inner surface of bone is called the endosteum. Both the periosteum and endosteum are made up of a layer of flattened osteoprogenitor cells, osteoblasts and osteoclasts (see section 1.5). When the periosteum and endosteum are active during bone growth, repair and remodelling, the osteoclasts or osteoblasts in these layers can act to either resorb or deposit bone respectively.

1.5 Bone cells

The four main types of cells which can be found in bone are osteoprogenitor cells, osteoblasts, osteocytes and osteoclasts. Osteoblasts are derived from osteoprogenitor cells, which are mesenchymal[2] in origin, located on bony surfaces. These osteoblasts produce the organic components of the matrix (collagens, proteoglycans and glycoproteins) called osteoid. Scientist seemed to have agreed that once the osteoblast is surrounded by osteoid, the matrix mineralises and advances to the next maturity level, the osteocyte (Villee *et al.*, 1989; Voet and Voet, 1990; Alberts *et al.*, 1994; Lodish *et al.*, 1998). Although the cells are embedded in these chambers, they are still connected to one another via small cell processes, found in small canaliculi (Fig. 1-5). This continuity between cells allows for the transfer of nutrients, hormones, wastes, and mechanical messages.

---

[2] Mesenchymal cells: derived from stem cells but have had some differentiation. They are pluripotent, which means that they can still differentiate into several kinds of cells.

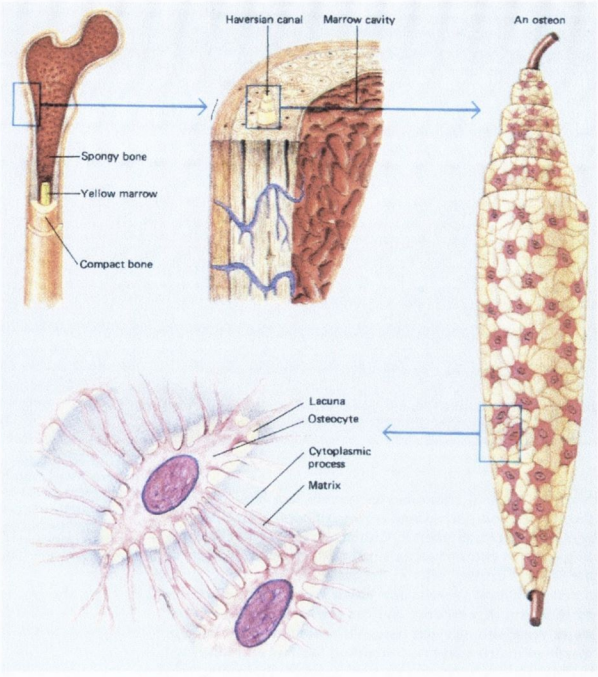

Fig. 1-5 Osteocytes and canaliculi (Villee *et al.*, 1989)

Histologically, osteocyte ultrastructure resembles that of osteoblasts. However, they are not as well understood due to the difficulty in isolating cells for study (Burger and Klein-Nulend, 1999). Osteoclasts are large multinucleate cells derived from the monocyte / macrophage cell family, and function to resorb bone tissue. They do so by secretion of acids and proteolytic enzymes that dissolve the matrix and the collagen. This erosion process, called resorption, is important in the regulation of calcium and phosphate concentrations in body fluids. The balance between the bone forming cells (osteoblasts) and the bone resorbing cells (osteoclasts) is very important in maintaining the mechanical integrity of the structure. Commonly this balance in elderly people can be lost, resulting in osteoporosis or osteopenia.

1.6 The development of bone

Bones are formed by two different mechanisms, intramembranous or endochondral ossification. The formation of bone tissue requires a number of external signals as well as the proper materials for construction. Hormonal signals control the behaviour

of bone cells, while a balanced diet and a good blood supply ensures a constant supply of building materials.

Most flat bones of the cranium, face and clavicle are formed by intramembranous ossification. Bones formed by intramembranous ossification, start with the differentiation of mesenchymal cells into osteoblasts, which begin to produce the organic components of the matrix or osteoid which is then mineralised to form bone. During this process, blood vessels are entrapped supplying the embedded osteocytes from nutrients. Once growth has slowed down, connective tissue around the bone becomes organised, forming the periosteum.

The majority of the skeleton is formed by endochondral ossification. This process starts with the differentiation of mesenchymal cells into chondrocytes, resulting in a cartilage pattern. Once blood vessels start growing around the edges of the cartilage, matrix calcification occurs. Over time, blood vessels penetrate the cartilage. These blood vessels convey osteoclasts, which reabsorb the calcified cartilage, and osteoblasts. Following this, the process of bone formation begins, resulting in a so-called primary ossification centre. The next major step is when the centres of the epiphysis begin to calcify. Migrating blood vessels and osteoblasts form the secondary ossification centres. These blood vessels carry osteoprogenitor cells and stem cells to the centre of the bone. The cartilage facing the exterior becomes the articular cartilage of the joint while the cartilage facing the primary ossification centre (diaphysis) becomes the epiphyseal (growth) plate.

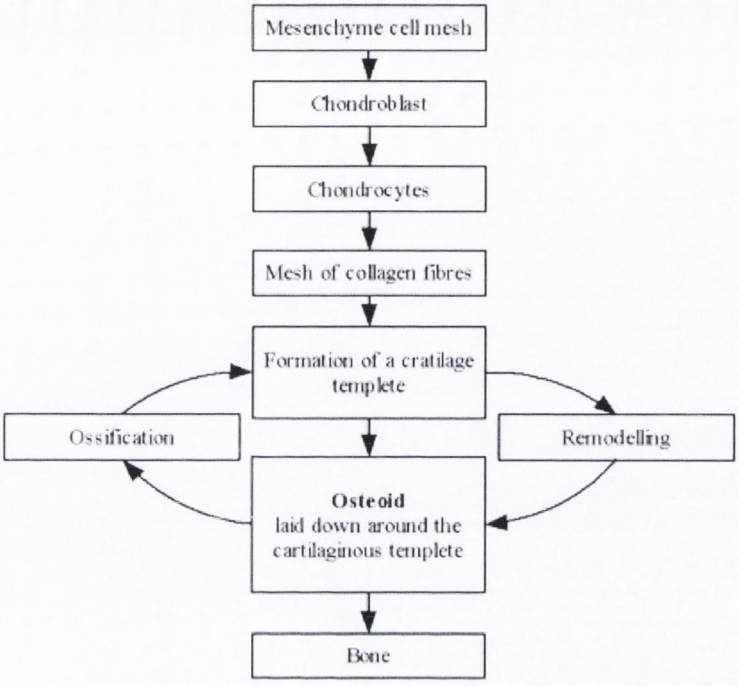

Fig. 1-6 Endochondral ossification; from mesenchymal cells to bone (Atkinson *et al.*, 2003)

1.7 Bone adaptation

Development of the adult skeleton is achieved by growth, modelling and remodelling. Growth and modelling are the two dominant processes that are present in normal growing individuals. The combination of these two processes is often referred to as adaptation. In long bones, growth increases bone length and diameter (both internal and external) controlled by the genes. This baseline architecture is modified by the modelling process, which sculpts the bone's size, shape, and curvature to optimally sustain the mechanical loads typically borne by that bone. Modelling adjusts bone architecture and mass via modelling drifts, which add bone to the surfaces and remove (resorb) it from others. This increases or decreases the cross-sectional area of bone. In the normal developing skeleton, growth and modelling result in the production of organized parallel sheets of primary lamellar

bone visible in diaphyseal cross-sections. Some of the early deposited lamellae are removed or "modelled out" as the bone drifts.

Once skeletal maturity is reached, modelling is reduced to a trivial level compared to that which occurred during development. Renewed modelling in the adult skeleton can occur, however, in some diseases and in cases where the mechanical loading environment has been altered radically (Inoue *et al.*, 2000; Hazelwood *et al.*, 2001; Rubin *et al.*, 2001).

Unlike modelling, which involves either resorption or formation, bone remodelling follows an activation, resorption, formation sequence. Remodelling of bone requires a complex arrangement and interaction of cells, collectively called basic multicellular units (BMU, see Fig. 1-7). Intracortical BMUs nearly always tunnel through the bone diaphysis in the longitudinal direction. The leading region of a BMU is lined with osteoclasts. The diameter of the tunnel is roughly 200 μm, which defines the size of the osteon that might be formed. This space is known as the resorption cavity. Following closely behind the osteoclasts is a group of mononuclear cells. The exact function of these cells remains unclear (Eriksen and Langdahl, 1995). These mononuclear cells line the resorption tunnel during the reversal phase (period between resorption and formation) and are suspected of forming the cement lines that surround secondary osteons. Behind the mononuclear cells, rows of osteoblasts adhere to the reversal zone and deposit a layer of osteoid centripetally. At a specific point, deposition ceases, resulting in a secondary osteon with a Haversian canal in the centre, which has a diameter of approximately 50 μm. A BMU progresses at a rate of approximately 40 μm/day, taking it almost 200 days to form a secondary osteon (Martin *et al.*, 1998).

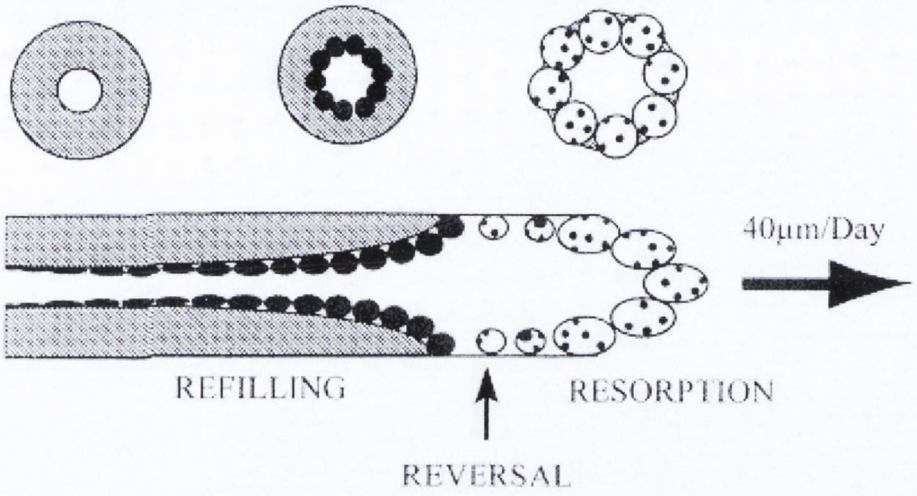

Fig. 1-7 Schematic diagram of a BMU (Martin *et al.*, 1998)

These processes of modelling and remodelling have been observed in animals and humans and are commonly referred to as Wolff's Law. Wolff's law (1892) states that the trabecular architecture reflects an adaptation to mechanical influences. Quantifying Wolff's law, therefore, depends on deriving correlations between quantitative measures of mechanical stimuli and the induced bone adaptation. Although Wolff's ideas have been largely undisputed, some workers suggested that Wolff had an incorrect understanding of both mechanics and biology (Roesler, 1987; Lee, 1995; Lee and Taylor, 1999). The use of a static model, the use of homogeneous material properties and the assumption of maximum strength with minimal weight shows that Wolff did not understand the process by which structural and geometrical properties evolve (Huiskes, 2000). A contemporary of Wolff who considered this process was Roux (1881), who proposed that bone was a 'quantitative self-regulating mechanism'. In other words, bone adapts to its function by making use of a functional stimulus (Lee and Taylor, 1999). The example he used to support his argument was that a tibia thickens in the absence of a fibula. The explanation provided by Roux regarding functional adaptation in response to altered loading has had major consequences on our modern day understanding of bone adaptation.

The main purpose for bone remodelling is thought to preserve the function of bone, replacing old regions, which might compromise structural integrity. A secondary effect of osteoclast activity is maintaining calcium homeostasis required for various processes in the body. Due to bone's load bearing function, it is subjected to cyclic loading resulting in damage accumulation. Whether bone remodelling could be triggered by microdamage, as proposed by various authors, is unknown, as is the detection threshold for initiation and repair. From a positive point of view, microdamage repair by BMU activity results in the turnover of old bone and repair of damage. The downside of this process is that it weakens the bone, therefore increasing the local stresses which might result in formation of more microdamage. However, new bone formation improves the material's capacity to withstand external loads, suggesting that there is a trade-off between bone renewal and damage repair. Based on these observations, the question arises as to what is the optimal level of bone remodelling?

Low levels of bone remodelling would not be adequate to prevent damage accumulation, and would increase the incidence of (stress-) fractures (see Fig. 1-8). Clinical examples causing bone remodelling levels to reduce include radiation necrosis (Yanagawa *et al.*, 2001; Hain and Fogelman, 2002) and hypoparathyroidism[3] (Langdahl *et al.*, 1996; Miller *et al.*, 1998; Khosla *et al.*, 1999) which increase the risk of fracture. Increased remodelling in post menoposal woman is known to increase the risk of fractures as a result of osteoporosis (Tomkinson *et al.*, 1997; Frost, 1998). When skeletal remnants of pre-agriculture populations are compared to our modern day skeleton, remodelling rates have been shown to change with dietary intake (Ruff, 2000).

[3] Hypoparathyroidism is caused by underactive parathyroid glands, which in turn causes low levels of calcium in the blood stream.

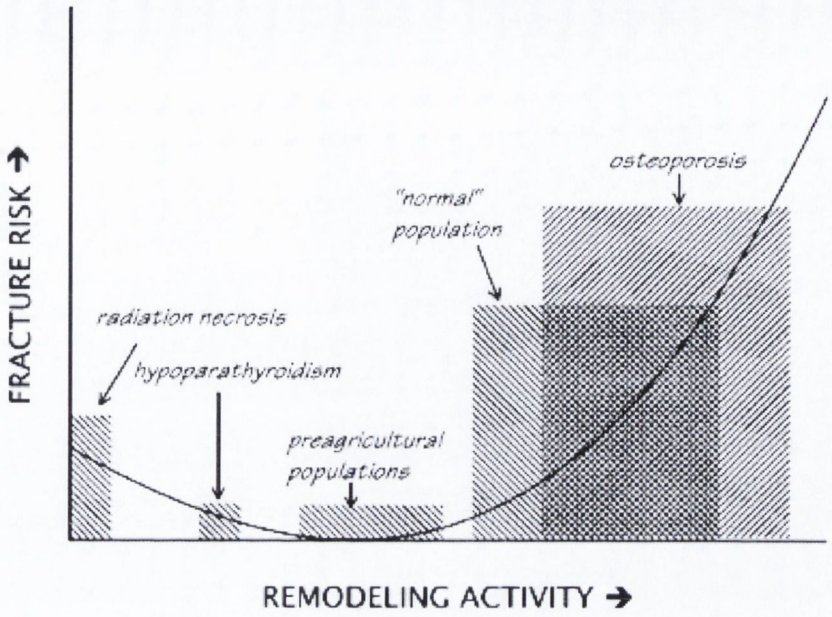

Fig. 1-8 Schematic depiction of the relationship between remodelling activity and osteoporotic fracture risk (solid line) (Heaney, 2003)

1.7.1 Cell signalling and cellular transducers

The ability of bone to adapt to its mechanical demands is generally well accepted, although the mechanism by which it does this is not fully understood. The process by which bone senses mechanical stimuli, and how the cells involved transduce this signal has not been established (Mullender and Huiskes, 1997). Because of their central location in the bone matrix, osteocytes have been proposed to play a major role in this process (Cowin *et al.*, 1991; Lanyon, 1993). There are approximately 10 times as many osteocytes as osteoblasts in normal human bone (Parfitt, 1977).

Several functions have been proposed for osteocytes. These include osteocytes as a calcium-sensor (Ypey *et al.*, 1992; Kamioka *et al.*, 1994; Kamioka *et al.*, 1995), regulator for osteoid matrix maturation and mineralization (Mikuni-Takagaki et al., 1995), and mechanosensor (Cowin *et al.*, 1991; Weinbaum *et al.*, 1994; Klein-Nulend *et al.*, 1995; Mullender and Huiskes, 1997; Owan *et al.*, 1997; Burger and Klein-Nulend, 1999; van der Meulen and Huiskes, 2002). The process by which

osteocytes respond to mechanical stimuli is often referred to as the mechanosensory mechanism (Frost, 1987). The sequence is thought to occur as follows:

- As a result of external mechanical loading, the cell system is stimulated.
- The system converts this mechanical load into an electrical and/or biochemical signal (Burger and Klein-Nulend, 1999).
- This signal is than transmitted to the effectors (osteoblasts or osteoclasts), causing a response, either by the formation of a BMU or by depositing or resorbing bone at the surfaces (Cowin, 2002).

The evidence that osteocytes play this primary role in the mechanosensory system is circumstantial. The osteoclasts may be eliminated directly because they are present in the bone tissue only when they are accomplishing their resorption function (Cowin, 2002). This leaves the osteoblasts and bone lining cells as the other remaining candidates. These cells can be found on the bone surfaces, which implies that they must be extremely sensitive to strain, which is in general very low in bone (0.2%) (Cowin et al., 1991). In other words, only osteocytes are the likely candidates based on their location, ability to communicate with other cells in the matrix and the cells on the bone's surfaces.

Marotti *et al.* (1992) hypothesised that osteocytes send out a inhibitory signal to bone lining cells preventing the formation of new BMUs. Based on work by Burr *et al.* (1985) and Bentolila (1998) showing increased bone remodelling activity following fatigue loading, it could be argued that microcracks disrupt this inhibitory signal and therefore BMUs are activated. On the other hand, a BMU-activation signal could be produced if microdamage interacts with the cellular network, increasing local strains and therefore triggering a remodelling response (Noble and Stevens, 2003). Parfitt (1984) proposed four different controlling mechanisms: 1) fatigue damage, 2) stress generated potentials, 3) hydrostatic pressure on the extracellular fluids under load, and 4) alterations in cell membrane diffusion due to direct load. Which of these (or a

combination) is the primary control mechanism involved in bone remodelling is unknown, but it seems clear that it is not possible to fully explain such complex processes with a single mechanism.

There has been increased interest in the nature of the remodelling process in bone. The reason for this is twofold. First, there is the clinical need to understand the mechanical and remodelling behaviour of bone tissue because the use of implanted bone prostheses has increased dramatically (Malchau *et al.*, 2000). Second, scientific experimental techniques developed in the physical and biological sciences in the last thirty years now provide the technology that was not available previously and thus blocked further development. Traditionally, animal experiments have been employed to investigate bone response from load alterations or during the progress of age related bone loss (Lanyon *et al.*, 1981; Lee *et al.*, 2002a). Since the time scale of the remodelling process is on the order of months or years, computational modelling offers a unique approach to study long term processes without the inconveniences of animal experimentation (Prendergast, 1997). Computer modelling is a potentially reliable, inexpensive and fast method by which different optimisation goals can be tried systematically until shape and architecture of bone can be reproduced. The relationship between bone structure and mechanical loading has been investigated theoretically and experimentally resulting in a variety of stimuli which will be discussed separately in the next two sections.

1.7.2 Experimental studies

Mechanically induced bone adaptation has been proposed to be a result of strain magnitude (Rubin, 1984), stress (Carter *et al.*, 1981c), cycle number (Adams et al., 1997), strain history (Fritton et al., 2000), strain rate (Mosley and Lanyon, 1998), strain energy density (Huiskes et al., 1987) and frequency of specific stimuli (Mosley and Lanyon, 1998). In general three regions are defined: I) decreased loading, II) normal loading and III) overloading. The two main methods by which decreasing loading can be achieved are by immobilisation and unloading. Immobilisation can be

realized via surgical or drug induced paralysis and by non-invasive casting. Unloading has been achieved by space flight and hindlimb suspension, resulting in a reduction in bone mass (van der Meulen *et al.*, 1995; Hardiman *et al.*, 2002). Clinically this occurs in patients with paralysis and in cases of prolonged bed rest (Vico *et al.*, 1987; Kiratli *et al.*, 2000). Normal loading is classified as the type of loading that maintains bone mass, i.e. neither bone deposition nor resorption is required and is better known as the lazy-zone. Overloading results in a stimulus which requires deposition of new bone on the outer surfaces, thereby reducing the amount of stress to which it is subjected. These three regions are shown in Fig. 1-9.

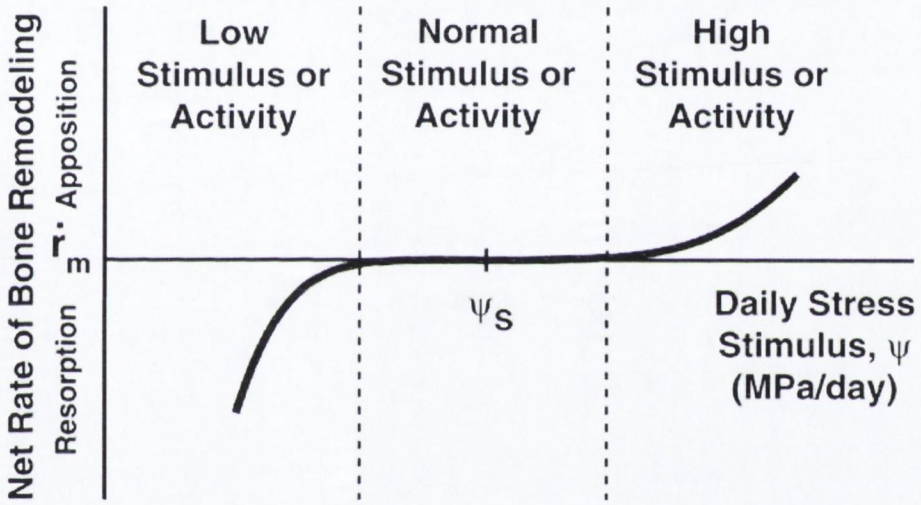

Fig. 1-9 Theoretical net rate of apposition/resorption as a function of mechanical loading (Carter, 1982)

Rubin and Lanyon (1984) showed that new bone formation occurred in ulnae using 2000 με and 36 cycles/day. Additional cycles were found to have little effect, suggesting that the stimulus for bone adaptation quickly saturates (Burr *et al.*, 2002). Strain gauge analysis carried out on dogs, sheep and turkeys (Adams *et al.*, 1997; Fritton *et al.*, 2000) showed that the number of incidents where large strain (> 1000 με) occur during daily activities only happen a few times a day, which might be enough to maintain bone mass. Increased bone mass has been observed in studies carried out on animals (sheep, dogs) in which the ulna is resected, causing increased

loading in the radius (Caler *et al.*, 1981; Carter *et al.*, 1981b; Carter *et al.*, 1981c; Lee, 1995; Lee *et al.*, 2002b), typically resulting in strains higher than 1500 με.

Experiments on foxhounds subjected to rigorous exercise regimes were carried out by Yoshikawa *et al.* (1994), showed that muscle fatigue increased the strains in bone by 26-35%. As well an increase in strain, a change in strain distribution was observed averaging a 25° rotation of the neutral axis. Besides strain gauge analysis carried out on animals, humans have been subjected to similar experiments. Milgrom *et al.* (2000b; 2002) and Arndt *et al.* (2002) reported on the amount of strain which occurs during various activities, such as walking, running, cycling, stepping, and leg presses using strain gauges stapled to human tibia and metatarsal bones as shown in Fig. 1-10.

Fig. 1-10 Stain gauge implanted on the dorsal surface of the 2nd metatarsus (Milgrom *et al.*, 2000a)

Cycling was found to produce the least amount of strain (< 500 με) in the tibia, whereas running resulted in tensile and compressive strains between 1000 με and 2000 με. In the metatarsal bones, a peak compressive strain of 5766 με was recorded during barefoot jogging on a treadmill.

Due to the wide variety of experimental methods applied in animal models (see Fig. 1-11), it is difficult to determine the dominating mechanism, controlling bone adaptation. The model by Qin et al. (2003), a modification of a previous model described by Rubin and McLeod (1994) , involved drilling two holes in the ulna of turkeys through which two pins were placed. Fluid was pumped in the marrow cavity followed by dynamic loading. Another, by Mosley and Lanyon (1998), flexes the rat ulna between two padded cups, followed by cyclic loading (Fig. 1-11). These experiments typically apply loads which result in strains of 500 με to 4000 με at frequencies ranging from 1 Hz to 20 Hz (Mosley *et al.*, 1997; Bentolila *et al.*, 1998; Mosley and Lanyon, 1998; Hsieh *et al.*, 2001; Hsieh and Silva, 2001; Hsieh and Turner, 2001; Mosley and Lanyon, 2002).

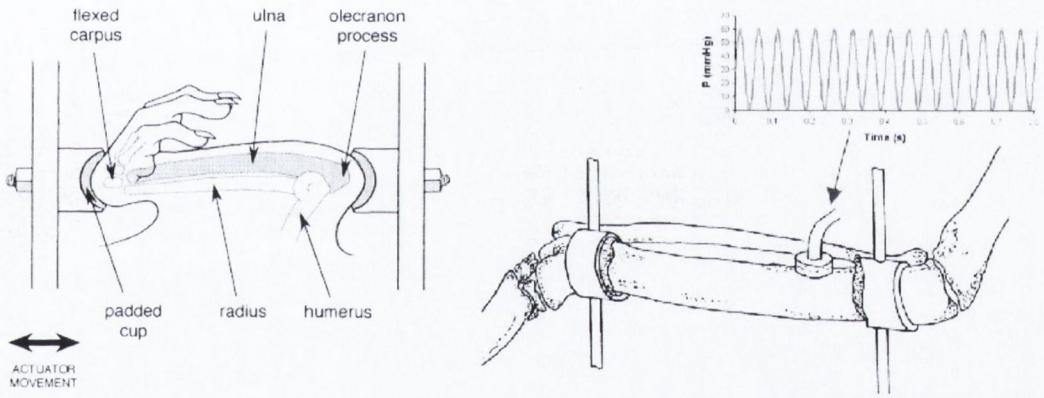

Fig. 1-11 Schematics of two different *in vivo* bone stimulation models by Mosley and Lanyon (1998) (left) and Qin *et al.* (2003) (right).

Other investigators have used four-point bending rigs to study the effect of mechanical loading on bone response. However, surgically implanting pins in limbs and applying a cyclic load (Qin et al., 1996) and similar fatigue tests using non-invasive procedures (Hsieh et al., 1999) are difficult to compare. Some of these experiments cause more (emotional) stress in animals than others, which has been shown to have great effects on bone properties (Seireg and Gray, 1978; Nijs *et al.*, 2003).

Besides these various techniques, different types of bone (e.g., woven bone, Haversian bone, plexiform bone) may have different sensitivity levels with regard to adaptation and its response to trauma (Brunski, 1999). Although this is difficult to prove, at a cellular level variations have been observed between the osteocyte-canalicular distribution during fracture healing (Kusuzaki et al., 2000). The osteocytes in newly formed woven bone appear at an early stage. Straight after woven bone formation only a few short and irregularly distributed canaliculi can be found in this new matrix, whereas osteocytes in lamellar bone, typically show many canaliculi that are long and are regularly distributed. Based on this observation, Kusuzaki et al. (2000) concluded that woven bone osteocytes may be necessary for induction of the lamellae.

Others have hypothesised that osteocytes are mechanically stimulated by the canalicular fluid flow resulting from strain. Flow of fluid, as a result of loading, has been linked to stress-generated potentials or streaming-potentials (Cowin et al., 1991). Cowin hypothesised that, in intact bone, the osteocytes are mechanically activated by flow of interstitial fluid through the lacuno-canalicular porosity. Here the dominant stimulus for bone adaptation is the strain-driven motion of the interstitial flow, which is sensed and transduced by the osteocytes. In order to do this the fluid shear stresses, to which bone cells are very sensitive in comparison with hydrostatic pressure (Klein-Nulend et al., 1995), have to be of the right order of magnitude. The only place where this can occur is in the canaliculi, due to their small diameter in comparison to Haversian and Volkmann's channels which have diameters which are several orders of magnitude bigger (Burger and Klein-Nulend, 1999). Theoretically it was shown by Weinbaum et al. (1994) and Steck et al. (2003) that bending-induced fluid flow could produce similar fluid shear stresses as those that cause responses in osteoblasts and other cells. Knothe-Tate et al. (1997; 1998), provided experimental proof that fluid flow in bone can occur in bending. In order to estimate the levels of shear stress or strain that are required for a cellular response, *in vitro* studies can be conducted using various techniques (see Brown (2000) for a review). The majority of these experiments have been criticised for either applying

stimulus levels which are several times (between 5-fold and 125 fold) higher than those normally experienced in bone, or for example, by employing stimulation systems that induce unintended physical signals (You et al., 2000). Bending substrates in a bath of culturing media causes unintended flow, which is complex and may be turbulent in nature. This not only makes it difficult to estimate the level of stimuli but also makes the experiments difficult to repeat. Three independent studies (Owan *et al.*, 1997; Smalt *et al.*, 1997; You *et al.*, 2000) have shown that bone cells on substrates are more sensitive to fluid shear stresses than mechanical stretching. These studies are a better indication of the nature of the stimulus since they are exposed to the same magnitude of stimuli. You *et al.* (2000) showed that there was a significant increase in both Ca^{2+}[4] and OPN[5] mRNA at strain levels greater than 5000με, below this level no increase was found to occur. Although arguments concerning the extremely high mechanical strains required to cause cell response might be valid, other arguments might need to be considered before conclusions can be drawn. In general, strain levels which are found to be acceptable are those on a macroscopic level. However, at a microstructural level strains might be much higher due to the microstructure (Nicolella et al., 2001) or microdamage (Prendergast and Huiskes, 1996).

As a result of cyclic loading, damage accumulates. As long as the accumulation rate is below the repair rate, the mechanical integrity of bone is guaranteed. Experimental evidence has demonstrated that fatigue loading of canine bones resulted in increased BMU activity (Burr and Martin, 1993; Mori and Burr, 1993). Microdamage was estimated to be four to six times more likely to be the cause of this than would be expected by chance alone. Intracortical bone remodelling in rats (which normally does not occur) was shown to be triggered by fatigue loading by Bentolila *et al.* (1998). In this experiment 14 out of a total of 16 rats showed microcracks in the bone

---

[4] Ca^{2+} is an early response messenger that plays a role in a number of metabolic pathways, typically observed to increase dramatically within seconds of stimulation.

[5] OPN is a matrix protein called osteopontin, which is believed to be an important factor in bone remodelling.

cortex. After 10 days of fatigue loading, resorption cavities were observed. However, two rats had no microdamage following fatigue loading. In these two specimens no resorption cavities were observed, creating more evidence that microdamage and bone remodelling are linked. Observations of increased osteocyte apoptosis in regions were microcracks are present suggests that local damage affects osteocyte homeostasis (Dunstan *et al.*, 1993; Schaffler *et al.*, 1995b; Noble and Reeve, 2000; Schaffler and Verborgt, 2000; Verborgt *et al.*, 2000). Recent experimental work which has tried to investigate this phenomenon has indicated that osteocyte apoptosis increases osteoclastic activity (Noble *et al.*, 2003; Noble and Stevens, 2003).

1.7.3 Theoretical studies

Approaches in which bone remodelling is mathematically described to be a self organizational process, are typically based on the hypothesis that bone contains mechanoreceptors, which can "measure" a mechanical signal and stimulate the osteoblasts and osteoclasts in their vicinity to adapt bone mass accordingly (Cowin et al., 1991). Most models are primarily based on load-driven adaptation using a single mechanism to stimulate bone remodelling. These computational studies, carried out over the last few decades, have been based on a variety of mathematical models (both time dependant and time-independent) mimicking bone's ability to adapt to mechanical stimuli. Both types of models are used to study the changes in bone morphology or the response to altered load due to prosthetic implants. These models are typically split into two processes (internal remodelling and external surface modelling), which in reality occur simultaneously. These models are either based on stress (Carter *et al.*, 1987; Beaupre *et al.*, 1990; Jacobs *et al.*, 1997), strain (Hart *et al.*, 1984a; Stanford and Brand, 1999) or strain energy density (Huiskes et al., 1987).

Huiskes et al. (1987) developed an adaptive bone remodelling algorithm for implant analysis based on the hypothesis that bone minimizes the difference between a homeostatic apparent strain energy density (SED) level and the implant induced apparent SED level. While the algorithm predicted cortical bone remodelling

consistent with clinical results, the prediction of trabecular bone remodelling was unstable and the homeostatic SED level could not be restored.

Other researchers have developed theoretical models based on the idea that adaptation is controlled by the level of fatigue damage, i.e. by the number and length of cracks (Viceconti and Seireg, 1990; Prendergast and Taylor, 1994; Martin, 1995). Martin (1995), for example, uses the amount of damage (mean crack length times crack density) as the stimulus for bone remodelling. In his model the activation frequency of the BMUs is directly related to the amount of damage present in a local area. As a consequence of damage formation, BMUs are activated, which increase the porosity resulting in increased strain. This promotes damage accumulation, which is not critical while the load remains below a critical level. The increasing damage removal overtakes the rising damage formation rate, resulting in a new state of equilibrium. On the other hand when the effective strain levels are below a critical value, BMUs are activated causing resorption of bone. This idea is an attractive one because the level of damage provides a direct measure of the potential danger of failure. If the damage, and particularly its rate of increase, is greater than can be repaired, then failure will occur unless adaptation is initiated to reduce the stress level. An advantage of this approach is that it automatically accounts for the dynamic loading history as the driving force for the remodelling process. However, whilst the concept of damage-stimulated remodelling and adaptation is an attractive one, it suffers from a number of problems. In particular, the lack of knowledge by which bone detects damage and 'decides' to initiate repair or adaptation.

1.8 Mechanical properties of bone

From a mechanical point of view, bone is a composite consisting of a solid and a fluid phase. In general, the mechanical properties are primarily related to the solid phase of bone, although it has been estimated that the fluid phase contributes to the material properties. Other factors that have been shown to affect the mechanical

behaviour of cortical and trabecular bone are the porosity, the orientation of the microstructure and the degree of mineralisation (Martin and Boardman, 1993; Sevostianov and Kachanov, 2000). Hence, bone is complex, inhomogeneous and anisotropic in its behaviour. This anisotropy in cortical bone is caused by the osteons which run along the longitudinal axis of the bone, resulting in a longitudinal stiffness that is approximately twice that of the transverse direction. In trabecular bone, the orientation of the trabeculae causes anisotropy. It is evident that there is clearly a preferential direction with respect to the loading direction in these two types of bone. Cortical bone is usually found in regions where there is unidirectional loading (e.g. long bones of the lower extremities) whereas trabecular bone is usually subjected to multi-axial loading, especially near the joints (e.g. hips and knees). Since the exact anisotropic values might not be known for implementation in a mechanical model, a good compromise can be found in using transverse isotropic material properties (Martin et al., 1998).

In general, the elastic constants (defined in Fig. 1-12), which are reported in various papers (e.g. Sevostianov and Kachanov (2000)) seem to agree well (see Table 1-1). Three factors that have a significant effect on bone are the orientation of the specimen with respect to its natural orientation, moisture content and the strain rate applied to bone.

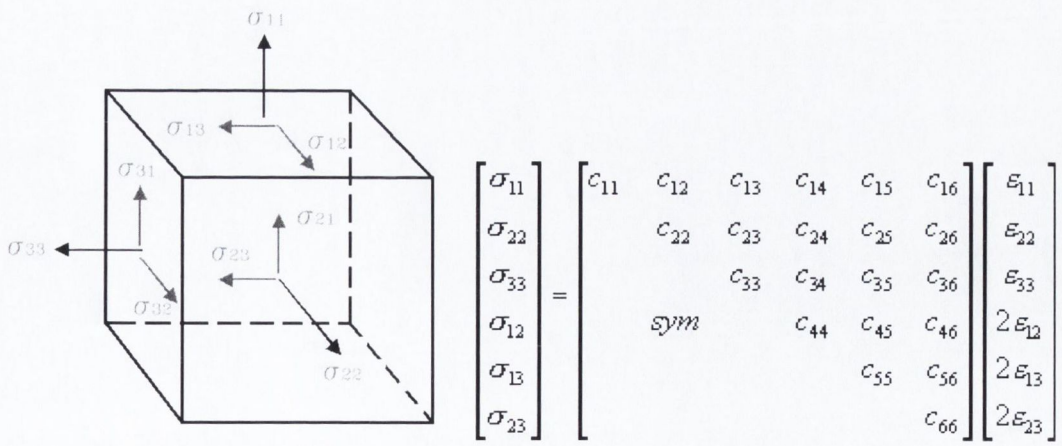

Fig. 1-12 Definition of stress components and stiffness matrix

Reference	(Lang, 1970)	(Van Buskirk et al., 1981)	(Katz et al., 1984)	(Reilly and Burstein, 1975)	(Zioupos et al., 1995)
Bone type	Bovine phalanx (dry)	Human femur (fresh)	Bovine femur (fresh)	Bovine femur (fresh)	Bovine femur (fresh)
Method	Ultrasound	Ultrasound	Ultrasound	Mechanical testing	Mechanical testing
C_{11}	19.7	20.0	21.2	17.0	13.69
C_{22}	19.7	21.7	21.0	17.0	13.96
C_{33}	32.0	30.0	29.0	29.6	24.88
C_{44}	5.4	6.56	6.3	3.6	4.92
C_{55}	5.4	5.85	6.3	3.6	4.92
C_{66}	3.8	4.74	5.4	3.4	4.14
C_{12}	12.1	10.91	11.1	10.2	5.42
C_{23}	12.6	11.45	11.7	9.8	8.58
C_{13}	12.6	11.53	12.7	9.8	8.58

Table 1-1 The anisotropic material properties of bone

Besides mechanical testing and ultrasound, nanoindentation can be used to determine the material properties of bone, which commonly gives values for the stiffness in the principal directions (Turner *et al.*, 1999; Rho *et al.*, 2002). This method can be very useful in measuring differences between various structures like lamellae (Rho et al., 1999) and differences between cortical and trabecular bone at a microstructural level (Rho et al., 1997). Other material properties such as ultimate tensile and compressive stresses, yield stress and fracture toughness values can be found for various species in books by Martin *et al.* (1998) and Currey (2002).

1.9 Microcracks

Microcracks have been observed within compact bone *in vitro* (Wright and Hayes, 1976b; Carter and Hayes, 1977b;a) and *ex vivo* (Frost, 1960; Wenzel *et al.*, 1996; Zioupos, 1999) due to fatigue loading. As a result of microcracking, bone is able to absorb a considerable amount of energy (Schaffler *et al.*, 1994; Martin *et al.*, 1996). Observations have been made of different microcrack appearances due to tension and

compression. Cracks induced by compression are usually relatively long, straight and start at obvious stress concentrators, such as channels and lacunae (Reilly and Currey, 1999; Reilly, 2000). Tensile cracks are often orientated with the grain of the bone and are associated with planes of weakness such as cement lines and inter-lamellar debonding (Carter and Hayes, 1977a; Vashishth *et al.*, 1997). Regarding the classification of microcracks, two types are commonly reported; long individual cracks (typically 100 μm, Fig. 1-13) and diffuse damage (Fig. 1-14). Diffuse damage consists of small cracks in the order of 2-10 μm, showing flame-like arrays, orientated roughly normal to the loading direction. The problem with diffuse damage, compared to long cracks, lies in its characterisation.

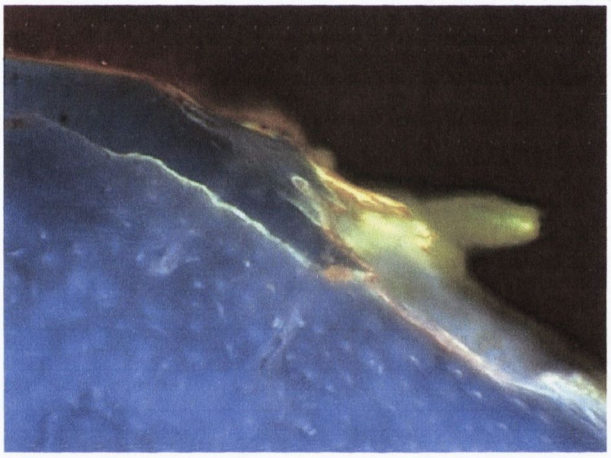

Fig. 1-13 Microcrack labelled with calcein (green) (Lee *et al.*, 2000)

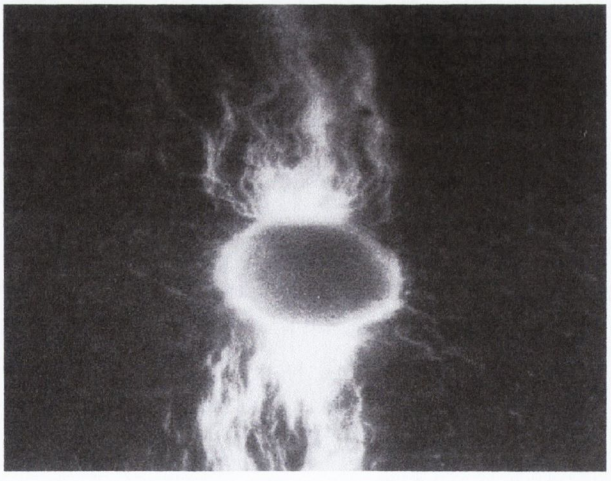

Fig. 1-14 Diffuse damage in bovine tibia (Reilly and Currey, 2000)

According to Martin and Burr (1982), microcracks formed in interstitial bone propagate to the cement line (Fig. 1-15) or concentric lamellae and debond or separate the Haversian canal from the surrounding bone.

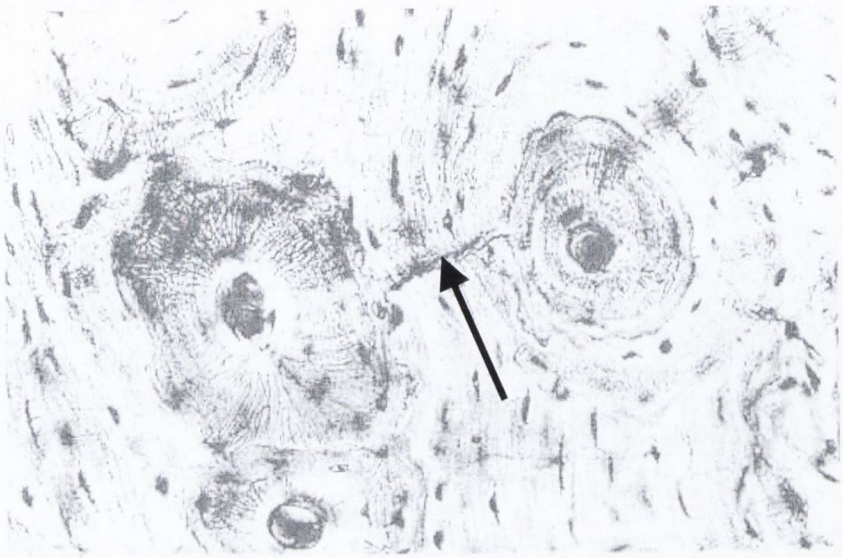

Fig. 1-15 A microcrack entrapped between two osteons (Martin *et al.*, 1998)

This would imply a greater incidence of microcracks at cement lines than at any other location within the bone microstructure. A number of researchers have noted that the vast majority of the cracks can be found in interstitial bone. The percentage of cracks found in interstitial bone by various researchers (Schaffler *et al.*, 1995b; Norman and Wang, 1997; O'Brien *et al.*, 2002) are respectively 87%, 62.4% and 85%. Corondan and Haworth (1986) showed that crack propagation in bone is inhibited by increasing numbers of osteons and by larger osteons. Additionally, it was found that crack densities are significantly higher in females than in males (Schaffler *et al.*, 1995a; Norman and Wang, 1997) and increase with age (Schaffler *et al.*, 1995a; Norman and Wang, 1997; Frank *et al.*, 2002).

Besides the influence of the microstructure and the interaction with microcracks, *in vitro* experiments have been carried out to study the mechanism of damage accumulation. These tests are typically stopped before failure occurs, taking 10 or 15 percent reduction in stiffness (Carter and Hayes, 1977a; Carter *et al.*, 1981a;

Schaffler *et al.*, 1995b; Boyce *et al.*, 1998) as the cut off point, followed by histological analysis of these specimens. Four point bending tests, carried out by Burr et al. (1998) on canine femora, found an increase in crack density with decreasing elastic modulus. Akkus and Rimnac (2001) observed that microcrack growth rates in bone specimens under uniaxial tension, initially reduced, going through a minimum rate, either becoming arrested or accelerating to macroscopic lengths. Work carried out by O'Brien et al. (2003), describes fatigue test carried out on bovine tibia, using various fluorescent stains allowing microcrack growth to be monitored. They found an initial strong increase in microdamge accumulation (first 10,000 cycles), followed by a period where hardly any new cracks initiated or propagated (10,000 – 50,000 cycles), and finally a rapid increase was observed resulting in failure of the specimen. This characteristic curve is shown in Fig. 1-16, supporting the theory that the cement lines, surrounding the osteons, act as a microcrack-arresting feature.

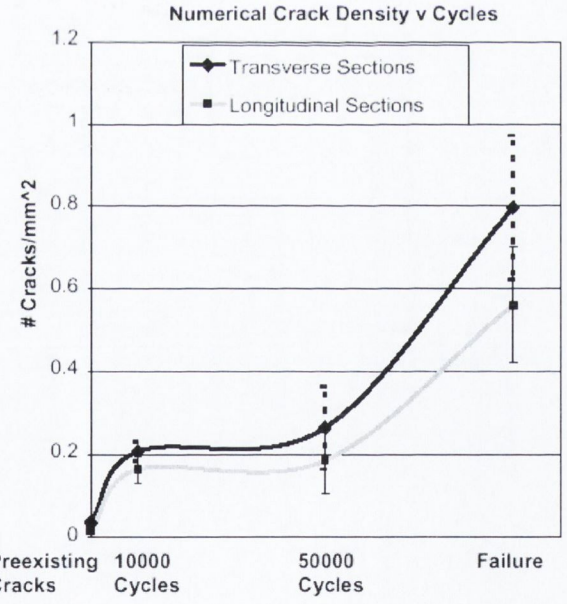

Fig. 1-16 Microdamage accumulation during testing (O'Brien *et al.*, 2003)

Experimental measurements of cracks tend to be made from histological sections oriented transversely to the bone's long axis. Individual cracks have an average length (measured tip-to-tip) of 60 to 100 μm. Table 1-2 summarizes this data. In

longitudinal sections, which have rarely been used, crack lengths appear significantly longer than those in transverse sections (Burr and Martin, 1993; O'Brien *et al.*, 2000). This implies that they are taking advantage of a relatively easy growth direction afforded by the anisotropic 'grain' of the material.

Reference	Bone	Mean length (μm)
(Burr and Martin, 1993)	Equine metacarpal	88
(Burr and Stafford, 1990)	Human rib	88
(Lee et al., 1998)	Human rib	82
(Lee, 1995)	Ovine Radius	55
(Muir et al., 1999)	Canine tibia	68 (left), 74 (right)
(Donahue et al., 2000)	Human metatarsals	75.04 (female), 81.67(male)
(Burr and Martin, 1993)	Human rib*	296

Table 1-2 Microcrack lengths found in bones of various species
(*crack length taken from longitudinal sections)

1.10 Clinical relevance

Bone adaptation is a naturally occurring event, which takes place throughout life. In general, bone modelling stops once adulthood is reached. Bone remodelling usually continues in order to repair damage and remove old bone. Several factors can have an effect on these processes, such as aging, exercise, disease, drug use, diet and malnutrition. Besides these 'naturally' occurring factors, in some cases surgical intervention is required such as fracture repair and joint replacements. In the following paragraph, some examples are given detailing the effects of microdamage on bone.

Clinically it has been observed that, with aging, people become more susceptible to fractures, which can be attributed to changes in the bone (Frost, 1998; Bailey *et al.*, 1999; Burr, 2002a). With aging, the process of coupled bone resorption and formation is affected by the reduction in osteoblast differentiation, which is further amplified in the menopausal years with hormone deprivation and increased osteoclast activity. Age-related bone loss is not only a consequence of hormone

deprivation, but also the result of changes in bone formation and cell-cell interactions (Chan, 2002). With the menopause comes a reduction in oestrogen levels, thereby favouring osteoclast formation and inhibition of osteoclast apoptosis. This increase in active osteoclast numbers with an increase in life expectancy results in uncoupling of bone turnover. As we age, our bones are less able to absorb energy, which might be the primary factor increasing the risk of fracture in elderly people with low bone mass (Burr, 2002a). As mentioned in section 1.2, bone tissue is primarily composed of collagen and mineral, both of which change with time, therefore affecting the material properties. Collagen may be considered the primary toughening mechanism in bone. Collagen has a greater effect on the fracture toughness of bone than on its strength and stiffness (Bailey *et al.*, 1999; Wang *et al.*, 2001; Zioupos, 2001). Studies by Currey *et al.* (1996), Zioupos *et al.* (1996) and Norman *et al.* (1995) showed that the fatigue strength and toughness of bone decrease with age. As bone gets older it becomes more mineralised, making it weaker, independent of the porosity and quantity of bone (Currey, 1970). Bone strength and toughness have been positively correlated to the bone mineral content. If the bone becomes hyper-mineralised, it tends to become brittle (Currey et al., 1996), making it more susceptible to crack initiation and damage accumulation.

Clinically the bone mineral density can be measured using DEXA and has been reported to differ according to sex, and race (Aloia *et al.*, 1998; Iwamoto *et al.*, 2000; Tanno *et al.*, 2001).

Besides these two components, microdamage is known to increase with age, which might contribute to a further deterioration of the mechanical properties (Schaffler *et al.*, 1995b; Mori *et al.*, 1997; Fazzalari *et al.*, 1998; Zioupos, 2001; Frank *et al.*, 2002). Age accounts for 70-80% of the variation in crack density (Burr, 2002a). The accumulation of cracks in woman is greater than in men after the age of 40 (Frost, 1960; Schaffler *et al.*, 1995b). As the amount of microdamage increases with age, the osteocyte density tends to decease (Vashishth *et al.*, 2000b; Frank *et al.*, 2002). Although this mechanism is poorly understood, it might indicate that cracks interfere

with generation or transmission of the osteocytic signals (Martin, 2000). It has been suggested that, as a direct or indirect result of microcracks, osteocytes become apoptotic (Dunstan *et al.*, 1993; Noble and Reeve, 2000; Schaffler and Verborgt, 2000; Verborgt *et al.*, 2000). Apoptosis, or programmed cell death, is an important determinant of the life span of cells in regenerating tissues.

Even when normal stresses are well below the failure level, cyclic loading induces microdamage in the bone structure resulting in microcracks. If the accumulation rate of microdamage is higher than the repair rate, fatigue fractures or stress fractures can occur. The rate depends on two factors. Firstly the rate of initiation of new cracks and secondly the rate of propagation by pre-existing cracks (Martin, 1992). Stress fractures can be classified into two types: fatigue fractures and insufficient (or fragility) fractures. Fatigue fractures occur in bone subjected to abnormal stress or torque, typically described in the metatarsal bones of military recruits (Beck et al., 2000) and in the lower extremities in athletes (Karlson, 1998), dancers, joggers and runners (Miller *et al.*, 1975; Goergen *et al.*, 1981; Daffner *et al.*, 1982; Micheli *et al.*, 1985). Insufficient fracture results from the application of normal force on a bone weakened by underlying conditions such as rheumatoid arthritis, osteoporosis, osteomalacia and congenital defects (Major and Helms, 1997).

Various diseases can cause damage or limit the use of a joint. Rheumatoid arthritis is the most common chronic inflammatory disease of joints, affecting 3% of woman and 1% of men (Dandy, 2003). Diseases in which bone is lost are osteomalacia (decreased mineralisation), osteolysis (increased removal by osteoclasts) and osteopenia (decrease in osteoid tissue). These processes usually occur together in varying degrees. The resulting bone loss is called osteoporosis of which there are three common types. Idiopathic osteoporosis (lack of oestrogen reduces the amount of collagen), disuse osteoporosis (lack of mechanical stimuli) and steroid osteoporosis (hormone treatment seen in patients with e.g. Rheumatoid arthritis).

Because of these diseases, joint arthroplasty can be a solution to relieve pain, improve function, increase social mobility and contribute to total psychological well-being (Laupacis et al., 1993). The majority of joint replacements are on hips and knees. The first successful low friction designs were made by Charnley (hip) in 1962 (Charnley, 1968) and by Gunston (knee) in 1969 (Gunston, 1971). Total hip arthroplasty is one of the most successful medical interventions developed during the 20^{th} century (Healy et al., 2001). Although there is a high success rate, infections, implant failure and calcar resorption and distal hyperthropy as a result of stress shielding can occur as a result of these implants (Harris, 1997). Therefore, theoretical models, simulations, and finite element analysis are needed to predict adaptation.

1.11 Aims and objectives

The aim of this project is to investigate, using fracture mechanics, the nature of the cellular transducer by which microcracks are detected, repaired and adaptation is regulated.

The specific objectives, which we aim to investigate, are:

- Is there a mechanism by which cracks can stimulate osteocytes?
- Is the size of a crack a determining factor in bone adaptation?
- Is there a threshold crack size that triggers modelling / remodelling?

The work presented in this thesis aims to answer the above questions by using fracture mechanics. In Chapter 2 some basic concepts, commonly used in fracture mechanics, will be discussed which will be applied in the subsequent chapters.

Microcrack analysis has mainly focussed on two-dimensional histological sections. As a result, no account has been taken of the three-dimensional shape of microcracks. In Chapter 3, a crack growth and shape development model will be presented which not only takes 3D crack growth into account, but also

microstructural features. Furthermore, fracture mechanics will be used to investigate the nature of the cellular transducer. Two different mechanisms will be discussed; damage to the cellular material and strain detection by the osteocytes.

Chapter 4 discusses the experimental work carried out to validate the predictions made in Chapter 3. This involves staining of cellular material, identifying how the microstructure affects crack growth and establishing what methods best describe microcrack behaviour.

Chapter 2 Fracture Mechanics

2.1 Introduction

As noted in Chapter 1, cyclic load stimulates the accumulation of microcracks in a structure. This principle also applies to bone. During daily activities our bones experience tensile, compressive and torsion loads. Microdamage is commonly found in bones of humans and animals. This triggers a repair process by the cells in the bone matrix. Although this relationship between microdamage and the repair process has been observed experimentally, the mechanism involved still unknown. A possible solution might lie in our ability to understand the formation, behaviour during growth and interaction of microdamage with the cellular system. Various authors have tried to explain crack growth phenomena in bone by using fracture mechanics. In order to understand the methods applied and their implications, some basic methods used in fracture mechanics will be discussed in this chapter.

Fracture mechanics is a relatively young discipline, in which the majority of developments are the result of accidents. Ever since there have been man-made structures, people have had to deal with the problem of failure. Especially in the time of the industrial revolution when trains, planes and automobiles were introduced, failure was common and cost many lives. The general aim of fracture mechanics is to gain more knowledge and insight into crack behaviour and ways in which the chance of a failure can be reduced.

2.2 Fracture Mechanics concepts

Over the last number of centuries, the variety of materials used in the construction of various objects has expanded rapidly, especially those that are optimised for their

function, like the use of fibre-reinforcements. That not all these materials behave in a similar way is obvious. In general, two concepts are used in the discipline of fracture mechanics. These concepts are Linear Elastic Fracture Mechanics (LEFM) and Elastic Plastic Fracture Mechanics (EPFM). In LEFM analysis, it is assumed that the material in the vicinity of a crack tip is linear-elastic. Plastic deformation might be present, but has little effect on the overall behaviour of the crack. For materials that do not obey Hooke's law near the crack tip the EPFM method was developed. This method is to be applied when large amounts of plastic deformation are present near the crack tip or in the whole specimen.

2.3 Linear elastic fracture mechanics (LEFM)

The following sections will discuss the most common methods used in fracture mechanics with respect to the linear elastic behaviour of materials. Energy and stress based approaches, as well as crack tip plasticity will be addressed. At the end of this section information will be given on when LEFM and when EPFM should be used.

2.3.1 Griffith energy balance

In 1920, Griffith studied brittle crack propagation in glass, which led to the development of the energy balance approach. This approach states that the extension of a crack can only occur when there is enough energy available for the crack to overcome the resistance of the material. The change in elastic energy (U_a) in an infinite plate was defined by Griffith as:

$$U_a = \frac{\pi\sigma^2 a^2}{E} \qquad \textbf{Equation 2-1}$$

Where σ is the remote applied stress, a is half the crack length and E is Young's modulus of the material. The crack is a straight, through-thickness crack in a finite plate loaded in tension normal to the crack faces.

The resistance of the material may be caused by surface energy, plastic deformation and surface roughness (Griffith, 1920). Although this model works very well for brittle solids, it leads to underestimations if applied of metals since no account is taken of plastic flow. Irwin (1948) and Orowan (1948) independently modified the Griffith equation to take account of this plastic flow. In an ideally brittle solid, a crack can only be formed by breaking the atomic bonds. However, in metals, dislocation motions will occur near the crack tip, which results in an additional energy dissipation. This called for modifications of existing methods, which eventually led to the development of the energy release rate.

2.3.2 Energy release rate

The energy release rate, G, was developed by Irwin (1956) based on previous work by Griffith. By definition, G, expresses the rate of change in potential energy with crack area for a linear elastic material. Here, the crack area is meant as the projected area normal to the crack plane of the newly formed surface. It is evident that, in order for crack growth to take place, the value of G has to be larger than a certain critical value (G_c), assuming that the material resistance R is a constant. This means that fracture only occurs when:

$$G = \frac{\pi\sigma^2 a^2}{E} > G_c = R \qquad \textbf{Equation 2-2}$$

In order to determine the critical value G_c, measurements can be taken of the stress (critical stress) that is required to fracture a plate with a crack of size $2a$. The modification made by Irwin resulted in the definition that states that the resistance, 'R', is dependent on the sum of the surface energy (γ_c) and the plastic strain work (γ_p), both per unit crack surface area. Therefore, R is defined as:

$$R = 2\left(\gamma_c + \gamma_p\right) \qquad \textbf{Equation 2-3}$$

For relatively ductile materials $(\gamma_p)>>(\gamma_c)$, meaning that R is mainly dependant on the plastic energy and the surface energy can be neglected. In order to assess the crack growth resistance of a given material, R-curves can provide useful information.

2.3.3 The stress intensity factor

Besides the energy-based approaches, stress-based models are frequently used. In the 1950s, Irwin developed the stress intensity approach. The stress intensity factor K describes the effect of the crack geometry on the local crack tip stresses. Solutions for a wide variety of geometries like penny shape, elliptical and straight cracks can be found in handbooks (Murakami, 1987). Due to all possible configurations with respect to geometry and loading conditions, it can be said that for every case a different K-value will be found. The value of K is linearly related to stress and directly related to the square root of a characteristic length. The general form of the stress intensity factor is given by:

$$K = F\sigma\sqrt{\pi a} \qquad \textbf{Equation 2-4}$$

Where F is a dimensionless correction factor that depends on geometry and loading, a is the crack length and σ is the (remote) applied stress. In Fig. 2-1 a centre crack and an edge crack can be seen. For specimens with a finite width, the stress intensity has to be corrected, due to the changes in the tip stress field. Specimens that are loaded in tension will have some closing due to compressive stresses near the crack. This closing effect is absent in edge crack specimens due to the free boundary conditions. This increases the value of F, usually taken to be 1.12.

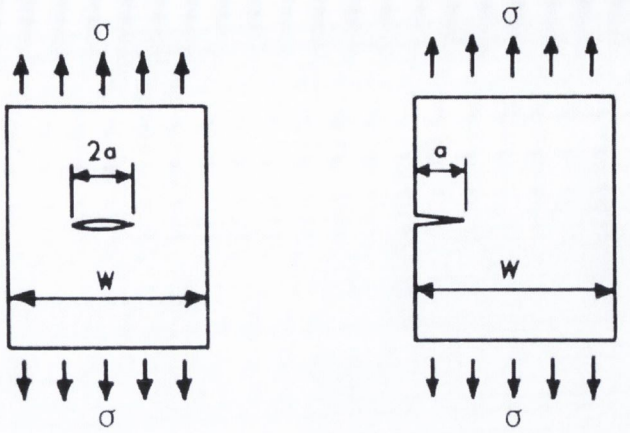

Fig. 2-1 Centre cracks and edge cracks (Ewalds and Wanhill, 1989)

Depending on the type of loading, the parameter *K* might have different subscripts. Subscript I refers to mode I loading, i.e. the crack opening mode. Other modes of deformation at the crack tip are the sliding mode II and the tearing mode III.

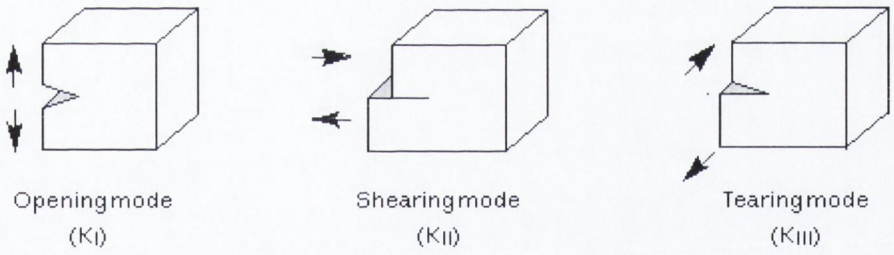

Fig. 2-2 Modes of failure (Ansys)

2.3.3.1 Crack shape analysis

Many crack analyses can be reduced to two-dimensional problems. In reality, this is not always possible. Many cracks have a three-dimensional shape where, for example circular, elliptical and ellipsoidal cracks can be distinguished. The major problem is that limited methods are available to assess the crack shape and monitor the growth and shape development in solid materials during fatigue tests. Two non-

destructive methods that have been used are the AC potential drop technique and ultrasonic methods. Both techniques use the fluctuations in electrical and acoustic resistance to monitor fatigue crack behaviour (Marsh *et al.*, 1991). The majority of studies investigate the crack shape post-testing. Commonly, specimens are fractured in liquid nitrogen following testing, after which the fracture surfaces can be analysed using SEM (Scanning Electron Microscopy). Experimental studies that have investigated the crack shape following fatigue loading are very limited and the majority have been qualitative and not quantitative. Elliptical cracks and circular cracks can form as surface cracks (Lee *et al.*, 2001; Murakami *et al.*, 2003).

Elliptical cracks can also form inside a structure, as a result of an edge crack that develops into an elliptical shape. Wang and Hadfield (2002) found that elliptical cracks form in brittle solids subjected to a rolling motion. Propagation occurred in the direction of the rolling motion but also in the opposite direction, resulting in elliptical crack formation. Similar observations have been made in coated materials. In these materials, the coating is a crack arresting feature. As the crack propagates in two directions, the coating prevents one axis from propagating, resulting in an elliptical crack shape. This shape is maintained if fatigue testing is continued and has been shown to grow in a stable manner (Kim *et al.*, 2001). Fractography observations have shown that the propagating fronts of ellipsoidal cracks tend to achieve an elliptical form (see Fig. 2-3) and to stay approximately elliptic during their fatigue propagation, even when the initial crack shape is far from an ellipsis (Castro *et al.*, 1995).

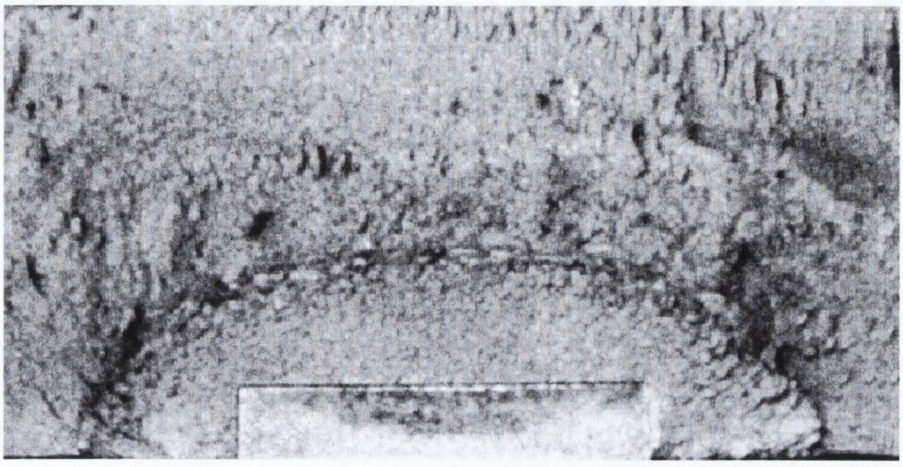

Fig. 2-3 Rectangular notch developing into an ellipse during fatigue testing (Miranda *et al.*, 2002)

That the crack shape has an influence on the stress intensity factors has been widely discussed in the literature. Various theoretical models are available to calculate the stress intensity factors (Wang and Huang, 1995; Guozhong *et al.*, 1996; Chen *et al.*, 1997; Huang and Liu, 1998). These models vary in complexity, depending on the incorporation of anisotropy and boundary problems. In general, for elliptical cracks, the stress intensity factor is calculated for the minor axis a and major axis b (Fig. 2-4) using equation 2-5 and 2-6.

$$K_a = \frac{\sigma \sqrt{\pi\, a}}{E(k)} \qquad \textbf{Equation 2-5}$$

$$K_b = \frac{\sigma \sqrt{\pi\, a}\left(\frac{a}{b}\right)}{E(k)} \qquad \textbf{Equation 2-6}$$

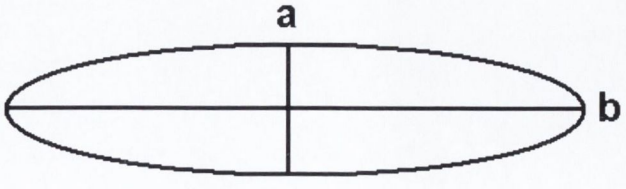

Fig. 2-4 Major and minor axis of an elliptical crack

Where K_a is the stress intensity at the minor axis of the ellipse and K_b is the stress intensity at the major axis of the ellipse, the complete elliptical integral of the second kind (*E(k)*) is calculated by:

$$E(k) = \int_0^{\frac{\pi}{2}} \left(1 - \left(1 - k^2\right) \sin^2 \phi\right)^{\frac{1}{2}} d\phi \qquad \textbf{Equation 2-7}$$

with k being the ratio a/b. In some cases an approximate equation can be used to calculate *E(k)* using:

$$E(k) = 1 + 1.464\left(\frac{a}{b}\right)^{1.65} \qquad \textbf{Equation 2-8}$$

Both methods are commonly used, although the approximate method should only be used where $b>>a$. Fig. 2-5 shows that the values for *E(k)* are higher with the approximate method at smaller axis ratios, resulting in lower stress intensity factors for both the major and minor axes.

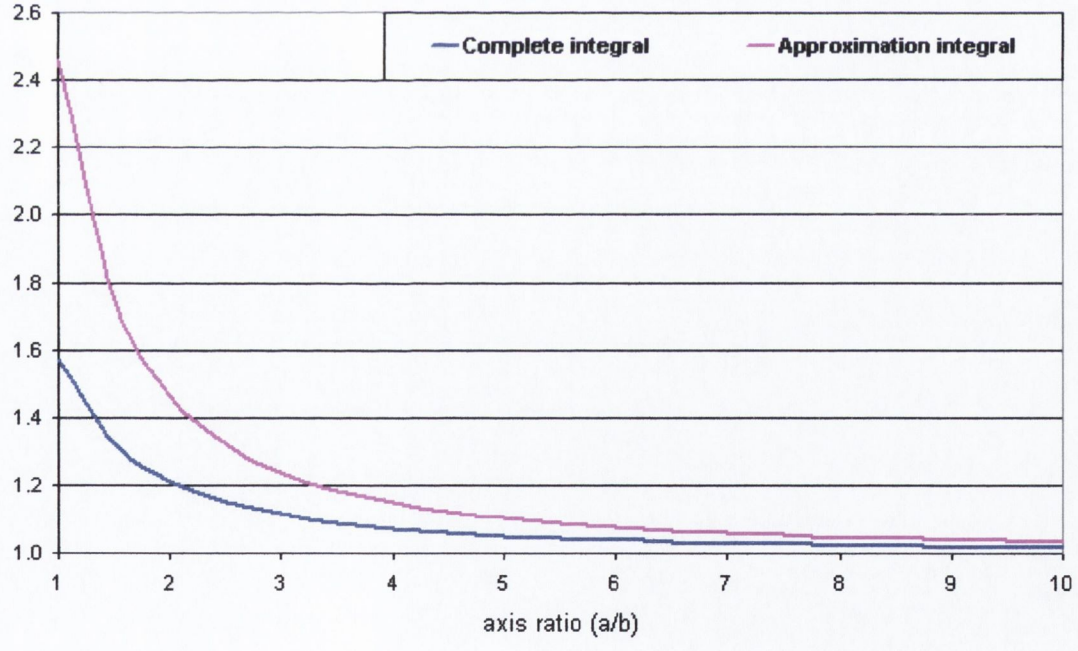

Fig. 2-5 Comparing the complete integral with an approximation method

Both methods obtain similar values when the ratio a/b becomes greater than 10. Since these equations are commonly used for axis ratios ranging from 1 to 10,

different values are obtained for the stress intensity factor using either one of these methods. Furthermore, limitations are present concerning the accuracy of these equations. This depends on the size of the body in which the elliptical crack is present, as shown in Fig. 2-6.

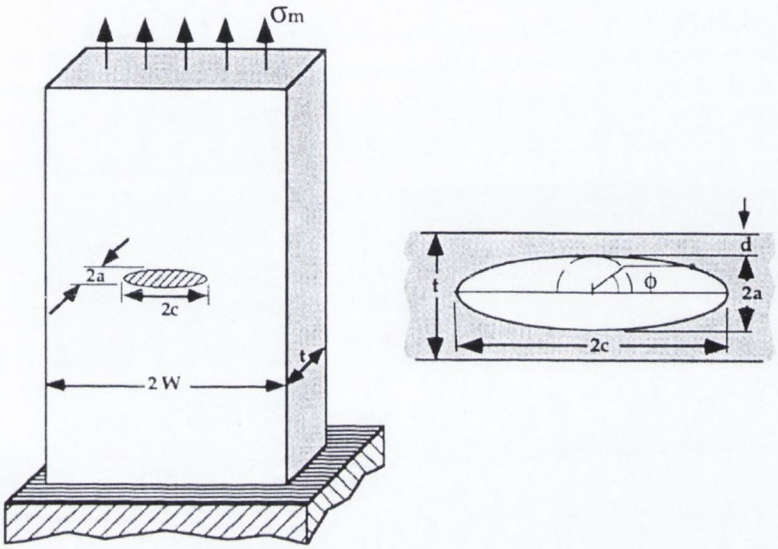

Fig. 2-6 Correction factors for an elliptical flaw in a solid body (Anderson, 1995)

The correction factor F for elliptical cracks in a finite body is dependant on various geometrical parameters and can be calculated as follows:

$$F = \left(M_1 + M_2\lambda^2 + M_2\lambda^4\right) g f_\phi f_w \qquad \textbf{Equation 2-9}$$

The correction factor F can be calculated for an elliptical crack in a finite body using equation 2-9, more details can be found in Anderson (1995).

2.3.4 Relationship between *K* and *G*

So far, two parameters have been discussed that can be used to describe the behaviour of a crack; the energy release rate G and the stress intensity factor K. The energy release rate method is based on the change in potential energy and the stress intensity factor is based on the description of the stresses, strains and displacements that occur near the crack tip. Although these methods are based on different approaches, K and G are related through the following expression.

$$G = \frac{K_I^2}{E} \text{ (plane stress)}, \quad G = \frac{K_I^2}{E}\left(1-\upsilon^2\right) \text{ (plane strain)} \qquad \textbf{Equation 2-10}$$

Where K_I is the mode I stress intensity factor, υ is Poisson's ratio and E is the Young's modulus of the material. The plane stress and plane strain conditions will be discussed in section 2.3.8. In some cases, combinations of loading modes might be present, for those cases the energy release rate can be calculated as follows.

$$G = \frac{K_I^2}{E} + \frac{K_{II}^2}{E} + \frac{K_{III}^2}{2\mu} \qquad \textbf{Equation 2-11}$$

Where μ is the shear modulus, E is the Young's modulus and K_I, K_{II} and K_{III} are three modes of failure. In cases where the stress intensity factor is used, the various modes can be combined as follows:

$$K_{total} = \sqrt{K_I^2 + K_{II}^2 + K_{III}^2} \qquad \textbf{Equation 2-12}$$

2.3.5 Crack tip plasticity

Due to the presence of a crack, high stresses are found near the crack tip. When the stress intensity factor is high enough, local plastic deformations near the crack tip will occur in the material. Theoretically, the stresses at the crack tip will go to infinity, assuming that the crack tip radius is infinitely small. In reality this is not completely true. Several factors can contribute to cause the crack tip to blunt (plastic zone, microstructural features). These elastic analyses become increasingly

inaccurate as the plastic region at the crack tip grows. In standard fracture mechanics, two approaches are available to estimate the size of the plastic zone. These methods are Irwin's model (Irwin, 1960), which is based on the elastic stress analysis and Dugdale's yield strip model (Dugdale, 1960).

2.3.5.1 The Irwin approach

Irwin (1960) considered a circular plastic zone to exist at the crack tip under tensile loading. The size of this circle has a diameter of $2r_y$ as shown in Fig. 2-7. The plastic zone or process zone size, r_y, is calculated to be:

$$r_y = \frac{1}{2\pi}\left(\frac{K}{\sigma_y}\right)^2 \qquad \textbf{Equation 2-13}$$

Where K is the stress intensity factor and σ_y is the yield strength of the material.

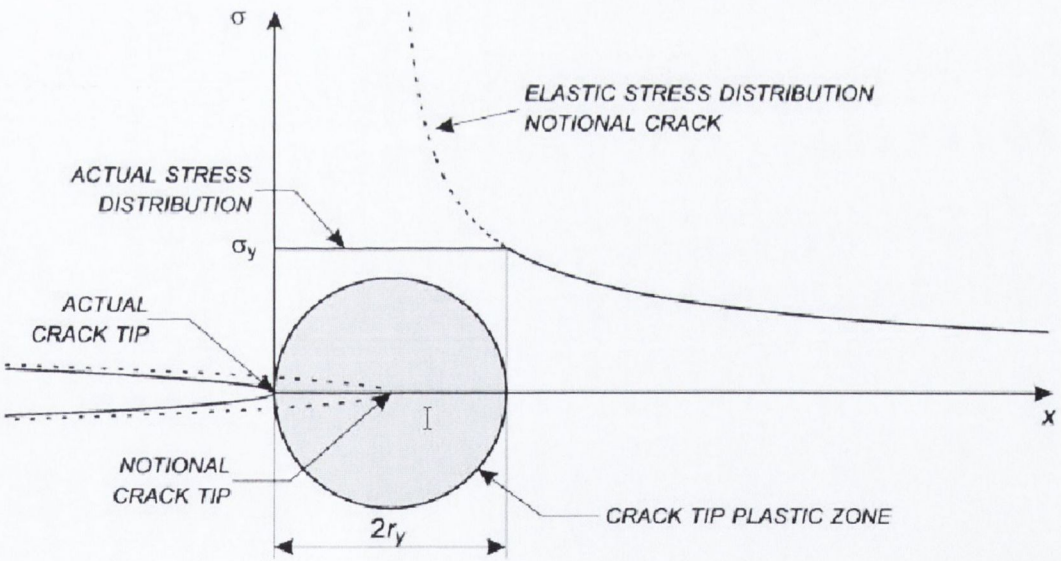

Fig. 2-7 The crack tip plastic zone according to Irwin (Janssen *et al.*, 2002)

Irwin argued that the occurrence of plasticity makes the crack behave as if it were longer than its physical size. As a result, the crack tip opening displacements are larger and the stiffness is lower than in the elastic case. He showed that the crack

may be viewed as having a notional tip at a distance r_y ahead of the real tip, *i.e.* in the centre of the circular plastic zone (see Fig. 2-7). Beyond the plastic zone the elastic stress distribution is described by the K, corresponding to the notional crack size. As shown in Fig. 2-7, this elastic stress distribution takes over from the yield stress at a distance $2r_y$ from the actual crack tip. Since the same K always gives the same plastic zone size for materials with the same yield stress, the stresses and strains both within and outside the plastic zone will be determined by K. For these cases the stress intensity approach is valid.

2.3.5.2 The Dugdale model (strip yield model)

Dugdale's (1960) analysis assumes that all plastic deformation concentrates in a strip in front of the crack, the so-called strip yield model. This type of behaviour does occur in a number of materials, but certainly not in all. Just as in Irwin's analysis, Dugdale argued that the effective crack length is longer than the physical length. The notional crack increment Δa_n (similar to r_y mentioned by Irwin) is considered to carry the yield stress as shown in Fig. 2-8 (here the assumption of elastic- perfectly plastic material behaviour and a state of plane stress are made).

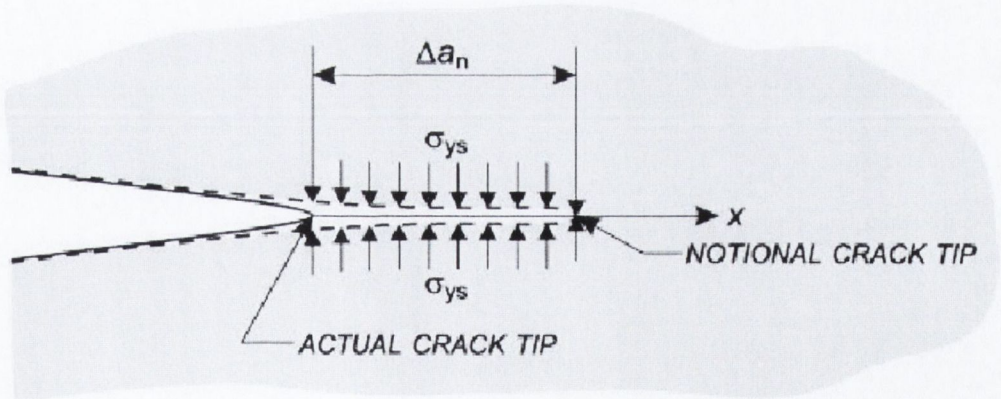

Fig. 2-8 Size of the plastic zone according to Dugdale (Janssen *et al.*, 2002)

The size of the plastic zone is calculated to be:

$$\Delta a_n = \frac{\pi}{8}\left(\frac{K}{\sigma_{ys}}\right)^2$$ **Equation 2-14**

2.3.6 Plane stress and plane strain

The majority of solutions have been reduced to two dimensions. This can be done if at least one of the principal stresses or strains is equal to zero. In a limited number of cases this can be applied, resulting in a good approximation. However, the majority of cracks show neither plane strain nor plane stress conditions, but are subjected to complex three-dimensional stress and strain fields.

In order to assess if plane strain or plane stress conditions should be applied, the following rule can be used. If the plate thickness is of the same order as the plastic zone size or smaller, contraction can occur freely and the plane stress state can be used. On the other hand, if the plate thickness is much larger than the plastic zone size, contraction is constrained by the elasticity of the material. The strain in the thickness direction will then be small, implying that a plane strain state exists everywhere except at the surfaces.

2.3.7 Crack opening displacements

Due to the presence of a crack in a strained body under tension, crack opening or crack flank displacement will occur (see Fig. 2-9). The amount of opening within the crack can be calculated with (Ewalds and Wanhill, 1989):

$$\delta = \frac{2\sigma}{E}\left(1-\upsilon^2\right)\sqrt{a^2-x^2}$$ **Equation 2-15**

for plane strain conditions (v = Poisson's ratio) and

$$\delta = \frac{2\sigma}{E}\sqrt{a^2-x^2}$$ **Equation 2-16**

for plane stress conditions.

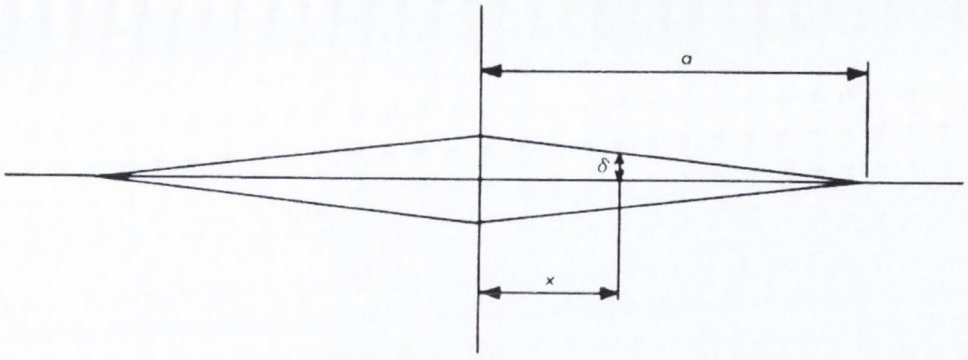

Fig. 2-9 Definition of crack-face displacement (Ewalds and Wanhill, 1989)

The total crack opening displacement (COD) is equal to 2δ, i.e.

$$COD = \frac{4\sigma\sqrt{a^2 - x^2}}{E} \qquad \textbf{Equation 2-17}$$

For this purely elastic case, the crack tip opening displacement (CTOD) would be zero and COD maximal in the centre of the crack. As shown in Fig. 2-7, crack tip plasticity can be accounted for by using Irwin's proposal for an effective crack length $2(a + r_y)$, and considering the crack opening displacement at the actual crack tip (Fig. 2-10).

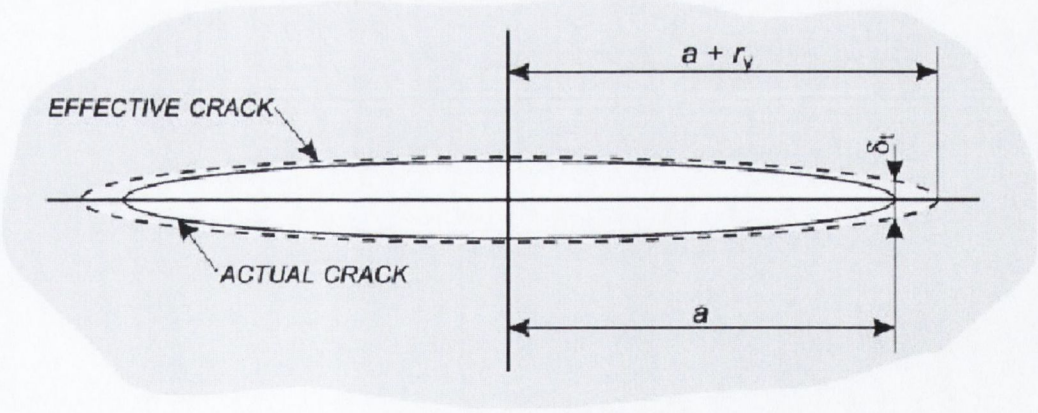

Fig. 2-10 Crack tip opening displacement according to Irwin (Janssen *et al.*, 2002)

Therefore δ_t should be:

$$\delta_t = \frac{4\sigma\sqrt{a^2 + 2ar_y + r_y^2 - a^2}}{E} \approx \frac{4\sigma\sqrt{2ar_y}}{E}$$ **Equation 2-18**

substituted in equation 2-11 results in the following expression for the CTOD,

$$\delta_t = \frac{4}{\pi}\left(\frac{K^2}{E\sigma_y}\right)$$ **Equation 2-19**

2.3.8 Mixed mode fracture and kinked cracks

In linear elastic isotropic materials, crack growth paths are typically perpendicular to the maximum tensile loading direction, resulting in a Mode I crack propagation. In materials like fibre-reinforced composites with non-isotropic material properties, the crack growth direction is strongly influenced by the microstructure and less by its loading conditions. This can be accounted for by calculating the stress perpendicular to the crack faces and the shear in the crack faces from the remote applied stress σ_∞. For cracks at some arbitrary angle (β), the tensile and shear stresses can be calculated according to equations 2-20 and 2-21 (Fig. 2-11).

$$\sigma = \sigma_\infty \cos^2(\beta)$$ **Equation 2-20**

$$\tau = \sigma_\infty \sin(\beta)\cos(\beta)$$ **Equation 2-21**

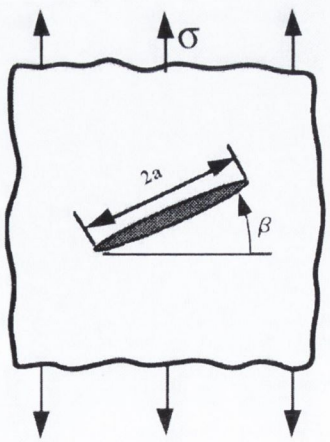

Fig. 2-11 Definition of crack angle β (Anderson, 1995)

As a result of the angle (β), a combination of loading modes (i.e. mixed mode conditions) can be found. Mixed mode loading appears if the crack is at an angle, but also if cracks start to kink. Kinked cracks are formed if microstructural features like defects, such as variations in crystal structure or fibres in laminates, deflect the crack from the primary growth direction. When a crack was not formed in the primary growth direction, kinking is also likely to occur. In the literature, kinked cracks have various descriptions. To avoid confusion, crack kinking is the out-of-plane growth of a pre-existing straight crack. The kink angle is defined as the angle between the initial straight crack and its out-of-plane extension (θ), see Fig. 2-12.

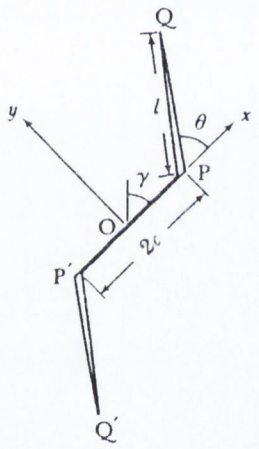

Fig. 2-12 Pre-existing crack PP' and a 'secondary' kinked crack PQ (Horri and Nemat-Nassar, 1986)

Although kinked cracks are commonly found in metals (Duncan *et al.*, 1999), wood (Jernkvist, 2001), rock (Steward and Alvarez, 1991) and laminates (Ireman *et al.*, 2000), they still have not had adequate attention (Nemat-Nassar and Horii, 1982; Hammouda *et al.*, 2003). Only a limited number of studies have addressed this issue.

Horii and Nemat-Nasser have done extensive research on kinked cracks in solids, especially rock. Their model, like most others, is based on the idea that frictional sliding of a pre-existing crack produces, at the crack tips (*P* and *P'* in Fig. 2-12),

tension cracks that grow in the direction of the compression axis. Horii and Nemat-Nasser showed analytically and experimentally that, under axial compression, tension cracks nucleate from the tip of the flaw at an angle close to 70° with respect to the flaw orientation, which was independent of the primary crack orientation. They continue to grow with increasing load, curving towards the direction of maximal axial compression. If axial compression is accompanied by any amount of lateral tension, the crack growth becomes unstable at a certain crack length, resulting in axial splitting. On the other hand, if some lateral compression accompanies the axial compressive load, the tension cracks grow to a certain length and then stop.

Scholz *et al.*(1986) showed that isolated cracks, subjected to hydrostatic pressure in pyrex glass, start to kink and grow in a stable manner from tiny flaws not greater than 20 μm. From Horii and Nemat-Nasser's analysis, it was shown that even a 10 μm initial crack would be large enough to initiate kinking cracks. From these studies it was shown that kink angle is approximately 70° and that this is independent of the angle of the initial crack and the friction coefficient within the crack faces. Other materials were shown to have similar behaviour, like CE-TZP/alumina composites and PMMA (Lin and Shetty, 2003).

For straight cracks subjected to a uni-axial load, it can be shown that K_I and K_{II} are of the same order of magnitude at an angle of 45° (using equations 2-20 and 2-21). For kinked cracks, there is a shift towards 70° (Lin and Shetty, 2003). This was also shown from an FE-analysis by Becker et al. (2001) and Hutchinson and Suo (1991). Fatigue tests on C-steel under mode II showed that as the crack grows, ΔK_{II} decreases towards the threshold value, and cracks will start to branch in the direction for mode I (Murakami *et al.*, 2003). The angle between crack propagation in mode II and mode I was found to be around 70.5°.

In order to calculate the stress intensity factor for embedded kinked cracks, standard fracture mechanics approaches are not sufficient without using a large number of

correction factors. Horii and Nemat-Nasser (1986) calculated the stress intensity factor for kinked cracks in solids using:

$$F_{split} = 2c\tau^*$$
$$\tau^* = -\frac{1}{2}(\sigma_1 - \sigma_2)\sin(2\gamma) - \tau_c + \mu\frac{1}{2}\left[\sigma_1 + \sigma_2 - (\sigma_1 - \sigma_2)\cos(2\gamma)\right] \quad \textbf{Equation 2-22}$$

The representative crack QQ' is subjected to a far field stress σ_1 and σ_2 (see Fig. 2-12). The stress intensity factor at Q and Q', produced by the splitting force F_{split}, can be calculated with:

$$K_I = \frac{F_{split}\sin(\theta)}{\sqrt{\pi * l}} \quad \textbf{Equation 2-23}$$

$$K_{II} = \frac{-F_{split}\cos(\theta)}{\sqrt{\pi * l}} \quad \textbf{Equation 2-24}$$

However, this method cannot be applied in every configuration. These estimates are valid when L is rather large compared to PQ and $P'Q'$. The solutions break down as L becomes small. For very small cracks, K_I and K_{II} can be calculated using:

$$K_{II}^0 = \sigma\sqrt{\pi a} * \left(-\sin\beta\cos\beta + \mu\sin^2\beta\right) \quad \textbf{Equation 2-25}$$

$$K_I^\theta = +0.75K_{II}^0\left[\sin(\theta/2) + \sin(3\theta/2)\right] \quad \textbf{Equation 2-26}$$

$$K_{II}^\theta = 0.25K_{II}^0\left[\cos(\theta/2) + 3\cos(3\theta/2)\right] \quad \textbf{Equation 2-27}$$

Here the Mode II stress intensity factor is calculated for the 'primary' crack PP' using equation 2-25. This value is then used in equations 2-26 and 2-27 to estimate the stress intensity factor at the tip (Q and Q') of the kinked crack. This method is simple in nature and has been proven to give a good indication. The only minor problem is that this method does not work if mode II is absent. This can happen in certain circumstances where the 'primary' crack is orientated, with respect to the loading direction, at an angle of 90°.

Kinked cracks from edged notch specimens present problems that are even more complex. The analyses for centre cracks with branching cracks (kinks) have so far only led to approximate equations as discussed above, which is in general enough to get a good indication. Due to the boundary conditions, present when dealing with edge cracks a more considered approach is required (Liu and Wu, 1997). For simple straight edge cracks, a 12% increase in stress intensity is usually accounted for due to the different boundary conditions at the free edge. For kinked cracks originating from edge cracks, this method results in inaccurate indications for K. To establish the magnitude of the stress intensity factor, FEA and analytical solutions might be considered. An FE model will give a good indication of the K-value and especially with complex geometries, it is advisable to use this. The two other commonly used solutions are by Denda and Dong (1999) and Chen (1999), see Fig. 2-13 and Fig. 2-14.

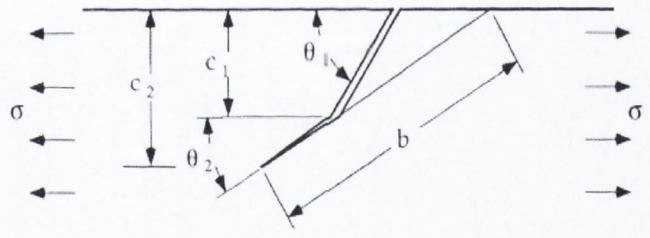

Fig. 2-13 Kinked crack (Denda and Dong, 1999)

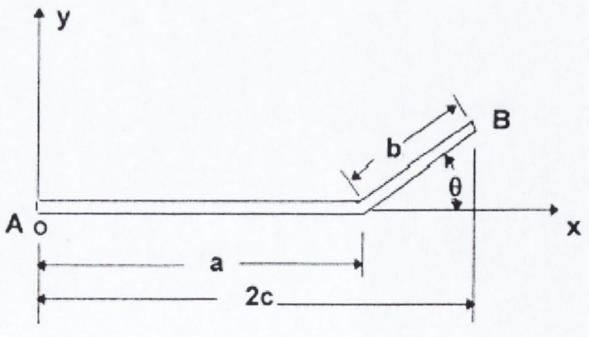

Fig. 2-14 Kinked crack (Chen, 1999)

The stress intensity factor at the crack tip of the kinked crack increases strongly with the length of the initial crack or notch. Both methods use the initial crack or notch length to calculate the representative crack lengths b (Denda & Dong) and c (Chen). Both methods use equation 2-4 to calculate the stress intensity factor. The geometry correction factors can be found in tables provided with these papers since they are dependent on the ratio (crack length/ kinked length), kink angle, width and thickness of the specimen.

2.4 Elastic-Plastic Fracture Mechanics (EPFM)

Linear Elastic Fracture Mechanics (LEFM) is, despite its denotation, valid also when plastic deformation occurs. However, this plastic deformation has to be confined to a small region ahead of the crack tip. In many materials, and for many combinations of loading and geometry, these conditions are not fulfilled. This calls for models that can deal with larger plastic zones. Elastic Plastic Fracture Mechanics (EPFM) deals with these situations. Two common parameters that can be used even in the presence of relatively large plastic zones are the crack tip opening displacement (CTOD) and the J-integral.

2.4.1 Crack Tip Opening Displacement (CTOD)

A variety of materials can be used in building structures, of which in some cases high toughness is required. Materials like that could not be characterised by LEFM according to experiments by Wells (1961). He observed that the crack faces moved apart prior to fracture. As a result of plastic deformation, the crack tip blunted the initial sharp crack tip (see Fig. 2-15). This crack blunting increased in proportion to the toughness of the material. The crack tip opening displacement (CTOD) is therefore one more way in which the fracture toughness can be quantified.

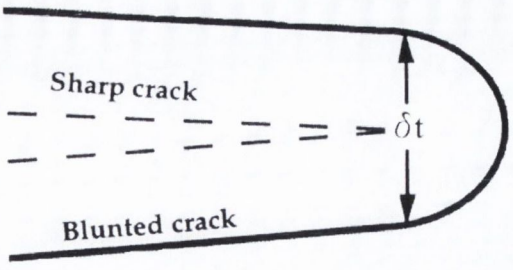

Fig. 2-15 Crack blunting as a result of plastic deformation (Anderson, 1995)

The CTOD can therefore be quantified in terms of the stress intensity according to equation 2-19 previously.

$$\delta_t = \frac{4}{\pi}\left(\frac{K^2}{E\sigma_y}\right) \qquad \textbf{Equation 2-19}$$

This equation can be rewritten in terms of:

$$\delta_t = \frac{4}{\pi}\frac{G}{\sigma_y} \qquad \textbf{Equation 2-28}$$

Thus, in cases where small scale yielding occurs, CTOD is related to G and K. The big advantage of the CTOD is that it can still be used when LEFM is no longer valid. This was proven to be correct when a unique relation between the CTOD and the J-integral (see section 2.4.2) was established.

2.4.2 J-integral

The J-integral concept is an energy balance based method, developed by Rice (1968). In this concept the elastic-plastic deformations are idealized as a non-linear behaviour that can be used for LEFM and EPFM. The J-integral can be seen as the balance between the internal strain energy U and the external energy represented by the work done by the applied traction t_i on a volume enclosed by the closed path S. The integral is evaluated along the path S surrounding the crack tip.

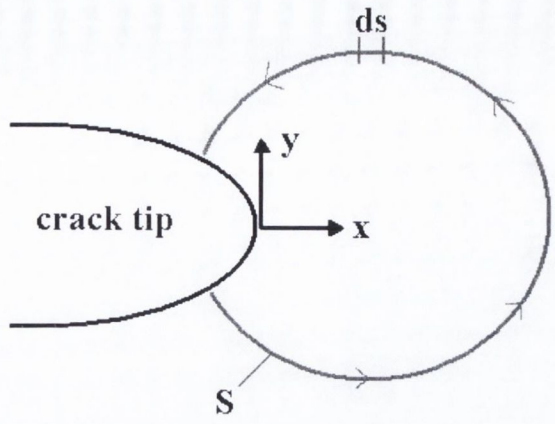

Fig. 2-16 Definition of the path 'S' around the crack tip

The initial point and the end point defining the path *S* must be located on the surface of the crack. The equation defining the J-integral is:

$$J = \int_s \left(U dy - t_i \frac{\partial u_i}{\partial x} ds \right)$$ **Equation 2-29**

where U is the strain energy density, t_i are the components of the traction vector, u_i are the displacement vector components, and ds is a length increment along the contour S. Rice showed that the J-integral is path independent. For linear elastic materials it was shown that J=G, therefore the J-integral can also be related to the stress intensity factor, K.

$$J = \frac{K^2}{E'}$$ **Equation 2-30**

With $E' = E$ for plane stress conditions and $E' = E/(1-\nu^2)$ for plane strain conditions.

2.4.3 Relation between CTOD, G, K and J

For linear conditions, the relationship between CTOD, G and J is given by equation 2-31.

$$J = G = \frac{K^2}{E'} = m\ \sigma_y \delta$$ **Equation 2-31**

Where m is a dimensionless constant depending on the stress state and the material properties.

For linear elastic fracture mechanics all failure criteria G, K, CTOD and the J-integral are inter-related and can be used. In the elastic-plastic domain only CTOD and the J-integral are useful since the plastic deformation is taken into account.

2.5 Fatigue Crack Growth

Under applied stress, a crack exceeding a critical size will suddenly advance breaking the cracked member into two or more pieces. This failure mode is called brittle fracture. But, even sub-critical cracks may propagate to a critical size if crack growth occurs during cyclic (fatigue) loading. Crack growth resulting from cyclic loading is called fatigue crack growth (FCG).

Paris and Erdogan (1963) were the first to discover the power law relationship for stable fatigue crack growth. They proposed that the stress intensity factor range, ΔK, could be used for characterisation of crack growth. Fatigue crack growth rates (increments of crack growth per load cycle, da/dN) were related to ΔK, the cyclic range of crack-tip stress intensity, for constant loading amplitude. A schematic of typical constant amplitude load cycles are shown in Fig. 2-17, where the stress intensity factor, K, is plotted as a function of time. The stress intensity factor oscillates between minimum and maximum values, K_{min} and K_{max}, respectively. Arrows indicate change in K with increasing time. ΔK is shown schematically on the right side of the figure and is defined as K_{max} - K_{min}.

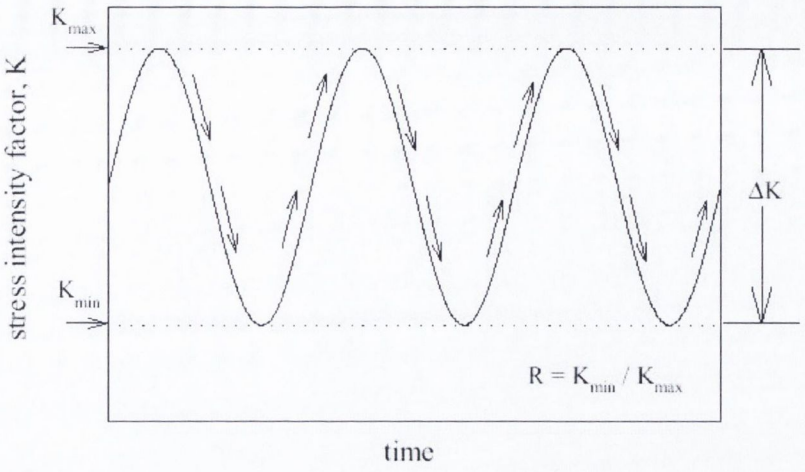

Fig. 2-17 Schematic of constant amplitude load cycles

For a constant amplitude loading the load ratio, R is defined in Fig. 2-17 as the ratio of K_{min} and K_{max}. Paris implied that resemblance exists for fatigue cracks subject to the same ΔK (Paris and Erdogan, 1963). In other words, fatigue cracks of different length but subject to the same ΔK will grow at the same FCG rate, da/dN. Therefore, FCG data obtained from laboratory specimens can be used to predict the FCG response for any crack configuration.

A schematic of typical (constant R) FCG behaviour for engineering metals is shown in Fig. 2-18, where the logarithm of FCG rate, log (da/dN), is plotted against log (ΔK). FCG behaviour is divided into three regions (see Fig. 2-18). At intermediate values of ΔK, the FCG curve is nearly linear on log-log plots. This region is called the Paris regime. Taking advantage of this linear relation, Paris presented an equation relating FCG rates (da/dN) to ΔK using two empirical parameters (C and m) as shown in equation 2-35, (Paris and Erdogan, 1963). Depending on the slope of the FCG curve in the Paris regime, 'm' ranges from 2 to 4 for most engineering metals. As ΔK increases beyond the Paris regime, unstable crack growth occurs. Here, the FCG curve becomes steep (i.e. da/dN increases rapidly with increasing ΔK) as K_{max} approaches the fracture toughness, K_c, or large scale yielding occurs.

$$\frac{da}{dN} = C(\Delta K)^m$$ **Equation 2-32**

As ΔK decreases into the threshold region, the FCG curve becomes steep as da/dN rapidly decreases with ΔK reduction. It is assumed that no detectable FCG occurs if ΔK is below the threshold value ΔK_{th}. Threshold FCG is interesting from a research point of view, since under constant cyclic loads, short fatigue cracks grow faster as the crack length increases. This region is also interesting because, for high-cycle (long life) fatigue, cracks spend most of their time at near-threshold values.

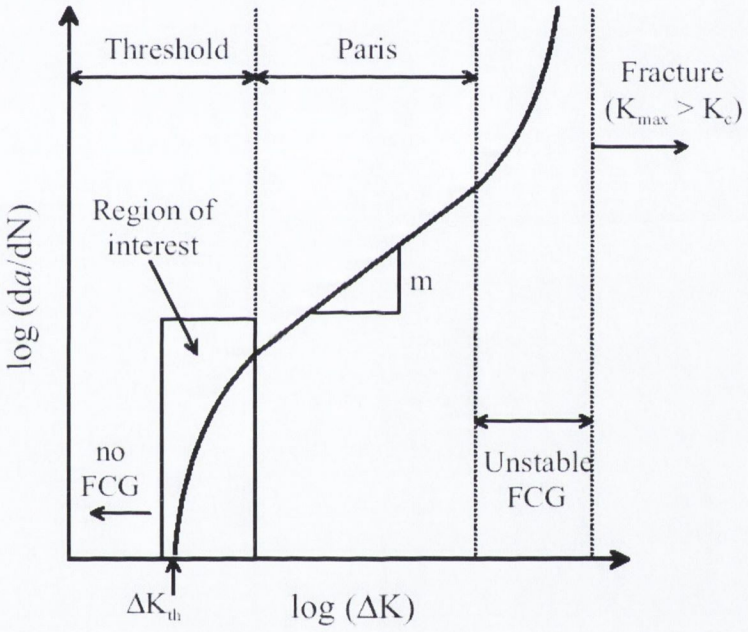

Fig. 2-18 Schematic of typical fatigue crack growth (FCG) data (Newman, 2000).

2.5.1 Short crack problems

Short cracks are known to propagate faster than long cracks subject to the same ΔK and R, since crack propagation also occurs at levels below ΔK_{th}. Therefore, a distinction should be made between "short" cracks and "small" cracks. A crack is considered small when all crack dimensions are similar to or less than a characteristic microstructural feature, likely a grain size. Therefore, small cracks are generally

contained within a limited number of grains, perhaps even a single grain. Because individual grains are highly anisotropic, the stress intensity factor is not a good descriptor of crack-tip driving force. The difference between "short" crack and "long" crack behaviour can be explained in terms of fatigue crack closure.

Several papers have identified that grain and phase boundaries act as barriers to crack propagation since it is in such locations that cracks are either arrested or temporarily halted (Tanaka and Akiniwa, 1988; Aniniwa *et al.*, 1996; Chapetti *et al.*, 2001). As a result of these dominating features, the fatigue damage process might be separated into microstructural short crack (MSC) and physical small crack stages (PSC) (Zhao *et al.*, 1999). Several experimental studies have shown that the short fatigue crack growth rate slowly decreases in the MSC-stage at relatively low stress levels (Pearson, 1975; El Haddad *et al.*, 1980; Lankford, 1983; Miller, 1987). This effect of crack growth rate reduction (or arrest) might fade away resulting in an increase in crack growth rate. This occurs in the PSC-stage were cracks have grown beyond the microstructural effect. In this stage, fatigue crack growth rates are mainly dominated by the level of loading. The point of transition between these two stages has been widely investigated, since crack growth in the MSC and PSC stages is more rapid than would be expected from LEFM analysis (Miller *et al.*, 1986; Taylor, 1986; Goto, 1994). The point of transition between MSC-stage and the PSC-stage is of great importance since crack growth rates can no longer be controlled by the microstructure of the material, increasing the chance of catastrophic failure.

2.6 Fracture in composites

Laminate composites have been widely employed in different applications for their light weight and high strength. By incorporating fibres in materials like polymers and ceramics, great improvements can be made in their ability to withstand loading in various directions. Damage growth in composite laminates is a complex process involving interaction among various damage modes on both microscopic and

macroscopic scales. Distinguishable damage modes in composite laminates include microdamage, transverse matrix cracking, delamination, and fibre-failure. Variances in the geometry of the laminate plies make it difficult to determine how these damage modes interact with one another (Wharmby *et al.*, 2003).

Recent theoretical and experimental studies have shown that the effectiveness of this reinforcement is dependent on the efficiency of stress transfer between the matrix and fibres (Chou and Sun, 1980; Belnap and Shetty, 1998; Jiang and Goa, 2001; Banerjee *et al.*, 2002). It is widely acknowledged that the fibre/matrix interface influences the mechanical behaviour of fibre-reinforced composites (Bennett and Young, 1998). Under cyclic loading, the mechanical behaviour of long-fibre-reinforced ceramic-matrix composites changes progressively as a function of the number of cycles and can lead to fatigue failure. The main mechanism involves matrix cracking in the longitudinal and transverse fibres on the first loading cycle (depending on the architecture of the reinforcement). Cracking is followed by debonding and a cyclic sliding along the fibre/matrix and fibre/fibre interfaces. Repeated sliding causes wear phenomena at the interfaces, resulting in a reduction of the stress transfer capability and a corresponding increase of the fibre failure probability (Reynaud *et al.*, 1998).

In general, crack growth can be seen as a mutual competition between intrinsic microstructural damage mechanisms, which promote crack extension ahead of the tip, and extrinsic crack-tip shielding mechanisms, which act primarily behind the tip (Ritchie, 1988). Intrinsic damage mechanisms typically involve processes that create microcracks or voids, leading to classical failure by cleavage, inter-granular cracking or micro-void coalescence. Other comparable mechanisms appearing due to cyclic loads involve the repetitive blunting and re-sharpening of the crack tip. The extrinsic shielding mechanism results from the creation of inelastic zones surrounding the crack wake or from physical contact between the crack surfaces via wedging, bridging, sliding or combinations of these mechanisms (Ritchie, 1988). A schematic representation can be found in Fig. 2-19.

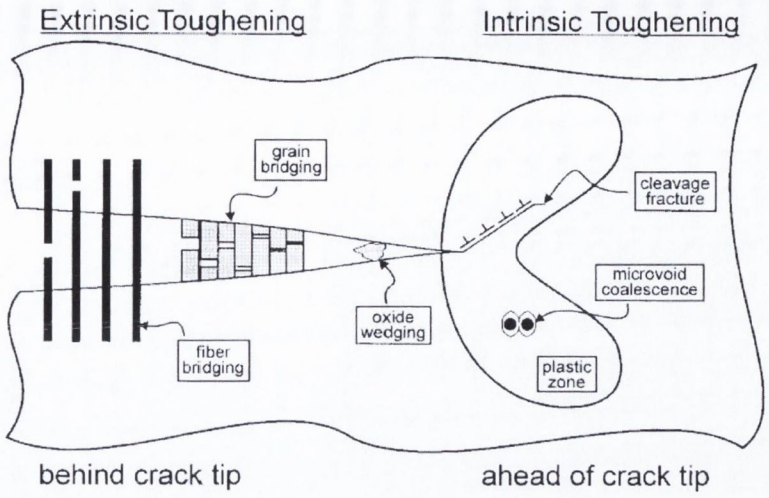

Fig. 2-19 Schematic of competition between intrinsic and extrinsic mechanisms (Ritchie, 1999)

An important toughening mechanism in fibre-reinforced composites is crack bridging by embedded fibres; other toughening mechanisms include interfacial debonding and frictional sliding associated with fibre pullout. The overall toughness may be affected by the strength of the interface (Bennett and Young, 1998).

2.7 Fracture Mechanics applied to Bone

The majority of this chapter has been dedicated to explain commonly used concepts in fracture mechanics. These methods are applied to gain more understanding of crack behaviour in general. In bone, cracks can be found *in vivo* and *in vitro*, in numbers varying approximately from 0.01 to 1 cracks/mm^2, depending on age, mineralisation and loading conditions (Taylor and Lee, 2003). It is therefore not surprising that fracture mechanics is a method that is extremely suitable to study how these cracks interact with a biological tissue like bone.

In order to know which of the previously described methods to apply, choices have to be made. The first obvious choice to make is a decision if the LEFM or the EPFM concepts should be used. Commonly the LEFM concept is applied to bone (Norman

et al., 1995; Tanabe *et al.*, 1998; Yeni *et al.*, 1998; Feng *et al.*, 2000; Yeni and Norman, 2000; Taylor, 2002). The problem is that the size of the plastic zone is not known and therefore the choice of this concept can not be validated (Akkus and Rimnac, 2001; Malik *et al.*, 2003). It is evident that the lack of knowledge concerning the fracture behaviour and especially plastic deformation within bone make researchers choose LEFM. This does not mean that such a method cannot be applied. The majority of cracks found in bone are generally relatively small ~100 μm, with crack densities ranging from 0.01 to 1 cracks / mm^2, making it plausible to assume that plastic deformation by individual cracks or due to interactions between cracks are unlikely. Robertson *et al.* (1978) theoretically estimated that the size of the plastic zone is about the thickness of lamellae (1-5 μm) using Westergaard's stress field analysis. The plastic zone size was calculated using equation 2-33.

$$r_{\max} = \frac{1}{2}\left(\frac{\sigma_c}{\sigma_y}\right)^2 a \qquad \textbf{Equation 2-33}$$

where a is the crack length, σ_y is the yield stress and σ_c is the gross fracture stress. Lakes *et al.* (1990) used a similar approach to estimate the size of the plastic zone using the Dugdale solution. Using a crack length of 1 mm, a yield stress of 100 MPa and an applied stress of 64 MPa, results in a plastic zone size of 0.25 mm. Since this size was less than the root radius of their machined specimens, the crack blunting effect due to plastic deformation was assumed to be minimal.

In order to gain more insight into the accumulation of microdamage, mechanical tests can be carried out. In these tests, bone specimens are subjected to cyclic fatigue at various stress ranges. By knowing the effective stress range and the number of cycles it took to cause failure, fatigue life predictions can be made, using S-N curves (see Fig. 2-20).

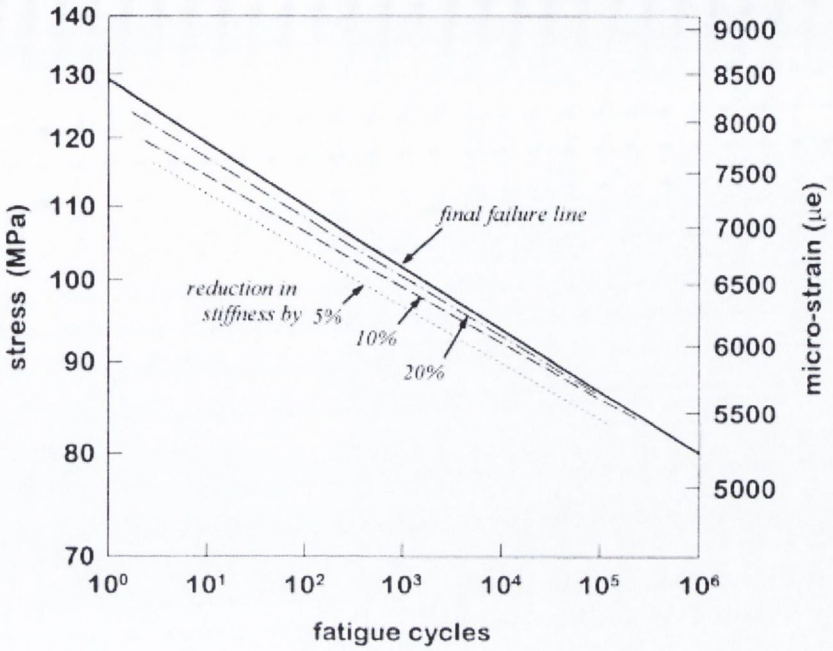

Fig. 2-20 S-N curve of human femoral bone (Zioupos *et al.*, 1996).

The fatigue life of a specimen depends on the number of cracks that develop at a certain stress level, but ultimately the worst crack will be the dominating factor. Typically this process can be subdivided in three progressive stages of failure. The first stage is characterised by the degradation of the stiffness of the material. In the second stage of fatigue, the rate of change in stiffness stabilizes to a constant level. The final, third phase is where catastrophic failure occurs (Tami *et al.*, 2003). In this first stage, damage accumulation requires existing cracks to propagate and new cracks to initiate. The ease by which this occurs depends on the fracture toughness of the material and has received a lot of attention in the literature.

Typically fracture toughness tests are carried out on coupons according to the ASTM[6] standard E399 (Norman *et al.*, 1995; Yeni *et al.*, 1997; Norman *et al.*, 1998; Tanabe *et al.*, 1998; Feng *et al.*, 2000; Yeni and Norman, 2000). This is a standard

[6] ASTM= American Society for Testing Materials

test method for plane-strain fracture toughness of materials. The shape of these specimens for mode I and Mode II testing can be seen in Fig. 2-21.

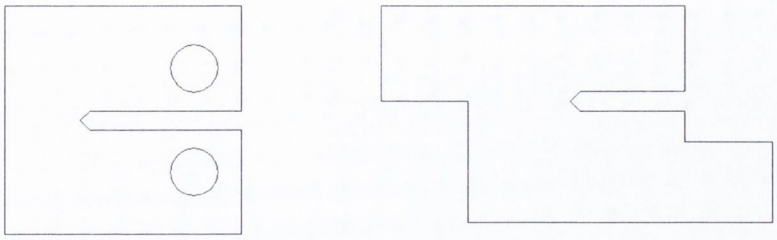

Fig. 2-21 Schematic of toughness testing specimens for mode I and II redrawn from Yeni and Norman (2000).

Studies on the fracture behaviour of bone are useful to gain an overall understanding of crack initiation and propagation. This may contribute to our ability to predict and reduce the risk of fractures associated with aging, incidents and repeated loading. However, the majority of research on bone's resistance to initiation and propagation has mainly focused on tensile loaded cracks (Norman *et al.*, 1995; Tanabe *et al.*, 1998; Akkus and Rimnac, 2001), e.g. mode I fracture. Long bones, which in reality are irregular in shape and have anisotropic material properties, are usually subjected to a combination of loads during daily physiological activities. Therefore cracks in bone will have a random orientation with respect to the loading axis of the bone, which is seldom in pure tension (Taylor *et al.*, 2003a). Clinical examples are transverse-, spiral- and impact-fracture to the lower extremities as shown in Fig. 2-22, which also indicate that a combination of fracture modes occurs.

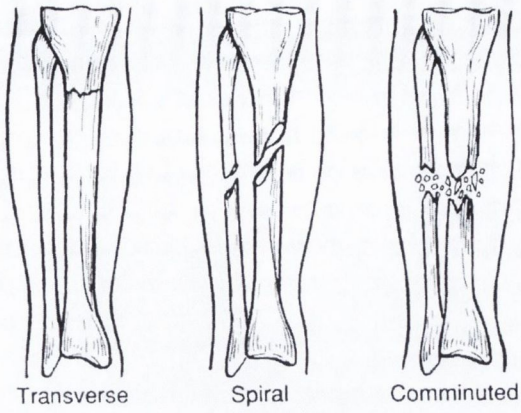

Fig. 2-22 Pattern of fracture (Dandy, 2003)

The fracture toughness may be tested at various sites, using various modes of failure, and having notches orientated transverse or perpendicular to the osteon direction. Commonly, the bones of the lower extremities are taken for these tests, examples are human tibia and femora (Yeni *et al.*, 1998), human femora (Akkus and Rimnac, 2001), bovine tibia (Norman *et al.*, 1995), bovine femora (Tanabe *et al.*, 1998; Feng *et al.*, 2000) and equine metacarpal (Malik *et al.*, 2003). Feng *et al.* (2000) investigated all three modes of failure in both directions, transverse and perpendicular to the osteon direction. Their results are shown in Table 2-1.

	Mode I	Mode II	Mode III
	K_{Ic} (MPa$\sqrt{m}$)	K_{IIc} (MPa$\sqrt{m}$)	K_{IIIc} (MPa$\sqrt{m}$)
Longitudinal fracture	3.0±0.24	6.3±1.2	6.5±0.9
Transverse fracture	6.0±0.41	12.5±1.7	10.5±1.3

Table 2-1 Fracture toughness of cortical bone (Feng *et al.*, 2000)

Their results show that K_c-values in both modes II and III are higher in longitudinal and transverse fracture than K_{Ic}. These results are consistent with the results by Norman et al (1996). According to Tanabe (1998), the critical initiation stress intensity value (K_c) decreases with an increasing loading rate, having an estimated minimum value of 0.2 MPa$\sqrt{m}$, and increases with an increasing load rate that is independent of the initial crack orientation.

Although significant differences might be found between different locations within bone, most analyses, assume that the microstructure is similar throughout the bone. However, Malik et al. (2003) found that the crack growth initiation toughness in equine metacarpal was significantly higher in the lateral region compared to the dorsal region. This might be influenced by the architecture of the bone, since there are significant differences in osteon density in equine bones in various regions (Mason *et al.*, 1995). Therefore, the influence of the microstructure needs to be considered in the analysis.

Yeni *et al.* (1998) found that the variation in composition of the bone can explain 35%-59% of the variation in fracture toughness. The parameters causing this variation has been suggested to depend on delamination of the material, which increases the fracture toughness (Ascenzi and Bonucci, 1967; Pope and Murphy, 1974; Simkin and Robin, 1974). Osteonal pullout could also be a crack arresting feature, which would indicate that a higher osteon density might be beneficial to prevent catastrophic failure. Malik *et al.* (2003) found in regions of stable slow crack growth, that osteonal pullout was present. All specimens that showed stable crack propagation, presented a rising *R*-curve prior to failure, i.e. an increase in the *K* needed to cause continuing crack growth. They observed that cracks appear to deflect into interstitial bone and eventually run parallel to the osteonal structure. This deflection of cracks might be one of the mechanisms in bone to absorb energy and therefore contribute to its toughness. Two good examples that have implemented this information in analytical fracture mechanics models are by Gou *et al.* (1998b) and Yeni and Fyhrie (2003).

From a microstructural and mechanical perspective, cortical bone shares several similarities with fibre-reinforced ceramics. The fibres are represented by the osteons, which support the matrix represented by the interstitial bone. At a more nanostructural level, the same applies to the collagen fibres embedded in the hydroxyapatite matrix. Gou *et al.* (Guo *et al.*, 1998a) found that cortical bone can

either encourage or slow down crack propagation in interstitial bone. This process is dominated by the modulus difference between the osteonal and interstitial bone. Using the stress intensity factor as a failure criterion, it could be shown that softer osteons tend to direct cracks in the interstitial lamellae toward the osteon, thereby increasing the likelihood of crack arresting mechanisms such as cement line debonding. This model might also explain why crack densities increase with aging. In older bones, osteons are more mineralised. If the osteon stiffness, due to mineralisation, exceeds the matrix stiffness, osteons lose their ability to attract or repel cracks.

Where osteons provide a toughening mechanism at a microstructural level, collagen fibres might do something similar at a nanostructural level. Yeni and Fyhrie (2003) made a rate-dependant model of fibres bridging the crack faces. Such a model allows investigation of the major toughening mechanism in bone e.g. strength, stiffness or microdamage itself. The choice of a rate dependant model is important since the overall behaviour of bone is load rate dependent. They concluded that the apparent yield strength of bone could be predicted directly from stiffness measurements of bone and depends on the failure strain of the collagen matrix.

Although these models are based on various assumptions and are highly idealized, they provide a method whereby various parameters can be assessed in a relatively short time. In other words, the crack orientation, fibre orientations, local anisotropic behaviour and impurities in the material are not taken into account. These models contribute to the general understanding of processes that happen in the bone. Taylor *et al.*(2003a) used the ratio of the effective tensile ($\Delta\sigma_t$) and compressive ($\Delta\sigma_c$) fatigue strength to calculate the crack orientation with respect to the longitudinal axis of the bone. Based on data from Caler and Carter (1989) , who found this ratio to be 1.16, an angle of 30.5° was calculated using:

$$\cos(\theta) = \Delta\sigma_t / \Delta\sigma_c = 1/1.16 \qquad \textbf{Equation 2-34}$$

Besides the ratio of tensile and compressive loading in bones, loss of stiffness has been used to estimate microcrack growth parameters. The loss of stiffness during fatigue testing is related to crack size and density. As cracks grow, elastic strain energy is released. Microcracks are typically 100 μm long, which implies that cracks of this length become non-propagating and new cracks will initiate and grow until this length is reached. Taylor (1998b) used changes in measured stiffness to make estimations of the value of K, crack length a, and the crack growth rate (da/dN). Based on the specimen length, cross sectional area, crack density and crack shape (assumed to be elliptical and constant) an expression was derived for the stress intensity factor K. Although this assumes that all cracks would have a similar shape, which is in reality not true, it provides a nice theoretical basis to predict microcrack growth using fracture mechanics.

Based on microcrack growth behaviour, a control mechanism for bone maintenance and remodelling was proposed by Taylor (1997). The balance between crack growth rates and the rate of repair is of great importance. As long as these two processes are in balance, the mechanical integrity of bone is secured. However, if crack propagation exceeds the repair rate, stress fracture or catastrophic failure might occur. Fig. 2-23 shows the model used.

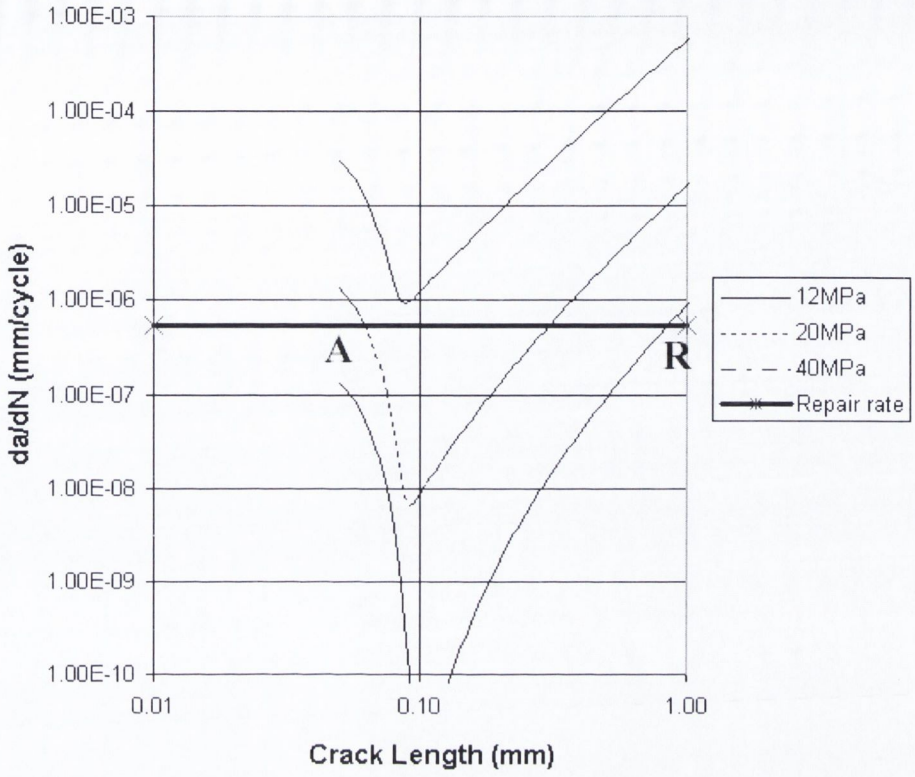

Fig. 2-23 Predicted crack growth rate with constant repair rate (Taylor, 1997)

- High stresses, causing crack growth rates which are always higher than the repair rate of bone, will cause stress fracture unless new bone is deposited on the surfaces.
- Intermediate stresses, which are stresses which will produce crack growth rates that will intersect with the repair line between points *A*, and *R*. Since a constant repair rate is assumed, which can mathematically be expressed as negative crack growth, any crack with a length between zero and *R* will be reduced to a crack length *A*.
- Low stresses, with crack length less than *R*, become dormant and will therefore become completely remodelled.

The results of this type of simulation produced crack lengths ranging form 42 μm at 15 MPa to 82 μm at 35 MPa, which are crack lengths commonly found in the literature at stress levels which are to be expected under normal loading conditions. This model shows that stability can occur between crack growth and the repair mechanism in bone using a constant repair rate, resulting in various crack lengths. Other models that have acknowledged that variations in local microstructure and loading condition produce various crack lengths have been described in the literature. Gou *et al.* (1994) describes a damage accumulation model in trabecular bone, combining finite element analysis and fracture mechanics. They achieve various crack lengths by using a random beta probability distribution. Using this type of analysis allows a wide range of mean crack lengths, with scatter, to be investigated. Other models that use a probability approach have been used to predict e.g. stress fractures in bone using a so called 'stressed volume concept' (Taylor, 1998a; Taylor *et al.*, 1999; Taylor and Kuiper, 2001). Since larger specimen sizes will have more defects and a larger number of weak regions from which cracks can initiate the probability of failure can be calculated using a Weibull analysis. These models (Taylor *et al.*, 2004) now take account of repair and deposition of new bone on the surface and could be valuable in predicting the risk of stress fracture based on the type of exercise and its intensity.

These models may be used to predict damage accumulation during activities, using various techniques either by using a probability approach or by incorporating crack growth rates, fracture mechanics, and microstructural features. However, they do not explain the underlying biological processes by which these cracks are detected. Examples of questions which still remain to be answered regarding microdamage in bone are:

- When does bone know to initiate bone remodelling?
- Is bone able to estimate the size of the crack?
- If so, by which means does it do so?
- How are the basic multi-cellular units (BMUs) directed to the damage site?

Chapter 3 A Theoretical Model of the Cellular Transducer

3.1 Introduction

It has been known for over forty years that bone, *in vivo*, contains small cracks, typically 100 μm long in the transverse direction (Frost, 1960; Burr and Stafford, 1990; Lee *et al.*, 1998; Muir *et al.*, 1999; Donahue *et al.*, 2000). These cracks are the visual manifestation of fatigue damage, caused by the cycles of stress that occur during running, walking and other daily activities. They have been the subject of considerable research, for two reasons. Firstly, there is evidence that cracks are detected and repaired by the body, through the action of BMUs (Basic Multicellular Units) (Frost, 1969; Martin *et al.*, 1998) in a process known as "remodelling". In cases where repair is not possible, or cannot act quickly enough, cracks grow to macroscopic lengths, causing stress fractures (Burr, 1997; Harmon, 2003; Iwamoto and Takeda, 2003; Sanderlin and Raspa, 2003).

Secondly, it has been suggested that these cracks act as a signal to regulate the process known as "bone adaptation", by which bone changes its geometry (e.g. cortical thickness) and other properties (e.g. cancellous bone density) in response to increases, or decreases, in applied stress levels (Bentolila *et al.*, 1998; Noble and Reeve, 2000). Adaptation is a very important subject for study because it emerges in various clinical conditions (e.g. disuse osteoporosis in humans and animals) and also because it affects the quality of bone in the vicinity of implants such as the hip joint arthroplasty, which may lead to aseptic loosening (Havelin *et al.*, 1995; Ang *et al.*, 1997; Bauer and Schils, 1999; Chambers *et al.*, 2001). It is evident both from clinical studies (Vico *et al.*, 1987; Kiratli *et al.*, 2000; Elmann-Larsen and Schmitt, 2003; Schneider *et al.*, 2003) and animal experiments (Rubin and Lanyon, 1985; van der

Meulen *et al.*, 1995; Trebacz, 2001; Allen and Bloomfield, 2003) that bones become thicker when loaded with cyclic stresses of high magnitude, and thinner if loaded at unusually low magnitudes. Evidence suggests that bone is able to detect the amount of strain which it is experiencing, and to initiate appropriate responses. However, currently it is not known how this is achieved. Neither the mechanism of strain detection (the 'cellular transducer') nor the process by which decisions are made to produce the result (e.g. repair or deposition) have not been discovered.

Research activities in this field tend to be divided into two types. On one hand, biologists have studied the changes, which occur at the cellular level when bone cells are exposed to cyclic strains. Typically, experiments are conducted *in vitro*; by culturing cells on a substrate, which can be stretched to generate cyclic strains. Various outcomes are measured which may be linked to the adaptation process, including up- or down-regulation of gene expression. For example Mikuni-Takagaki *et al.*(1996) reported that following stretching, elevated levels of two early response genes, cyclooxygenase 2 (COX-2) and c-fos, were recorded as well as elevated levels of osteocalcin and IGF-I. Furthermore, these studies report that significant responses occur only if the loading regimes are outside the physiological range, i.e. more than 3000 με at physiological frequencies (Burger and Klein-Nulend, 1999; Stanford and Brand, 1999; Brown, 2000). In order to understand the amount of strain to which bones are subjected during various activities, strain gauges can be attached to bones in animals and humans. During normal activities, bones experience between –1500 and 1000 με (Yoshikawa *et al.*, 1994; Adams *et al.*, 1997; Judex *et al.*, 1997; Fritton *et al.*, 2000). Higher stains (>1400-2000 με) on the periosteal surface have been shown to result in new bone formation (McLeod and Rubin, 1992; Turner *et al.*, 1994; McLeod *et al.*, 1998). Peak physical activities are typically in the range of 2000-3000 με (Rubin, 1984; Rubin and Lanyon, 1984; Cullen *et al.*, 2001).

On the other hand, many researchers have developed computer simulations of adaptation, which are capable of predicting changes in bone density and thickness, usually working from finite element (FE) analyses to estimate stress/strain levels.

These programs generally do not consider how the adaptation signal is generated, but assume that it is related to one or more chosen mechanical parameters, such as stress, strain or strain-energy density (Hart *et al.*, 1984a; Carter, 1987; Carter *et al.*, 1987; Huiskes *et al.*, 1987; Beaupre *et al.*, 1990).

Other theoretical models have been developed based on the idea that bone adaptation is controlled by the level of fatigue damage (Prendergast and Taylor, 1994; Martin, 1995; Levenston and Carter, 1998; Doblare and Garcia, 2001; Garcia *et al.*, 2001; Ramtani and Zidi, 2001). This idea is an attractive one because the level of damage provides a direct measure of the potential danger of failure. If the damage, and particularly its rate of increase, is greater than can be repaired, then failure will occur unless adaptation is initiated to reduce the stress level. However, 'damage-stimulated remodelling and adaptation' suffers from a number of problems. These models are generally based on continuum damage mechanics (CDM). CDM considers the presence and effects of a large number of microdefects distributed widely and randomly throughout the matrix (McDowell, 1997), which is useful in studying the effect of microdamage on a whole bone, but does not take into account the underlying biological mechanism. Furthermore, there is no knowledge of the means by which bone detects damage and 'decides' to initiate repair or adaptation, i.e. what are the threshold values causing stimuli to trigger a response?

A number of other workers have considered this biological mechanism, but to date the experimental evidence is very limited. For example, Schaffler and Verborgt (2000) examined osteocytes located near cracks. They found evidence of cells undergoing apoptosis (programmed cell death) in regions where microdamage was present. According to Noble and Reeve (2000), osteocyte death through apoptosis is most likely at very high and very low strain levels. Since the strain fields surrounding cracks would produce high strains near the crack tip and low strains in other regions, it was hypothesised that microdamage could be the main cause. In a later experiment (Noble *et al.*, 2003), loading regimes of 8000 με were required to cause intra-cortical remodelling, which is normally not found in rats. Their experiments indicated that in

regions where microdamage was present, osteocyte apoptosis occurred and that osteocyte apoptosis preceded osteoclastic activity. However, it only provides more circumstantial evidence that microdamage and bone remodelling are linked and does not explain the mechanism by which the cells sense microdamage. Other researchers (Frost, 1987; Martin, 2000) suggested that microdamage might interfere with the signalling process between adjacent cells. Osteocytes are assumed to be in constant contact with the surface of the bone, therefore the presence of a crack might inhibit this signal (Marotti *et al.*, 1992; Martin, 2000). This suggests that a minimum critical number of osteocytes are required for an operational network that ensures effective repair of microdamage. This would be consistent with data found by Vashishth *et al.* (2000b) and, Frank *et al.* (2002) which show that the osteocyte lacunar density decreases exponentially with age whereas crack density increases after the age of 40 (Burr, 2002a).

3.1.1 Aims and objectives

The main objective of this chapter is to use fracture mechanics to investigate which mechanisms might be present, and provide insight to why microdamage causes bone adaptation. The use of fracture mechanics allows different mechanisms to be investigated for individual cracks. These mechanisms could be split into destructive and non-destructive stimuli. Whilst loaded, an individual crack might locally generate strains that are higher than the failure strain of the osteocytes. If cell rupture would follow from such an event, apoptosis of adjacent cells within the network is likely to occur, which has been shown to happen in cartilage (Tew *et al.*, 2000). It is therefore possible that such a mechanism is present in bone, acting as a cellular transducer, stimulating bone adaptation.

In order to transduce this signal, various researchers have proposed that osteocytes and their processes orchestrate the bone-tissue modifications required (Parfitt, 1984; Frost, 1987; Cowin *et al.*, 1991; Burger and Klein-Nulend, 1999). Due to the large numbers of osteocytes (12,000 to 20,000 ostoecytes/mm^3 (Martin and Burr, 1989),

with up to 60 processes per osteocyte (Cowin, 2002)), and their random distribution throughout the matrix, it is likely that they are subjected to microdamage. Therefore, cell-processes bridging the crack faces could be stretched, subjecting them to strain levels higher than the failure strain of the material. Alternatively, cracks orientated at an angle with respect to the loading direction, will be subjected to tensile, compressive and shear loads. Due to repetitive loading, cell-processes crossing the crack faces might lose their ability to communicate with neighbouring osteocytes, interfering with the inhibitory signal by the cellular network, generating a signal to initiate repair.

The aim of this chapter is to investigate the possible biological mechanism triggering the modelling and remodelling process due to damage accumulation using a theoretical model. Existing theoretical models based on damage tend not to consider the nature of the biological process which links microcracks to osteocytes. Martin (1995), for example, defines the remodelling stimulus as the crack density times the mean crack length in a given volume. Improvements could be made to these models if the three-dimensional shape of the crack is taken into account. Furthermore, there is little knowledge of the nature of the cellular transducer. Therefore the following questions were set:

- Can the three dimensional crack shape be predicted?
- How can osteocytes detect the presence of cracks?
- How can they decide whether a crack is dangerous enough to initiate repair?
- How can they decide whether the level of damage is high enough to require adaptation, i.e. deposition of bone on the surface?

3.2 Crack growth and shape development model

Various researchers have observed a difference in microcrack propagation behaviour, compared to macrocracks in the same material (Laird, 1967; Tanaka *et al.*, 1986; Taylor, 1986; Sciti *et al.*, 2002). At short lengths, crack behaviour is dominated by microstructural features such as grain boundaries which act as barriers arresting or temporarily halting crack growth (Tanaka and Akiniwa, 1988; Aniniwa *et al.*, 1996; Chapetti *et al.*, 2001). The point of transition between microcracks and macrocracks is of great importance to bone. Once cracks have obtained lengths which exceed the microstructural boundaries, crack growth rates might exceed repair rates, jeopardising the mechanical integrity of the bone. Microcracks in bone are known to be affected by the microstructure. In regions where osteon populations are high, a greater fatigue life is expected (Evans and Riolo, 1970). A study by Corondan and Haworth (1986) showed that regions where osteons are less numerous could be related to fracture sites. These findings support the idea that crack propagation is inhibited by increasing osteon numbers and support the theory that the combination of osteons and cement lines is able to arrest or divert cracks (Burr *et al.*, 1988). This interaction between microstructure and crack propagation was also shown by Zioupos and Currey (1994), who suggested that crack growth directions were mainly influenced by the orientation of the lamellae. Various authors have shown experimentally that the majority of these cracks develop in the interstitial tissue and become dormant at the osteonal boundaries (Schaffler *et al.*, 1995b; Norman and Wang, 1997; Boyce *et al.*, 1998; O'Brien *et al.*, 2002). Using this information from the literature, the following model was set up to predict crack growth and shape development (see Fig. 3-1).

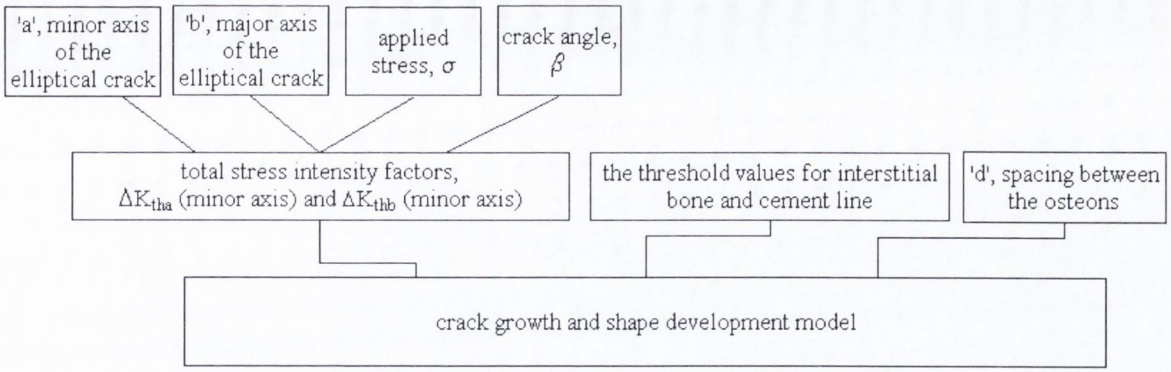

Fig. 3-1 Input variables for crack growth and shape development model

The three input parameters are the total stress intensity factor, the threshold values (interstitial bone and cement lines) and the spacing between the osteons. These parameters will be individually discussed in the next section.

3.2.1 The input parameters

The total stress intensity factor:

In order to calculate the stress intensity factor, four input variables are required (see Fig. 3-1). These are the minor (*a*) and major (*b*) axis of the elliptical crack (see Fig. 3-2), the applied stress and the angle of the crack with respect to the loading direction. The choice for the elliptical crack shape is based on work carried out by O'Brien *et al.* (2000). In their study longitudinal sections were taken from human ribs, containing *in vivo* microcracks which were bulk-stained with basic fuchsin. Two different computer-based methods were used to reconstruct individual cracks; the first was based on a serial sectioning technique using fluorescent markers, the second technique was based on laser scanning confocal microscopy. The size and shape of these nine microcracks (see Table 3-3) were found to be similar using both techniques, showing that *in vivo* microcracks are approximately elliptical in shape. Mean crack lengths were found to be 97 μm in the transverse direction and 404 μm in the longitudinal direction. These crack lengths were consistent with findings by other researchers (Burr and Stafford, 1990; Burr and Martin, 1993; Mori and Burr,

1993; Lee *et al.*, 1998). The total stress intensity factors for the minor (a) and major axis (b) can be calculated as shown in Table 3-1:

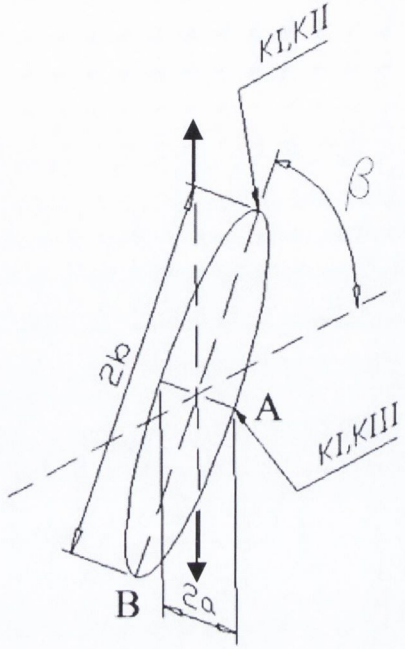

Fig. 3-2 Geometry and orientation of an elliptical crack in cortical bone.

For the minor axis a	For the major axis b
$K_{Ia} = \frac{\sigma * \sqrt{\pi * a}}{E(k)} \cos^2(\beta)$	$K_{Ib} = \frac{\sigma * \sqrt{\pi * a} * (a/b)}{E(k)} \cos^2(\beta)$
$K_{IIIa} = \frac{\sigma * \sqrt{\pi * a}}{E(k)} \cos(\beta)\sin(\beta)$	$K_{IIb} = \frac{\sigma * \sqrt{\pi * a} * (a/b)}{E(k)} \cos(\beta)\sin(\beta)$
with $E(k) = \int_0^{\frac{\pi}{2}} \left(1 - \left(1 - k^2\right) * \sin^2\phi\right)^{\frac{1}{2}} d\phi$, where k is the ratio a/b	
$K_{a,total} = \sqrt{K_{Ia}^2 + K_{IIIa}^2}$	$K_{b,total} = \sqrt{K_{Ib}^2 + K_{IIb}^2}$

Table 3-1 Total stress intensity factor calculations for minor *a* and major *b* axis of an ellipse (Pickard, 1985)

The crack angle:

The angle (β) of the crack is defined as the angle between the crack and the axis perpendicular to the loading direction (see Fig. 3-2), which has been related to the orientation of the lamellae (Zioupos and Currey, 1994) or osteon direction. This angle was estimated to be 10 and 20 degrees to the normal loading direction (Cohen and Harris, 1958; Martin and Burr, 1989), e.g. β ranges from 70 to 80 degrees. Taylor and Lee (1998) made theoretical estimates from two-dimensional sections that this angle would be similar to the osteonal direction (~70°). In a later paper Taylor et al.(2003b) used the ratio between the tensile and compressive fatigue strength to predict the crack angle β, which was estimated to be 59.5 degrees.

The applied stress:

Although cracks are commonly found *in vivo*, the loading regimes to which these cracks have been subjected during crack initiation and propagation remain unknown. Strain gauge measurements show that bone experiences between 1000 and 2000 με (McLeod and Rubin, 1992; Turner *et al.*, 1994; Yoshikawa *et al.*, 1994; Judex *et al.*, 1997; Fritton *et al.*, 2000). Since the exact strain levels in human ribs are not known, it is assumed to be around 2000 με, which would be approximately 40 MPa.

Osteon spacing:

The osteon spacing ($2d$) is defined as the distance between osteons (cement line to cement line). Various authors have suggested that osteons can arrest or divert cracks similar to the grain boundaries in metals. Experimental evidence showed that cracks which become dormant at the osteonal boundaries have a typical length of 100 μm. The distance 'd' has to approximate to this value as a consequence of these findings (Schaffler *et al.*, 1995b; Norman and Wang, 1997; Boyce *et al.*, 1998; O'Brien *et al.*, 2002).

The input data for the theoretical model discussed above were taken from clinical measurements, observations made on histological sections and well established

methods in fracture mechanics. The only missing data are the threshold values for various features in cortical bone.

3.2.1.1 Estimating the threshold values

Once bone growth has ceased, modifications to the bone shape barely occur in healthy individuals. However, the existing bone is constantly renewed by osteoclast and osteoblast activity. As a result, variations in microstructure and mineralization levels occur. Therefore, within a microstructural region of bone, sections of old and new bone can be found which can be highly or less mineralised. Since crack initiation is predominantly concentrated in the older, higher mineralized regions of bone, whereas crack arrest mainly occurs near the less mineralized cement lines, variations in material properties are present. As a result, crack growth threshold values for the cement lines ($\Delta K_{th,\ cement\ line}$), intra-osteonal[7] bone ($\Delta K_{th,\ intra\text{-}osteonal}$), and the interstitial[8] bone ($\Delta K_{th,\ interstitial}$) differ, as shown in Fig. 3-3.

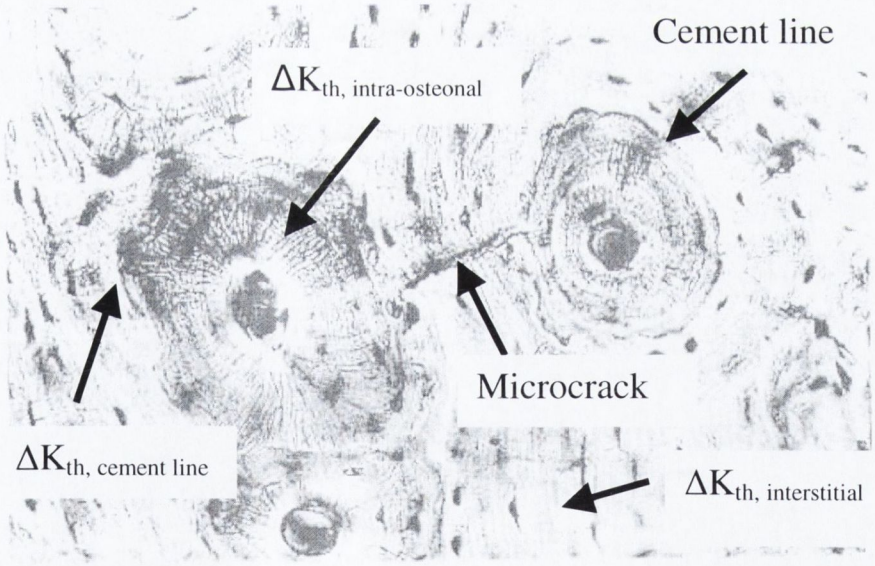

Fig. 3-3 Microcracks and cortical bone regions (Martin *et al.*, 1998)

[7] Bone found within the osteons enclosed by the cementline
[8] Bone found outside the osteons e.g. the remnants of old primairy bone

In an attempt to find the threshold values for the interstitial bone ($\Delta K_{th,\ interstitial}$) and cement lines ($\Delta K_{th,\ cement\ line}$) the elliptical cracks found by O'Brien (2000) were used. It is assumed that crack growth will only occur if the stress intensity factor is higher than the threshold value of the material. Table 3-2 shows the calculated stress intensity factors for all cracks found by O'Brien (2000), using an angle of 70° and a stress of 40 MPa.

Crack no.	Transverse length ($2a$), (μm)	Longitudinal length ($2b$), (μm)	Ka_{tot}, MPa√m	Kb_{tot}, MPa√m	Ratio (b/a)
1	79	559	0.176	0.066	7.07
2	83	553	0.179	0.069	6.66
3	96	543	0.190	0.08	5.65
4	111	482	0.198	0.095	4.34
5	69	459	0.163	0.063	6.65
6	181	338	0.203	0.148	1.86
7	120	253	0.173	0.119	2.11
8	56	242	0.140	0.068	4.32
9	75	206	0.148	0.089	2.74
(Average)	97	404			4.16

Table 3-2 Calculated stress intensity values for the nine cracks found by O'Brien (2000)

These values were calculated to get an initial indication of an order of magnitude for the stress intensity factors for elliptical cracks during normal activities. The stress intensity values calculated ranged from 0.140 MPa√m to 0.203 MPa√m for the minor axis ($2a$) of the ellipse and 0.063 MPa√m to 0.148 MPa√m for the major axis of the ellipse ($2b$). Cracks 6 and 7 (Table 3-2) have a relatively small axis ratio, but they have a very large transverse length, resulting in a very high stress intensity factor. If these are eliminated from the analysis, the stress intensity factors are almost the same (S.D. < 0.02) for all found cracks in both directions. For crack growth to have taken place, the threshold value for the cement lines (transverse direction) must be higher than the Ka_{tot} of the biggest crack, assuming that none of these cracks have broken through the cement line. Furthermore, the threshold value for the interstitial bone must be lower than the lowest value for these cracks in the longitudinal direction.

3.2.2 Predicting crack shapes

In this section various initial threshold values will be estimated, which will then be used as input data for a computational model of crack growth and shape development in cortical bone. In order to investigate if the values for the threshold values and crack angles could be used to predict the 9 cracks found by O'Brien *et al.* (2000), a computer program was written in Fortran 90 (Visual Fortran Professional, edition 6.1, Compaq, USA).

The variable input values for the model were:

- The threshold value for cement lines was taken as 0.23 MPa$\sqrt{m}$ which is slightly higher than the highest value calculated (see Table 3-2, Ka_{tot}) to prevent computational problems with crack number six.
- A range of values was used for the interstitial bone threshold (0.06, 0.065, 0.07 and 0.075 MPa$\sqrt{m}$), to investigate the effect of this parameter.
- Crack growth directions, reported in the literature indicate that crack angles are similar to the osteonal direction. This is approximately 10 to 30 degrees to the loading direction, therefore following crack angles were considered (β = 60°, 65°, 70°, and 75°).
- A stress of 40 MPa was taken for all models, which is assumed to be the physiological stress occurring in human ribs.

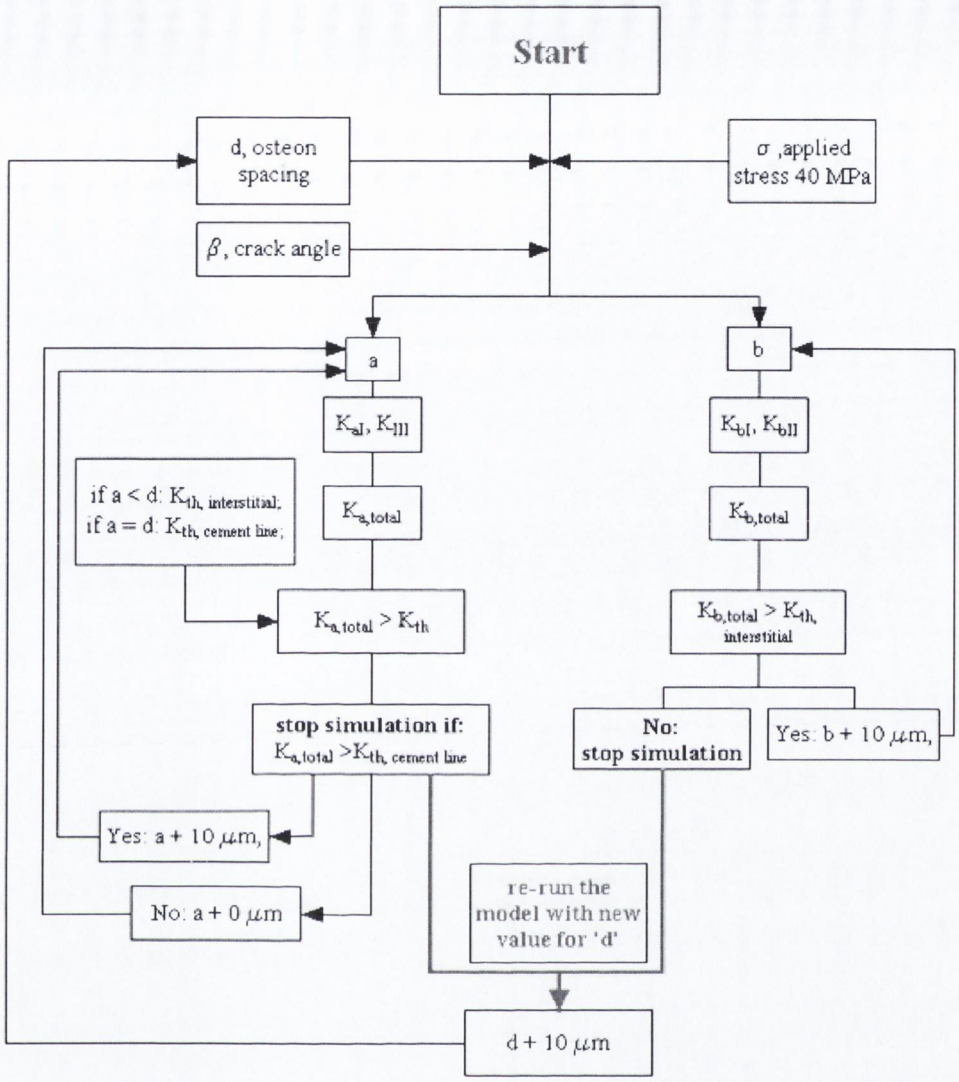

Fig. 3-4 Flow chart used for the computer model (variables crack angle, osteon spacing and threshold values).

The computer program (see also Fig. 3-4) starts by assuming that the initial crack shape is circular ($a = b$). The program calculates the total stress intensity factors for the transverse (a) and the longitudinal axes (b). If the K-value is higher than the threshold, the program will add 10 μm to both axes. This process will continue until the K-value is less than the threshold for the interstitial bone, since most cracks are known to initiate here. For the transverse axes, there is an exception to this process. Since cracks are known to stop at the cement lines of the osteon (growth in the transverse direction), the threshold changes when the length of the transverse axis is

equal to the distance between two osteons (*2d*). When this length is reached, the threshold value changes from the interstitial to the cement line threshold value. The effect is that the crack changes shape, becoming more elliptical (Fig. 3-5).

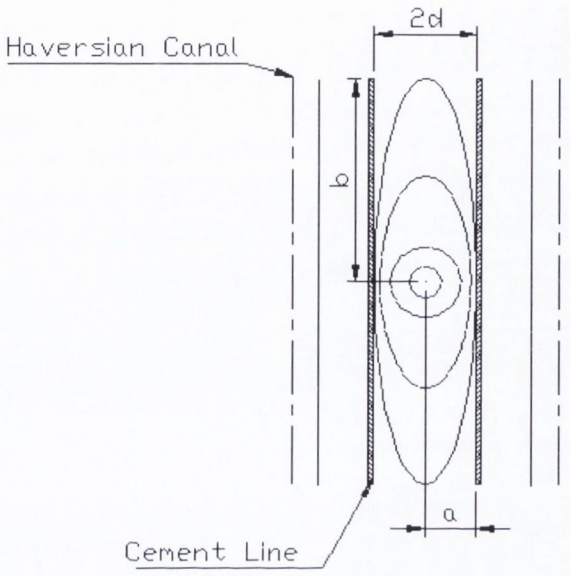

Fig. 3-5 Shape development for a crack trapped between two osteons.

Provided that the stress intensity factor at the longitudinal crack-tip has not reached the threshold value, then the crack will continue to become more elongated. The program stops if the calculated values meet the following requirements:

- The stress intensity factor at the crack-tip of the longitudinal axis is equal to, or less than the threshold value of the interstitial bone, assuming that $K_{b,\ total} > K_{th,\ interstitial}$ for crack growth to take place.
- The stress intensity factor in the transverse axis becomes higher than the specified threshold value of the cement lines. When the computer model predicts that the crack would break through the cement line, the threshold value in the transverse direction becomes higher than the threshold. It is not of great importance what happens beyond this point; it presumably meets a second boundary.

One interesting observation that was made during the analysis of the model was that as the crack changes its shape with a = constant, with increasing b, ΔK decreases in the b dimension and increases in the a dimension (Fig. 3-6).

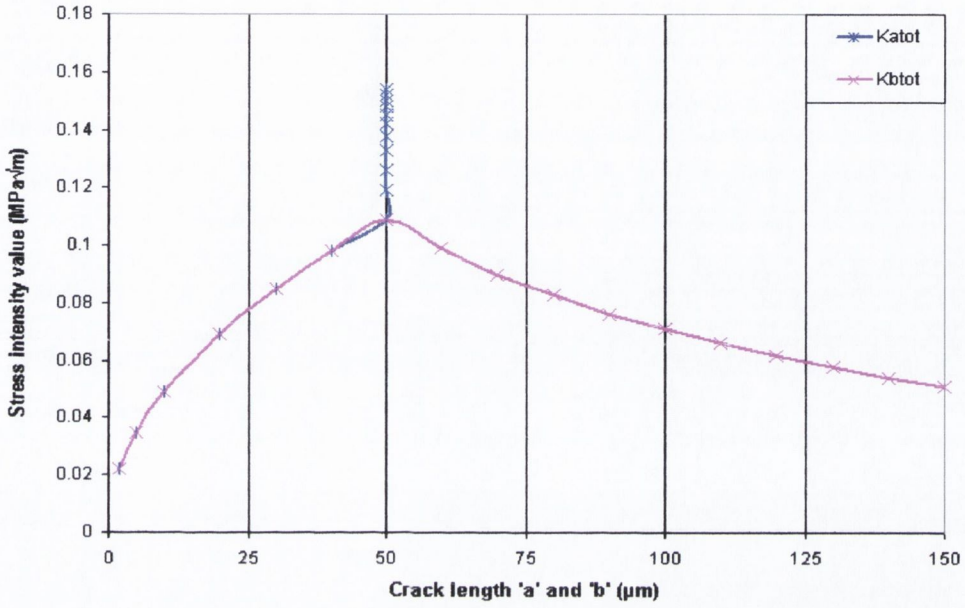

Fig. 3-6 Change in stress intensity factor due to a change in crack shape

As a result of this effect, the crack may either stop (at b) or break out (at a). Fig. 3-7 shows the results of the simulations (solid lines). The dots in the same figure are the crack shapes found by O'Brien *et al.* (2000).

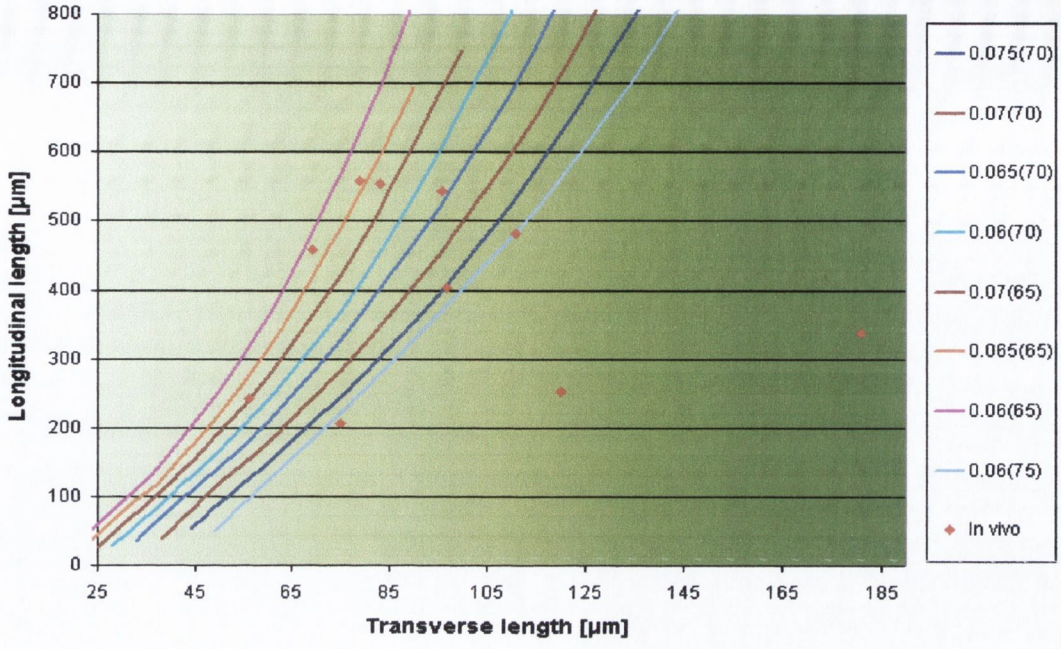

Fig. 3-7 Transverse length versus longitudinal length. Solid lines represent predicted threshold values at various angles, red dots are experimental data form O'Brien *et al.* (2000)

From the calculated results (see Fig. 3-7) estimations can be made as to which calculated threshold and angle best fits the cracks identified by O'Brien (2000). The results are shown in Table 3-3.

Crack no.	Crack width (*2b*) µm	Crack length (*2a*) µm	Ratio (*b/a*)	Best prediction: threshold (angle), (see also Fig. 3-7)
1	79	559	7.07	0.065(65)
2	83	553	6.66	0.065(65) / 0.07(65)
3	96	543	5.65	0.065(70)
4	111	482	4.34	0.06(75)
5	69	459	6.65	0.06(65)
6	181	338	1.86	Breaks out
7	120	253	2.11	Breaks out
8	56	242	4.32	0.07(65)
9	75	206	2.74	0.06(75)
Average	97	404	4.16	0.075(70)

Table 3-3 Experimental data from O'Brien *et al.* (2000) and calculated results

Good predictions could be made using thresholds for the interstitial bone ranging between the 0.065 and 0.075 MPa$\sqrt{m}$ and an angle (β) between 65 and 75 degrees (Table 3-3) except for cracks 6 & 7. It suggests that these two cracks have broken out, growing beyond the cement line, and no predictions could be made for these cracks. With exception of these two crack, all crack fall in a very narrow range for both threshold values and crack angles.

In fact if various other stress levels or angles would be used an increasing error in predicting the crack shape occurs. The optimal predictions occur at approximately 40 MPa and an angle of 70 degrees as shown in Fig. 3-8.

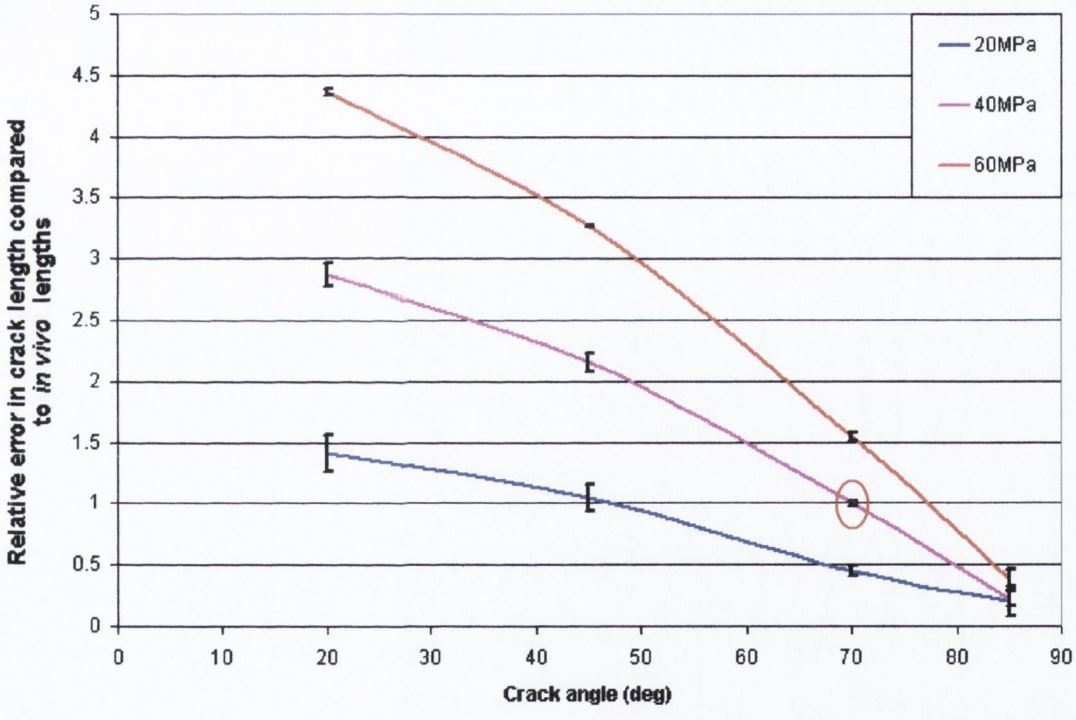

Fig. 3-8 Sensitivity analysis for different stress levels and varying crack angles

In the model described above, the crack stays circular until it meets the cement lines. However, the model takes no account of the fact that crack growth rates might vary in the two main directions. Previous work by Taylor (1997), used an equation to

predict crack growth in bone, based on a modification of Paris law (Paris and Erdogan, 1963). These equations can be formulated as:

$$\frac{da}{dN} = C(\Delta K - \Delta K_{tha})^n + C'\Delta K^{n'}\left[\frac{(d_1 - a)}{d_1}\right]^m \qquad \textbf{Equation 3-1}$$

$$\frac{db}{dN} = C(\Delta K - \Delta K_{thb})^n + C'\Delta K^{n'}\left[\frac{(d_2 - b)}{d_2}\right]^m \qquad \textbf{Equation 3-2}$$

Here the parameters a and b are the crack lengths in the transverse and longitudinal directions and d_1 and d_2 are the half-spacing between the osteons. The values used here were ΔK_{tha}= 0.23 MPa$\sqrt{m}$, ΔK_{thb}= 0.07 MPa$\sqrt{m}$ (as described above); the constants n=n'= 4.5; m= 5; C= 1.3x10^{-5} mm/cycle and C'= 0.013 mm/cycle were taken from previous work by Taylor and Prendergast (1997).

The model described in the previous paragraph, was expanded by incorporating the crack growth equations. Simulations were run until the cracks were breaking through the cement lines or had stopped growing. Although these simulations depend on various assumptions, they were very successful in predicting the *in vivo* crack shapes (Fig. 3-9).

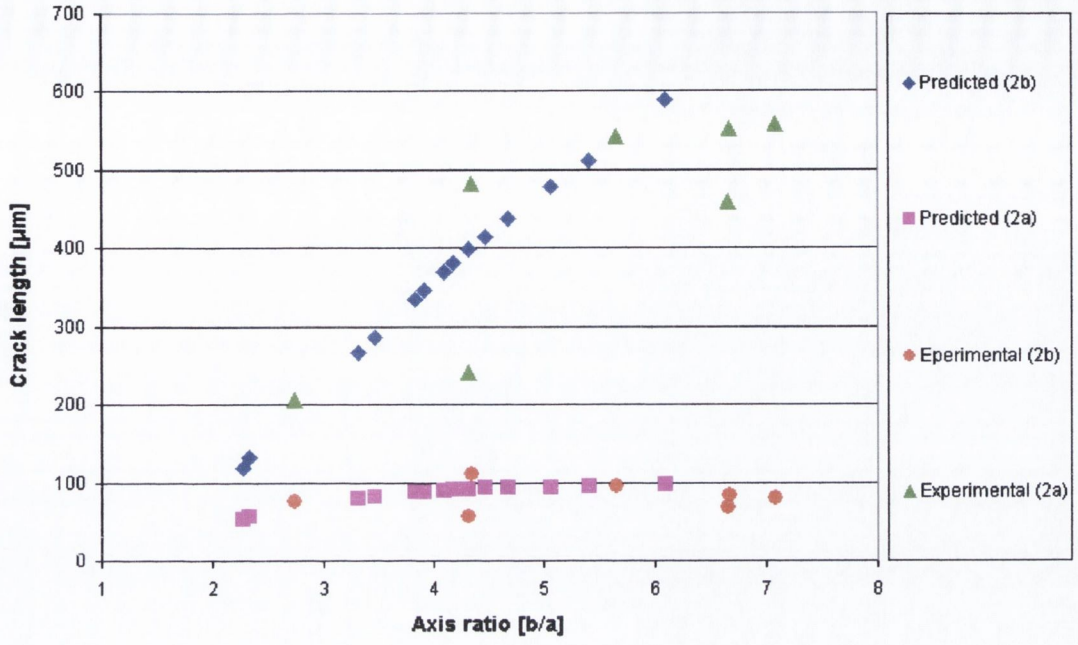

Fig. 3-9 Experimental data (O'Brien (2000)) versus predicted crack lengths and shapes.

This model shows that useful insights can be gained into the behaviour of cracks in bone using a fracture mechanics analysis of the type which is commonly applied to fatigue cracks in other materials. It can be used to help to establish crack sizes, shapes and orientations for typical cracks which could be used with confidence in the simulations described below.

3.3 Establishing the rules for bone repair and adaptation

When making predictions, it is important to have something to predict. Unfortunately, there is a lack of precise experimental data in this field, making it difficult, if not impossible, to test and compare different theoretical models. Animal experiments and clinical measurements have established beyond doubt that microcracks can be repaired and that bones become thicker as a result of increased loads and/or increased cycles of load. Computer simulations are able to predict these qualitative trends, but precise quantification is not possible. Based on data from the

literature and common sense, simple rules for the behaviour of bone will be proposed in the following paragraphs. In what follows, a normal physiological stress of 40 MPa is assumed, which is typical of the stresses attained during strenuous daily activities such as running. This is equivalent to a strain of 2300 με in a bone of typical elastic modulus E= 17.4 GPa (Martin et al., 1998).

3.3.1 Crack lengths related to repair and adaptation

As noted above, cracks typically attain lengths up to $2a$=100 μm (in the transverse direction) *in vivo*, so clearly they must either become dormant at this length or, if they continue to grow, they must be removed. Therefore 100 μm was set as a limit for repair: cracks above this length, growing in material loaded at the physiological stress, should emit a repair signal which will initiate a BMU. Cracks which are significantly smaller, say 30 μm (thus having a total area which is an order of magnitude less) are proposed not to give rise to a repair signal. Neither will a crack of length 100 μm growing in a bone which is experiencing a lower-than-normal stress of 10 MPa (which would represent a person with a very sedentary lifestyle). At the other extreme, cracks of length 300 μm (in the transverse direction) are proposed to be so large that repair alone would be inadequate, requiring the deposition of bone on the surface in order to reduce the local stresses. The reason being that a crack of this length will be growing much faster than a 100 μm crack: so fast that it will reach a length sufficient to cause a stress fracture in a very short time. Crack growth accelerates very rapidly because the rate of crack propagation (da/dN) is a strong function of K: Wright and Hayes (1976a) showed that, for long cracks, da/dN increases as $K^{4.5}$, which would imply that the 300 μm crack will grow about 10 times faster than the 100 μm crack. However, Taylor (1997) showed that, for short cracks, these differences are even greater: a factor of more than 100 can be expected. Another reason that a 300 μm crack would be very dangerous is that it is larger than the diameter of a BMU (typically 200 μm) so it will be impossible for a single BMU to repair it. Fundamental to this approach is the idea that the bone can fail due to the actions of a *single* crack, which is a common concept in the analysis of fatigue in

engineering materials. It is important to detect and measure the worst (i.e. largest, fastest-growing) crack, in order to establish whether failure will occur. The only exception to this rule is when failure occurs by the interaction of many cracks, but this is not the case for bone because the *in vivo* crack density is not high enough for these interactions to occur (typically 0.01-1 cracks/mm^2). Finally, a crack of the normal length, 100 μm, should stimulate bone deposition if the stress level is abnormally high, say about 60 MPa, which is the maximum value recorded (Milgrom *et al.*, 2002) *in vivo* (equivalent to 3450με).

3.4 The source of the signal

Two alternative methods were considered by which cracks might be detected by cells: (a) by rupturing of the cells themselves, due to high local strains, and; (b) by the cells' ability to measure strain.

3.4.1 Rupturing of Cells

If the presence of a crack can cause rupture of osteocytes or their processes, then the split cells will release many chemical agents into the surroundings, any one of which could act as a signal. There are two ways in which cells may be ruptured. Firstly, cells immediately ahead of the crack tip may experience a strain (ε) which is sufficiently high to rupture them; secondly, the relative displacements of the crack faces may be sufficient to rupture cellular processes: the long, thin extensions of the cell which link one cell to another, via gap junctions. Some of these processes will pass across the crack faces: Fig. 3-10 shows schematically how a process could be ruptured.

3.4.1.1 Failure criteria and material strength

No data could be found on the rupture strengths of osteocytes; therefore it is assumed that they behave in a manner similar to other soft-tissue materials (e.g. skin, cartilage, blood vessels) which have failure strains of the order of 0.5-1.0. However, in this study the fatigue strength of the material is of importance, i.e. the strain at which rupture occurs after a large number of cycles. Unfortunately, there have been very few studies of the fatigue strengths of soft tissues. The only detailed study has been the work of Ker et al. and co-workers (2000) who carried out tests on tendons. They showed that the stress needed to cause failure after a large number of cycles (10^5) was approximately 5 times smaller than the stress needed for instantaneous failure. Assuming the same applies to osteocytes gives us an estimated strain to failure of $\varepsilon_f = 0.15$.

Cell processes have a typical length L= 40 μm and diameter D= 0.2 μm. For a crack oriented at an angle β to the stress axis, the total displacement, 2δ, can be divided into a tensile separation 2δT and a shear displacement $2\delta S$ (see Fig. 3-10). Under compressive loading, the crack faces remain together and experience only the shear displacement. It was assumed that the process would rupture if $2\delta S > D$, causing it to be cut by the surrounding hard tissue. For tensile loading rupture might occur if 2δS is large enough whilst $2\delta T$ remains small. The assumed failure criterion was 2δS>D whilst $2\delta T < D$. Alternatively, rupture might occur if the failure strain was reached along the entire length of the process, thus $\varepsilon_f = 2\delta/L$. However, it was calculated that this would not occur in practice. Even under a 'worst case' scenario with a long crack ($2a$ = 300 μm) and a high applied stress (80MPa), the calculated strain was only 0.0005, much less than the failure strain. This model ignores the fact that the processes are attached to the walls of the canaliculi by fibres, which would tend to increase local strains, but probably not be sufficient to reach the failure strain. Thus, in both compressive and tensile loading, the proposed mode of failure is cutting of the cell process by the shearing motion between crack faces.

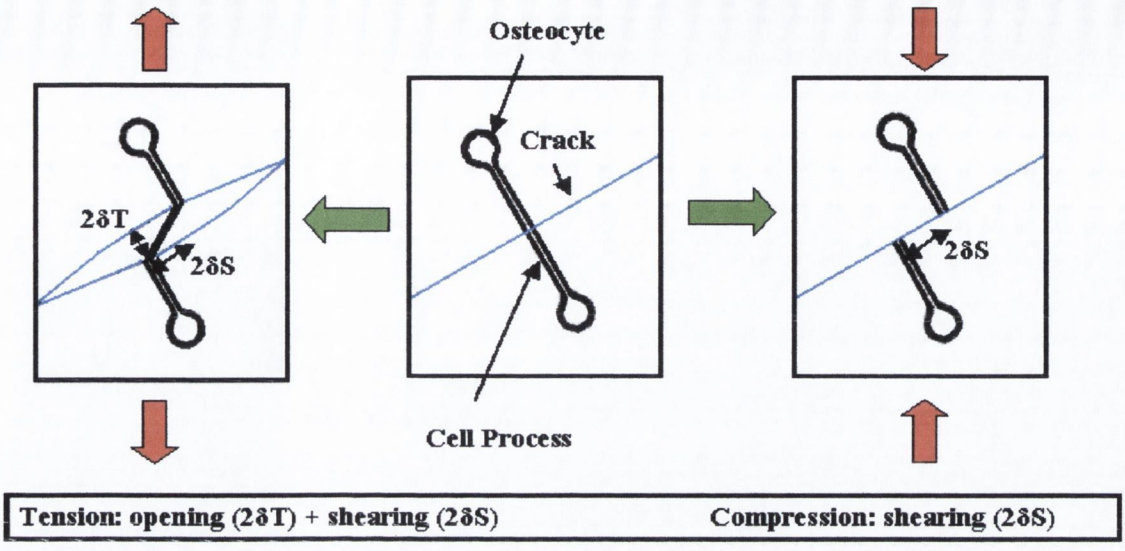

Fig. 3-10 Cell processes spanning a crack subjected to tensile and compressive loading.

3.4.1.2 Estimating crack-face displacements.

No data could be found in the literature for estimating crack-face displacements in the three-dimensional case of an elliptical crack, oriented at an angle to the loading axis. There is a well-known solution for a two dimensional crack, originally formulated by Irwin (1957). The crack opening displacement (δT) can be calculated using equation 3-3.

$$\delta T = \frac{2\sigma}{E}\left(1-\upsilon^2\right)\sqrt{a^2-x^2} \qquad \textbf{Equation 3-3}$$

Here σ is the applied tensile stress, E is Young's modulus, v is Poisson's ratio, a is the half-length of the crack and x is distance along the crack, measured from the crack centre. Maximum displacement occurs in the middle of the crack (x= 0). Only a few papers (Huang and Liu, 1998; Saha *et al.*, 1999; Ahmed and Noor, 2000; Martin, 2001) have addressed the issue of crack opening displacements in elliptical cracks. The majority concern maximum crack opening displacement (COD) and maximum crack shear displacement (CSD). However, the area within the cracks face needs to be quantified that meets the criteria as set in the previous paragraph. A full

description of crack face displacements was developed by assuming that the equations for δT and δS for an elliptical geometry would be of the same form. As such, modifications are required to account for the crack shape, considering the two crack dimensions a (minor axis) and b (major axis). It is evident that for a crack with $a = b$ that the COD and CSD would be equal in the centre of the crack. As a result of a changing axis ratio, three possible options are:

- The COD and CSD are dominated by the major axis.
- The COD and CSD are dominated by the minor axis.
- The COD and CSD are dominated by the axis ratio. In other words, the axis ratio of the minor axis is restricting the COD and CSD of the major axis

It is therefore more convenient to have a similar expression for the second axis of the elliptical crack. Rewriting the equations gives us:

$$\delta(x) = \left(\frac{2\sigma}{E}\right)\left(1-\upsilon^2\right)\sqrt{\left(a^2 - x^2\right)} \qquad \textbf{Equation 3-4}$$

$$\delta(z) = \left(\frac{2\sigma}{E}\right)\left(1-\upsilon^2\right)\sqrt{\left(b^2 - z^2\right)} \qquad \textbf{Equation 3-5}$$

Where a is along the x-axis and b is along the z-axis (see Fig. 3-11).

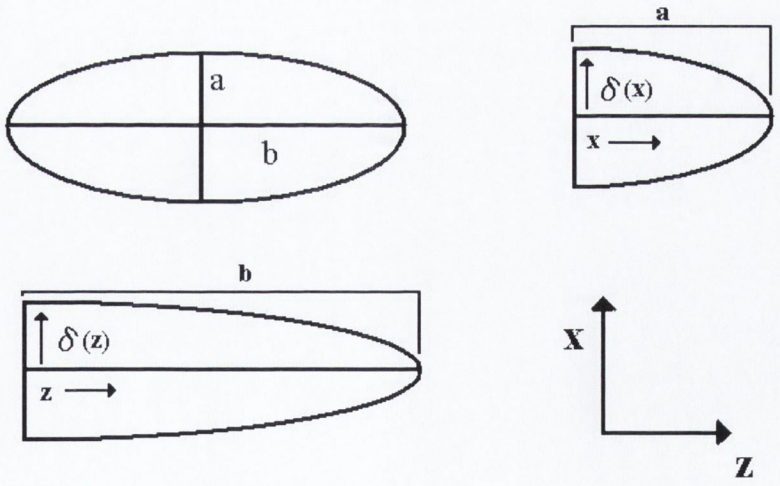

Fig. 3-11 Axis definition for an elliptical crack

From these two equations, it is evident that a discrepancy will occur: the crack opening will be different for the same applied load, e.g. in the centre of the ellipse where $x = z = 0$. The relationship between equation 3-4 and 3-6 is $\delta(x) = (a/b)x\delta(z)$, making $\delta(x) = \delta(z)$ for $x = z = 0$. This leads to a new form for $\delta(z)$:

$$\delta(z) = \left(\frac{a}{b}\right)\left(\frac{2\sigma}{E}\right)\left(1-\upsilon^2\right)\sqrt{\left(b^2 - z^2\right)} \qquad \textbf{Equation 3-6}$$

To find the relation between 2D solutions and the 3D problem, nine different FEA models where made using the following isotropic material properties (E=17.4 GPa, G=4.140 GPa and v=0.39), listed in Table 3-4:

Crack number	Length a[mm]	Axis ratio	Length b[mm]	FEA: 3D COD [μm]
1	0.1	2	0.2	0.323
2	0.075	2	0.15	0.240
3	0.05	2	0.1	0.158
4	0.05	4	0.2	0.180
5	0.038	4	0.15	0.134
6	0.025	4	0.1	0.089
7	0.033	6	0.2	0.122
8	0.025	6	0.15	0.091
9	0.017	6	0.1	0.060

Table 3-4 Crack opening calculated for nine different cracks using FEA

For all of these 9 cracks, the crack opening displacement (COD) was calculated in a horizontal plane, perpendicular to the loading direction. The results show (see also Fig. 3-12) that, if the crack length is kept constant and the axis ratio is increased (crack becomes more elongated), the crack opening is reduced. If the axis ratio is kept constant and the crack length b is increased, the crack opening is increased.

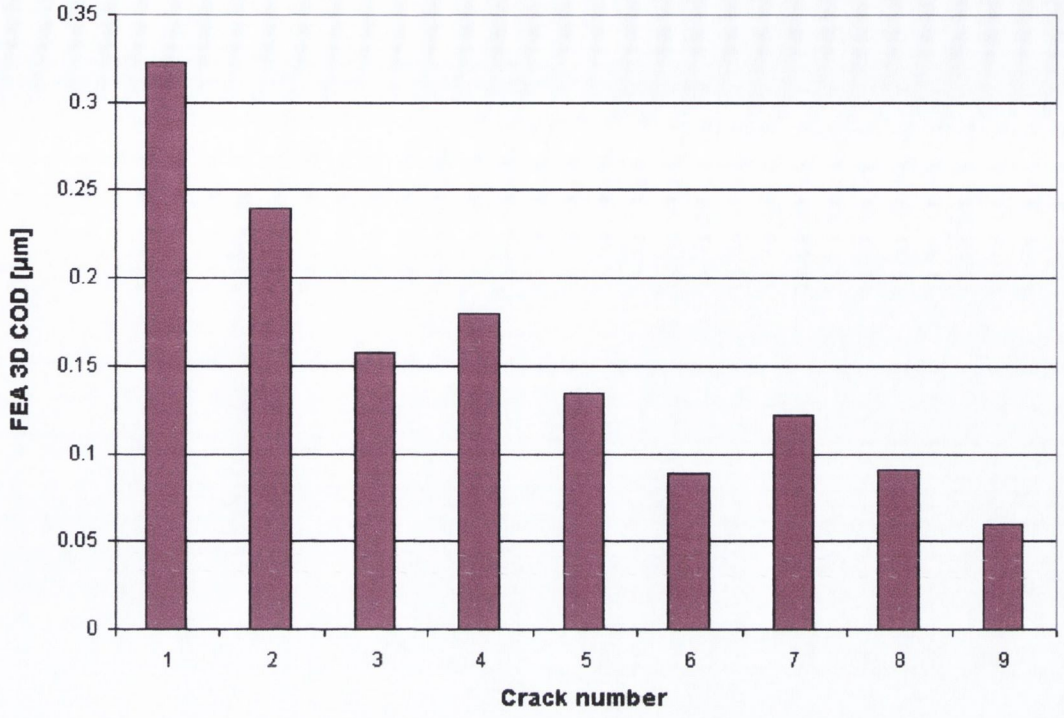

Fig. 3-12 Effect of axis ratio on crack opening displacement

It is obvious that both the crack length and axis ratio have an effect on the amount of crack opening. In order to express this relationship between the crack opening displacement and the existing equations, the following relationship was chosen:

$$C_{ratio} = F\left(\frac{a}{b}\right)^{\alpha} \qquad \textbf{Equation 3-7}$$

Here F is a geometrical correction factor and α is a dimensionless variable. Therefore the equations for crack opening displacement become:

$$\delta(x) = \left[F\left(\frac{a}{b}\right)^{\alpha}\right]\left(\frac{2\sigma}{E}\right)\left(1-\upsilon^2\right)\sqrt{\left(a^2-x^2\right)} \qquad \textbf{Equation 3-8}$$

$$\delta(z) = \left[F\left(\frac{a}{b}\right)^{\alpha}\right]\left(\frac{a}{b}\right)\left(\frac{2\sigma}{E}\right)\left(1-\upsilon^2\right)\sqrt{\left(b^2-z^2\right)} \qquad \textbf{Equation 3-9}$$

In order to compare equations 7 and 8 with the results from the FEA study, various values were chosen to estimate the two unknown variables α and F. It was found that

values of F=1.53 and α=0.1 gave the best possible solution, resulting in the following expressions:

$$\delta(x) = 1.53\left(\frac{b}{a}\right)^{0.1}\left(\frac{2\sigma}{E}\right)\left(1-\upsilon^2\right)\sqrt{\left(a^2-x^2\right)} \qquad \textbf{Equation 3-10}$$

$$\delta(z) = 1.53\left(\frac{b}{a}\right)^{0.1}\left(\frac{a}{b}\right)\left(\frac{2\sigma}{E}\right)\left(1-\upsilon^2\right)\sqrt{\left(b^2-z^2\right)} \qquad \textbf{Equation 3-11}$$

Table 3-5 and Fig. 3-13 compares equations 3-10 and 3-11 to the results from the FEA analysis, showing that the resulting equations produce similar results as predicted by the FE-analysis ($R^2 = 0.998$).

Crack No.	FEA 3D [µm]	Calculation [µm]	Ratio (FEA / calculation)
1	0.323	0.320	1.012
2	0.240	0.240	1.001
3	0.159	0.160	0.992
4	0.180	0.171	1.051
5	0.134	0.128	1.046
6	0.089	0.086	1.034
7	0.122	0.119	1.025
8	0.091	0.089	1.019
9	0.060	0.059	1.016

Table 3-5 Results for the final corrections including major axis and axis ratio

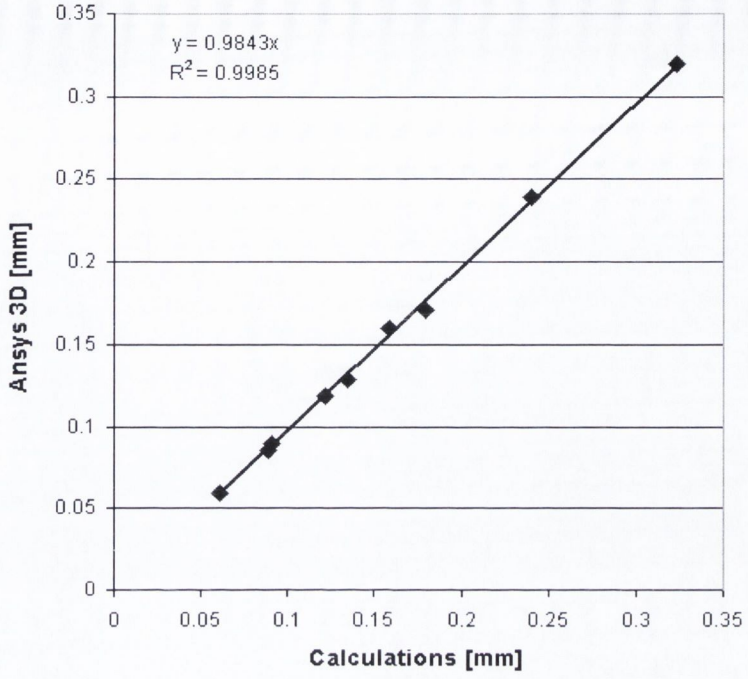

Fig. 3-13 Comparing the calculated values with the FEA results

The same approach was taken for orthotropic material properties. The crack displacements were calculated by making 27 finite-element models of cracks of different sizes, with $2b$ varying from 100-200 μm and the axis ratio b/a varying from 2 to 6, using the following material properties: v= 0.39; E_{11}= 17.4, E_{22}=E_{33} = 9.6 GPa. The following equations were found to best describe the displacements for cracks at various angles (β):

$$\delta T(z) = \left(F\left(\frac{b}{a}\right)^{0.1} \left(\frac{a}{b}\right) \frac{\sigma}{E}\left(1-\upsilon^2\right)\sqrt{\left(b^2-z^2\right)} \right) \cos(\beta)\cos(\beta) \qquad \textbf{Equation 3-12}$$

$$\delta s(z) = \left(F\left(\frac{b}{a}\right)^{0.1} \left(\frac{a}{b}\right) \frac{\sigma}{E}\left(1-\upsilon^2\right)\sqrt{\left(b^2-z^2\right)} \right) \sin(\beta)\cos(\beta) \qquad \textbf{Equation 3-13}$$

$$\delta T(x) = \left(F\left(\frac{b}{a}\right)^{0.1} \frac{\sigma}{E}\left(1-\upsilon^2\right)\sqrt{\left(a^2-x^2\right)} \right) \cos(\beta)\cos(\beta) \qquad \textbf{Equation 3-14}$$

$$\delta s(x) = \left(F\left(\frac{b}{a}\right)^{0.1} \frac{\sigma}{E}\left(1-\upsilon^2\right)\sqrt{\left(a^2-x^2\right)} \right) \sin(\beta)\cos(\beta) \qquad \textbf{Equation 3-15}$$

Here $\delta T(x)$ is the tensile displacement in the x direction and $\delta T(z)$ is the tensile displacement in the z direction, and similarly for δS. The constant F has the following values: in isotropic material F= 1.53; in orthotropic material F= 2.0 for tensile displacement and F= 3.25 for shear displacement. Fig. 3-14 and Fig. 3-15 show a comparison of total shear and opening displacements. These equations agree very well with the predicted FEA-values (COD, R^2= 0.992 and CSD, R^2= 0.988). The benefit of the equations over FEA is that they are more convenient for calculating displacements for any combination of crack size, shape and loading angle.

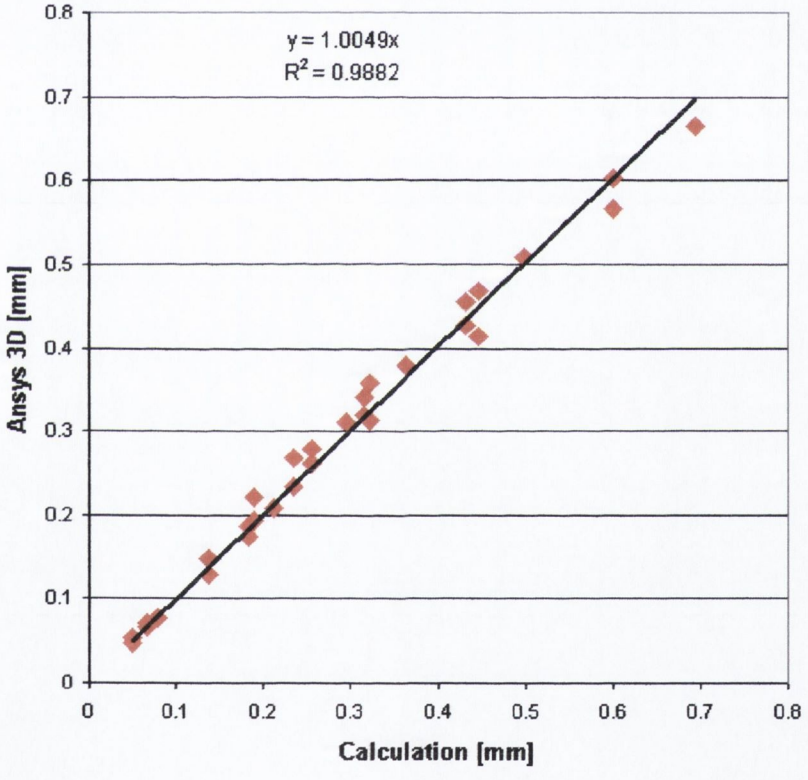

Fig. 3-14 Comparing calculated CSD using equations 3-12 & 2-14 with FEA.

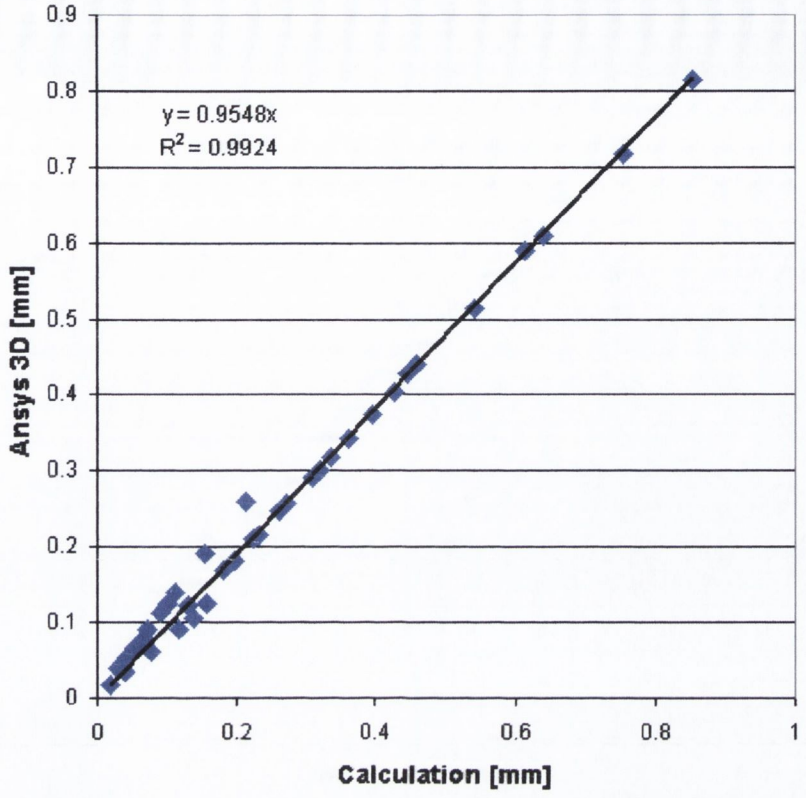

Fig. 3-15 Comparing calculated COD using equations 3-13 & 3-15 with FEA.

The only objective of the study was to analyse various crack geometries using FEA, within the range of those typically found in bone, and to find the two constants (F, α), which could be used in an equation which could describe the COD and CSD without having to reconstruct every configuration of crack shape in a FE-model. The model was tested at various crack angles, therefore the equations are valid for cracks between 0 and 90°, axis ratio's between 1 and 7 and transverse crack lengths of 50 to 300 μm.

3.4.1.3 Predicting the number of ruptured osteocyte processes.

Fig. 3-16 shows the maximum displacements predicted for a typical *in vivo* crack ($2b$= 400 μm (longitudinal), and $2a$= 100 μm (transverse)), loaded at various angles with a physiological stress of 40 MPa. Results are the same for tensile and

compressive loading except that, in compression, the tensile displacement will be zero. Predictions were made using both isotropic and orthotropic elastic properties, showing significant differences. Clearly it is important to assume orthotropic behaviour, so this was done in all subsequent work. At a crack orientation of 70°, failure of cell processes will occur during compressive loading because $2\delta S$>0.2 μm. Failure will also occur under tensile loading because 2δS>0.2 μm and $2\delta T$<0.2 μm (see section 3.4.1. failure criteria).

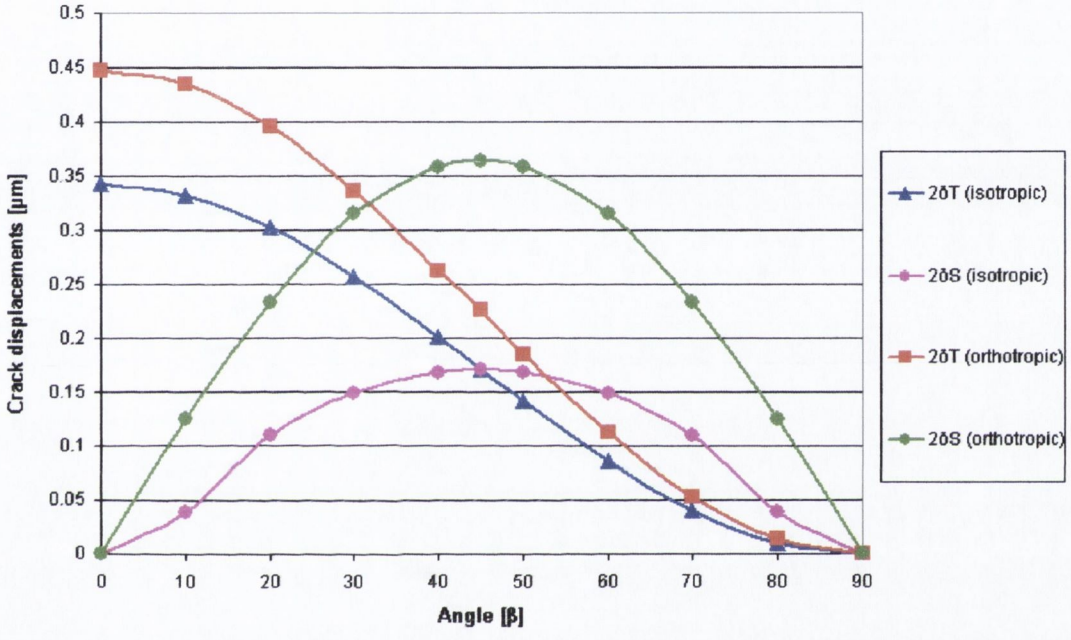

Fig. 3-16 Maximum COD and CSD due to shear and tension, assuming isotropic and orthotropic elastic properties.

Using this type of analysis, predictions can be made for the number of cell processes that will be ruptured by calculating how much of the crack's area experiences displacements conforming to the failure criteria. Fig. 3-17 shows results for cracks of length $2a$= 30, 100 and 300 μm (at the usual orientation of 70°), using two osteocyte densities: high (740 osteocytes/mm^2) and low (350 osteocytes/mm^2) (Martin and Burr, 1989; Mullender *et al.*, 1994; Kagayama *et al.*, 1997; Power *et al.*, 2002; Vashishth *et al.*, 2002).

For the 30 μm crack, no failures occur, even at stresses above the normal physiological level. For the 100 μm crack, cell processes begin to rupture at a threshold level of 28MPa; for the 300 μm crack the threshold is 10MPa. Large numbers of ruptured cell processes (more than 1000) occur for the large crack at normal stress levels and for the normal crack at high stress levels.

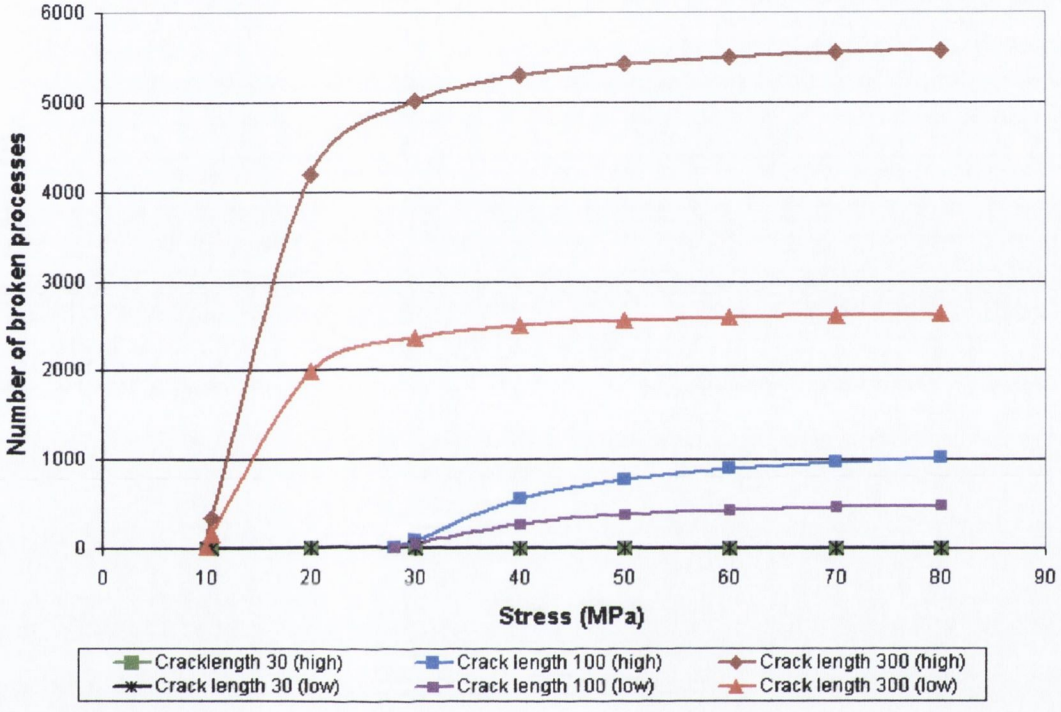

Fig. 3-17 Predicted number of cell-processes that failed, using high and low osteocyte densities for three different crack lengths.

The density of osteocytes was found to have only a small effect on the threshold. The results found above can be expressed as a simple equation, rewritten from equations discussed in section 3.4.1.2:

$$D_{cp} = \pi \left(-\left(\frac{f_c}{H}\right)^2 + a^2 \right)^{0.5} \left(-\left(\frac{f_c}{H'}\right)^2 + b^2 \right)^{0.5} OD \qquad D_{cp} \subset \mathbb{Q}^+ \qquad \textbf{Equation 3-16}$$

with:

$$H' = H\left(\frac{a}{b}\right) \quad \text{and} \quad H = \left(F\left(\frac{b}{a}\right)^{0.1} \frac{\sigma}{E}\left(1-\upsilon^2\right)\cos(\beta)\sin(\beta) \right)^{-1}$$

Here D_{cp} is the number of ruptured cell processes, OD is the number of cell processes/mm^2, f_c is the failure criteria (0.2 μm), a and b are the crack lengths in mm. The number of cell processes/mm^2 is dependant on the cell density (cd, osteocytes/mm^2). It was assumed that there are 50 cell processes per osteocyte (Cowin et al., 1991), with osteocytes equally distributed. A negligible difference was found between tensile and compressive loading.

3.4.1.4 Rupture of cells ahead of the crack.

Cells located just ahead of the crack tip will fail if they experience cyclic strains of more than the predicted fatigue strength, estimated earlier to be $\varepsilon = 0.15$. Fracture mechanics theory states that the stress near a crack tip decreases with distance from the tip according to:

$$\sigma(r) = \left(\frac{K}{\sqrt{2\pi r}} \right) \qquad \textbf{Equation 3-17}$$

Here r is the distance from the crack tip, K is the stress intensity factor and $\sigma(r)$ is the stress at a distance 'r'. For our 'worst-case scenario' (a crack with a transverse length $2a$= 300 μm at an applied stress of 80 MPa) the strain falls to 0.15 at r = 0.025 μm from the crack edge. This distance is far smaller than the size of a single osteocyte (4-10 μm), therefore it was concluded that it is highly unlikely that any osteocytes will be ruptured ahead of the crack. For a typical crack with a length of 100μm, subjected to a stress of 40 Mpa, the failure strain of the material has to drop by a factor 10 to produce strains which might rupture the cell. Even for a extreme long crack with a length of 300 μm subjected to a stress of 80 MPa the failure strain has to drop by a factor of 1.5 in order to introduce strain levels to be potentially harmful to the osteocytes.

3.4.2 Strain sensing by cells

Another possible option for the cellular transducer is that the osteocytes themselves are able to detect, and measure, the level of strain which they are experiencing. Experiments carried out on animals *in vivo* have shown that bone modelling occurs at

strain rates and magnitudes higher than physiological normal. Furthermore, passive and active cellular responses have been observed in *in vitro* cell cultures subjected to similar loading conditions as the animal studies. In principle this would allow osteocytes to signal the fact that they were experiencing unusually high (or low) levels of strain. The idea of strain measurement is implicit in the theories advanced by Carter et al (1987), Beaupré et al., Huiskes et al.(1987) and others, who have developed adaptation schemes based on local values of strain, stress, and strain-energy density. In those approaches the strain value was used directly as the signal for adaptation. However, the main question is how this strain signal could be used to indicate the presence of a microcrack, and to distinguish between microcracks of different sizes.

One conclusion which can be drawn immediately from a simple knowledge of fracture mechanics, is that the signal cannot be proportional to the strain. The reason for this is as follows: in the region of the crack tips there will be cells which experience high strains, whilst other cells, close to the crack faces, will experience unusually low strains. If each cell emits a signal which is directly proportional to strain, then the net signal, as seen from a point at a large distance from the crack, must be exactly equal to the nominal applied strain, i.e. the crack would be invisible. There will be local variations near the crack, which might be sufficient to signal for repair, but an adaptation signal would be impossible. This implies that there must be a non-linear relationship between the signal (S) and the strain (ε). One possibility is an equation of the form:

$$S = \varepsilon^n \qquad \textbf{Equation 3-18}$$

If n>1 then the net signal will be larger than the nominal value, if n<1 it will be smaller. Another, simpler possibility is that cells only emit a signal if they experience a strain which is higher than the normal physiological range. Such high strains could only occur due to the local stress concentration caused by a crack, so this would be an efficient way to detect damage. Though there is some experimental evidence that cells *in vitro* can detect cyclic strain (see above) it is not known what strain levels

can be detected *in vivo* for cells embedded in the bone matrix. Lets assume a value of 4000 με because this lies above any normal physiological strain (the maximum being 3000 με) but is less than bone's failure strain (typically 20000 με). In fact the exact value assumed is not important in demonstrating the general principle.

Using the fracture mechanics theory, values for the distance r can be found (in equation 3-17) over which strains greater than 4000 με exist, which is labelled here as the 'high-strain zone'. The relevant zone here is a three-dimensional volume, which has a toroidal shape, of varying thickness because the stress intensity changes as one moves around the elliptical crack. The volume of this torus V can be expressed as:

$$V = \frac{\pi\left(\frac{k\ (r_a + r_b)}{k+1}\right)^2 L}{\cos^4(\beta)} \qquad \textbf{Equation 3-19}$$

Here 'r_a' and 'r_b' are the extent of the zone at points a and b on the crack (see Fig. 3-2), $k = b/a$ and L is the length of the torus which is approximated by:

$$L = \pi\sqrt{2(a + r_a)^2 + (b + r_b)^2} \qquad \textbf{Equation 3-20}$$

The relationship (k (r_a+r_b))/(k+1) estimates the average estimated value for the size of the high strain zone for an elliptical crack, since $r_a \neq r_b$. However this relationship should still be valid if the crack were circular in those cases $a=b$ and therefore $r_a \approx r_b$. Fig. 3-18 shows the numbers of cells in the high-strain zone as a function of crack length, stress and osteon density. Cracks of length 30 μm do give rise to a signal in this case, but will for stresses above the physiological range. The thresholds for the signal with cracks of length 100 μm and 300 μm in the transverse direction were 26 MPa and 19 MPa respectively. Results for tension and compression were significantly different: the number of cells affected can be expressed in the following forms, which were found by curve fitting:

$$CA_{(tension)} = cd\ 12e^{(2a+0.9)\ 1.8\sqrt{\sigma}-21.5} \qquad \textbf{Equation 3-21}$$

$$CA_{(compression)} = cd\ 12e^{(2a+0.9)\ 1.8\sqrt{\sigma}-22} \qquad \textbf{Equation 3-22}$$

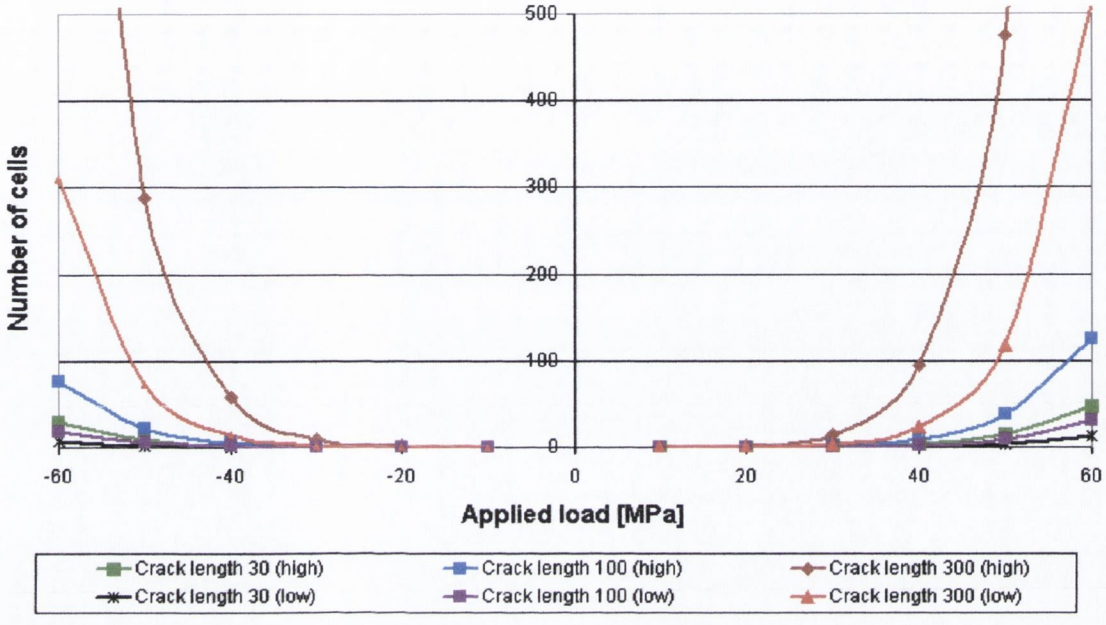

Fig. 3-18 Predicted number of cells experiencing more than 4000 με, using two osteocyte densities: high (20,000 osteocytes/mm^3) and low (5,000 osteocytes/mm^3)

3.5 Discussion

The most important finding from this analysis was that it is highly likely that cellular material will be ruptured as a result of the presence of a crack. A new failure mechanism was proposed: cutting of cell processes by shear across the crack faces, which has not been considered before. These results rest on an assumption about the displacements needed to cause rupture ($2\delta S > D$) which, whilst it seems reasonable, has not been proven experimentally. This however is the only important assumption. The rest of the analysis uses well-established procedures in elastic fracture mechanics and finite element analysis and is likely to be quite accurate. This has established a very simple source for the cellular transducer: broken cell processes release cellular material into the extra-cellular matrix, which can then diffuse through the matrix and be detected elsewhere, causing BMU formation and bone deposition.

It is very encouraging that the quantitative results are also of the correct order of magnitude, both for repair and deposition. For a 100 μm crack, processes begin to rupture at a stress of 28 MPa, which is somewhat lower than the normal maximum physiological stress of 40 MPa. In fact the crack length which has a threshold of exactly 40 MPa is 91 μm, which is within the range of average crack lengths measured experimentally (Burr and Stafford, 1990; Burr and Martin, 1993; Mori and Burr, 1993; Lee *et al.*, 1998). Given the assumptions made in the model, especially the use of average quantities and not considering their variability from one crack to another, this analysis demonstrates quite accurately that repair could be instigated by detecting the first ruptures of cell processes.

On the other hand, a longer crack (300 μm) generates a much larger number of ruptures, several thousand even at normal physiological stress levels. The number of ruptured processes exceeds 1000 also for 100 μm cracks if the stress level becomes abnormally high (>70 MPa), suggesting that extensive failures of this magnitude could act as the signal for bone adaptation, being detected some distance away by osteoblast progenitors located on the bone surface.

It was also shown that similar results can be obtained if one proposes a different signal source, whereby cells detect the presence of unusually high strains near the crack tip. Results are essentially similar (compare Fig. 3-17 and Fig. 3-18) indicating that this is also a potentially viable way to control repair and adaptation. However there are significant differences between the two results, as shown in Fig. 3-19 for a typical crack. The dependence of the signal on stress level is qualitatively different: though the thresholds are similar the strain-sensing mechanism has a rapidly increasing, exponential form. It is also greater in tension than in compression.

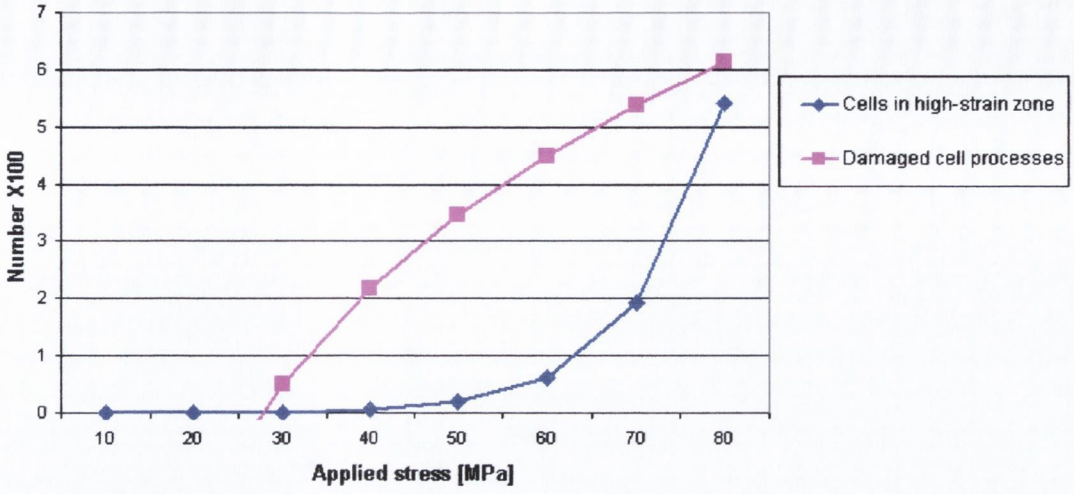

Fig. 3-19 Comparison of the signals from the high-strain zone and from ruptured cell processes, for a typical crack of length 2a= 100 μm at different applied stresses.

Furthermore a crack growth and shape development model was developed which is able to predict microcrack shapes that are similar to *in vivo* cracks found by O'Brien *et al.* (2000). These predictions were made using existing crack growth equations and fracture mechanics solutions. Although this approach was based on various assumptions, seven of the nine cracks found by O'Brien *et al.* (2000) could successfully be predicted using thresholds for the interstitial bone between 0.065 and 0.075 MPa$\sqrt{m}$ and an angle (β) between 65 and 75 degrees. The remaining two cracks had axis ratios of approximately two, with a transverse length higher and a longitudinal length lower than the other seven.

The analysis carried out in this chapter has resulted in a proposal for two new mechanisms by which microdamage can be detected. Specifically the quantification of the number of osteocytes signalling or ruptured cell-processes could explain how crack sizes could be estimated allowing adequate action to be taken to prevent catastrophic failure due to microdamage. Although the results from the theoretical analysis were encouraging, various assumptions which were made in this chapter require further research to validate the two mechanisms proposed. These were:

- The theoretical model presented was based on linear elastic fracture mechanics, which was not validated. Plastic deformation near the crack tips and the dynamic nature of propagating cracks could affect crack opening and shear displacements which might potentially result in an over- or under prediction.
- Although the criteria for rupturing cell-processes due to crack opening and shear displacements seem reasonable, it is not known if this would occur *in vivo*.
- Various effects, such as crack kinking, which have been known to occur during crack growth and propagation have not been considered. The direction of crack growth was assumed to be mainly affected by the local orientation of the microstructure of bone, and less by the loading confirmation. As such, it is not known how well the theoretical model mimics the *in vivo* crack behaviour in cortical bone.

Some of these concerns will be addressed in the following chapter.

3.6 Conclusions

- It is possible to predict crack size and shape development using a simple fracture mechanics model.
- Cracks in bone will not cause rupture of osteocyte cells, because they do not develop sufficient strain over volumes equivalent to the cell size.
- Cell processes which pass between the crack faces can be ruptured by a cutting process due to shear displacements. The number of processes that rupture is related to crack size and applied stress. Signal strengths (assumed proportional to the number of ruptured processes) will be zero for very small cracks, positive for cracks which need repairing, and much greater if surface deposition is required.
- Cell processes cannot be ruptured by tensile strains between the crack faces, because the strain levels reached are much less than the material's fatigue strength.
- If osteocytes can detect strain, and signal the presence of strain levels higher than normal physiological values, then this also could be used to detect the presence of cracks and to distinguish between cracks of different sizes.

Chapter 4 Experimental Validation of the Theoretical Model

4.1 Introduction

In Chapter 3 a theoretical model was proposed, in which cell processes, spanning a crack, rupture due to relative crack-face opening and shear displacements. These displacements could be calculated with the theory developed and therefore an estimate regarding the number of broken cell-processes could be made. This chapter discusses the experimental work carried out to validate this theory.

The theoretical model predicts that cell-processes can be broken by the crack-face displacements, assuming that a linear elastic fracture mechanics (LEFM) model is valid. Therefore the validation of this theoretical model is two fold:

I) Do cell-processes break due to crack displacements *in vivo*, i.e. are the failure criteria set in Chapter 3 valid?

II) Is it valid to use LEFM to predict these displacements?

In order to assess this, growing cracks in bone were analysed. This required a test rig in which cracks can be grown and monitored. Subsequently, post-test analysis was used to analyse whether the failure criteria, as discussed in Chapter 3, cause failure of the cell-processes. Crack opening and shear displacements were measured during crack growth, to indicate whether the use of linear elastic fracture mechanics was justified.

4.1.1 Visualisation of cell-processes

In order to assess if cell-processes were broken by a given displacement, visualisation of the crack faces and cell processes was required. Osteocytes and their

lacunae are large enough to be easily identified in most preparations. Commonly paraffin sections of decalcified bone are used, stained with haematoxylin[9] and eosin (H&E-staining). The fine canaliculi, radiating from the osteocytes, are less easily seen. Often thick celloidin[10] sections require strong staining with haematoxylin, or impregnation with silver nitrate to visualise canaliculi. The major problem in visually observing canaliculi is that the spaces are too fine to be identified by merely staining the surrounding tissue. In general it requires the use of a second substance, which will provide enough contrast between the canaliculi and the surrounding tissue. A traditional method is called the 'air injection' method (Taylor *et al.*, 1993). Un-decalcified ground sections are dried and mounted in balsam. By melting the balsam, air is entrapped within the canaliculi, making them appear as black threads against the unstained bone. However this method does not work if sections are too thin or if the balsam is too liquid. Besides balsam, resin can be impregnated in cortical bone sections as shown in Fig. 4-1.

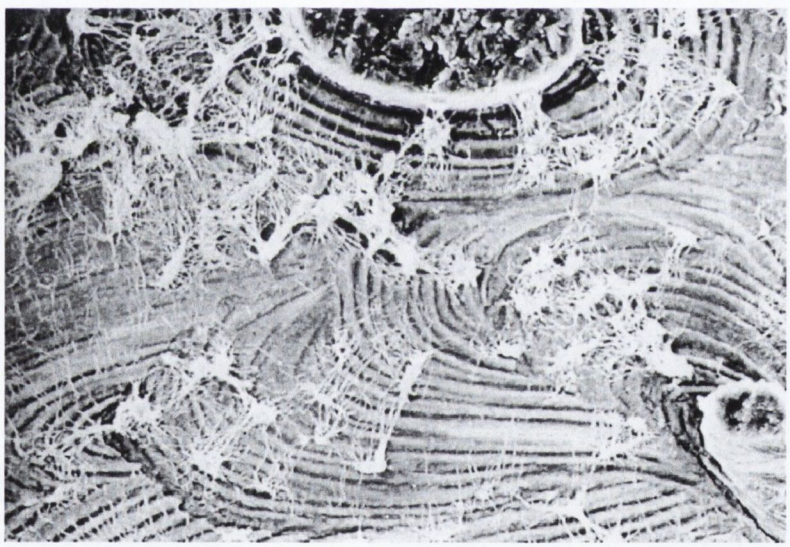

Fig. 4-1 Scanning electron micrograph of a resin-impregnated section of human cortical bone (Currey, 2002)

---

[9] H&E is the most widely used natural dye in histotechnology, obtained from logwood. It will stain tissue components such as myelin, elastin and collagenic fibres, muscle striations, mitochondria and so on, but its most common application is as a nuclear dye.

[10] Nitrocellulose is a compound derived from pyroxylin, used in a solution of alcohol and ether for embedding specimens before cutting sections.

Other methods, like a modified Bodian method using protargol[11], commonly used for detection of nerve fibres, have been described in the literature to investigate osteocytes and their processes (Kageyama *et al.*, 1991; Kusuzaki *et al.*, 1995; Kagayama *et al.*, 1997; Kusuzaki *et al.*, 2000). However, the majority of studies on osteocytes and their processes have been based on conventional transmission electron microscopy of demineralised bone tissue (Jande, 1971; Jande and Belanger, 1971; Palumbo, 1986; Palumbo *et al.*, 1990). The limitation of this kind of study is the lack of understanding of the three-dimensional distribution of cell-processes throughout the matrix. Furthermore, these techniques require bone specimens to be decalcified, which means that fluorescent dyes, commonly used for microdamage detection cannot be used. These dyes bind to free exposed calcium, which is removed during the decalcification process. Recently Kamioka *et al.* (2001) used confocal laser scanning (CLS) microscopy to study the three-dimensional distribution of cell-processes through the matrix. In combination with recent developments in fluorescent antibody labelling techniques, high detailed images can be obtained.

4.1.1.1 Antibody staining

Antibodies are serum proteins or immunoglobulins, secreted by B-lymphocytes. These proteins comprise a memory system, which detects specific antigens and then links antigens to an effector system that defends against the antigen and associated structures. Antibodies may be free-floating in the serum, or may be attached to cell-surfaces, acting as receptors. These site-specific binding proteins can be used to identify specific components within tissues and cells. All eukaryotic[12] cells contain complicated systems of internal membranes, which set up membrane-enclosed compartments within the cell. The cell membranes form the cytoskeleton of the

---

[11] Protargol (silver protein) is used with the addition of copper metal. The copper replaces the silver in the connective tissue, allowing a greater differentiation between the nerve fibers and the connective tissue.

[12] Cells found in various organisms like plants, animals and humans, which are defined as membrane-bound structures containing organelles such as nucleus, mitochondria, chloroplasts, endoplasmic reticulum (ER), Golgi apparatus, lysosomes, vacuoles, peroxisomes, etc. Prokaryotic cells do not have organelles.

cellular network. This universal feature within all cells (the plasma membrane or cytoskeleton), can be used for antibody staining.

The cytoskeleton is made up of three kinds of protein filaments:

- Actin filaments
- Intermediate filaments
- Microtubules.

Actin microfilaments form a layer just beneath the plasma membrane called the cortex. Actin is the product of different genes in cells. Actin is commonly divided into *G-actin* (G for globular), which polymerises under under physiological conditions to *F-actin* (F for fibrous). *F-actin* is sub-divided into α-,β-, and γ-actin. In bone cells only β-actin is found in the membranes whereas α-actin is usually found in muscles and γ-actin is only found in the lining of the gut (Villee *et al.*, 1989; Voet and Voet, 1990; Spector *et al.*, 1998).

Commercial kits are available to stain these proteins using antibodies (Lodish *et al.*, 1998). The production of these antibodies involves the synthesis of antibodies created by living organisms. For example, *F-actin* from a cow can be injected into a goat. The goat will react to these proteins as if it were a virus. The response is the production of anti-actin antibodies. These antibodies kits may contain a 'primary-secondary' system or a pre-mixed combination of these two. The primary antibody will stick to the *F*-actin. The secondary antibody, containing a fluorescent marker, will then bind to the primary antibody. The secondary antibody will only show up if it has successfully bound to the specific site. In order to check if the secondary antibody does not bind to other proteins, a negative control needs to be carried out to investigate binding specificity.

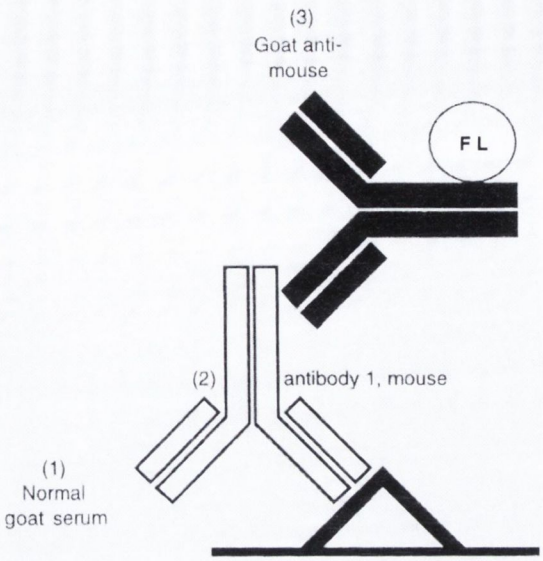

Fig. 4-2 Primary-secondary antibody staining schematic (van der Loos, 1999)

Fig. 4-2 illustrates the principle of this staining process. Due to the wide variety of proteins in bone, non-specific sites are blocked using goat serum. This is followed by the primary antibody, which in this case is an antibody that was grown in a mouse. The next step is to attach the secondary antibody, which is a goat anti-mouse. If the secondary antibody binds to the primary antibody, the fluorescent marker can be visualised, using a confocal microscope.

4.1.2 Linear elastic fracture mechanics

In order to apply fracture mechanics, one has to consider if linear elastic fracture mechanics (LEFM) or elasto-plastic fracture mechanics (EPFM) should be used. This choice is generally made on the basis of the overall material behaviour. Bone can be considered to be I) a linear elastic material, II) a composite material or III) elastoplastic material. The elasticity theory is the simplest constitutive relation, suitable to describe the mechanical behaviour of bone. It is considered adequate for the description of whole bones subjected to small deformations (Lakes *et al.*, 1990). In cases where linear elastic behaviour can be assumed, LEFM can be used. However, at a semisolid level anisotropy and variations of local material properties suggest that bone should be treated as a complex multi phase composite.

Analysis of microcrack behaviour in bone is typically done using notched coupons. These specimens are subjected to a constant load rate, causing different failure modes (Currey, 2002), providing data on stress intensity threshold values (Bonfield and Datta, 1976; Lakes *et al.*, 1990; Norman *et al.*, 1992;1995; Yeni *et al.*, 1997; Yeni *et al.*, 1998) and crack growth rates (Vashishth *et al.*, 1997; Vashishth *et al.*, 2000a). Quantitative observations on crack angle, crack densities and location of crack formation provide valuable information in our understanding of damage formation and behaviour.

4.1.3 Aims and objectives

In order to investigate if the assumptions made in the theoretical model are correct, various aims and objectives were set, which were split into three categories. The first section concerns the individual behaviour of cracks and their interaction with the microstructure. The second section concerns visualisation of damage to the cell-processes. The third section asks if linear elastic fracture mechanics adequately describes crack face displacements.

The overall aims are:

1. Does linear elastic fracture mechanics describe crack opening and shear displacements?
2. Are the failure criteria set in the previous chapter valid?

However the theoretical analysis in Chapter 3 takes no account of the dynamic nature of propagating cracks. During the crack growth experiments, to validate the use of linear elastic fracture mechanics, various effects were observed that required further study.

4.2 Materials and methods

4.2.1 Design of the rig and specimens

The limitations to the design of a rig that could be used for crack growth observations under a microscope were as follows:

- The size of the rig should be small enough that it could be placed under an optical microscope, which means that the maximum size of the rig is 20x200x150 (height x length x width, mm).

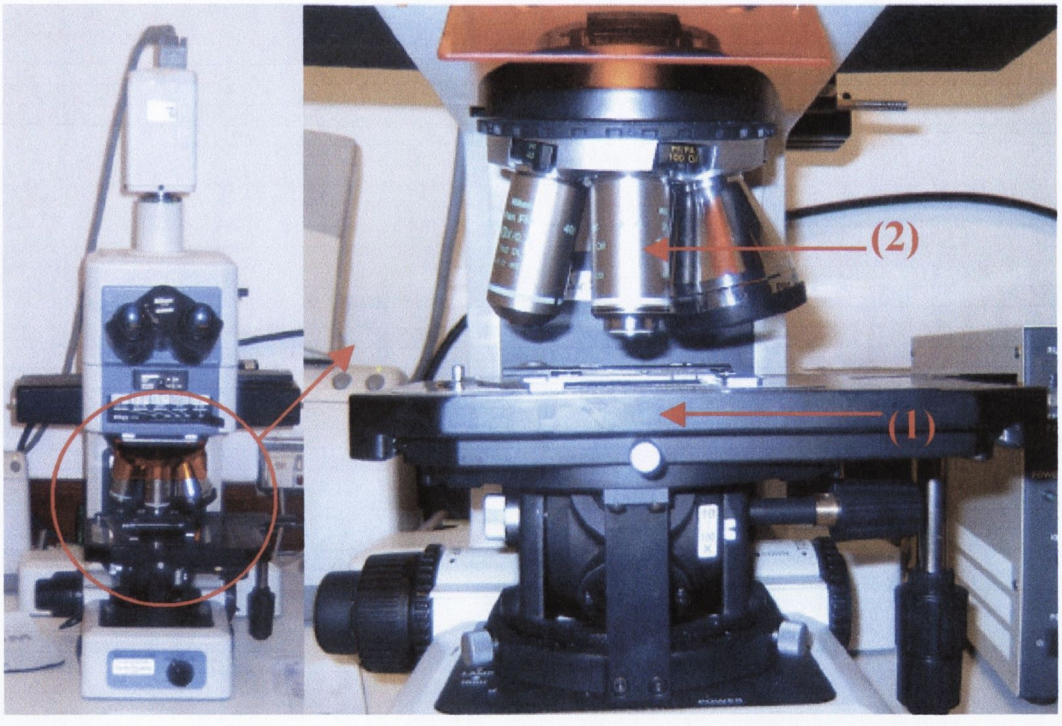

Fig. 4-3 Microscope: space between stage (1) and lenses (2).

- It should be able to apply load to a bone sample whilst placed under the microscope.
- The applied load should be quantified.
- The rig should be constructed as rigidly as possible, so as not to distort under load.
- If a bone sample or a rig component fails, damage to the microscope should be avoided, especially to the lenses

The final rig design, as shown in Fig. 4-4, consisted of two grips, one attached to a load cell to monitor the forces applied during testing and one attached to a spindle in order to apply a load.

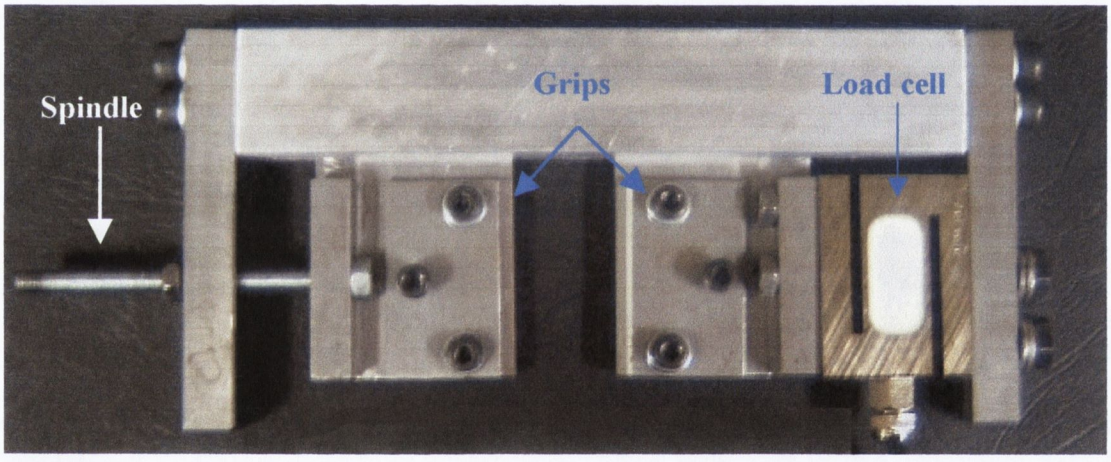

Fig. 4-4 Test rig used for crack growth analysis

These components are held together by a C-shaped frame measuring 165x68mm, having a thickness of 16 mm. The load cell (KD 40S, ME-Meßsyteme Germany) which is attached to one of the grips, measures tensile or compressive forces in a range of 0-2000N. These measured forces were amplified (GSV-2, ME-Meßsyteme Germany) and directly read out to a PC. The spindle by which the loads are applied was made of a standard threaded metal rod (M6), which is attached to the second grip. Each grip has three bolts; two for fixing the bone specimen (Fig. 4-5 'a' and 'b') and one to adjust the grips to the thickness of the specimen (Fig. 4-5 'c').

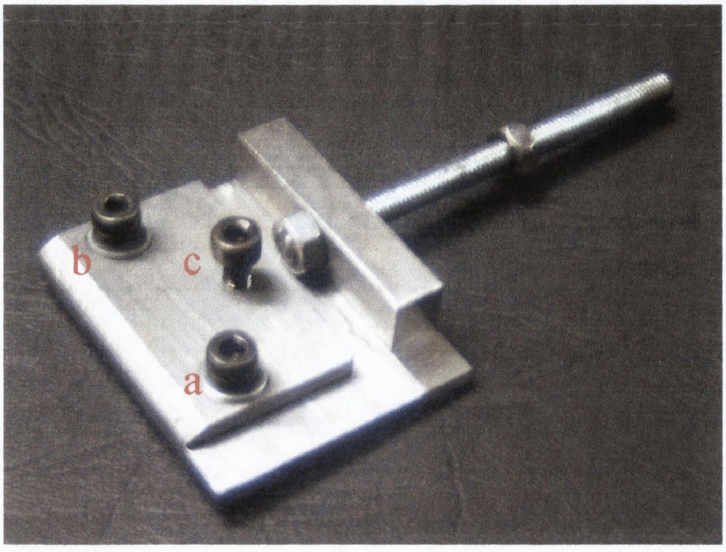

Fig. 4-5 Grip used in test rig

Once the bone specimens were placed between the grips, a strain was applied by rotating the nuts on left side of the frame. The two grips side in a slot, which was milled along the length of the frame to prevent any axial rotation (Fig. 4-6).

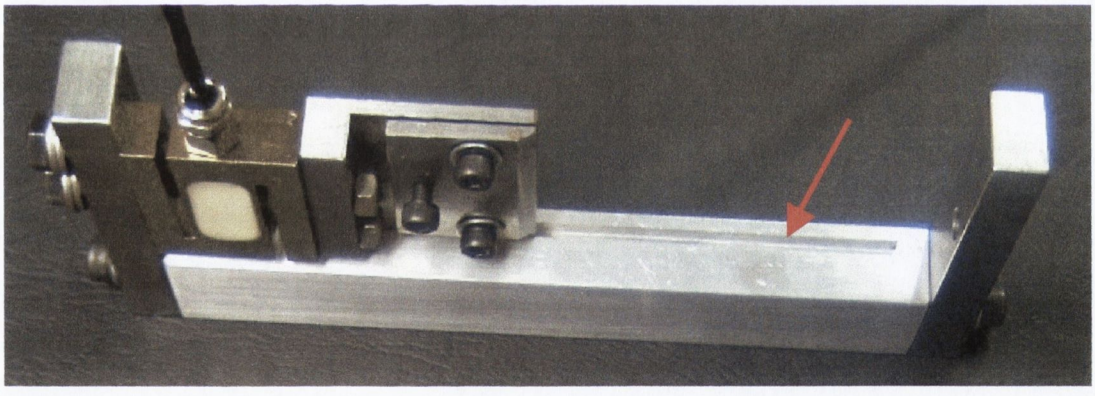

Fig. 4-6 Milled slot (red arrow) in frame of test rig

An example of crack propagation in a notched bone specimen is shown in Fig. 4-7.

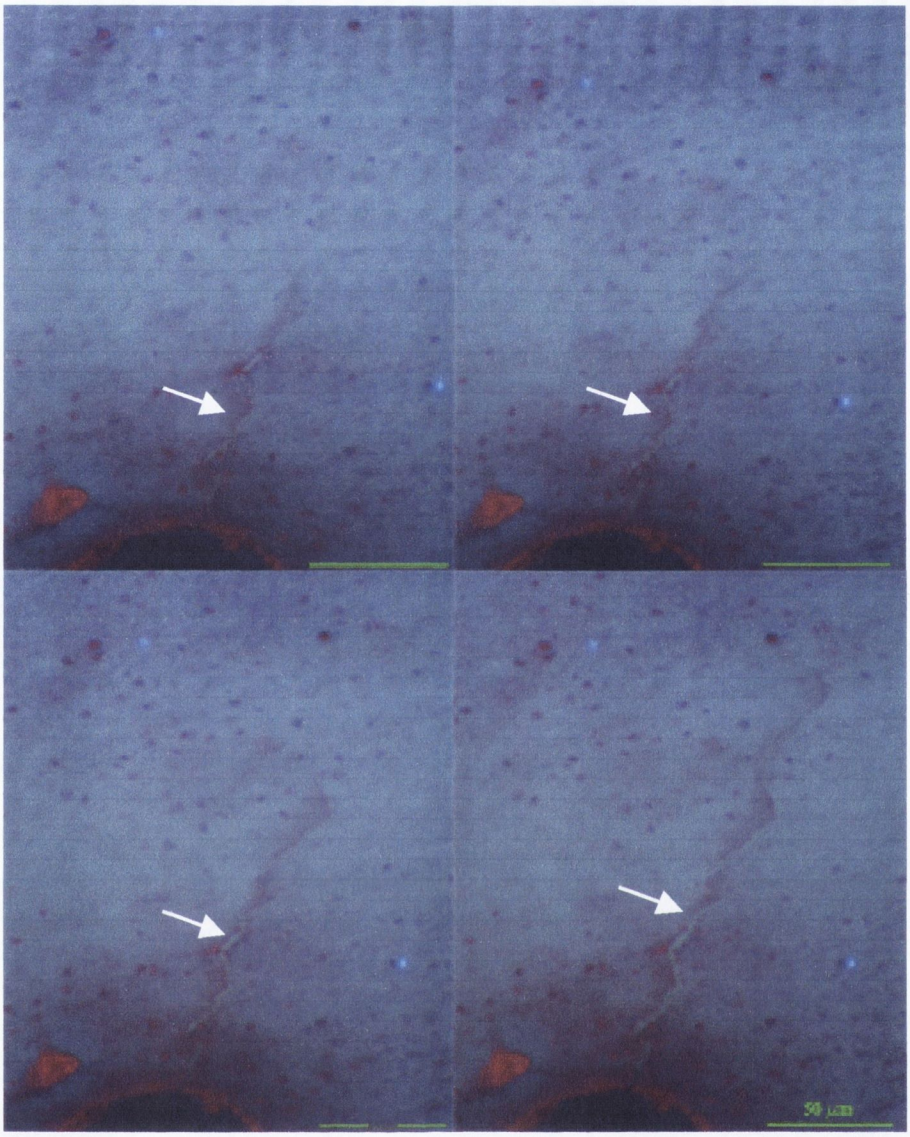

Fig. 4-7 Crack growth in bone sample D8s3 (scale bar = 50 μm)

4.2.2 Testing procedure

Fresh frozen bone samples were taken from the mid-diaphysis of bovine femur and tibia. In total 31 rectangular longitudinal specimens were cut, using a diamond saw cutting wheel (Struers Minitron, Copenhagen, Denmark). The sections were divided in two groups: I) Transverse notches and, II) Longitudinal notches (see Fig. 4-8).

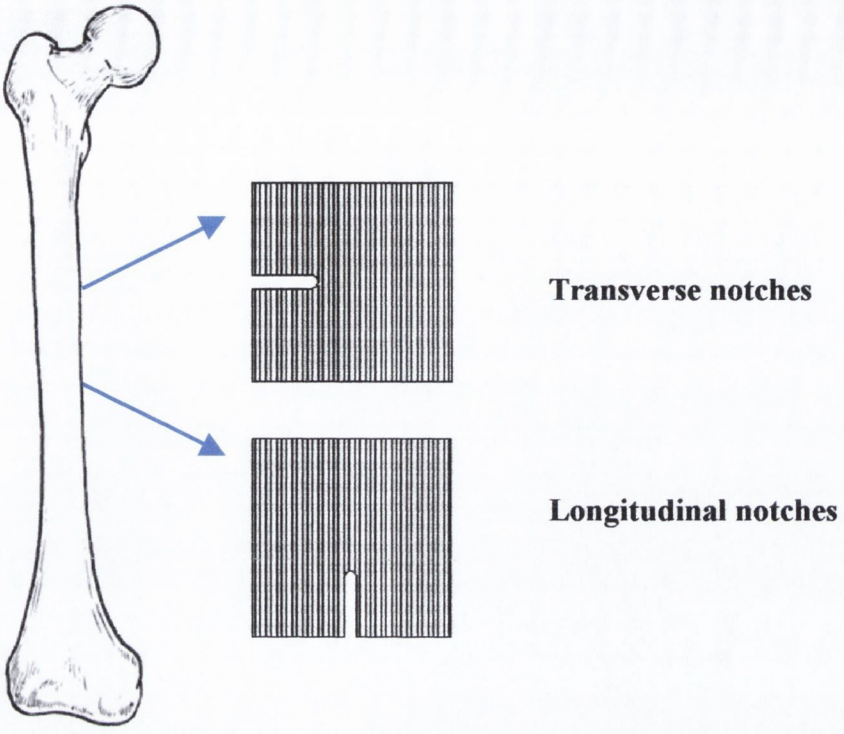

Fig. 4-8 Osteon orientation for specimens

Specimens with longitudinal notches had a thickness of 1 mm, specimens with transverse notches had a thickness of 0.6mm. From initial tests it was found that it was more difficult to initiate cracks from transverse notches. The thickness values of 0.6 and 1 mm were found to work best. Thicker sections made it more difficult to control growth and resulted in sudden cracking. Thinner sections made it more difficult to create the notch.

Sections of bone were manually ground down between two pieces of silicon carbide paper (400 and 1200 grade successfully) in a circular fashion using light pressure. Sections were then stained for 24 hours using Alizarin (fluorescent dye, Sigma Aldrich, UK) in a vacuum desiccator.

Two hours prior to testing specimens were taken out of the freezer (-20°C) and kept at 4°C in saline, to prevent drying out of the specimens. Specimens were clamped in the rig, first adjusting the grips to the right thickness as shown in Fig. 4-9.

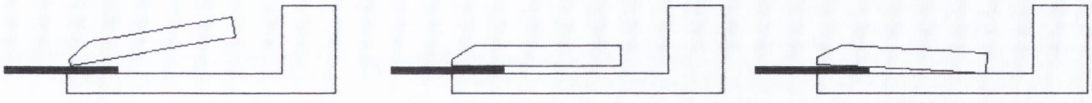

Fig. 4-9 Adjusting the grips to the right position

The rig with specimen was then positioned under the microscope (Fig. 4-10) and the loadcell amplifier was zeroed. The amplifier was switched on two hours prior to testing; allowing it to warm up. This prevents drifting of the output values during testing. The amplifier was set to take readings every 0.1 seconds, which were directly displayed on a screen. Under a 100 times magnification, focused on the notch tip, the sample was loaded by rotating the nut. The displacements were kept constant during the test. However, in some cases the applied load was not sufficient to initiate a crack from the notch and therefore reloading was necessary. Images were taken using Nikon ACT-1 image acquiring software. The optimum configuration was to take images in TIFF-format at 15-second intervals. Shorter intervals were not possible due to technical limitations. Once the specimens were tested, they were kept refrigerated at 4 °C.

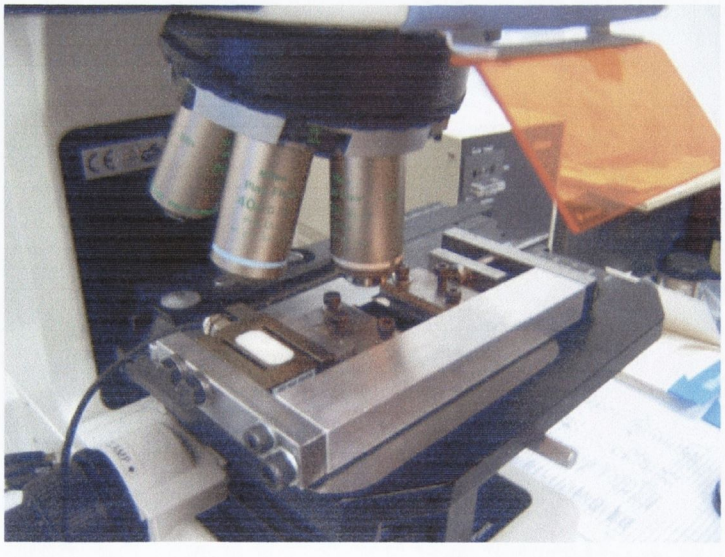

Fig. 4-10 Rig under microscope

4.2.3 Image analysis from microscopy

Once cracks were grown successfully in the specimens, the images were analysed using specialised image analysing software (Lucia Measurement version 4.7.1.) Accurate measurement was achieved by using a graticule to calibrate the software. Although the software is pre-calibrated, due to the manual processes of taking measurements, the accuracy of these measurements is operator dependant.

The crack length can be measured in two ways. Commonly the crack length is measured from tip to tip, or here from the origin (notch) to the crack tip. The 2-point option was used for this type of measurement in the Lucia program, which results in a straight line. On the other hand the crack length or crack path can also be measured using a polyline. Using the polyline option requires that the crack is redrawn, from this the number of pixels is counted which corresponds to a certain length. For one specimen, several images are taken at set intervals during crack growth. Analysing these images is easier when analysed in reversed order, i.e. starting with the last image in the set. This leads to better measurements since the crack is getting shorter and hence the direction is known.

The crack opening displacement (COD) was measured by two parallel lines on either side of the crack, near the origin of the crack, tangent to the crack growth direction. The crack shear displacement (CSD) was measured by drawing two parallel lines perpendicular to the first two. In Fig. 4-11 the crack opening is illustrated by the red lines, whereas the green lines demonstrate the crack shear displacement. The origin of the crack was chosen to take measurements of the COD and CSD, since it provides a reference point with a direction that does not alter during crack growth.

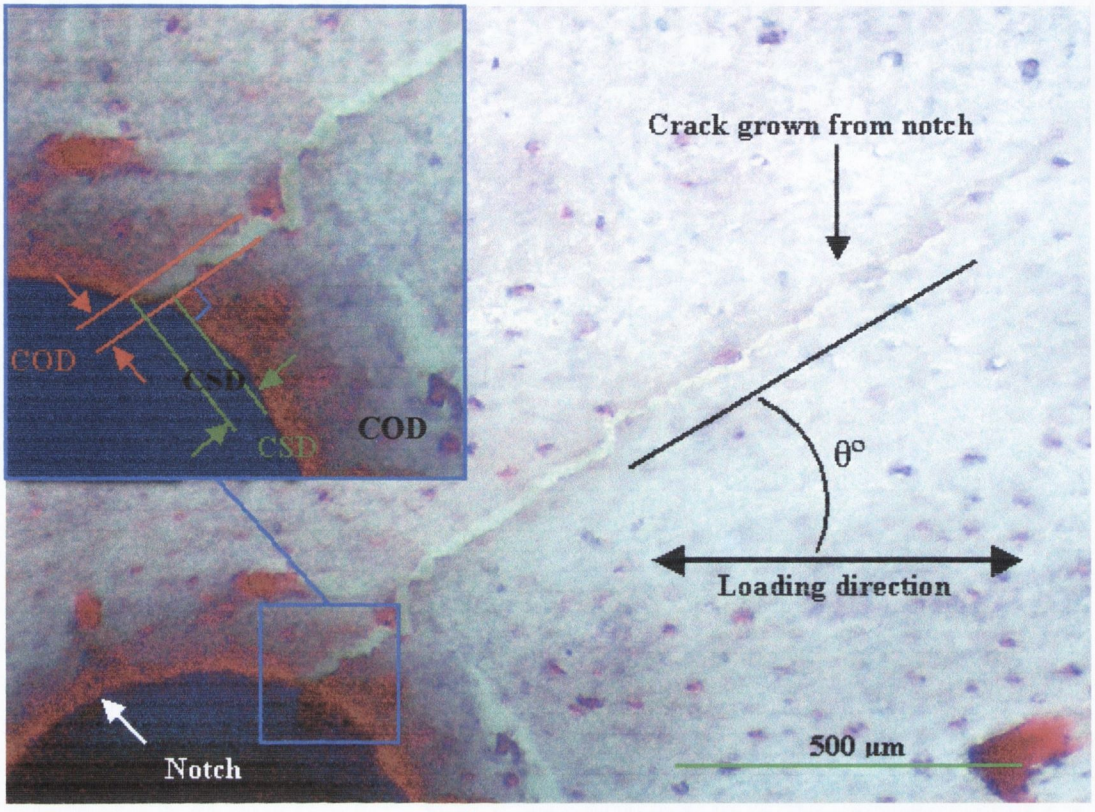

Fig. 4-11 Illustration on measurements taken for COD and CSD

By measuring the angles of these perpendicular lines, the displacements in the principal direction can be calculated, which can later on be compared with the FE analysis. The angle measurement option uses a reference line, which was perpendicular to the loading direction. The crack angle can be measured by specifying a point at the origin of the crack and a second point at the crack tip. The angle was then calculated by the program with respect to this reference line.

4.2.4 Protocol for staining cellular material

In order to establish if the cell-processes are ruptured, it is essential to see these cell-processes. This is difficult with an optical microscope since the cell-processes are randomly distributed throughout the matrix. In order to see the canaliculi, which are approximately 0.2 µm in diameter and 40 µm long, confocal microscopy can be used. The confocal microscope is similar to an epi-fluorescence microscope, however

instead of using a UV-light source, one or more excitation lasers are used (e.g. Argon, Hini-1, Hini-2 etc.). The laser causes the fluorescent dyes to excite at a specific wavelength, which is then detected by the confocal microscope. By altering the focal point of the laser in combination with specific filters, individual fluorescent markers can be selected. This allows specific features to be visualized within a given specimen.

The choice of stains is limited. The bone surfaces had been stained with Alizarin to obtain more contrast during crack propagation. The downside is that the stain also penetrates into the cellular network and therefore into the cytoplasm. To distinguish between the crack faces and the cellular material a second fluorescent dye is required.

Since there is limited knowledge of staining non-decalcified bone with antibodies, the following protocol commonly used in immunohistochemistry was used.

Three solutions were prepared:

solution 1: To 1000 ml of Phosphate Buffer Solution (PBS), 0.2 ml Triton X100 and 0.3 ml Tween was added. Triton X100 and Tween are detergents; Triton breaks the cell membranes, Tween removes debris and makes the proteins more hydrophobic. This is the main buffer used for the wash.

solution 2: 1x PBS solution with 0.2% Triton X100 which is stirred for 10 minutes due to the high viscosity of Triton X100. This solution is used to permeablise the cell membrane of the cells and cell processes.

solution 3: 1x PBS solution containing 3gr of BSA (Bovine serum albumin) in 100ml, which also needs to be stirred for 10 minutes. This is used to dilute the antibodies and provide them with a buffer.

The protocol used was as follows:

step 1: Sections were cut and polished with No.1200 silicon carbide paper

step 2: Bone sections were glued with super glue to glass-slides (only at the top edges)

step 3: Cell membranes were permeablised with Triton X100 (solution 2)

step 4: They were washed 3 times in solution 1

step 5: Non-specific sites were blocked with normal goat serum for 30 min.

step 6: They were washed 3 times in solution 1

step 7: Anti-actin was added for 1 hour (1/50 dilution in solution number 3, 100µl per slide)

step 8: They were washed 3 times in solution 1

step 9: Secondary Antibody was added for 30 minutes. Secondary antibody: Alexa Fluor 488 Phalloidin.

step 10: They were washed 3 times in solution 1

step 11: Slides were mounted with Dako Fluorescent (DAKO Corporation, CA, USA) mounting medium under a cover slip

step 12: Slides were kept stored in the dark at 4 °C

To get a clear image using the confocal microscope, a number of slides (3-5) were required to measure the intensity of the auto- fluorescence of bone. Three slides stained with Alizarin and three slides stained with the primary and secondary antibodies were used to measure the intensity of staining. Once the bone specimens were stained with both the antibodies and the Alizarin, the colours could be balanced since one may be more dominating than the other. A further 3-5 slides were required for a negative control with only the secondary anti-body.

4.3 Results

In total of 31 specimens were successfully tested, of which 13 specimens had longitudinal notches and 18 had transverse notches. Transverse notched specimens had a typical size of 15 x 35 mm, whereas longitudinal notched specimens had dimensions of 25 x 25 mm. The dimensions of individual specimens are given in appendix 4.

In order to quantify the accuracy and repeatability of the measuring technique various lengths, ranging from 5 and 1000 μm, were measured and repeated 10 times. The maximum error was 1.2% for smaller (5 μm) lengths and 0.1% for the longer lengths (1000 μm).

4.3.1 Specimen analysis

4.3.1.1 Force measurements

Fig. 4-12 and Fig. 4-13 show the changes in tensile force measured during crack growth. In some cases, the load was increased until crack initiation was observed. This resulted in a step-like pattern in the output data, as shown in the two images below. Transverse notched specimens required a mean force of 145 N to initiate a crack, whereas longitudinal notches required 95 N (see Table 4-1), though in the longitudinal notched specimens, one specimen, D3s2, required 140N to initiate crack growth. Table 4-1 shows a summary of the forces and stresses.

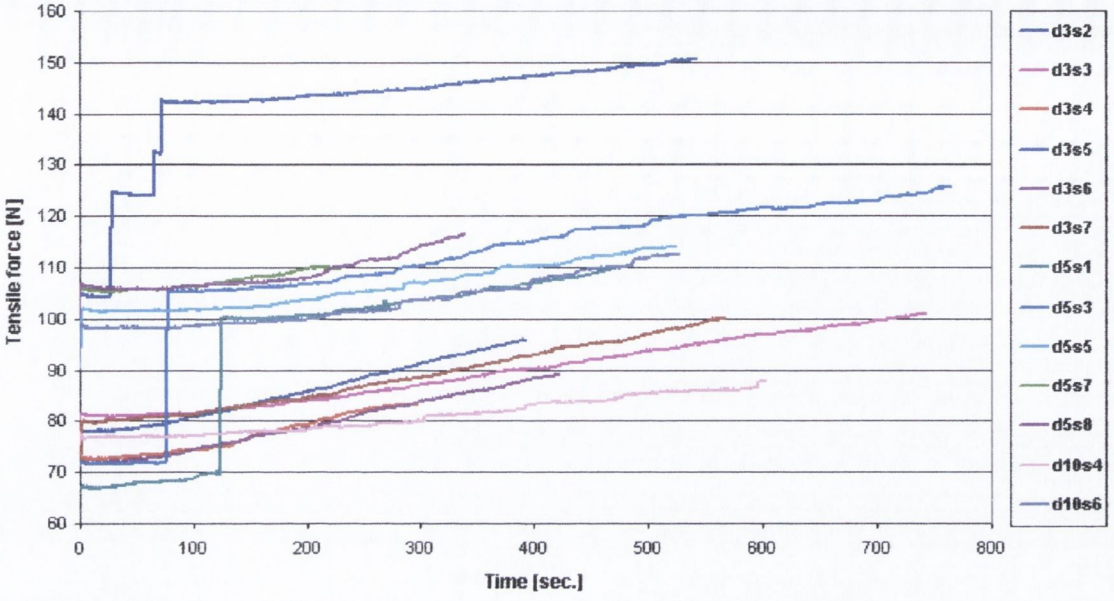

Fig. 4-12 Readings from loadcell for longitudinal notches

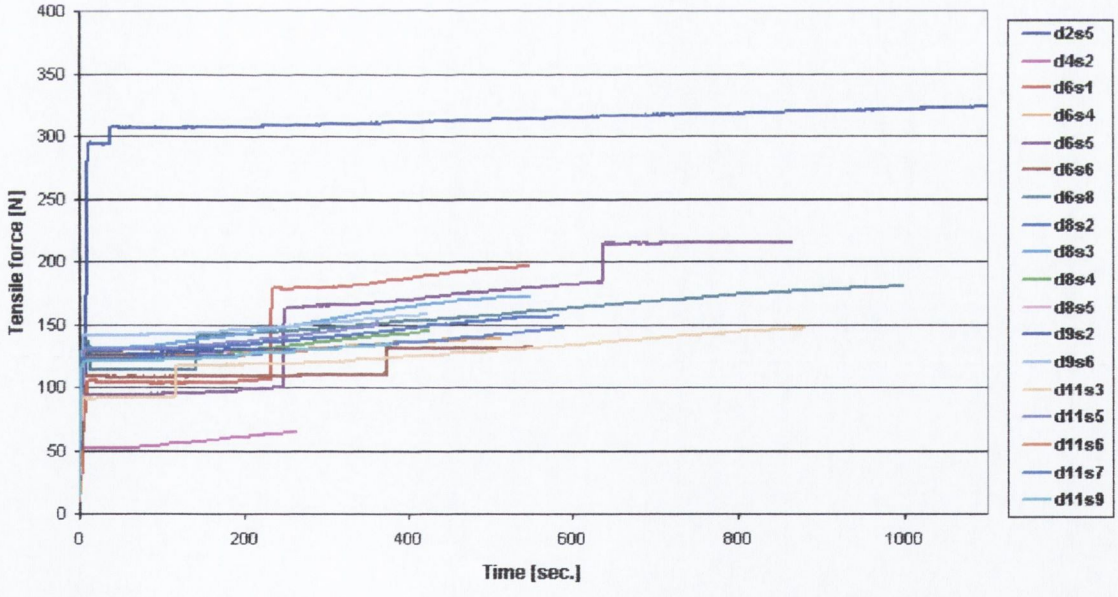

Fig. 4-13 Readings from loadcell for transverse notches

	Longitudinal notches	*Transverse notches*
Mean crack initiating force (N)	95.1 N, (S.D. 32.8) Min = 71.7 N Max = 142.3 N	145.7 N, (S.D. 53.4) Min = 51.5 N Max = 320.5 N
Mean stress at initiation (MPa), (Force / area)	5.1 MPa (S.D. 0.85)	19.6 MPa (S.D. 6.4)

Table 4-1 Analysis of the readings from the loadcell

As the crack starts growing one would expect to see a reduction in force measured by the loadcell. From the graphs above it is evident that this did not occur, in fact a gradual increase always occurred. In order to ascertain what causes this increase in force, un-notched bone specimens where wrapped in cling film. This allowed the UV-light to penetrate through, but kept the moisture content of the specimens constant. Tests were run for 15 minutes, which is equal to the testing time used in the notched specimens. All specimens without cling film showed an increase in force over time as indicated by the blue lines in Fig. 4-14, whereas the specimens wrapped in cling film showed hardly any change in force. It was therefore concluded that the increase was due to the drying of the bone during testing.

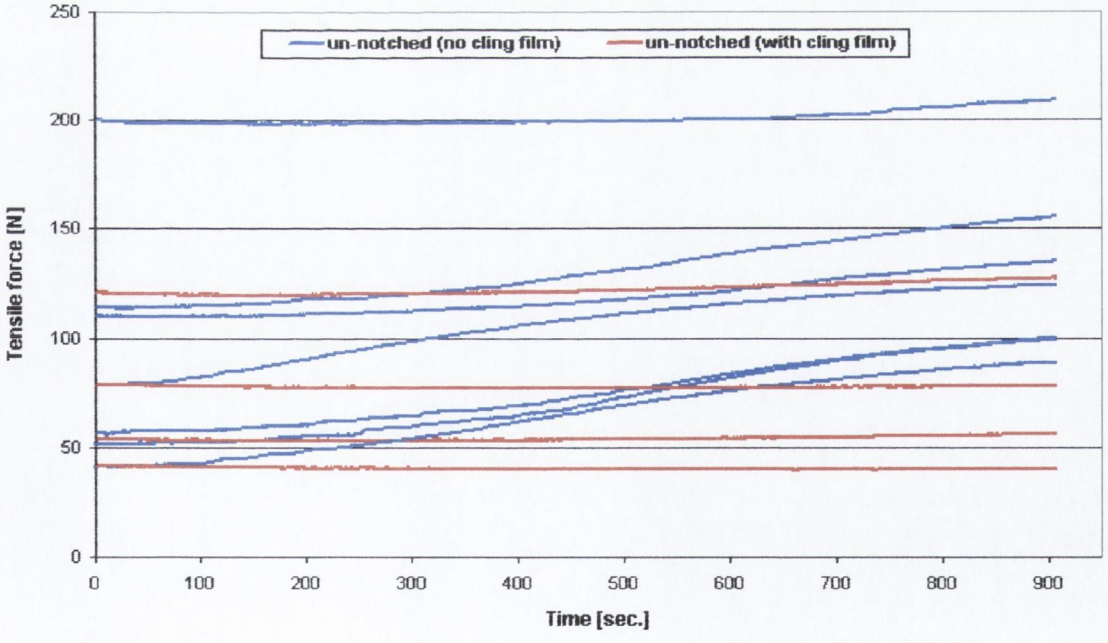

Fig. 4-14 Testing un-notched specimens with and without cling film

4.3.1.2 Crack growth observations

Crack lengths varied from 113 to 891 μm for longitudinal notches, and from 190 to 1345 μm for transverse notches. Crack paths ranged from 113 to 943 μm and 237 to 1547 μm for the respective groups. This is well within the range of typical crack lengths found *in vivo*. Cracks could have already started to grow before the observation was made. This is a common problem in fracture mechanics. Therefore the term 'initial' might be misleading. Testing had to be stopped once cracks obtained lengths that were longer than 1400 μm (angle dependant). Longer cracks were outside the field of vision, and in some cases crack growth rates were so high that specimens completely fractured which made them unsuitable for analyses of ruptured cell processes. During crack growth, various sub-stages were observed as shown in Fig. 4-15, indicated by the arrows.

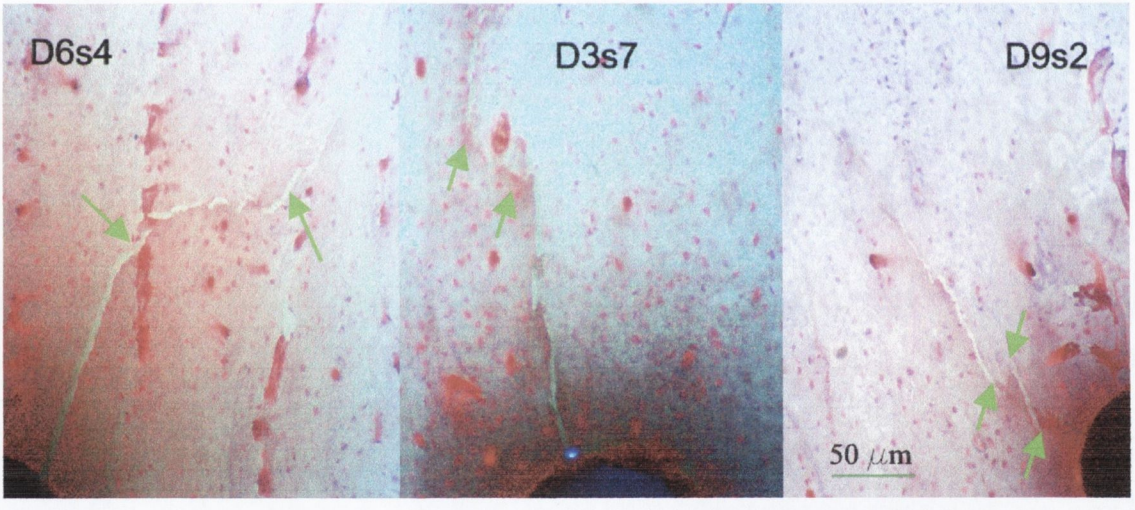

Fig. 4-15 Examples of sub-stages in specimens D6s4, D3s7 and D9s2

These sub-stages occurred when the crack was deflected by, presumably, a microstructural feature, causing the crack to change direction. This change in direction caused the surfaces to come into contact (see green arrows in Fig. 4-15), which in some cases clearly limited the amount of displacement between the crack faces. However the majority of cracks were found to continue in the direction in

which they originally started. Cracks which radically changed direction during propagation, occurred only in 4 out of 31 specimens (D3s7, D5s7, D6s4 and D9s2).

Although the majority of cracks did not show any deviation from their initial crack growth direction, SEM revealed more information that cannot be observed at a hundred times magnification. The images shown below were taken with a Hitachi S-3500N scanning electron microscope. Fig. 4-16 shows a SEM image at 50 times magnification. The crack appears to be straight and seems to have stopped at a cavity, indicated by the second black arrow.

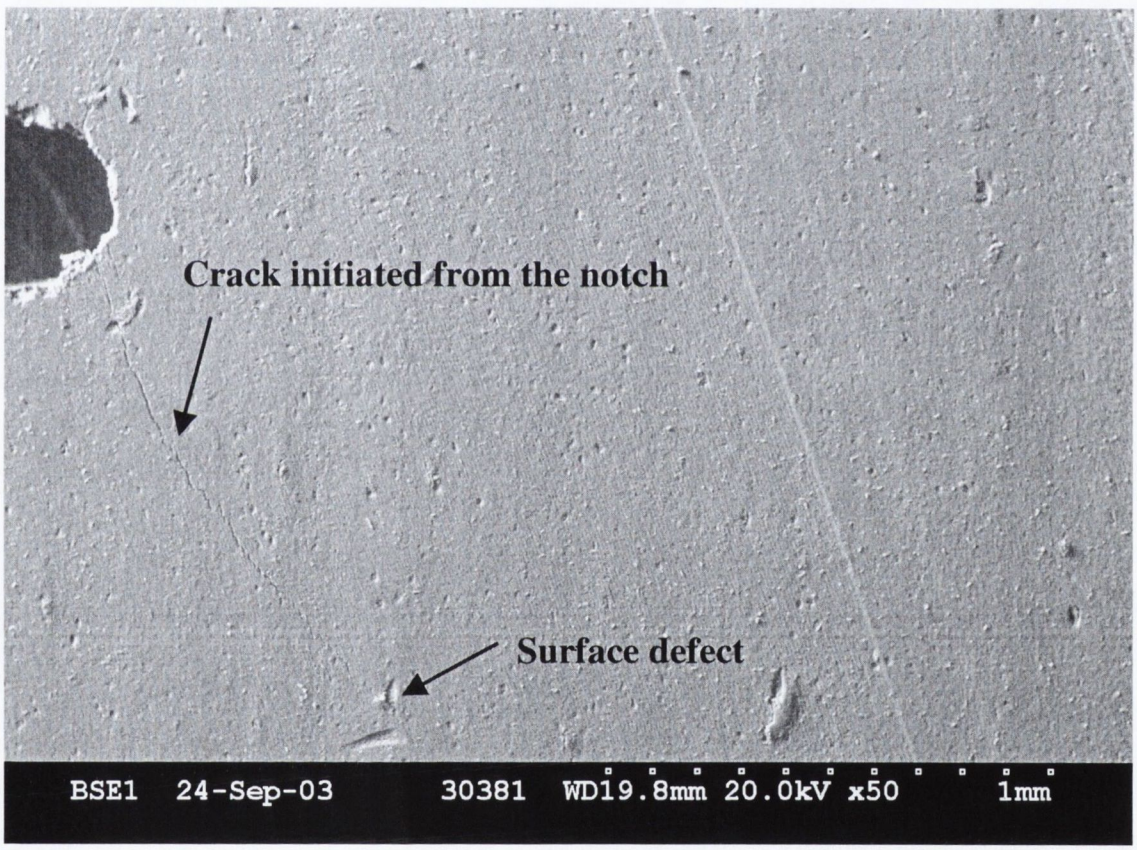

Fig. 4-16 Example of crack initiated from notch (taken from specimen D8s2)

Cavities are known to attract cracks in some materials, due to stress concentrations. However, using the SEM revealed that this is not always true. In Fig. 4-17 the crack is deflected from its original course. It might be argued that the feature responsible for this deflection might lie within the depth of the bone. It does not however,

explain why the crack did not choose to alter its course towards the two other features, lying on either side of the crack.

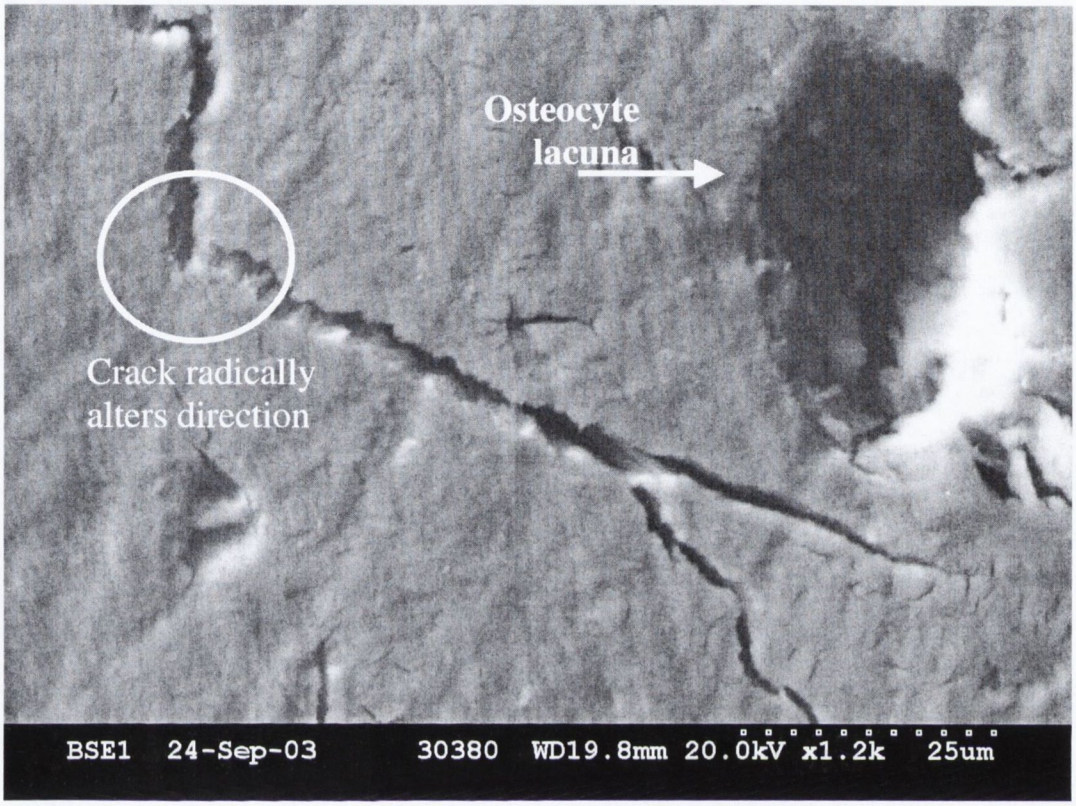

Fig. 4-17 Diverted crack near the tip of specimen D9s7

This is in contrast to Fig. 4-18, in which a crack crossed an osteocyte lacuna. Surrounding this lacuna secondary microdamage can be observed, indicating that the local material failed to cope with the local strains. The second lacunae also shows signs of secondary damage, resulting in the initiation of a microcrack.

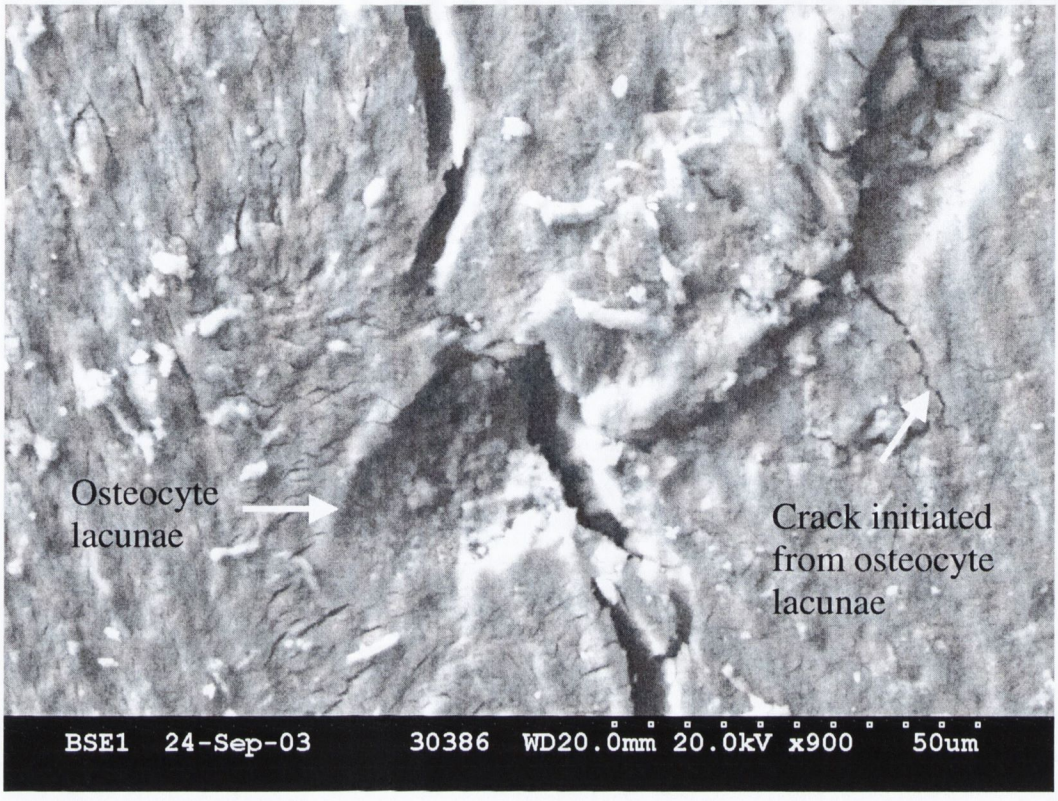

Fig. 4-18 Crack path crosses an osteocyte lacunae (specimen D8s2)

Both cracks still appear to take a straight path, in which the two crack faces are free to move. At higher magnifications it was found that this was rather deceptive. In Fig. 4-19 the two crack faces seem to interact with each other, providing a possible mechanism to prevent crack displacements. Consistent with the images above, secondary microdamage is present, suggesting that the main microcrack increases the local strains beyond its limits. This is a good example of what Ritchie (1999) calls an 'extrinsic toughening mechanism'. The crack face displacements are compromised making crack growth more difficult.

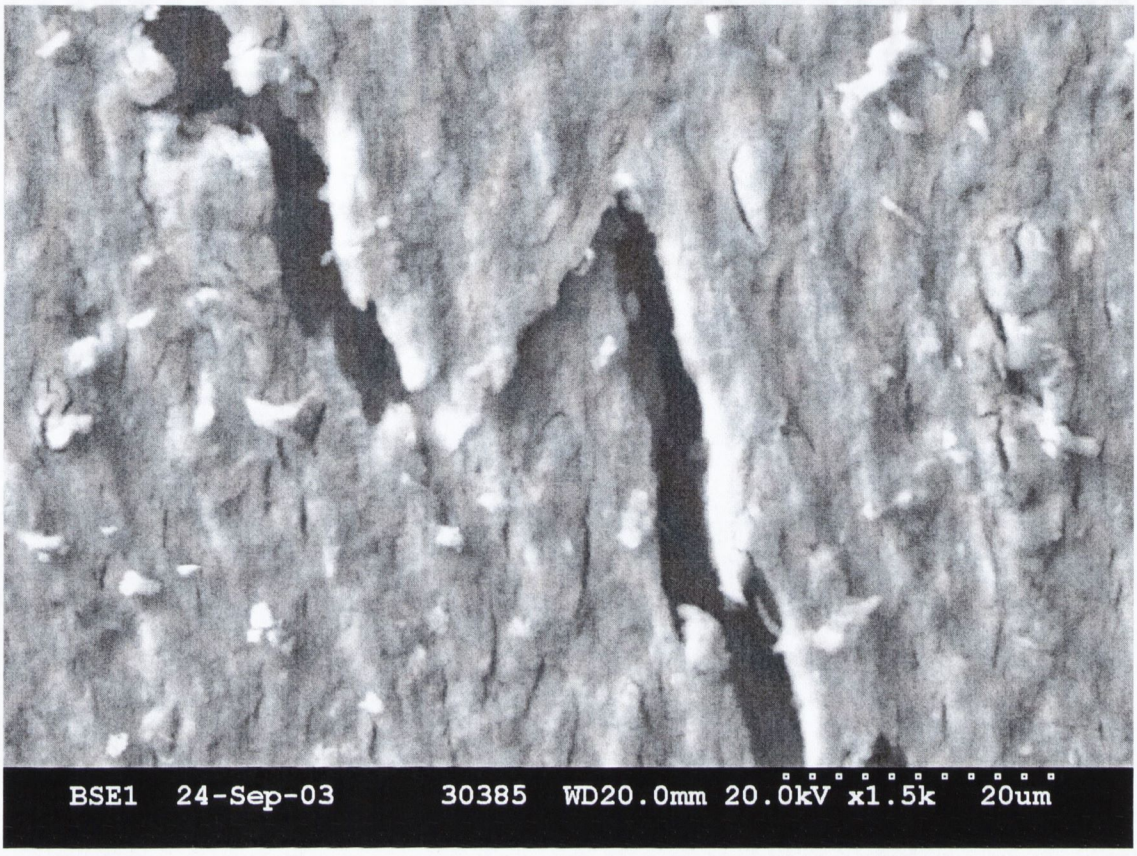

Fig. 4-19 Influence of the microstructure on the crack face displacements (specimen D8s2)

Although the crack seems to be one continuous straight line, closer examination shows that terraces occur ahead of the crack tip (Fig. 4-20), indicating that the material fails ahead of the crack. As the crack propagates, these terraces join up forming the new extension of the main crack which initiated from the notch.

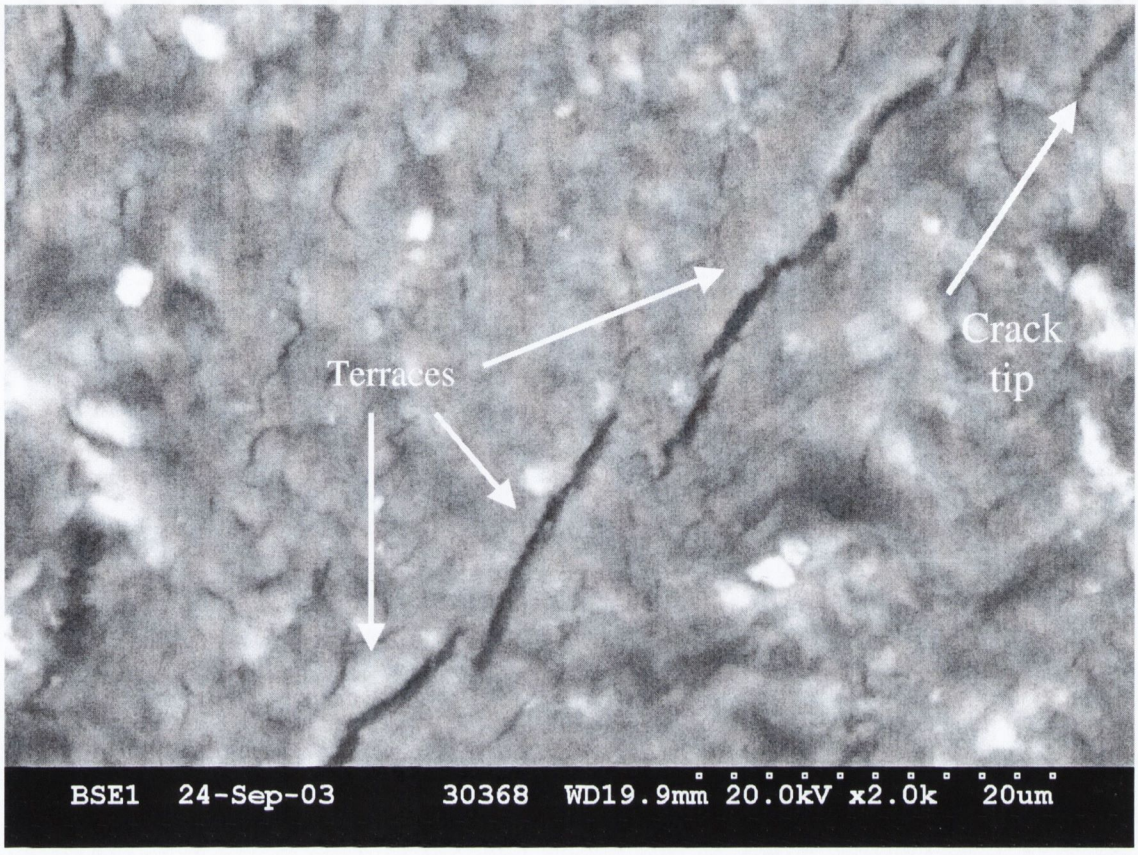

Fig. 4-20 Terraces near the crack tip of specimen D8s3

This is essentially damage ahead of the crack, though it could be connected to the main crack below the surface.

4.3.1.3 Crack growth angle

Table 4-2 records the angle of the main crack, which is defined as the angle between the crack and the longitudinal axis of the bone as shown in Fig. 4-21. The green arrows indicate the longitudinal axis of the bone and the red arrows show the loading direction.

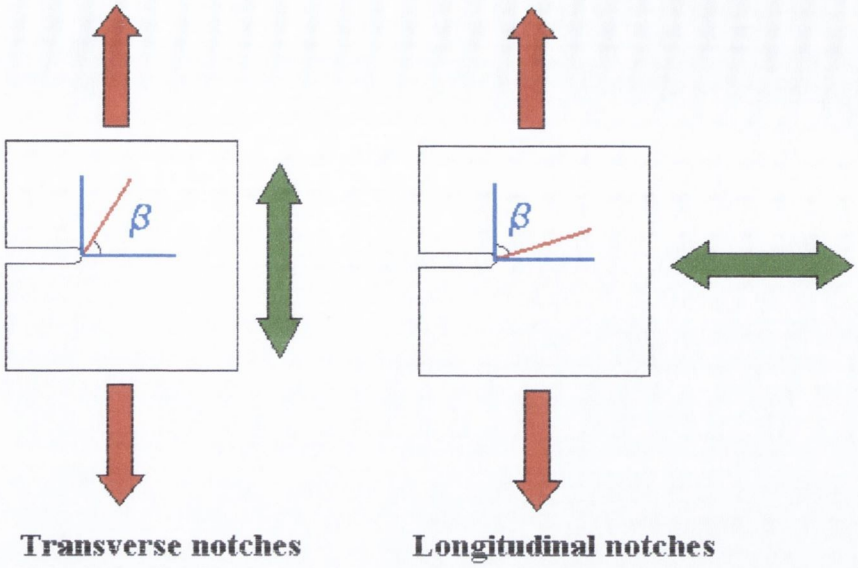

Fig. 4-21 Crack angle with respect to the longitudinal axis of the bone

	Longitudinal notches	Transverse notches
Mean crack angle (deg.)	80.56	53.6
S.D.	5.94	13.43
Maximum angle (deg.)	90	88.51
Minimum angle (deg.)	68.23	15.62

Table 4-2 Crack growth angles (β)

The crack angles measured for the longitudinal notches were rotated over 90 degrees to relate the angle back to the natural orientation in bone.

4.3.1.3 Crack displacements due to angle

Under uniform stress, the crack angle will influence the amount of opening and shear displacements within the crack faces. In Fig. 4-22, the total maximum displacement is plotted as a function the kinked crack angle. The total maximum displacement is defined as:

$$CD_{total_max} = \sqrt{2\delta T^2_{measured} + 2\delta S^2_{measured}} \qquad \textbf{Equation 4-1}$$

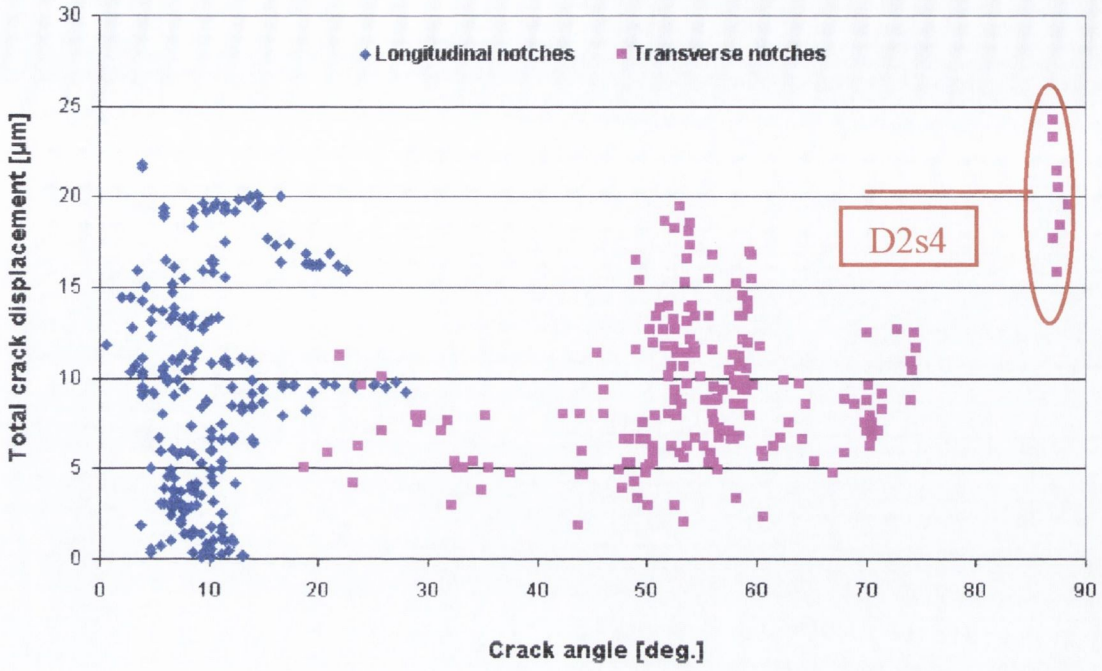

Fig. 4-22 Maximum crack displacement as a result of crack angle

Two peaks can clearly be distinguished. The first peak appears for crack angles ranging between 5-10 degrees. This is to be expected since the crack growth direction is approximately perpendicular to the loading direction. The second peak appears between 50-65 degrees. Here a mixture of mode I and II is present, except for specimen D4S2, which shows displacements that are extremely high, as shown in Fig. 4-23.

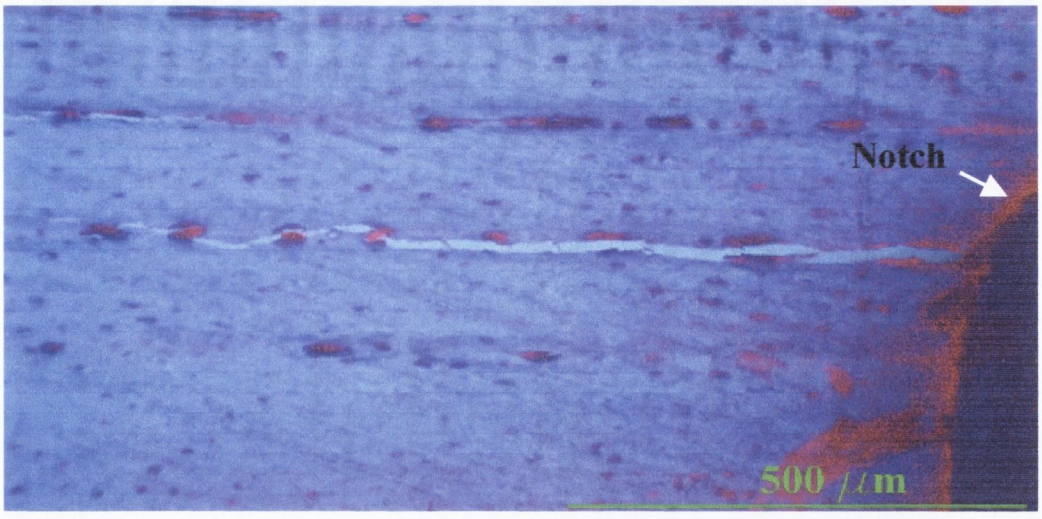

Fig. 4-23 Specimen D4s2, high COD and CSD values at 90° crack angle

4.3.1.4 Crack growth rate during testing

Fig. 4-24 shows a plot of crack length versus time for a selection of specimens. It shows that there is an initial jump indicating rapid crack growth, which stabilises within the first minute of testing.

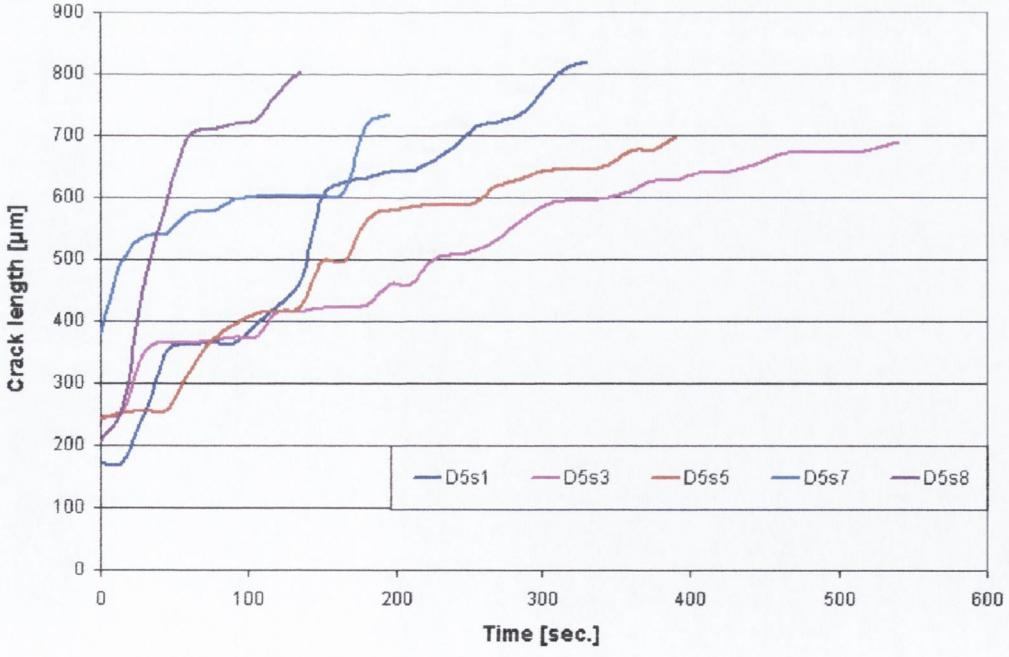

Fig. 4-24 Crack length versus time

The crack growth rates for both groups of specimens showed similar patterns (see Fig. 4-25). Since the images were taken at intervals of 15 seconds, data can only be analysed at these given points during testing. This means that crack growth rate (*da/dt*) could be several orders of magnitude higher than found during these tests.

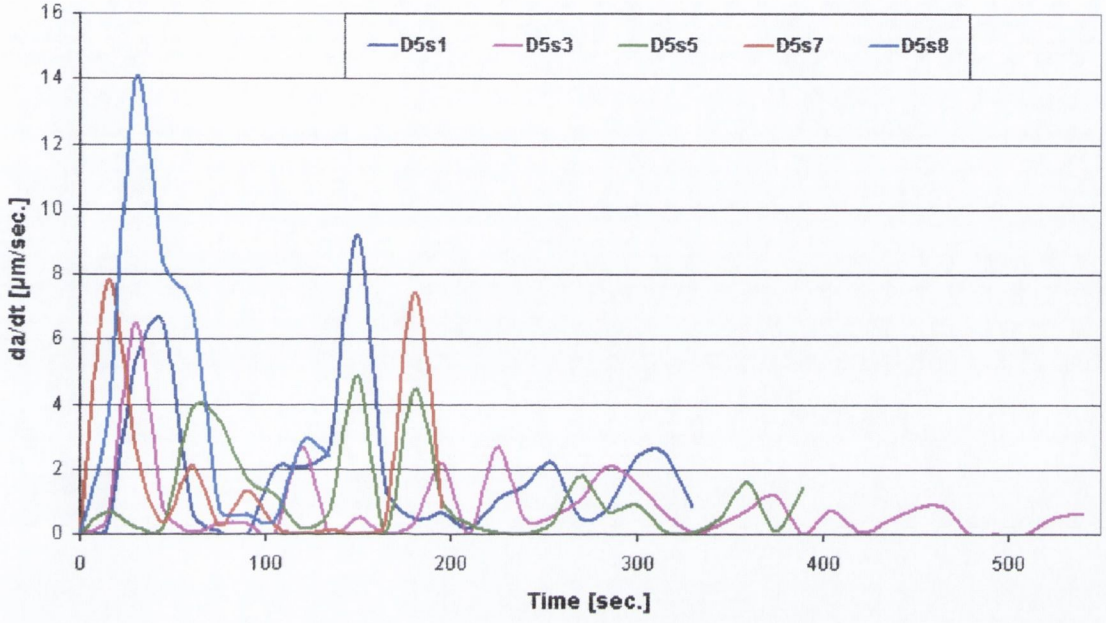

Fig. 4-25 Typical behaviour of crack growth during testing

This crack growth behaviour has been suggested to be the effect of microstructural features in bone (Corondan and Haworth, 1986; Schaffler *et al.*, 1995b; Norman and Wang, 1997; O'Brien, 2002). In Fig. 4-26, specimen D10s4 clearly showed canals that crossed the path. The size of these canals was measured to be 18-23 µm in diameter, the typical size of Volkmann's canals.

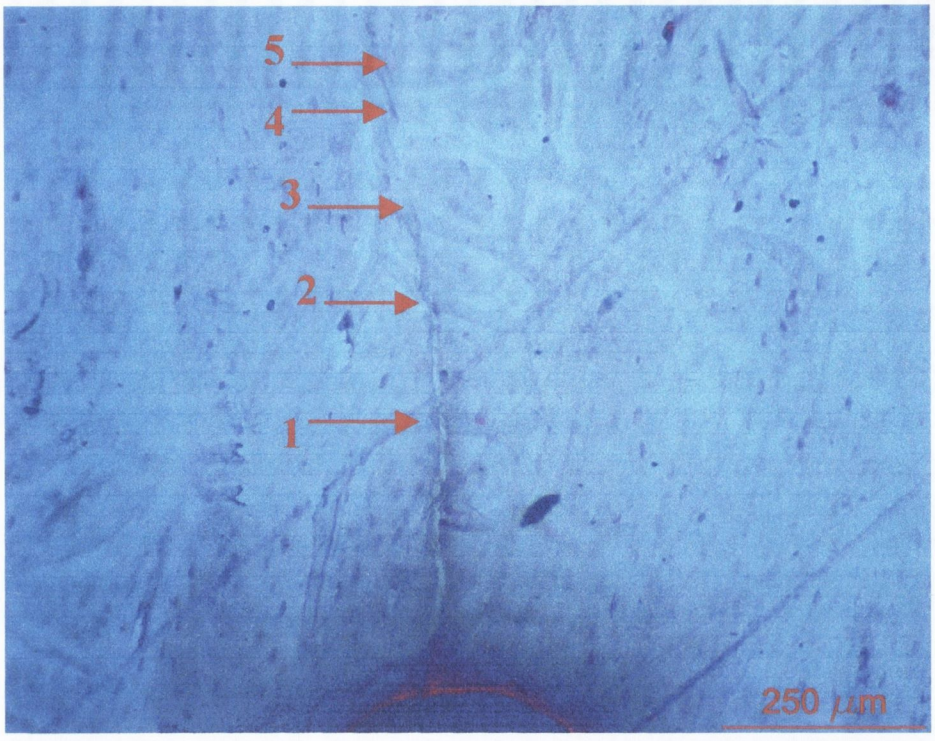

Fig. 4-26 A crack crossing Volkmann's canals (specimen D10s4)

That these features interfered with the cracks growth rate as can be seen in Fig. 4-27.

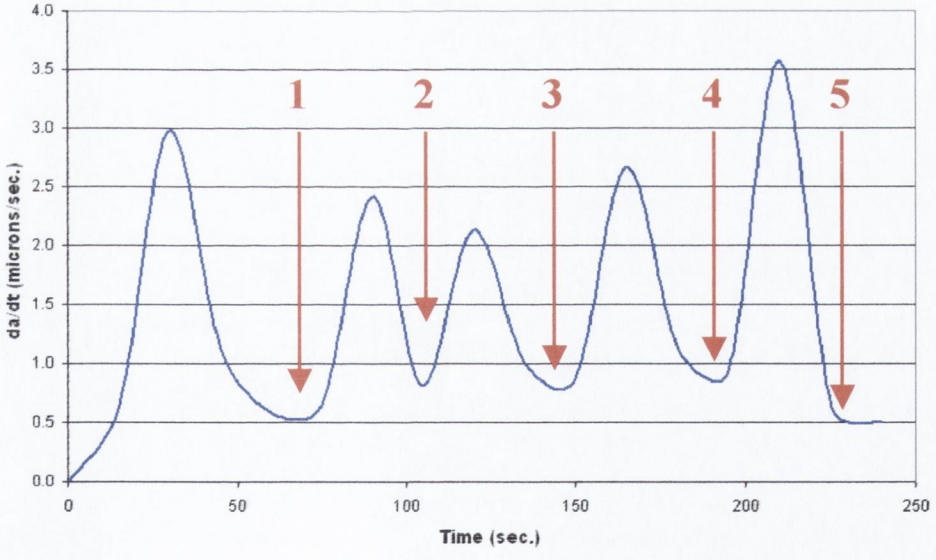

Fig. 4-27 Crack growth rate specimen d10s4, showing location of features

The spacing between these individual features are shown in Table 4-3.

Section	Spacing [μm]
Notch to 1	320.67
1 to 2	125.65
2 to 3	74.7
3 to 4	108.4
4 to 5	59.18

Table 4-3 Distance between feature 1 to 5 (specimens d10s4)

If the microstructure plays a role in the crack growth rate, one would expect that Haversian and Volkmann's cannels would stop or divert cracks. This would mean that if $da/dt \rightarrow 0$, such a boundary would be encountered. The drops in da/dt had a mean spacing of 89.9 μm (S.D. 108) for specimens with longitudinal notches and 139 μm (S.D. 97.6) for transverse notches.

Furthermore, observations were made that as the crack growth rate decreased and increase in crack opening and shear displacements occurred. Once crack growth rates increased, the opposite in COD and CSD was observed as shown in Fig. 4-28.

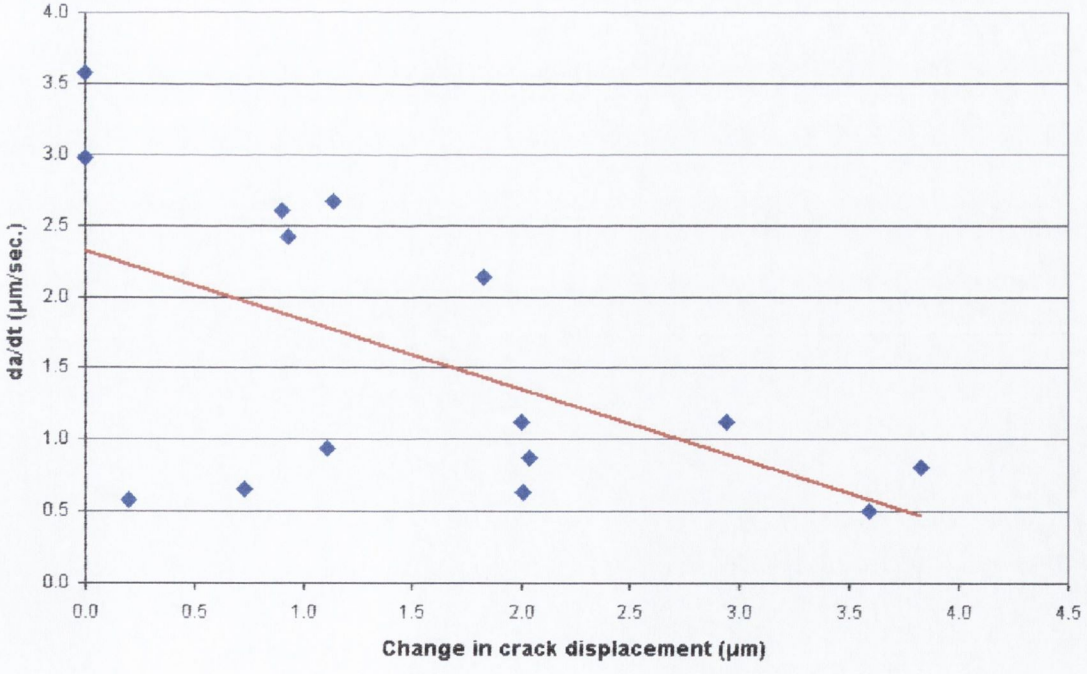

Fig. 4-28 Changes in crack growth rate as a result of changes in crack displacements (specimen D10s4)

Besides assessing the individual measurements from which *da/dt* were determined, the mean crack growth rate can be investigated. The mean crack growth rate was defined as the length of the crack at the end of the test minus the crack length at the beginning of the test divided over the time duration of the test.

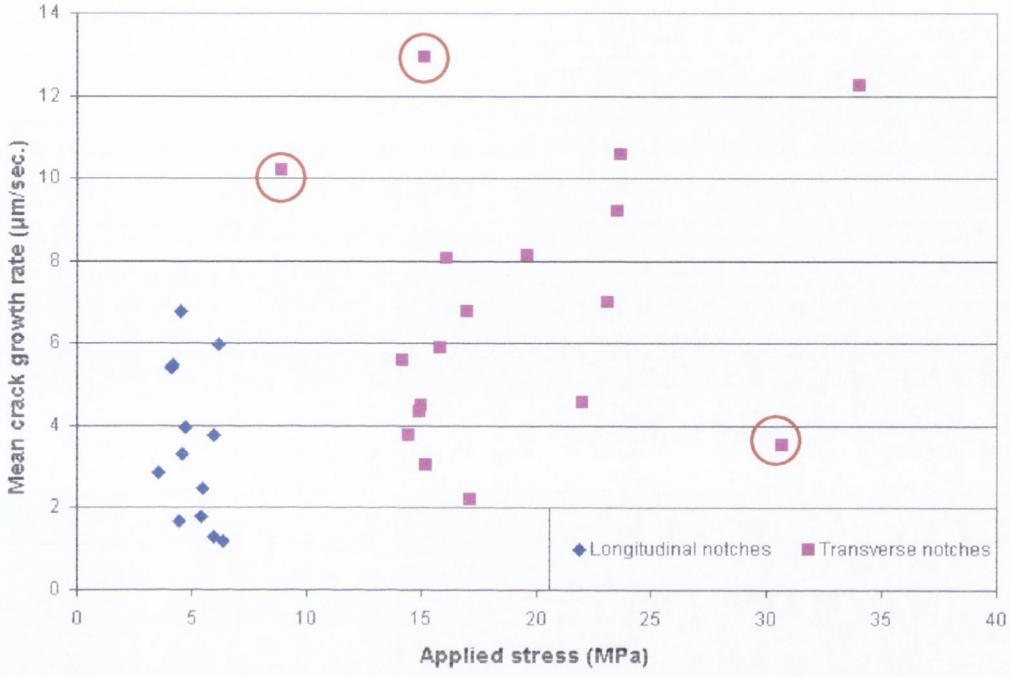

Fig. 4-29 Mean crack growth rate versus applied average stress

For both groups, longitudinal and transverse notches, higher stresses cause higher crack growth rates (*da/dt*), however there is some scatter. Three specimens behave differently, identified with the red circles in Fig. 4-29.

The reason why these specimens behaved in a dissimilar fashion might lie in the effect of the crack angle. Lower crack angle will result in a higher mode I, which is known to cause higher crack growth rates. A plot of crack angle versus mean crack growth rate can be found in Fig. 4-30.

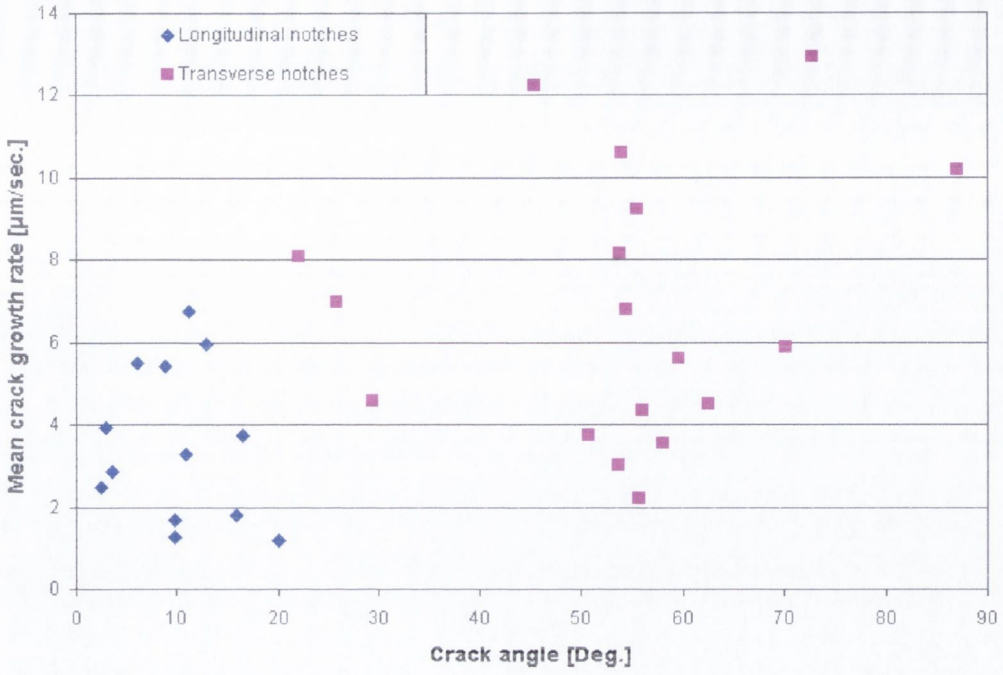

Fig. 4-30 Crack angle versus mean crack growth rate

The mean crack growth rate for specimens with longitudinal notches was between 1 and 7 µm/sec. This occurred for cracks ranging between 0 and 20 °, which does not explicitly show that the crack angle is a major influence since it is well known that the osteon direction usually varies in this range (Martin and Burr, 1989). For specimens with transverse notches, the majority of specimens fell in the range of 50-70°.

4.3.2 Ruptured cell processes

In Chapter 3 a model was presented from which it was concluded that there are theoretical grounds to assume that damage to cell-processes ought to be expected. Even at physiological stress levels, crack displacements were predicted to be sufficient to cause them to rupture, which might result in a signal to initiate a (re-) modelling stimulus. In general, Scanning Electro Microscopy (SEM) was performed in order to analyse the effect which cracks had on the local microstructure. However, to assess if crack displacements are able to break or disrupt canaliculi in bone, SEM

can only partly provide answers. The crack faces can be investigated in order to see if there is organic matter crossing from one side to the other, but no conclusions can be drawn as to whether these are collagen fibres or cell processes. This is illustrated in Fig. 4-31 where a SEM image is shown which clearly illustrates that fibres / tubes cross between the crack faces.

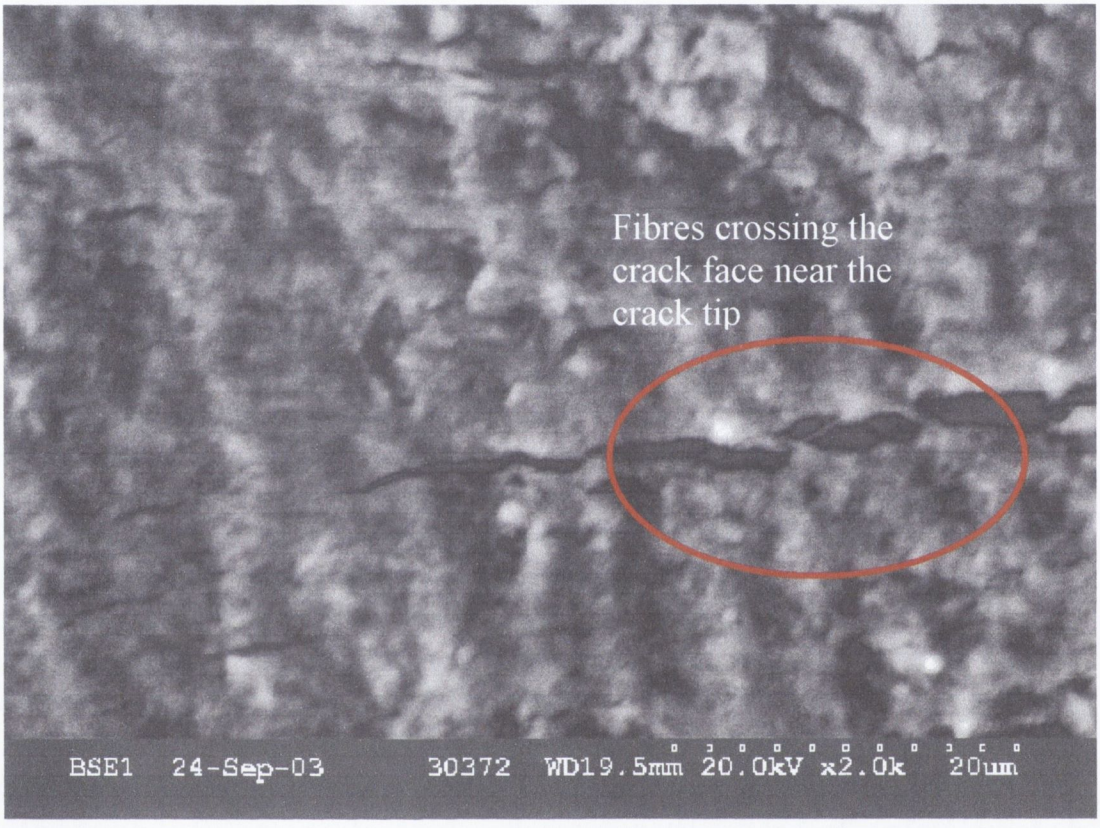

Fig. 4-31 SEM image of the specimen D5s6 at the crack tip (x2000 mag.)

In order to distinguish if the fibre/ tubes observed in Fig. 4-31 are comprised of collagen or if they are part of the cytoskeleton (contain actin filaments) specific staining techniques can be applied.

The combination of antibody staining and confocal microscopy (Zeiss LSM 510 META, Zeiss, Germany) allows scanning through surfaces, resulting in highly detailed images. Fig. 4-32 shows an osteocyte that is stained with Alizarin.

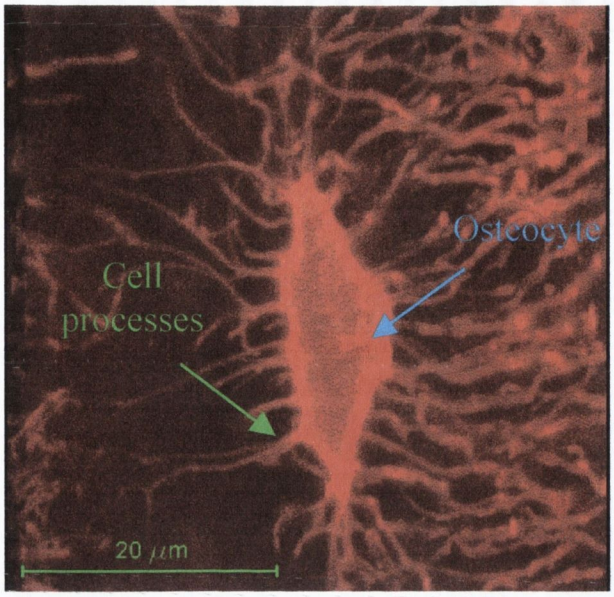

Fig. 4-32 Osteocyte stained with Alizarin

This method is able to provide the amount of detail required to investigate if there is damage to the cell-processes indicated by the green arrows in Fig. 4-32. The common procedure for hard non-decalcified tissue is to take a monochrome picture, which is overlaid with the image containing the stained feature as shown in Fig. 4-33.

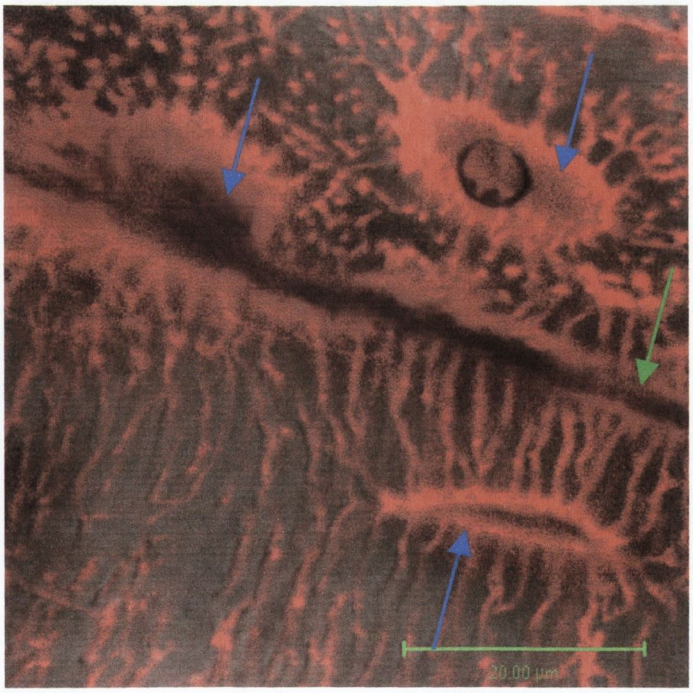

Fig. 4-33 Ruptured cell-processes (scale bar 20 µm)

The image shows three osteocytes indicated by the blue arrows. The crack has travelled through the lacuna of one osteocyte. The osteocyte however appears to have remained intact. The majority of processes are broken by the crack, although some processes seem to cross the crack faces (green arrow). This pattern was seen in all slides examined. Near the origin of the crack (notch), all canaliculi were found to be broken (see Fig. 4-34), whereas near the crack tip the majority of the processes were still intact.

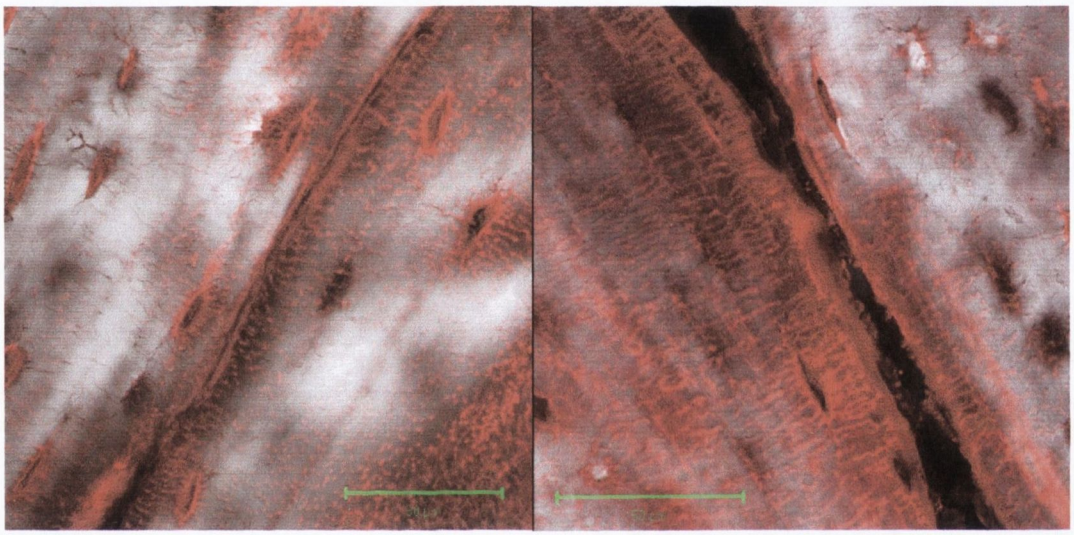

Fig. 4-34 Ruptured cell processes between the notch and the centre of the crack (scale bar 50 µm)

4.3.3 Theoretical analysis

In the following paragraphs crack growth will be analysed, comparing the difference between longitudinal and transverse notches regarding crack initiation, stress intensity factors, crack opening and shear displacements which occurred during the experiments. Existing fracture mechanics solutions and finite element analysis will be used in order to assess if these displacements can be predicted and if linear elastic fracture mechanics is adequate to describe these trends. The major errors, which occur as a result of the dynamic crack growth behaviour, will be analysed in order to

improve existing techniques. Finally, all methods will be compared to determine which method works best for bone.

4.3.3.1 Stress intensity analyses

The stress intensity factor at crack initiation for longitudinal and transverse notches, was calculated using:

$$K = F\sigma\sqrt{\pi a}$$ **Equation 4-2**

Here a is the notch length, σ is the remote applied stress (force/area) and F is the geometrical correction factor that can be calculated using (Janssen *et al.*, 2002):

$$F = 1.12 - 0.231\left(\frac{a}{W}\right) + 10.55\left(\frac{a}{W}\right)^2 - 21.72\left(\frac{a}{W}\right)^3 + 30.39\left(\frac{a}{W}\right)^4$$ **Equation 4-3**

For all tested specimens, this value was found to be 1.12, meaning that a/W is relatively small. The stress intensity factors at crack initiation are summarised in Table 4-4. Depending on the notch depth and its radius, it can be valid to use the 'Crack-like' approach to calculate the stress intensity factor for notches instead of the 'Notch-like' approach. The transition between Crack-like and Notch-like (blunt) notches can be calculated using the following equation:

$$\left(\frac{D}{a_0}\right) = \left[\left(2\sqrt{\frac{D}{\rho}}\right) + 1\right]^2$$ **Equation 4-4**

Where D is the notch depth, a_0 the fictitious crack length and ρ is the notch radius. The transition occurs around $D/a_0=3$, which should be seen as an approximation (Taylor, 2001). Since $D>>\rho$ (all specimens had notch depths bigger than the notch radius) the crack-like method can be applied. A summary of these results can be found in Table 4-5.

Specimen	*Direction*	*K crack initiation MPa\m*	*Specimen*	*Direction*	*K crack initiation MPa\m*
D3s2	L-notches	0.67	D2s5	T-notches	2.16
D3s3	L-notches	0.45	D4s2	T-notches	0.85
D3s4	L-notches	0.43	D6s1	T-notches	2.86
D3s5	L-notches	0.48	D6s4	T-notches	1.83
D3s6	L-notches	0.45	D6s5	T-notches	3.1
D3s7	L-notches	0.47	D6s6	T-notches	1.44
D5s1	L-notches	0.62	D6s8	T-notches	1.54
D5s3	L-notches	0.65	D8s2	T-notches	2.05
D5s5	L-notches	0.6	D8s3	T-notches	2
D5s7	L-notches	0.64	D8s4	T-notches	2
D5s8	L-notches	0.64	D8s5	T-notches	2.19
D10s4	L-notches	0.41	D9s2	T-notches	1.97
D10s6	L-notches	0.53	D9s6	T-notches	1.6
			D11s3	T-notches	1.72
			D11s5	T-notches	1.84
			D11s6	T-notches	1.86
			D11s7	T-notches	1.79
			D11s9	T-notches	1.85

Table 4-4 Stress intensity factors at crack initiation

	K_0 L-notches	K_0 T-notches	$Stress_0$ L-notches	$Stress_0$ T-notches
Mean	0.55	1.99	5.11	19.59
S.D.	0.09	0.50	0.86	6.40
Max	0.67	3.10	6.38	34.13
Min	0.41	0.85	3.56	8.94

Table 4-5 Stresses and stress intensity factors during testing

The mean stress intensity factor for crack initiation from longitudinal notches was found to be approximately four times smaller than for specimens that had transverse notches. The values quoted in Table 4-5 are the thresholds for slow crack growth.

For crack growth to occur, the stress intensity factor has to be higher than the threshold value of the material. If cracks are slowed down or diverted, energy is dissipated. In order to continue propagation, loads have to increase. For all tested specimens, stress intensity factors were calculated during the process of growth.

Stress intensity values were calculated using two methods, one that is commonly used for kinked cracks, and one that uses the crack opening displacement and shear displacement.

Method 1: Standard Fracture Mechanics (Chen, 1999)

$$K_I = \sigma\sqrt{\pi C}\,\cos^2(\beta) \qquad \textbf{Equation 4-5}$$

$$K_{II} = \sigma\sqrt{\pi C}\,(\sin(\beta)\cos(\beta)) \qquad \textbf{Equation 4-6}$$

$$C = \frac{\left(Nl + l_{kink}\,\cos(\beta)\right)}{2} \qquad \textbf{Equation 4-7}$$

In which the representative crack length is comprised of the notch length *Nl* and the length of the kinked crack L_{kink} (by which the crack originating form the notch is meant).

Method 2: Crack opening displacement (Seif and Dasari, 2001):

$$K_I = \frac{(COD)E\sqrt{\pi C}}{4C} \qquad \textbf{Equation 4-8}$$

$$K_{II} = \frac{(CSD)E\sqrt{\pi C}}{4C} \qquad \textbf{Equation 4-9}$$

This method uses the crack opening- (COD) and shear- displacements (CSD) to predict the stress intensity factors. In Fig. 4-35 the total stress intensity factors (square root of sum of squares) that were calculated with the standard method are displayed with the dashed lines. The solid lines in Fig. 4-35 show the results when the COD and CSD are used.

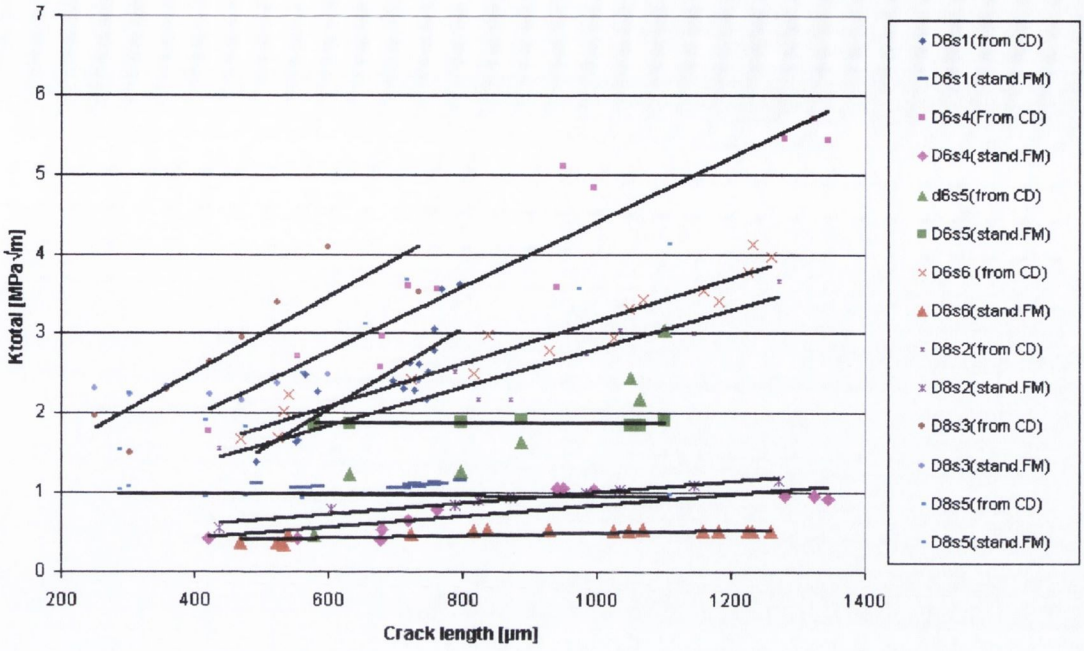

Fig. 4-35 Stress intensity factors during crack growth using standard fracture mechanics and crack displacements

Crack growth rates increased followed by a decrease and vice versa. In order to continue to dissipate energy during this process, cracks can achieve this by either changing direction or by increasing COD and CSD. For cracks to propagate the stress intensity based method, states that the stress intensity factor is required to be higher than the threshold value of the material. The effect of crack deflections, the dynamic nature and changes in COD and CSD are generally ignored.

The stress intensity values for similar specimens were predicted to be far lower using the standard method than if the crack displacements are used. Using the crack displacements showed that as the crack progressed, stress intensity values decreased even though cracks continued to propagate. The graph below (Fig. 4-36) shows how the stress intensity factor changed during crack growth for a selection of specimens.

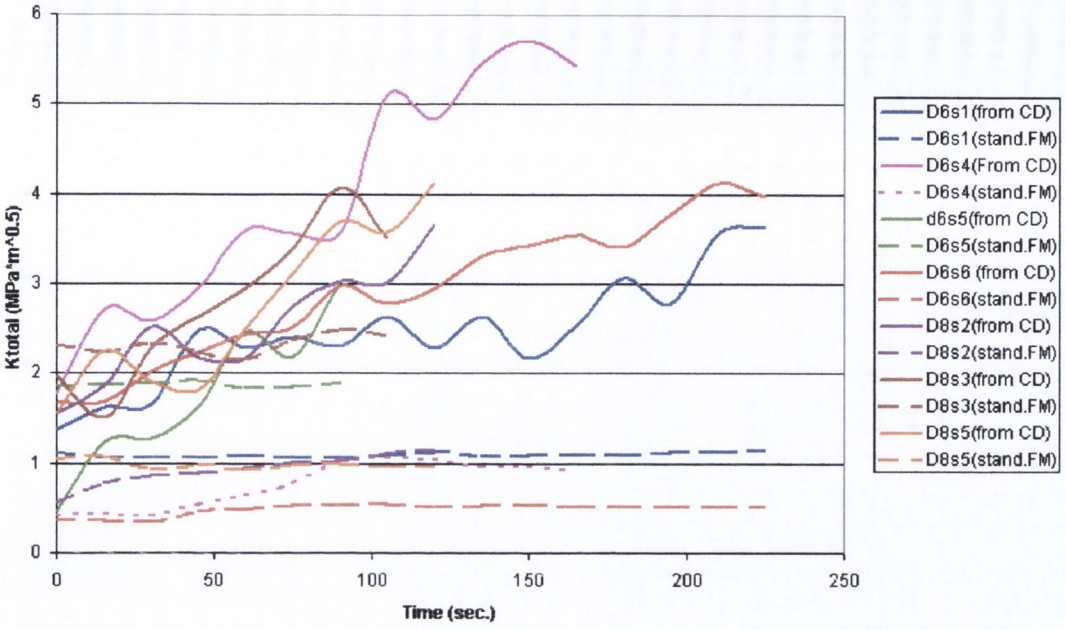

Fig. 4-36 Changes in stress intensity factor over time

4.3.3.2 Crack displacement analysis of tested specimens

Fracture mechanics analysis for edge cracks in finite plates subjected to various loading conditions has attracted some attention in the last decades because of its practical importance (Murakami, 1987). Although the crack displacement (*CD*) can be obtained by various methods, most of the solutions are in numerical form, especially for the crack face segment loading. The lack of closed form *CD*-solutions for edge crack geometries presents an obstacle to the crack-closure based growth analysis employing the modified Dugdale model (Liu and Wu, 1997). For simple edge cracks, standard analytical solutions tend to give a good indication. However, for crack geometries that are more complex, e.g. curved crack faces or kinked cracks from notches, these standard solutions break down. Two options remain to solve these situations, which are higher order complex integrals or approximate methods (Chen *et al.*, 1997; Liu and Wu, 1997).

4.3.3.2.1 Analytical estimation

To assess if crack displacements that were measured during crack growth could be predicted using LEFM, the following three methods were used:

Denda and Dong (1999):

The representative crack length for kinked cracks from notches is calculated as follows:

$$l_{rep.} = \frac{n_l + (a \sin(\phi))}{\sin(\phi)} \qquad \textbf{Equation 4-10}$$

Where n_l is the notch length, a is the kinked crack length, which is the length from the crack tip to the notch (point of initiation). The angle φ is the angle between the notch and the kinked crack. The crack opening- and shear- displacements are calculated using:

$$COD = F \frac{2\sigma}{E} \sqrt{\frac{l_{rep.}^2}{2} - a^2} \cos\left(\frac{\varphi}{2}\right) \cos\left(\frac{\varphi}{2}\right)$$

$$CSD = F \frac{2\sigma}{E} \sqrt{\frac{l_{rep.}^2}{2} - a^2} \sin\left(\frac{\varphi}{2}\right) \cos\left(\frac{\varphi}{2}\right) \qquad \textbf{Equation 4-11}$$

Chen *et al.* :

The representative crack length for kinked cracks from notches is calculated as follows:

$$l_{rep.} = nl + (a \cos(\phi)) \qquad \textbf{Equation 4-12}$$

The crack opening- and shear- displacements are calculated similarly to Denda and Dong (Equation 4-11).

Irwin (1957):

The representative crack length for kinked cracks from notches is assumed to be equal to a. Since the majority of methods use the notch length as an 'amplifying' factor, the standard method as described by Irwin might be represented in one

constant F. It follows that the crack opening- and shear- displacements are calculated using:

$$COD = F \frac{2\sigma a}{E} \cos\left(\frac{\varphi}{2}\right) \cos\left(\frac{\varphi}{2}\right) \qquad \textbf{Equation 4-13}$$

$$CSD = F \frac{2\sigma a}{E} \sin\left(\frac{\varphi}{2}\right) \cos\left(\frac{\varphi}{2}\right) \qquad \textbf{Equation 4-14}$$

The constant used for F are shown in Table 4-6:

Method	F
(Denda and Dong, 1999)	3
(Chen et al., 1997)	2
(Irwin, 1957)	6

Table 4-6 Constant used in analytical methods

The three methods were incorporated in a small Matlab program, in which data were imported from the main database. Both crack opening and shear displacements were calculated for transverse notches. The results for all tested specimens, using these three methods, are shown in Fig. 4-37 and Fig. 4-38.

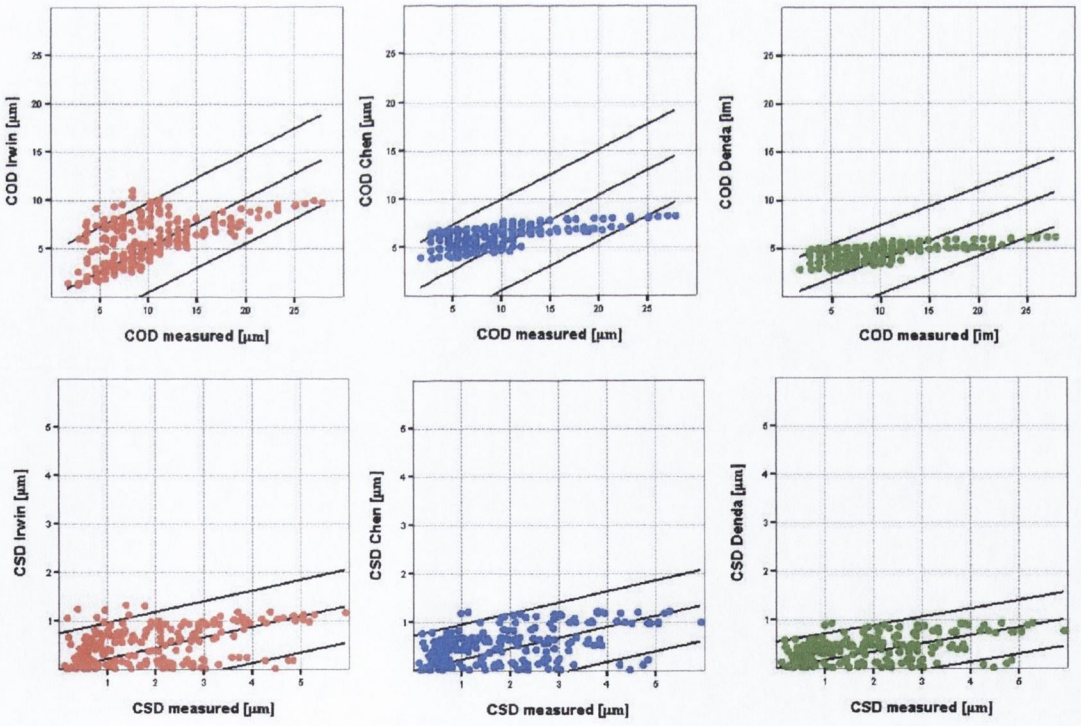

Fig. 4-37 Comparing the measured crack opening and shear displacement with analytical predictions in specimens with longitudinal notches (solid lines: mean and S.D.)

For longitudinal notched specimens, crack opening and shear displacement were clearly under predicted. The predicted shear displacements are small since the majority of cracks grew at an angle of 10 to 20 degrees resulting in a predominant opening mode. The crack opening displacements were predicted best using Irwin's model.

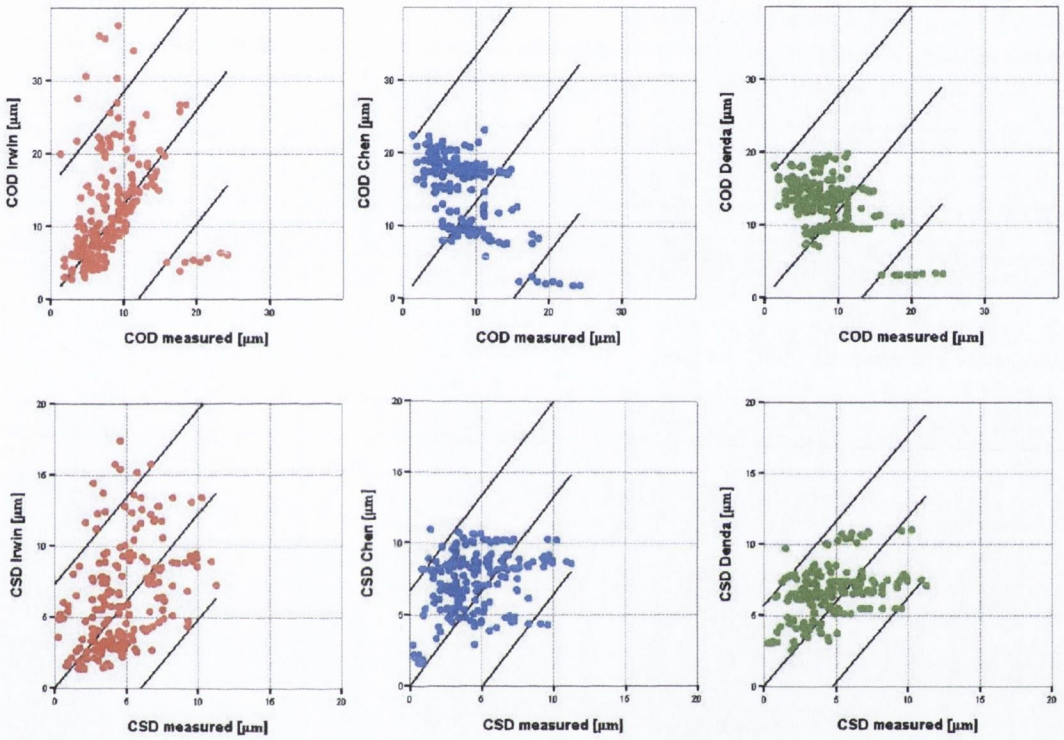

Fig. 4-38 Comparing the measured crack opening and shear displacement with analytical predictions in specimens with transverse notches (solid lines: mean and S.D.)

All three methods seem to predict the crack displacements satisfactorily for transverse notches. Irwin's method tended to over predict the crack displacements, whereas the results by Denda and Chen give approximately similar results. Although a lot of scatter was present, the method seems to give reasonable results.

4.3.3.2.2 Finite element analysis estimation

Since there are limitations to the analytical methods, 6 specimens with transverse notches, and 6 specimens with longitudinal notches were modelled in great detail, by which is meant that the exact path taken by the cracks was modelled using FEA. All models were made using a solid 6 node triangular element. For this analysis, orthotropic material properties were chosen.

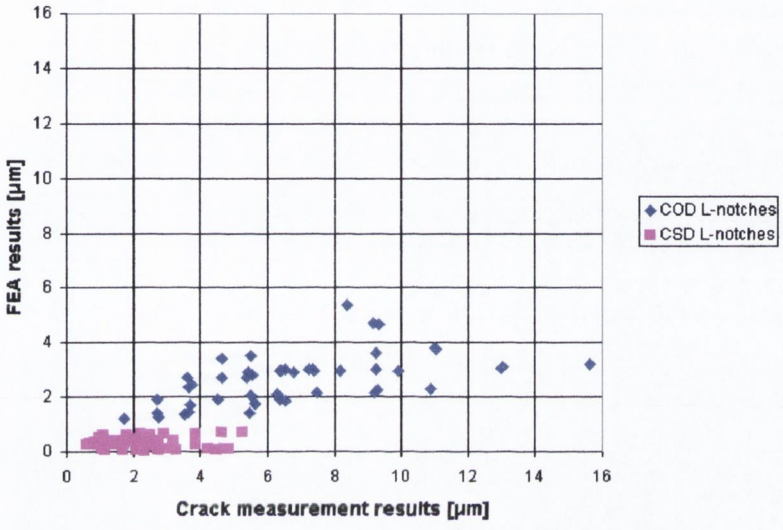

Fig. 4-39 Comparing the FEA results with the measured values for specimens with longitudinal notches

The cracks modelled for this exercise were D3s2, D3s3, D3s4, D3s5, D3s6, and D3s7. The values calculated for the crack opening and shear displacements for longitudinal notches are clearly under-predicted by the FEA, as shown in Fig. 4-39.

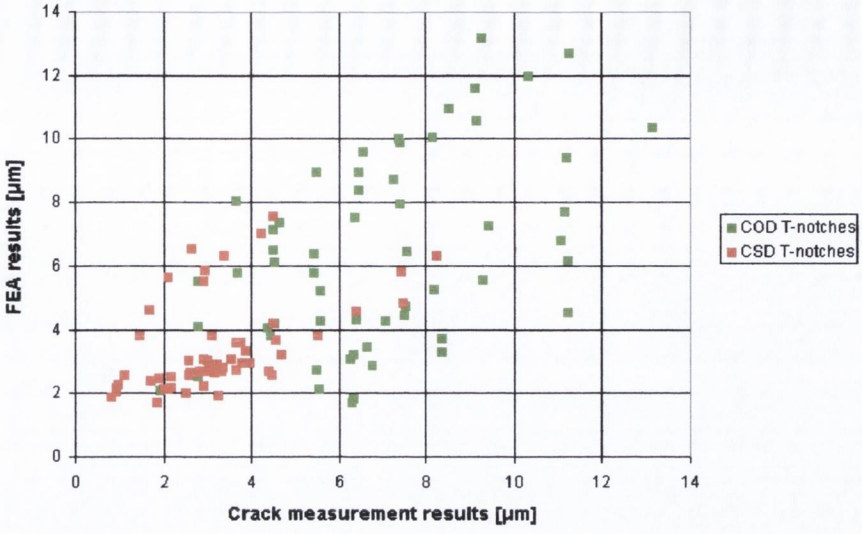

Fig. 4-40 Comparing the FEA results with the measured values for specimens with transverse notches

For longitudinal notches, the following specimens were used: D8s2, D8s3, D8s4, D8s5, D9s2, and D9s6. The crack opening and shear displacements predicted by the FEA-models shown in Fig. 4-40 indicates that this method can successfully be applied to this type of specimen.

Similar to the standard fracture mechanics approaches, finite element predictions of crack face displacements are better predicted for transverse notched specimens. These types of specimens are loaded in a manner similar to that which occurs *in vivo*, having crack growth directions similar to that, which have been described in the literature. However for the finite element analysis, only a selection of specimens were used in contrast to the analytical methods. If the crack opening and shear displacements predicted by the finite element models and standard fracture mechanics methods are compared it can be seen that similar results are obtained, as shown in Fig. 4-41

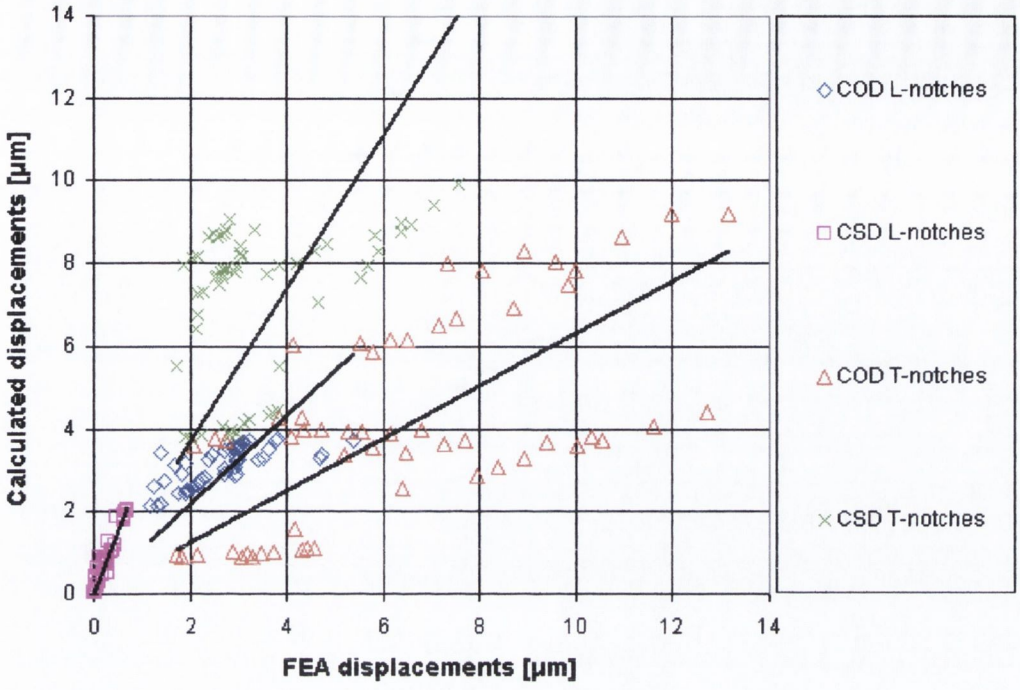

Fig. 4-41 Comparing crack displacements predicted by the FE-analysis with analytical solutions

Crack opening displacements are predicted to be higher using FEA, whereas crack shear displacements are predicted to be higher using the analytical methods. Therefore the smaller selection of specimens should have little effect of the final outcome as to which method works better.

4.3.3.3 Assessment of applicability of LEFM

In the analysis carried out so far the assumption was made that bone would behave in a linear elastic fashion. The fracture mechanics analysis carried out does not take account of the dynamic behaviour of the material during crack propagation. This mis-estimation of the COD and CSD, only for longitudinal notches, could be an effect of:

- A wrong estimation of the material properties
- Wrongly estimated COD and CSD values due to the crack growth rate
- Plastic deformation
- Damage formation at the crack tip

- Interface conditions between the lamellae; perhaps the results for the notches growing with the grain are not dominated by the Young's modulus of the material but depend on the cohesion of the lamellae

The influence of these points mentioned above will be discussed in the following paragraphs.

4.3.3.3.1 Effect of the material properties

If bone is seen as a laminate, in which the fibre orientation varies for different specimens, a new estimate can be made regarding crack opening and shear displacements. Therefore, the fibre orientation for a particular specimen needs to be known. Since it is well known that the crack growth direction in anisotropic materials is usually in the direction where symmetry of material properties are found, therefore the kink angle can be assumed to be the angle of the local fibre orientation.

For composites with a fibre direction neither parallel nor perpendicular to the loading direction, the stiffness in the major and minor axes can be calculated for a sheet (ignoring the 3 direction) as described in the literature (Talreja, 1987; Yum and Hong, 1991; Jernkvist, 2001; Poe *et al.*, 2001) as follows:

$$\sigma = Q\varepsilon$$ **Equation 4-15**

$$\begin{bmatrix} \sigma_1 \\ \sigma_1 \\ \tau_{12} \end{bmatrix} = \begin{bmatrix} Q_{11} & Q_{12} & 0 \\ Q_{21} & Q_{22} & 0 \\ 0 & 0 & Q_{66} \end{bmatrix} \begin{bmatrix} \varepsilon_1 \\ \varepsilon_2 \\ \upsilon_{12} \end{bmatrix}$$

Where 'Q' is the stiffness matrix.

When considering fibre-reinforced composites, generally thin sheets or plies are used. Therefore plane stress can be assumed and no through thickness stresses need to be considered, i.e. $\sigma_3 = \tau_{23} = \tau_{31} = 0$

The material properties are defined as followes:

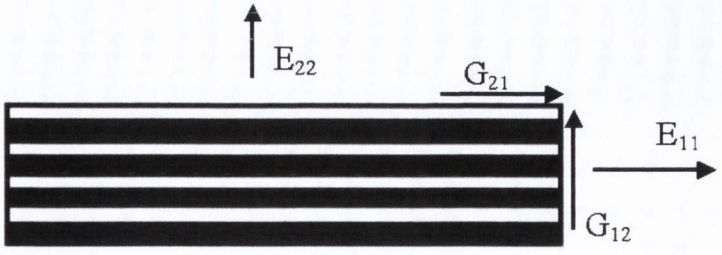

Fig. 4-42 Fibre orientation and axis definitions

The next step is to rotate the general '*x-y*' coordinate system which is aligned with the direction of the loading to the new coordinate system ('1-2') which is orientated with the fibres, where θ is the angle between the two systems.

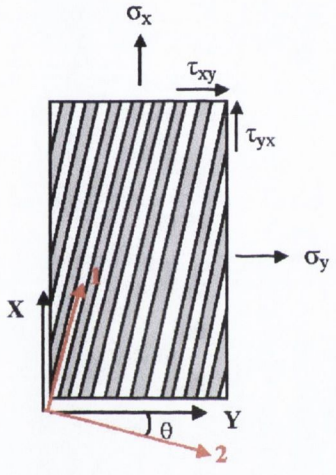

Fig. 4-43 The 'x-y' and '1-2' coordinate system

If the composite is loaded at an angle θ to the fibre direction, the new elastic properties can be determined as follows:

- The strains in the general 'x-y' orientation (the loading direction) need to be translated to the '*1-2*' orientation.
- Since $\sigma = Q\varepsilon$, the stresses and strains in the '*1-2*' system can be calculated using:

$$\begin{bmatrix}\sigma_1\\ \sigma_2\\ \upsilon_{12}\end{bmatrix} = Q\begin{bmatrix}\varepsilon_1\\ \varepsilon_2\\ \upsilon_{12}\end{bmatrix} = QT\begin{bmatrix}\varepsilon_x\\ \varepsilon_y\\ \upsilon_{xy}\end{bmatrix} \text{ and } \begin{bmatrix}\sigma_1\\ \sigma_2\\ \upsilon_{12}\end{bmatrix} = T\begin{bmatrix}\sigma_x\\ \sigma_y\\ \tau_{xy}\end{bmatrix}\begin{bmatrix}\sigma_x\\ \sigma_y\\ \tau_{1xy}\end{bmatrix} = T^{-1}\begin{bmatrix}\sigma_1\\ \sigma_2\\ \tau_{12}\end{bmatrix}$$

Where T is the tensor rotation matrix, defined as:

$$T = \begin{bmatrix}\cos^2\theta & \sin^2\theta & 2\sin\theta\cos\theta\\ \sin^2\theta & \cos^2\theta & -2\sin\theta\cos\theta\\ -\sin\theta\cos\theta & \sin\theta\cos\theta & \cos^2\theta - \sin^2\theta\end{bmatrix}$$

Applying this method implies that the strain in the '*x*-*y*'-coordinate system is rotated to the '*1*-*2*'-coordinate system. This is based on the assumption that the crack growth angle can be used as an indication of the local fibre orientation. In the new coordinate system, the strains are recalculated in order to predict the crack opening and shear displacements at the origin of the crack as shown in Fig. 4-11.

In order to do so, two methods by Chen *et al.* and Denda and Dong (1999) have been used, which have previously been described in section 4.3.3.2.1. Both methods use the notch length and the kinked crack length to calculated a representative crack length. For the representative crack length, which has a length of $2a$, the rotated x-axis is chosen along the length of the crack with its origin at the centre of the crack, meaning that the y-axis is positioned between $-a$ and $+a$ (i.e. the crack tips). For values between 0 and $+a$ standard fracture mechanics applies since the cracks opening at $+a$ is equal to zero. For values between 0 and $-a$ a non-singular term occurs due to a non-zero crack opening at $-a$, i.e. the crack mouth opening (CMO), which is not of interest for this work since all cracks are in the domain between 0 and $+a$. Although straight edge cracks have been known to satisfactorily describe the crack displacements, kinked edge cracks have only led to approximate equations, which should be seen as an indication and not the exact linear elastic answer.

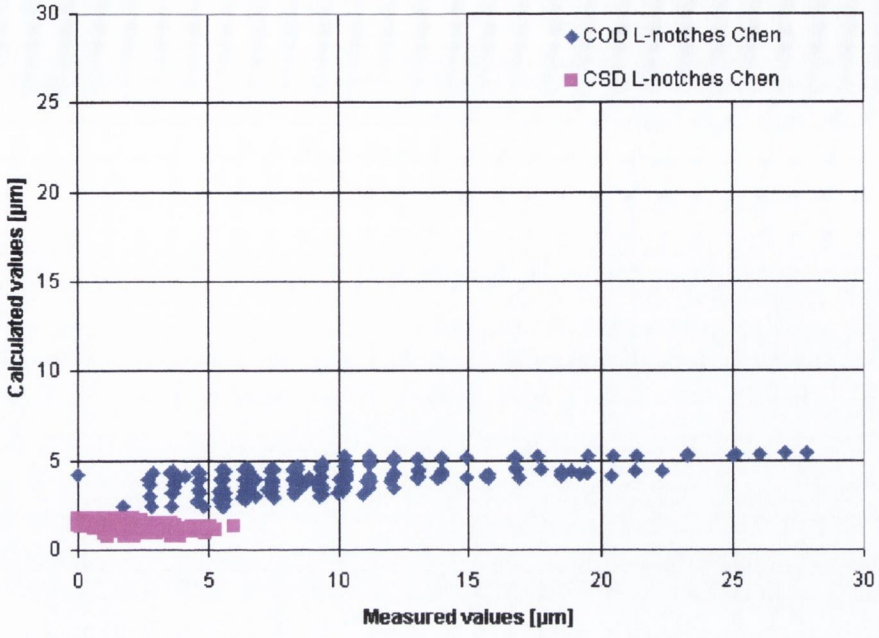

Fig. 4-44 Crack displacements for cracks from longitudinal notches, using Chen's method.

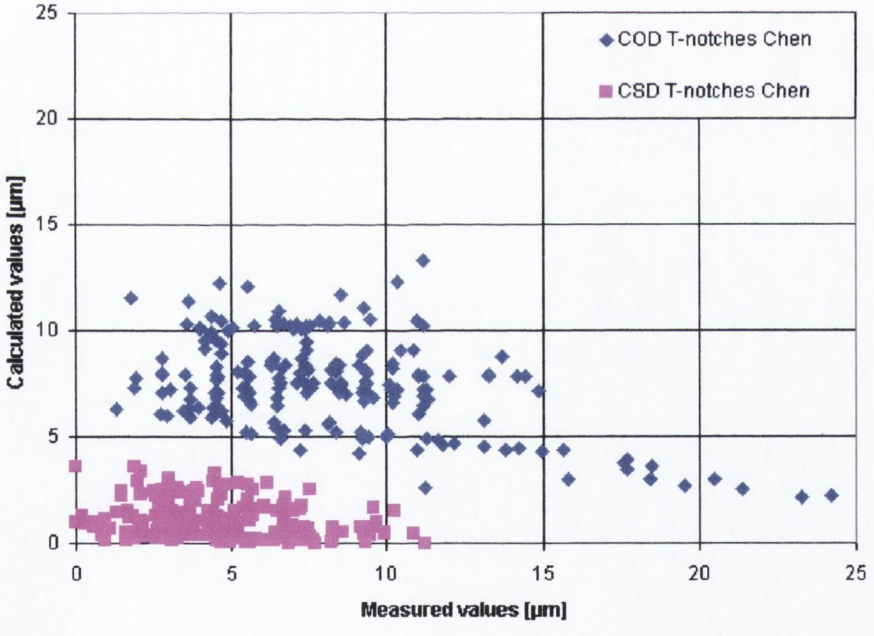

Fig. 4-45 Crack displacements for cracks from transverse notches, using Chen's method.

The method of Chen et al. (Fig. 4-44, Fig. 4-45) shows an under-prediction for both crack opening- and shear displacements for longitudinal notches. For these notches,

better predictions exist for the crack opening displacements than the crack shear displacements, except for specimen D4s2, which shows more crack opening than the other specimens.

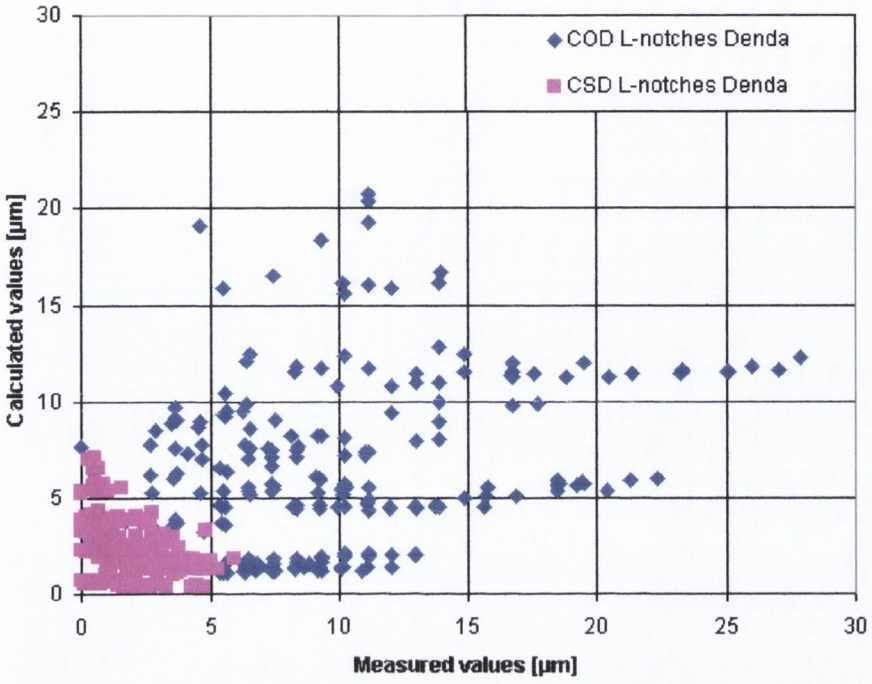

Fig. 4-46 Crack displacements for cracks from longitudinal notches, using Denda's method.

For longitudinal notches, better predictions are made using Denda and Dong's model, for both crack opening and shear displacements (Fig. 4-46), as compared with Chen's model. Extreme outliers seem to be specimens D5s3 and D5s5, which show more crack opening than predicted. When Denda and Dong's model is applied to transverse notches, this results in an under-prediction of both crack opening- and shear displacements as shown in Fig. 4-47. The only exceptions were found to be specimens D8s3 and D11s5, which exhibited less crack opening displacement than the calculations predicted.

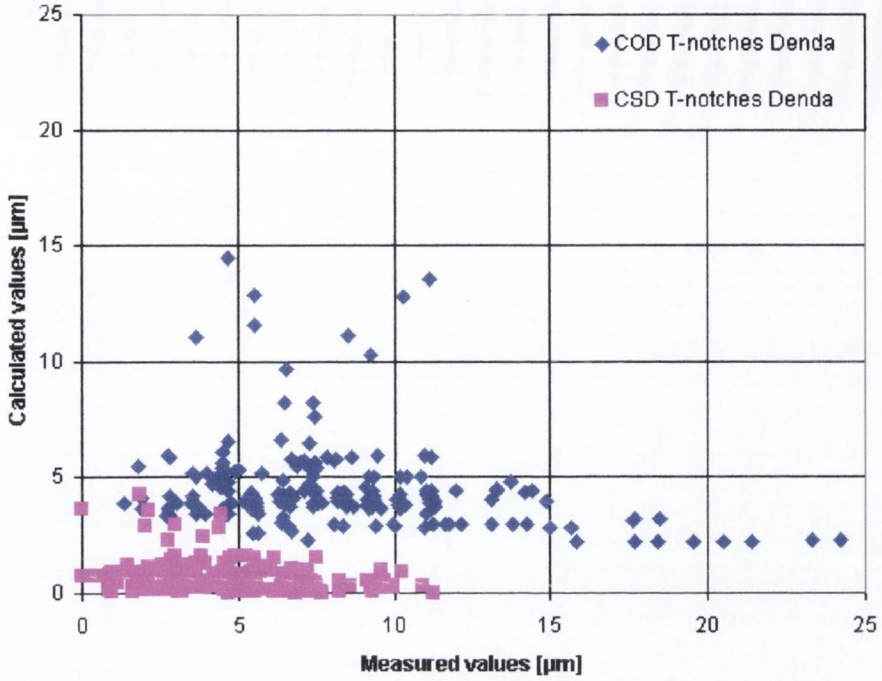

Fig. 4-47 Crack displacements for kinked cracks from transverse notches, using Denda's method.

Various methods will be compared for accuracy below.

4.3.3.3.2 Effect of crack growth and kink-angle on COD and CSD

In the analysis so far the assumption has been made that crack growth rate and kink angle had little effect. Unfortunately, this is not correct, both have an influence on the predictions. The prediction error can be calculated as follows:

$$\text{Relative error} = \frac{\text{measured value - calculated value}}{\text{measured value}} \qquad \textbf{Equation 4-16}$$

This relative error was calculated for all data points, i.e. longitudinal and transverse notches, as shown in Fig. 4-48.

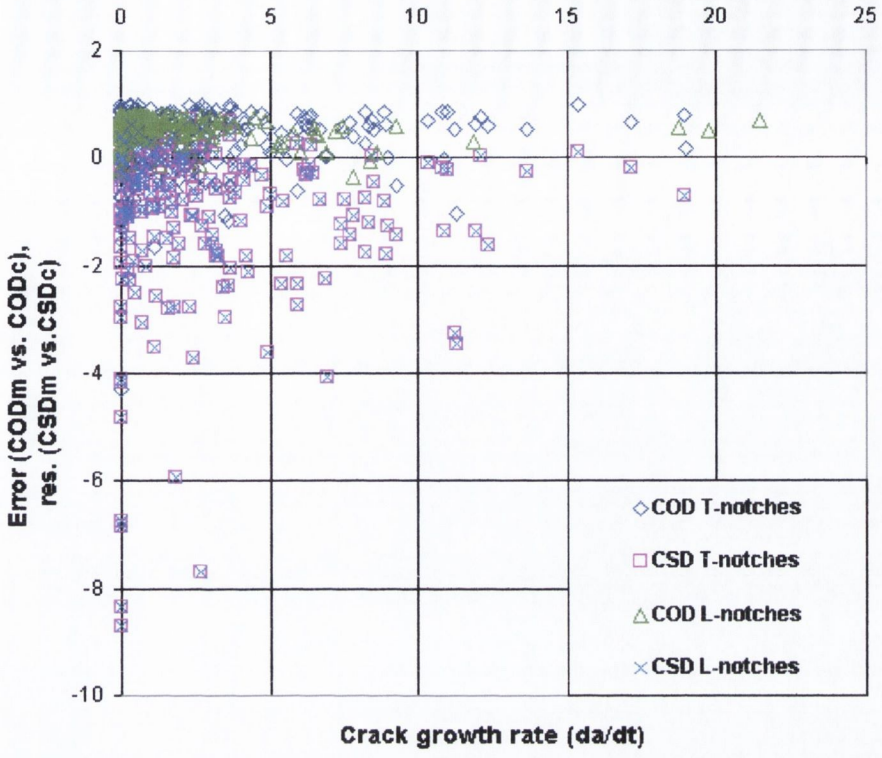

Fig. 4-48 Error calculated in COD and CSD due to crack growth rate

It shows that the majority of errors occur when crack growth is approaching zero. The component which causes the biggest problem is the amount of shear displacement, whereas the error concerning the crack opening displacement is relatively constant. This indicates that energy which cannot be released in the form of crack propagation might be used to increase crack opening and shear displacement.

These previous discussed results (Fig. 4-25, Fig. 4-28 and Fig. 4-48) indicate that crack growth initially increases. Once a boundary is approached, crack growth rates reduce and eventually stop. At this point crack opening and shear displacements tend to increase until crack growth resumes. This process repeats itself until failure of the specimen occurs.

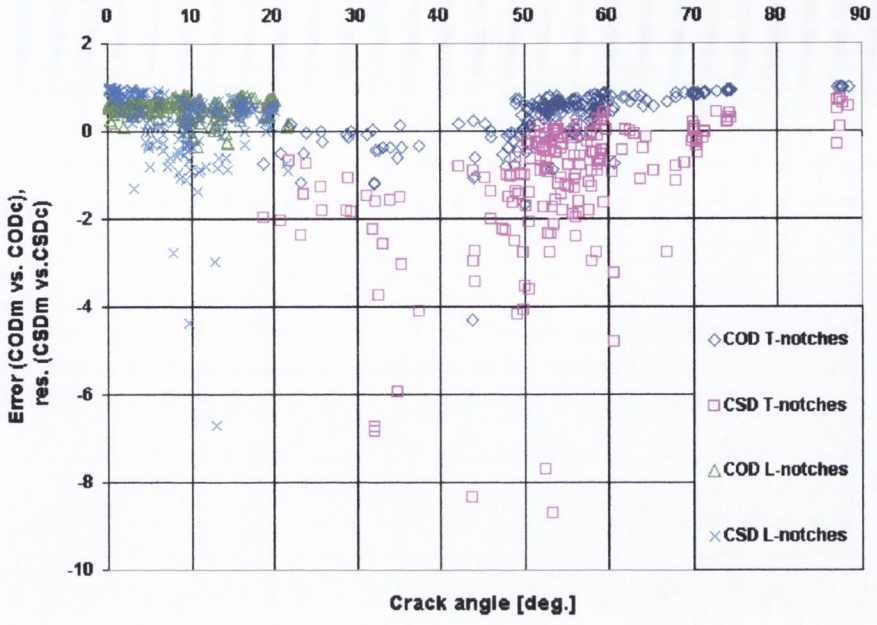

Fig. 4-49 Error calculated in COD and CSD due to kink angle

The effect of the kinked crack angle is similar to the effect caused by the crack growth rate, in that the major errors in predictions are found to be in crack shear displacements. For longitudinal notches, this error seems to peak between 10 and 20 degrees, whereas the major errors for transverse notches occur between 45 and 60 degrees.

4.3.3.3.3 Effect of plastic zone

High stresses a head o the crack tip cause a local region of plastic deformation and/or microdamage, known as the plastic zone. This can act to increase crack opening near the crack tip. In order to assess the effect of the plastic / process zone with respect to the specimens which were analysed, methods by Irwin (1960) and Dugdale (1960) were used.

Irwin (1960)

The plastic zone or process zone size is assumed to be circular, having a radius r_y, which can be estimated as follows:

$$r_y = \frac{1}{2\pi}\left(\frac{K}{\sigma_{ys}}\right)^2$$

Where K is the total stress intensity factor (K_I and K_{II} combined) and σ_y is the yield strength of the material taken to be 120 MPa (Robertson *et al.*, 1978).

Dugdale (1960)

This analysis assumes that all plastic deformation concentrates in a strip in front of the crack, the so-called strip yield model. The size of the plastic zone can be estimated using:

$$\Delta a_n = \frac{\pi}{8}\left(\frac{K}{\sigma_{ys}}\right)^2$$

In section 5.2.2. it was shown, that depending on which criterion is chosen, stress intensity factors can differ. Therefore both methods, standard fracture mechanics analysis and the stress intensity factor calculated using crack opening displacement, were used to estimate these values. The results in Table 4-7 show the maximum size of the plastic zone at the end of the test, i.e. the worst-case scenarios.

Method	K calculated with	Specimen type	Max plastic zone size [mm]
Max Irwin	Standard FM	L-notches	6.78E-05
Max Irwin	Standard FM	T-notches	6.36E-04
Max Irwin	Crack displacement	L-notches	4.36E-03
Max Irwin	Crack displacement	T-notches	5.56E-03
Max Dugdale	Standard FM	L-notches	1.69E-05
Max Dugdale	Standard FM	T-notches	1.59E-04
Max Dugdale	Crack displacement	L-notches	1.09E-03
Max Dugdale	Crack displacement	T-notches	1.39E-03
Max CTOD	Standard FM	L-notches	3.23E-07
Max CTOD	Standard FM	T-notches	3.03E-06
Max CTOD	Crack displacement	L-notches	2.08E-05
Max CTOD	Crack displacement	T-notches	2.65E-05

Table 4-7 Plastic zone and CTOD estimation

From all tests conducted specimens D6S5, D6s8, D8s3 and D8s2 had the highest values for plastic zone size when standard fracture mechanics analysis was used. These specimens all had transverse notches. When the crack opening displacement is used, specimens D5s3, D4s2 and D6s1 had higher values for the plastic zone than the other specimens. However, the values for the crack tip opening displacement (CTOD) are several orders of magnitude smaller than the plastic zone size, therefore plastic deformation near the crack tip can be assumed to have had little effect on the COD and CSD.

4.3.4 Comparing methods

Various methods have been described in the previous sections. These methods were FEA, standard fracture mechanics approaches and fracture mechanics approaches using the theory developed for composite analysis. To assess which methods best predict crack opening and shear displacements, a comparison can be made of their performances with respect to the measured values.

A commonly used approach in the literature is to plot the measured values against the calculated values, followed by a correlation analysis. Correlation is used when one wishes to quantify how consistently the two methods vary together. How well the two methods vary together, is expressed by the amount of correlation. The direction and magnitude of correlation is quantified by the correlation coefficient, r using a specifiable confidence interval. It also calculates a p-value. The p-value expresses what the statistical likelihood is that two sets of data are unrelated. For example, if the p-value is 0.05 there is only a 5 % chance that the two values are unrelated (i.e. they are statistically related to each other).

A better way of assessing the validity of two methods is through a linear regression analysis. Linear regression is used to analyse the relationship between two methods, which can be labelled method 1 and method 2. For each data point, the values according to method 1 and method 2 will be known. The objective is to find the

straight line which best explains the data. The p-value in linear regression determines the likelihood that the line is not at a significantly different slope to the horizontal axis. In other words it tests whether a change in one variable results in a set variation in the second variable.

Based on the correlation coefficient and in some cases a p-value, statements are made on the best methods to be used. Although these processes are commonly applied in clinical trials e.g. comparison studies, it is an incorrect method on which to base any conclusions. A paper by Bland and Altman (1986) discusses the effect of method comparison, using statistics. They describe an example in which two new peak flow meters are compared with the existing device. If the objective is to replace the existing device, the commonly used criterion is that there should be sufficient agreement with the old method. If the quantities measured by the new device are known and the results compare well with the true values one might consider replacing the existing devices. However, this decision cannot be taken since the true values remain unknown. Furthermore, what if both methods prove to be unequivocally correct, both show a good correlation and are found to give significant results with respect to the old method? Comparing methods is difficult and, according to Bland and Altman, often results in wrong interpretation of statistical data. This depends on:

- **Measured values:** both variables, COD and CSD, are measured values. The applied stress was calculated from the force measurements by the load cells and the specimen geometry, whereas the crack growth rate was based on measurements taken from images. Although both methods are likely to be accurate, they will contain some error. However it cannot therefore be said that these are the true (correct) values. For smaller length, measurement errors increase. If, for example, the measured crack opening displacement is to be compared with the calculated values, this effect may have significant influence on the results and therefore on the assessment of which method should prevail.

- **Scatter:** Besides the natural scatter in biological systems and materials, outliers might cause scatter. An outlier may be the result of an error in measurement, in which case it will distort the interpretation of the data having undue influence on many summary statistics. If an outlier is a genuine result, it is important because it may indicate an extreme behaviour of the process under study. For this reason, all outliers must be examined carefully before embarking on any formal analysis. Outliers should not routinely be removed without good justification.
- **Sample size:** If two methods are compared in which a lot of scatter is present and the sample size is relatively small, one is always likely to obtain answers which are not statistically significant. Scatter and outliers play an important role in these situations.
- **Repeatability:** If measurements are repeated, there is a likelihood that dissimilar results will be found. Taking several measurements of the same image will result in an indication of how good is the repeatability of a measurement. If one method has a poor repeatability, in other words, there is a lot of variation in repeated measurements, the agreement between the two methods is bound to be poor. The old method (containing the 'true values') may hold more variation, compared to the 'new' tested method. Even though the new method may be perfect, no agreement will be found between the old and the new method. When both methods have poor repeatability the problem becomes even more complex.

For biological materials in which a lot of scatter is to be expected regression lines and correlation coefficients may not be appropriate in assessing which method to use. A simple plot of the results of one method against the other without a regression line can be a useful start, but usually the data points will cluster near the line, making it difficult to assess the differences between methods. Bland and Altman (1986) proposed a new approach which allows different methods to be compared which provides a stronger indication as to which is more suitable. They suggest that a plot

of the differences (or the ratio of the differences) between the methods against their mean would be more informative.

COD and CSD data were analysed in MedCalc v7.2 (MedCalc Software, Mariakerke, Belgium), which is able to produce a 'Bland and Altman plot'. A typical graph is shown in Fig. 4-50, in which the ratio of the differences between the measured COD and the COD predicted by the FEA is plotted against their mean. The program calculates the mean ratio and the standard deviation of the ratio. A mean value higher than one expresses an under-estimation of the measured values. The 'limits of agreement' can be calculated according to:

lower limit = mean - (2 S.D.) **Equation 4-17**

Upper limit = mean + (2 S.D.) **Equation 4-18**

The ideal model would produce a mean ratio equal to 1, with the 'limits of agreement' having a small range.

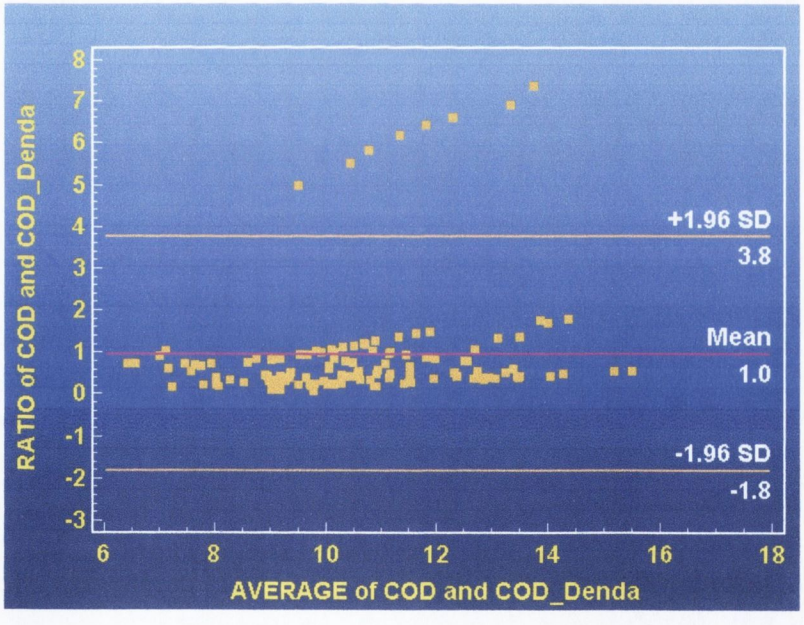

Fig. 4-50 Example 'Bland and Altman plot' comparing COD with the predicted COD using FEA

Using this method, specimens with longitudinal notches were analysed. The results are shown in Table 4-8. The results are shown in Fig. 4-51 and Fig. 4-52.

Method		Mean	S.D.
FEA	COD	2.642	0.929
	CSD	23.488	41.779
Chen (composite)	COD	2.213	0.730
	CSD	2.253	1.349
Denda (composite)	COD	2.494	2.110
	CSD	2.355	2.381
Irwin	COD	1.703	0.561
	CSD	16.150	36.890
Chen	COD	1.445	0.471
	CSD	12.479	27.479
Denda	COD	1.921	0.625
	CSD	19.793	52.335

Table 4-8 Results for notches with the grain

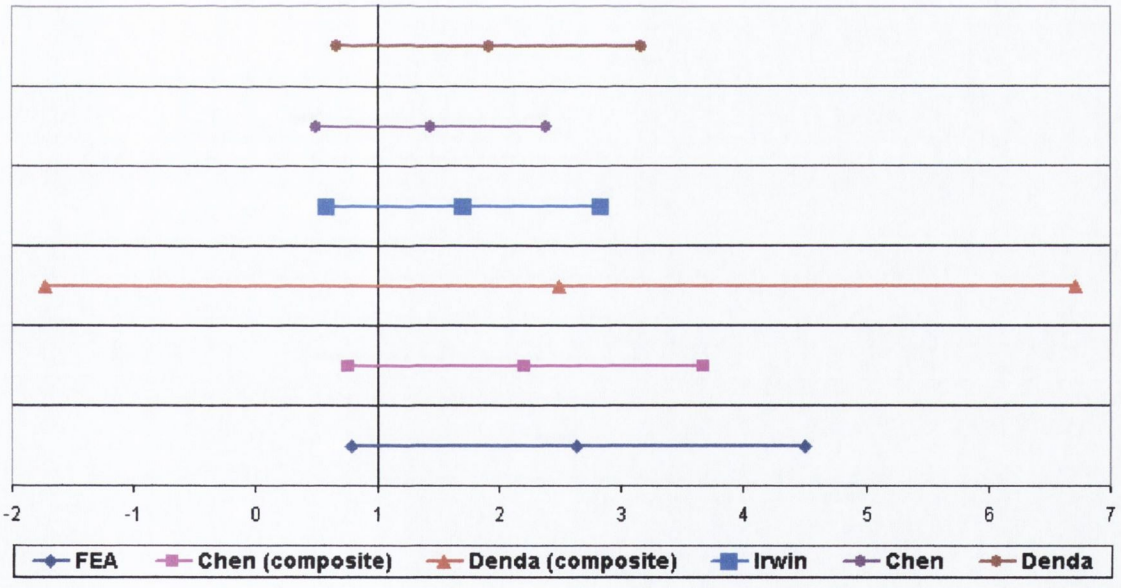

Fig. 4-51 COD limits of agreement for longitudinal notches

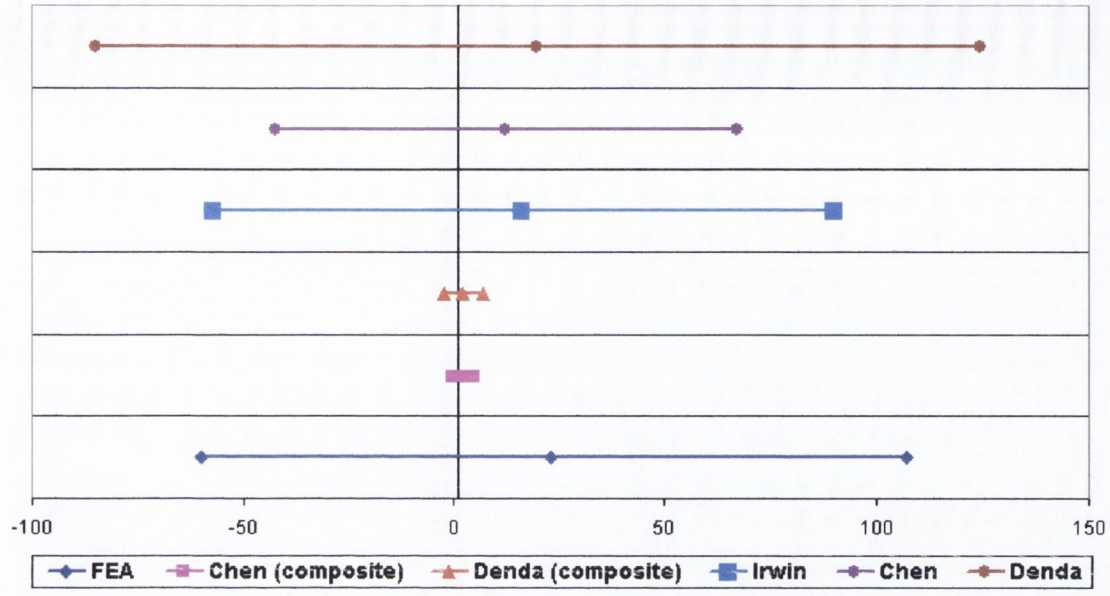

Fig. 4-52 CSD limits of agreement for longitudinal notches

Although all methods under-predicted the measured COD and CSD and the range of the limits of agreement are widespread, the composite approaches prevail over the other approaches, if COD and CSD are taken into account. With respect to the COD, Chen's method seems to work best, whereas the composite approach using Chen's method shows the best results in predicting CSD.

For specimens with transverse notches, the following results were found, as shown in Table 4-9, Fig. 4-53 and Fig. 4-54.

Method		Mean	S.D.
FEA	COD	1.291	0.772
	CSD	0.989	0.369
Chen (composite)	COD	1.598	1.888
	CSD	5.364	6.557
Denda (composite)	COD	2.348	2.134
	CSD	8.455	8.284
Irwin	COD	0.806	0.829
	CSD	0.639	0.315
Chen	COD	1.813	2.461
	CSD	0.633	0.412
Denda	COD	0.987	1.427
	CSD	0.640	0.347

Table 4-9 Results for transverse notches

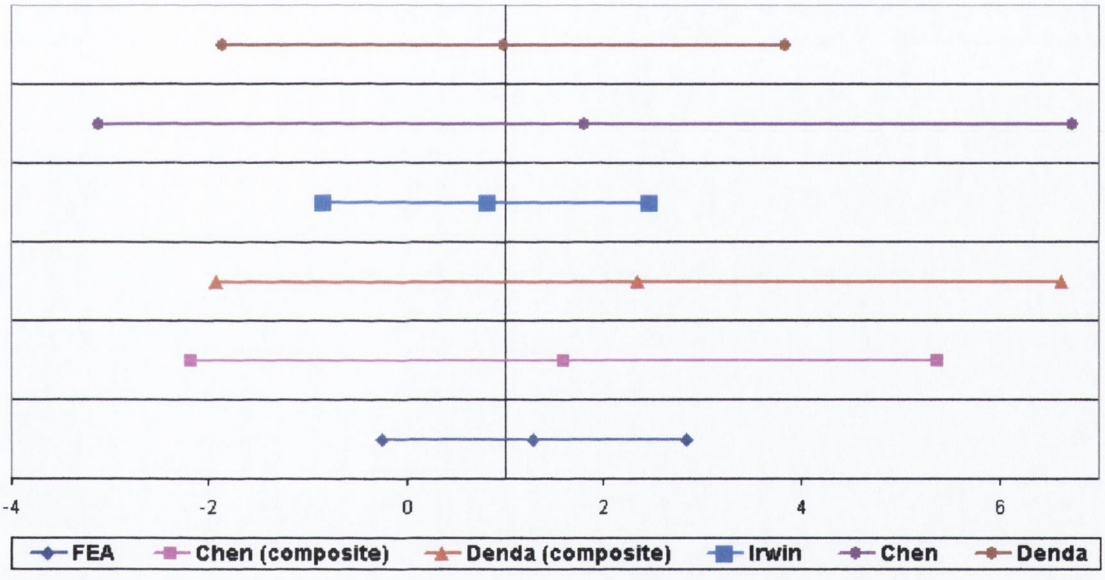

Fig. 4-53 COD limits of agreement for transverse notches

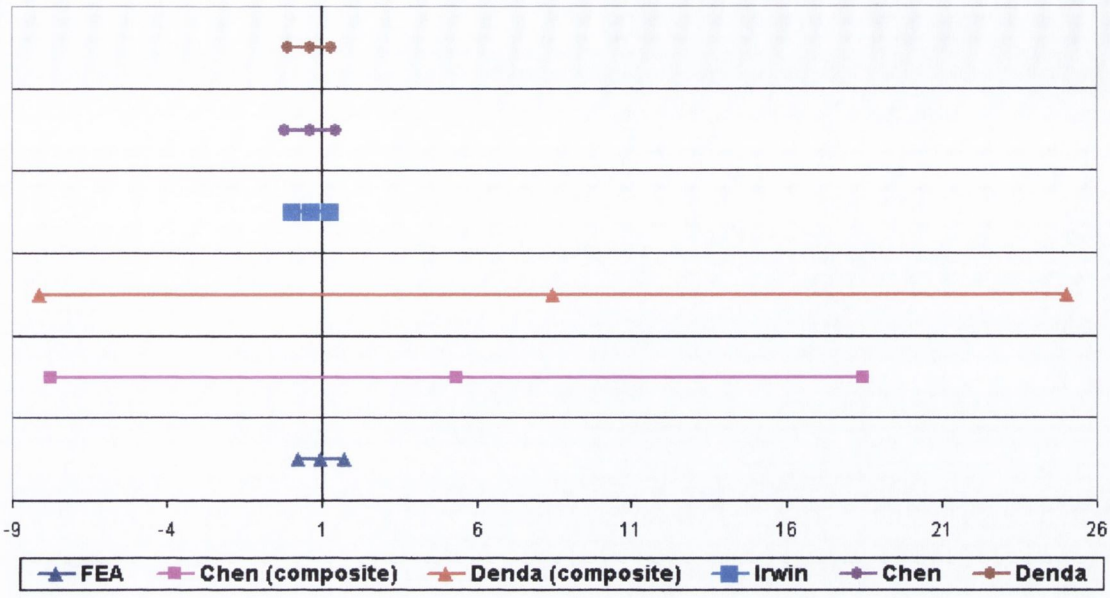

Fig. 4-54 CSD limits of agreement for transverse notches

The COD and CSD predictions made by the FE-analysis show the smallest range in the limits of agreement. All methods seem to produce very good results, except for the composite approach, which in general under-predicts the measured values.

Specimens D5s1, D5s3 and D10s6 caused the majority of errors for longitudinal notches. The composite approach was more influenced by these specimens than the other approaches. However, for transverse notches the composite approach had little effect (except specimens D4s2), whereas the other approaches showed larger errors regarding specimens D6s4, D6s5 and D11s3. As such, good predictions can be made in cases where bone is loaded in its 'natural orientation' with crack growth directions similar to the osteonal direction.

4.4 Discussion

The most important finding of the experimental work carried out in this chapter was that cell processes can rupture due to crack opening and shear displacement. Cell processes were only found to cross near the crack tip, where small crack face displacements occurred. The combination of antibody staining and confocal microscopy allowed these cell processes to be identified. Although the failure criteria, which were set in Chapter 3, could not be confirmed to be correct due to technical limitations, there was a transition from broken to intact cell processes along the length of the crack. This indicates that not all cell processes rupture due to the presence of a crack. Cell processes were also found to be intact in specimens which had longitudinal notches in which crack face displacements were approximately 2 μm. However, in these longitudinal sections, cell processes were stretched due to a crack opening mode resulting in a strain (0.05%), far less than the expected failure strain of soft tissues (15%,). This result confirms the theoretical estimation made in Chapter 3.

The second main objective of this chapter was to assess whether linear elastic fracture mechanics is adequate to describe crack faces displacements in cortical bone. The theoretical model presented in chapter 3 was based on this assumption, but effects such as plastic deformation, secondary damage accumulation and the dynamic nature of crack propagation were ignored. In order to assess whether linear elastic behaviour could be applied to cracks in bone, three methods were used; LEFM, FE-analysis and a composite approach.

Good predictions could be made for transverse notched specimens, mimicking *in vivo* loading conditions, specimens with longitudinal notches tended to under-predict these values. Finite element analyses resulted in good predictions for the crack opening and shear displacements for transverse notched specimens, whereas the specimens which had longitudinal notched specimens resulted in a under prediction

of these displacements. However, the best predictions where made when the fibre orientation was taken into account.

The method of Chen (1999) employs the projection of the crack from the notch in which a representative crack length is calculated. Denda and Dong (1999) use a similar approach, however the reconstruction of the representative crack length differs. This method requires some geometrical calculations to find the crack length to use. The third method is modified from Irwin's (1960) work. Here a correction factor 'F' is used to compensate for the notch and the crack originating from it. Although these methods are commonly used, their power tends to break down as the angle between the crack and the notch increases. If Chen's method is used, the representative crack length approaches a value equal to the notch depth when φ reals ninety degrees. Therefore the method hardly seems to distinguish between cracks at greater angles. By contrast, in the method of Denda and Dong, cracks approaching 90 degrees result in a crack length which goes to infinity. As a result the relation between the 'real' crack length and the representative length is lost. Therefore predictions of COD and CSD are compromised, with respect to the measured values.

In order to assess whether the crack opening and shear displacements could be better predicted by taking into account the fibre orientation of the material, a composite approach was used. The fibre direction was taken to be similar to the crack growth direction. Since it is well known in fracture mechanics that cracks tend to follow the path of the fibres, this seems a reasonable assumption. Although it was found to improve predictions for longitudinal notched specimens, it still under-predicted the values, whereas the transverse notched specimens showed little improvement. The reason for the under-predictions might be that bone is loaded in a configuration other than natural. In this study, the main focus was the microcrack grown from the notch and its surrounding area. Therefore, fibre debonding and the formation of microdamage in regions outside the domain compromising the mechanical integrity of the material cannot be excluded. As a result, a reduction in stiffness might have contributed to higher values of COD and CSD.

A direct comparison between methods, is not a good one to find the best one, according to Bland and Altman (1986), if the reference values are *measured* values in which the accuracy is unknown or, as in this case change with length. From the three methods assessed in this study, the composite approach best describes the overall results, resulting in narrower band for 'the limits of agreement'.

During crack growth analysis of the notched specimens various observations were made. An increase in crack growth was always followed by a decrease and *vice versa*. This behaviour is consistent with findings by Vashishth *et al.* (2000a), as shown in Fig. 4-55.

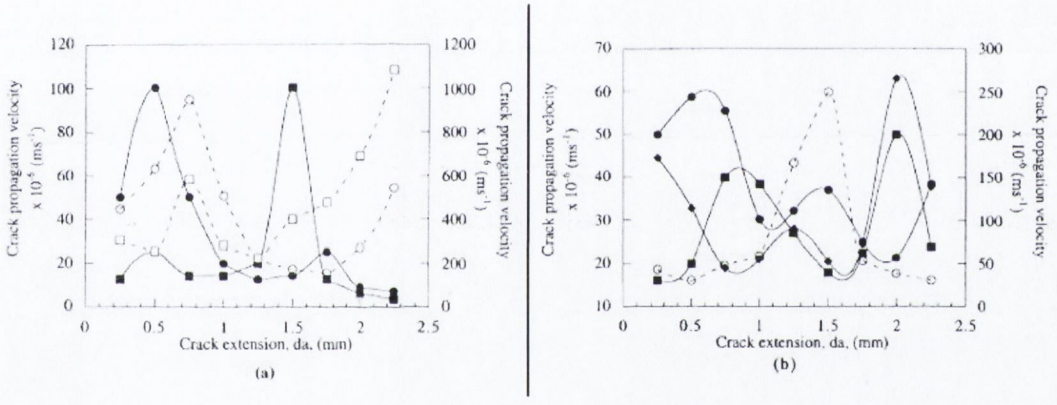

Fig. 4-55 Crack propagation velocity in (a) human bone, (b) bovine bone (Vashishth *et al.*, 2000a)

In their paper, similar specimens of human and bovine cortical bone were tested using a constant load rate. They showed that crack growth rates were approximately the same in human and bovine bone. This type of crack propagation behaviour has also been observed during fatigue loading (Nakai and Hiwa, 2002) and constant load rates (Kessler *et al.*, 2003) in carbon fibre reinforced epoxy laminates, where delamination of fibre bundles from the surrounding matrix causes this effect. This type of crack growth is typical in brittle materials and has been extensively described in the literature (Suzuki *et al.*, 1993; Ebeling *et al.*, 1997; Martin, 1997).

According to Vashishth *et al.* increased crack propagation followed by a decrease and *vice versa*, suggests that a plastic zone wake developed from the process zone. Nakai *et al.* relate this effect to crack tip shielding by fibres bridging the crack faces, which have been suggested to be present in bone (Yeni and Fyhrie, 2003) as well as in dentine (Kinney *et al.*, 1999). The mechanism proposed by Scott *et al.* (1980) is stick-slip. Stick-slip occurs when sharp cracks under low stresses start to blunt as the stresses rise. When the crack radius is deformed to a relatively large extent, a new sharp crack suddenly develops at the crack tip. This new formed crack rapidly speeds up, increasing its length markedly. Subsequently, the crack becomes dormant due to microstructural barriers. This process is repeated once stress levels increase again.

Although the mean values suggest that after every 90 to 140 μm crack growth rate is slowed down, it cannot be said that this is mainly due to osteons. As a result of the optical technique used, this behaviour could only be related to observations made on the surface. In some cases it was evident that Volkmann's canals caused this reduction in crack growth. The intervals between drops in crack propagation velocity were found to be smaller for specimens having longitudinal notches, compared to the transverse notches. Resection of specimens in order to investigate the microstructural feature responsible for the drops in crack growth rate was not possible due to the specimen size and the presence of the cracks.

The thresholds for crack growth and initiation are important since they express the ability of bone to withstand crack initiation and propagation. In practice, the point of crack initiation is taken when the first observation is made of new formed cracks. However, cracks might have been already been in the stage of propagation. Besides this, crack initiation and propagation, are known to occur at stress intensity values below their threshold value. The combination of these two factors makes it difficult to truly define the threshold values. This is a common problem if one wishes to apply fracture mechanics to bone. In order to obtain some indication, the first observation of a crack originating for the notch was taken as the crack initiation point. It was found that longitudinal notched specimens had a threshold value of approximately

0.55 (S.D., ±0.09) MPa√m, which is four times lower than the transverse notched specimens (1.99 ± 0.5 MPa√m). This ratio is similar to the critical stress intensity factor, K_c, found by other researches e.g. Tanabe and Bonfield (1999) with 1.3 to 1.6 MPa√m for longitudinal notches and 2.5 to 4.2 MPa√m for transverse notches. Similar test usually result in values higher than found here, typically 3.21 ± 0.43 MPa√m for longitudinal and 5.6 ± 0.52 MPa√m for transverse orientated notched specimens (Melvin and Evans, 1973).

Short cracks have not received much experimental attention. The only a few researchers investigated threshold and critical stress intensity values for short cracks in bone either using static or dynamic loading conditions (Lakes *et al.*, 1990; Taylor, 1998b; Akkus and Rimnac, 2001). Akkus and Rimnac found that cracks arrest when the stress intensity factor was 0.5 MPa√m, which is similar to the predicted 0.2 MPa√m by Taylor (1998b) and Tanabe *et al.* (1998). Although the values found in the 31 specimens tested here are well within the range of what is found in the literature, stress intensity factors are difficult to compare depending on the type of the test, testing conditions and the anisotropy of the material. That these factors have significant effects on the stress intensity factor was shown by Yum and Hong (1991) using graphite/ epoxy composites. In their study they found a decrease in stress intensity correction factors with increasing anisotropy of the material.

Besides crack growth rates, crack growth directions and the crack length, plastic deformation and the formation of microdamage are to be expected in the region of the crack. Studies by Robertson et al. (1978) and Lakes et al. (1990) showed that plastic zones in bone are small, which is similar to what was found in this research. Plastic zones sizes are predicted to be not bigger than 6.4×10^{-4} mm using standard fracture mechanics and 5.6×10^{-3} mm if crack displacements are used. Compared to the plastic zone, formation of small microcracks ahead of the main crack it is more likely, causing the material to soften. This contributes to an increase in COD and CSD. This formation of microdamage ahead of the main crack was confirmed to be present in the tested bone specimens using SEM-analysis.

Although antibody staining was successful, it was a tedious process which success depends on many variables. The freshness of the specimens, specimen thickness, permeablisation time, quality of antibodies, dilution levels and the number of osteocytes and canaliculi have major influence on the success of the staining procedure. Beside these factors, there are no standard protocols that describe the staining process for cellular material in non-decalcified hard tissue. The technique used requires further optimisation, especially the colour combinations of cell stain and fluorescent stains.

4.5 Conclusions

- Cell processes can be visualised near cracks in non-decalcified bone.
- Crack opening and displacements were found to cause damage to the cell-processes. Unbroken cell processes do exist near the crack, where crack face displacements are less.
- Crack opening and shear displacements can be predicted using standard linear elastic fracture mechanics, FEA and analytical methods.
- The best overall predictions for both types of specimens with least errors occurred when fibre orientation, and therefore the orientation of the stiffness gradients, was taken into account.
- Better predictions could be made if better methods where available to describe kinked crack behaviour from notches at various angles.
- The plastic near the crack tip is larger than the crack tip opening displacement. Therefore plastic deformation have little effect on the crack face displacements.
- During crack propagation, crack growth rates tend to increase followed by a decrease and *vice versa*. This appears to be caused by microstructural features.

- Crack growth rates show strong interactions with crack opening and shear displacements. A decrease in crack growth rate results in an increase in COD, CSD or combination of these two. A sudden increase in crack growth rate has the opposite effect with respect to the crack displacements.
- Crack initiation thresholds were found to be approximately four times lower for specimens with longitudinal notches compared to transverse notches. The values were 0.55 MPa$\sqrt{m}$ and 1.99 MPa$\sqrt{m}$ respectively.

Chapter 5 General Discussion

5.1 The cellular transducer

The work described in this thesis has addressed the problem of how microdamage could be detected and how targeted remodelling or deposition of new bone could be regulated. A theoretical analysis, using fracture mechanics, indicated that both damage to cellular material and strain sensing by the osteocytes could be a direct measure which regulates these two processes. Two bone adaptation mechanisms were investigated: I) detection by rupturing of the cellular material itself and, II) strain detection by the osteocytes. Using various osteocyte densities and a crack growth model, estimations were made of the number of ruptured cell processes and the number of stimulated osteocytes due to altered strain levels. Analysis of *in vitro* grown microcracks showed that crack opening and shear displacements could be adequately predicted using linear elastic fracture mechanics. Furthermore, cell staining showed that crack face displacements are sufficiently large to rupture cell processes, unbroken cell processes exist in regions where displacements are less.

5.1.1 Rupturing cell processes

Damage to the cellular material, in the form of rupturing of cell processes due to crack opening and shear displacements, could act as a cellular transducing mechanism in bone. Theoretical analysis showed that small cracks, of the order of 30 μm in the transverse direction, would not cause sufficient crack face displacements to rupture any cell processes. Cracks with a transverse length of 100 μm, a length typically found in bone, would damage cell processes at stress levels exceeding 28 MPa. For cracks of this length, more strenuous exercise would cause several hundred cell processes to rupture. For longer cracks (300 μm), several thousand cell processes could rupture, even when subjected to moderate loading conditions. Importantly, in

this last case, a single BMU would be unable to repair the crack completely. These longer cracks therefore pose a serious threat to the mechanical integrity of bone. In these cases, deposition of new bone on the outer surface could provide a means by which the stresses are reduced and crack growth rates decreased. Various researchers have reported that as osteocyte density decreased an increase in microcrack density was observed (Vashishth *et al.*, 2000b; Frank *et al.*, 2002). The model provides a possible explanation for why this occurs. Lower osteocyte densities result in fewer ruptured cell processes and hence a repair signal which is delayed or does not surpass the threshold value. Consequently, microcracks remain undetected in the matrix, causing an increase in microcrack densities. This may also answer the question which has often puzzled researchers as to why some microcracks in the bone matrix are repaired by targeted bone remodelling but others remain within the matrix and are not repaired. According to the predictions made, bone with normal osteocyte densities is able to detect microcracks that pose a threat i.e. cracks that are longer than those normally found (typical length of 100 μm) or highly stressed cracks.

The primary interest of the experimental work carried out was to investigate if crack opening and shear displacements could break cell processes? Secondly, what is the major cause of rupturing cell processes, crack opening or crack shear displacements? Near the crack tips, cell processes remained intact and were observed spanning the crack. Crack face displacements in this region were clearly not sufficient to cause rupture of cell processes. Specimens that had longitudinal notches had crack growth directions perpendicular to the loading direction. This resulted in stretching of cell processes (see Fig. 5-1A), whereas cracks at angles are subjected to a combination of crack opening and shear displacements (see Fig. 5-1B). However, more research is required regarding the effect of fracturing mode on the cellular response.

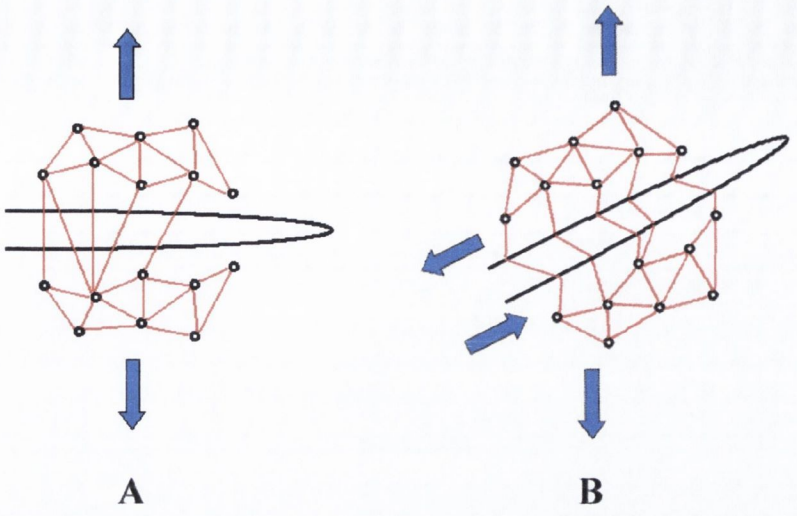

Fig. 5-1 Stretched cell processes by pure opening displacement (A) and by opening and shear displacements

The mechanism by which cell processes are broken due to crack opening and shear displacements could also explain observations of osteocyte apoptosis. Ruptures would interfere with nutrient and waste exchange and significantly alter the stimulus caused by fluid shear flow. Some scientists (Marotti *et al.*, 1992; Martin, 2000) have proposed that osteocytes continuously send out an inhibitory signal, preventing osteoclastic activity. Cell process rupture might introduce osteocyte death (apoptosis/necrosis) or a signalling response (passive or active) which might explain why Bentolila *et al.* (1998) observed BMU activity in rats which had microdamage and why no resorption cavities were found in those that had no microdamage in their bone cortex.

5.1.2 Strain sensing

When a different cellular transducer was proposed in the form of strain sensing by the cells themselves, similar results were obtained. *In vivo* experiments have shown that bone is more likely to respond to dynamic strain changes, rather than static strain (Lanyon and Rubin, 1984; Klein-Nulend *et al.*, 1995). It was however shown that both a constant strain magnitude and a constant strain rate result in a saturated

stimulus (Turner *et al.*, 1995; Burr *et al.*, 2002). The theoretical model described in this thesis (Chapter 3), showed that as a crack propagates, increasing numbers of osteocytes would be subjected to the 'high strain zone' which surrounds the microcrack. This might result in a continuous stimulus for bone adaptation due to crack growth. Osteocytes are known to respond to strain levels of 4000 με, hence this level was chosen as criterium for the 'high strain zone' which surrounds the crack. Osteocytes can detect strain levels of this magnitude since they are significantly different from the bulk strain, causing a response to be initiated. Mosley and Lanyon (1998) subjected growing male rat ulnae to strains of 4000 με at three strain rate levels for two days. Their data indicated that both strain magnitude and strain rate, have significant effects on new bone formation. High strain levels and high strain magnitudes suppress bone resorption and stimulate bone formation. Although these findings are consistent with findings by other researchers (Skerry *et al.*, 1990; Otter *et al.*, 1992; Burger and Klein-Nulend, 1999; You *et al.*, 2000; Hsieh and Turner, 2001), it is not known what signalling pathways are triggered by the bone cells as a result of these tissue deformations.

5.1.3 Crack growth and shape

As analysis of microdamage in bone has largely focused on transverse sections, little is known about crack lengths in the longitudinal direction. As a consequence theoretical models have not taken the three-dimensional shape of the cracks into account. In this work a theoretical model was presented, based on standard fracture mechanics rules, which is able to predict three dimensional shapes, similar to those found by O'Brien *et al.*(2000). Crack angles were predicted to range between 65 and 75 degrees which is similar to the mean crack angle found in the experimental analysis (67.6 ± 16.9) of growing cracks (see Chapter 4). The crack growth direction suggests a strong influence of the microstructural architecture and is similar to findings by other researchers (Carter and Hayes, 1977a; Vashishth *et al.*, 1997). Furthermore, a 'slip-stick' crack growth behaviour was observed in the notched specimens used in the experimental part of this work. Once crack growth had

initiated, crack growth rates initially increased followed by a decrease. When crack growth stopped, an increase in crack opening and shear displacement was observed. When some critical opening or shear displacement was reached, cracks started to propagate once more. This process repeated itself during crack propagation in all specimens tested. Similar crack growth behaviour was observed by Vashishth *et al.*, (2000a) where similar loading conditions and specimens were used. In their work, gauges were attached to the bone surface. During crack propagation these gauges broke, and crack propagation velocities were analysed. In both experiments the work described in this thesis and by Vashishth *et al.*, (2000a) there were relatively large intervals between measurements. As such the crack growth between the intervals is unknown and could therefore be several times higher than has been established from experiments.

5.2 Is there a need for mechanotransduction?

Bone adaptation occurs as a result of altered loading. Increased loading results in bone formation whereas, reduced levels of exercise and immobilization result in decreased bone mass. Secondary effects such as drug use, disease, osteonecrosis and congenital diseases, might lead to alterations in bone quality and quantity. This has led researchers to believe that bone contains mechanoreceptors. Due to their position, osteocytes with their fine cell-processes radiating from the cell, are believed to fill this function (Cowin *et al.*, 1991; Aarden *et al.*, 1994; Burger and Klein-Nulend, 1999; Cowin, 2002). This network allows for communication and transport of organic and inorganic matter between cells deep in the tissue and those located within the vicinity of vascular canals and bone surfaces. The osteocytes are believed to be able to sense strain levels and in some cases, scientists have proposed that they contain a memory system by which the signalling pathways are triggered (Turner and Forwood, 1995; Jacobs *et al.*, 1997; Turner, 1999).

The general mechanism by which mechanotransduction is believed to take place is that the altered loading environment, be it stress (Carter, 1987; Beaupre *et al.*, 1990;

Jacobs *et al.*, 1997), strain (Hart *et al.*, 1984b; Stanford and Brand, 1999) or strain energy density (Huiskes *et al.*, 1987) causes passive and active cellular responses. This is believed to cause altered gene and protein expression (biochemical signalling) (Wang *et al.*, 1993; Burger and Klein-Nulend, 1999; You *et al.*, 2001). Several paracrine signals have been reported to be expressed as a result of alterations in loading conditions, these are PGI_2 and PGE_2, nitride oxide and IGF. Recently Mason *et al.* (1997) found that expression of the glutamine transporters increased following loading suggesting that excitory amino acids may play a role in the transduction of the loading signal. Transmission of mechanical signals to the osteocyte skeleton via cell surface receptors (Wang *et al.*, 1993) can occur directly through the solid matrix of the tissue (Carter *et al.*, 1987; Frost, 1987; Burr *et al.*, 1990; Huiskes and Hollister, 1993; Burger and Klein-Nulend, 1999) as well as indirectly via fluid pressure and shear stresses (Cowin *et al.*, 1991; Turner and Forwood, 1994; Weinbaum *et al.*, 1994; Duncan and Turner, 1995; Forwood and Turner, 1995) impaired by fluid moving through the lacunocanalicular system sue to load induced fluid flow. All this requires bone cells to be sensitive in order to recognize and respond to mechanical and chemical stimuli.

Based on the experimental evidence, which can be found in the literature, and the current lack of biological data and knowledge of signalling pathways a theory like the mechanotransduction theory can remain undisputed for a considerable time. The two models in this thesis (cell process rupture and strain) show differences in their response (Fig. 3-19) with respect to both crack size and loading regimes. Antibody staining showed that cell processes were ruptured by crack opening and shear displacements. However, further research is required. The response by the osteocytes to this type of injury remains unknown. It could result in necrosis or apoptosis of the osteocytes in close proximity to the crack. Also, to what extent this affects the osteocyte-canalicular network and at what distance from the source of the trauma remains unknown. In other words, if rupture of cell processes or altered strain levels trigger a response (chemically, or by necrosis/ apoptosis of osteocytes), how is this 'message' distributed through the cellular network? Mechanotransduction might not

be neccesarry if ruptured cell processes due to relative crack face displacements is the stimulus for bone adaptation. Ruptured cell processes could secrete active and passive compounds in the extracellular matrix, which could diffuse through the matrix, triggering a cellular response of the osteoblast and osteoclasts. Signal transmission through direct cell-to-cell contact or by diffusion provides a much simpler mechanism to regulate bone adaptation compared to the existing mechanotransductioin theory.

The second model is based on strain sensing by the cells in the 'high strain zone' close to the crack. Work by Schaffler and Verborgt (2000) showed that osteocytes in close proximity to the crack were apoptotic. Noble and Reeve (2000) found that high peak strains resulted in an increase in apoptosis. They suggested that osteocyte apoptosis could be related to the high and low strain fields found in a close proximity to the crack. Growing cracks will have a strain field which is increasing in size and alters location during propagation. As a result, increasing numbers of cells will be subjected to altered strain levels, be it an increase or decrease. As a result, increased osteoclastic activity could be promoted, which is the first stage of the repair mechanism.

Various authors have proposed adaptation schemes based on stress (Carter *et al.*, 1987; Beaupre *et al.*, 1990), strain (Hart *et al.*, 1984a) or strain density (Huiskes *et al.*, 1987; Weinans *et al.*, 1992) to predict bone adaptation following total hip replacement. That these models could qualitatively predict bone density changes in these cases was shown by Huiskes *et al.* (1987). Prendergast and Taylor (1992) showed that similar results could be obtained using a damage based model. Damage models are typically based on either the rate of damage formation and the bone's repair rate or use mean crack length and densities to find a remodelling equilibrium. Consequently, they do not distinguish between variations in crack length, position or the threat they impose to the local region. An exception is the model presented by

Guo *et al.* (1994), who used a random β-distribution[13] to incorporate variations in crack length. The two theoretical models presented in Chapter 3 suggest that not all microcracks need to be removed. Small cracks would not be detected by the osteocytes since they neither rupture cell processes nor impose strain levels which are higher that the bulk strain of the bone. More importantly, it links in with the discussion as to "how much remodelling is optimal" (Heaney, 2003). A high level of remodelling activity weakens the bone, increasing the risk of additional damage formation and osteoporosis. Low levels of remodelling would leave the bone with numerous cracks and increase the chance of catastrophic failure. Burr (2002b) and Parfitt (2002) discussed this issue in their papers titled "targeted and non-targeted bone remodelling". The data in these papers indicated that microdamage could trigger BMU activity, which was calculated to be four to six times more likely to be associated with damage than by random BMU-activity. In the model proposed in this thesis, cracks that cause moderate damage to the cell processes or stimulate several osteocytes, require remodelling. Cracks which cause several thousand ruptured cell processes or stimulate large numbers of osteocytes by high strain levels not only require remodelling but also deposition of new bone on the surface to reduce the stresses. Although experiments as described by Mosley and Lanyon (1998) which showed bone modelling following cyclic loading, are similar to those carried out by Bentolila *et al.* (1998) which showed increased BMU activity, to what extent microdamage can trigger or is linked with bone modelling remains unknown (Lee and Taylor, 2004).

Although more extensive research is required to show the signalling pathways by which adaptation is regulated. Ruptured cell processes as a secondary effect of microdamage might provide a simpler regulating mechanism. It provides a new system compared to the existing mechanotransduction theory. There is no indication from the experimental work to date that indicates that this new theory is invalid.

---

[13] A distribution used for continuous random variables which are constrained to lie between 0 and 1, characterized by two parameters: shape and scale.

5.3 Implementation of proposed models in FEA

Theoretical models and finite element analysis have previously been employed to predict the effect of microdamage on bone (Prendergast and Taylor, 1994; Martin, 1995; Taylor and Prendergast, 1997). These types of models can theoretically mimic *in vivo* damage accumulation using continuum damage mechanics models. Other researchers have used models in which a statistical probability is used to assess the chance of stresses occurring under various loading conditions (Taylor and Kuiper, 2001). Theoretical models like those presented by Martin (1995) are highly sophisticated, and are even able to take into account the effect of remodelling. As a consequence of the repair process, alterations in mechanical properties occur, resulting in increased and decreased strain levels.

Finite element analysis has been widely accepted as an essential tool to investigate new hip implant designs. The two models developed in this thesis could be implemented into a finite element routine to investigate the effect of damage accumulation to various hip replacement designs. Various websites, such as those of 'The Standardized Femur program' (Viceconti *et al.*, 1996), provide pre-meshed femora which can be directly imported into various FEA packages. Following the work carried out in this thesis, it was proposed that:

- Small cracks remain undetected for both mechanisms proposed
- Typical crack lengths would only be detected and remodelled when subjected to loads higher than physiological
- Longer cracks would be detected even when subjected to low loading levels. Higher stress levels would require remodelling and deposition of new bone on the surfaces in order to reduce the stresses.

Therefore it is important to consider not only the crack length but also its position in the bone cortex. As such the following model (Fig. 5-2) could be proposed to set up a damaged based bone remodelling algorithm which incorporates the cellular transducer.

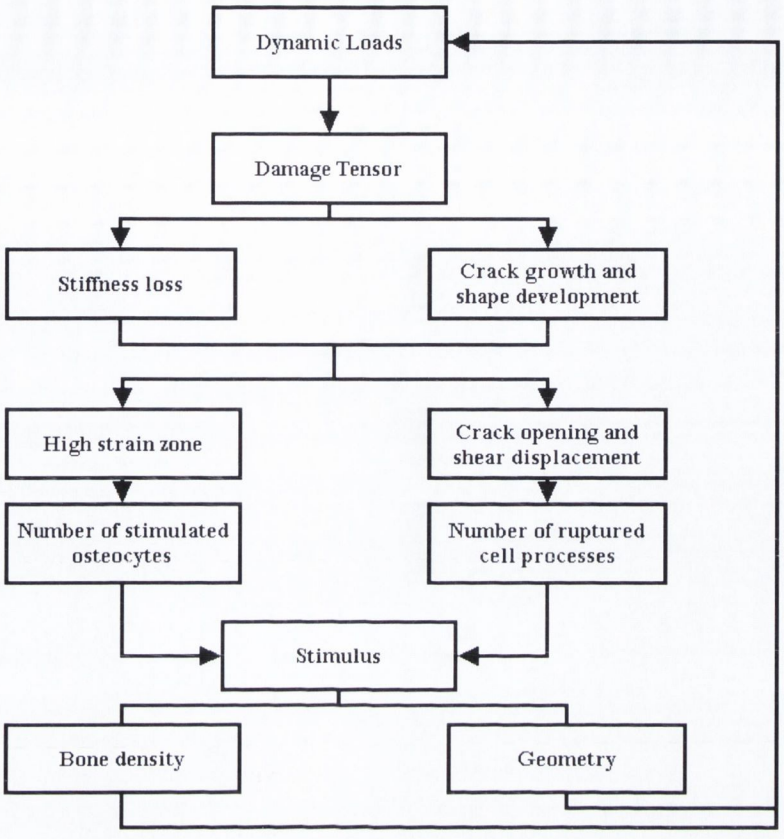

Fig. 5-2 Remodelling routine incorporating the cellular transducer

The local stresses at a tissue level are dependant on the porosity and the stress concentrations near the crack tip. The tissue level stresses due to the porosity can be calculated using (Carter and Caler, 1985):

$$\sigma_{TL} = \left(\frac{\rho_c}{\rho} \right) * \sigma_{\infty} \qquad \textbf{Equation 5-1}$$

where σ_{TL} is the stress at the tissue level, ρ_c is the cortical porosity, ρ is the apparent density and σ_{∞} is the effective stress at a continuum level. The singular stress state at the crack tip can be written as (Jernkvist, 2001):

$$\sigma_{ij} = \frac{K_I f_{ij}(\theta)}{\sqrt{2\pi r}} + \frac{K_{II} g_{ij}(\theta)}{\sqrt{2\pi r}} \qquad \textbf{Equation 5-2}$$

where r and θ are defined by the local fibre orientation and the angular functions f_{ij} and g_{ij} are dependent on the plain strain constitutive matrix C'. In a local Cartesian stystem (x_1, x_2, x_3), whose axes coincide with the principal axes of orthotropy, the material constitutive relation can be written $\varepsilon_k = C_{kl}\sigma_l$, or in explicit matrix from:

$$\begin{pmatrix} \varepsilon_{11} \\ \varepsilon_{22} \\ \varepsilon_{33} \\ \upsilon_{23} \\ \upsilon_{31} \\ \upsilon_{12} \end{pmatrix} = \begin{pmatrix} 1/E_1 & -\upsilon_{21}/E_2 & -\upsilon_{31}/E_3 & 0 & 0 & 0 \\ -\upsilon_{12}/E_1 & 1/E_2 & -\upsilon_{32}/E_3 & 0 & 0 & 0 \\ -\upsilon_{13}/E_1 & -\upsilon_{23}/E_2 & 1/E_3 & 0 & 0 & 0 \\ 0 & 0 & 0 & 1/G_{23} & 0 & 0 \\ 0 & 0 & 0 & 0 & 1/G_{31} & 0 \\ 0 & 0 & 0 & 0 & 0 & 1/G_{12} \end{pmatrix}$$

For plane stress conditions in the (x_1,x_2)-plane, only the components C_{11}, C_{22}, C_{12}, C_{21} and C_{66} are relevant. For plane strain problems, all governing equations are the same as in the plane stress, except that those four of the in-plane compliance need to be replaced by C'_{kl} according to:

$C'_{kl} = C_{kl} - C_{k3}C_{l1}/C_{33}$ (k=1,2 and l= 1,2)

The number of damaged processes, D_p, is dependant on the local stresses at a tissue level (σ_{TL}, σ_{ij}), the crack angle β, osteocyte density (OCD) and the amount of damage (D) in a representative volume element (RVE). In order to incorporate the variation in local fibre orientation, the crack angle could be varied using a random β-distribution (Euler's integral of the first kind.

Further more there will be an increase in stress due to the loss of stiffness as a result of damage accumulation. This depends on the amount of damage (D) present and the initiation of new damage. The formation rate of new damage can be calculated with (Martin, 1995):

$$D'_f = K_D S^q R_L \qquad \textbf{Equation 5-3}$$

Where D'_f is the damage formation rate, K_D is the damage rate coefficient, S^q is the strain rate and R_L is the loading frequency. Here 'q' is a dimensionless empirical constant which might be as high as 15. Depending on the number of cracks, loss of stiffness (Taylor, 1998b), crack growth rates (Taylor and Prendergast, 1997) and indirectly, the crack shape (Hazenberg *et al.*, 2002) can be calculated.

Subsequently, the crack opening and shear displacements can be calculated, followed by the number of broken cell processes. Alternatively, the high strain zones surrounding the cracks can give an indication of the number of osteocytes that are stimulated within a given domain. Certain elements, like loss of stiffness depending on the number of active BMUs can be taken from other models (Martin, 1995) which would mimic the *in vivo* adaptation process. Various parameters such as varying osteocyte densities and different BMU activation thresholds could be assessed. The two cell transducing mechanisms proposed here require new adaptation schemes to be developed regarding modelling and remodelling. However, further research is required regarding the effect of ruptured cell processes / strain stimulated cells on the stimulus triggered.

5.4 Limitations

Rupturing of osteocyte cell processes due to crack face displacements was theoretically predicted and experimentally shown to occur during crack growth. Although this process of rupturing, as well as the strain sensing mechanism, provide an excellent mechanism to detect and asses if modelling or remodelling is required, the signalling response remains unknown. The two models are, from a biological point of view, a basis for further research into the signalling pathways which are present in bone. Rupturing cell processes and strain sensing for a crack of the same length and loading conditions were predicted to result in significantly different responses. Additional experiments on osteocyte cultures might provide insight into the passive response signal (intracellular contents and secreted factors) by osteocytes

when cell processes are damaged, and the strength of this signal in relation to the number of cell processes ruptured. Damage to cell processes might also result in an active signal (protein production), necrosis or apoptosis. What is the relationship between the number of broken cell processes and the active signal and how many cell processes have to be damaged before apoptosis or necrosis is induced requires additional research.

In order to calculate the number of broken cell processes in elliptical cracks, a set of equations were developed based on standard fracture mechanics methods. These equations were based on linear elastic fracture mechanics (LEFM). In order to test if this was applicable to bone, crack growth in bone was analysed and compared to existing LEFM methods. Cracks grown in specimens with transverse notches, loaded like they would be *in vivo*, resulted in good predictions if the local fibre orientation was taken into account. For specimens that had longitudinal notches, both crack opening and crack shear displacements were under predicted using these methods. This could be attributed to several factors. The main suspected reason why specimens which had notches in the same direction as the fibres, produced an under-estimation of the crack opening and shear displacements was that the loading direct caused debonding of individual lamellae throughout the specimen. This could have caused the stiffness to reduce, and therefore increase the crack opening and shear displacements.

Other shortcomings were that the cell staining was not always successful. Permeabilisation of the cell, quality of buffer solutions, freshness of the antibody stains, storing and handling of the specimens and exposure times affect the success of staining. The use of epi-fluorescence microscopy does not provide insight into the three-dimensional distribution of osteocytes and their cell processes. Confocal microscopy improved this, however the resolution necessary to detect the cell processes was not always adequate. This was mainly due to the thickness of the specimens as the lasers had to be used at the maximum intensity available in order to visualise the fluorescent stains.

Chapter 6 General Conclusions and Future Work

- Theoretically models indicated that cell processes which pass between the crack faces can be ruptured by a cutting process due to shear displacements. The number of processes that rupture is related to crack size and applied stress. The signal strengths (assumed proportional to the number of ruptured processes) will be zero for very small cracks, positive for cracks which need repairing, and much greater if surface deposition is required. Crack opening and displacements were found to cause damage to the cell-processes in regions where the sufficiently large displacements take place, i.e. the centre or mouth of the crack.
- Experimental observations were made of unbroken cell processes near the crack tip. In regions where crack face displacements were larger cell processes were found to be broken. Indicating that not all processes break due to crack face displacements, therefore there is a critical displacement criteria which cause cell processes to rupture.
- If osteocytes can detect strain, and signal the presence of strain levels higher than normal physiological values, then this also could be used to detect the presence of cracks and to distinguish between cracks of different sizes. However rupture of osteocyte cells by cracks in bone is less likely to occur, because they do not develop sufficient strain over volumes equivalent to the cell size. Furthermore cell processes cannot be ruptured by tensile strains between the crack faces, because the strain levels reached are much less than the material's fatigue strength.
- Crack opening and shear displacements can be predicted using standard fracture mechanics, FEA and analytical methods if the load is applied in the same direction as that which occurs *in vivo*. If bone specimens are loaded in a perpendicular direction, all methods tend to under-predict displacements. The best overall predictions for all specimens, with the least errors, occurred when

fibre orientation, and therefore the orientation of the stiffness gradients, was taken into account.

- Plastic deformations do not contribute significantly to the crack opening and shear displacements in bone.
- During crack propagation under static loading conditions, crack growth rates tend to increase followed by a decrease and *vice versa*. This indicates that microstructural features are able to reduce and maybe arrest microcracks in early stages of their development. Crack growth rates show strong interactions with crack opening and shear displacements. A decrease in crack growth rate results in an increase in crack opening and shear displacements. A sudden increase in crack growth rate has the opposite effect with respect to the crack displacements.

6.1 Future work

Four possible future projects can be envisaged

Project 1

The two mechanisms proposed in this thesis, regarding the nature of the cellular transducer, could be directly implemented in a finite element model in combination with the theoretical model proposed by Martin (1995). This would present a more realistic model with both mechanisms having a criterion for bone remodelling and bone deposition. Such a model could then be used to analyse the effect of various hip implant designs as well as in analysis regarding stress fracture predictions.

Project 2

The second project involves analysing the effect of damage on a cellular network. This could be done by culturing osteocytes on a substrate. In culture osteocytes are known, to form cell processes, linking one cell to neighbouring cells. Two types of damage could be introduced. The first is by cutting cell processes using laser dissection and analysing their response, e.g. gene and protein expression, chemical release or cell death (necrosis or apoptosis). Relating the number of damaged cell

processes to the mode of death could also provide information as to how many osteocytes become apoptotic as a direct result of microdamage. The second type of damage is to induce apoptosis or necrosis to one or more cells within the network and measure the extent or number of cells affected by this damage. This might provide useful information on how many cells are required to trigger a response.

Project 3

Recent developments in the analysis of cell deformations have suggested that actin filaments, which make up the majority of the cytoskeleton, affect gene expression and play a role in mechanotransduction (Turner, 1999; Weinbaum, 2001). Deformations typically result in the release of CA^{2+} (You *et al.*, 2000), and increased expression of transcription factors such as c-fos and COX-2, all of which have been associated with bone mass regulation and growth. Due to the complexity of three dimensional stress fields surrounding the crack, this might be another mechanism by which microcrack detection takes place. To analyse this effect, a micro-mechanical finite element model should be made in which the cell deformations could be analysed, especially with respect to the deformations of the actin filaments. Various authors (Gittes *et al.*, 1993; Ingber, 1993) have described how cells could be modelled in finite element analysis.

Project 4

Osteocytes have been shown experimentally to be more sensitive to fluid shear stresses than to hydrostatic pressure. Theoretical analysis by Weinbaum *et al.* (1994) has shown that fluid shear stresses which occur within the canaliculi are of the same order of magnitude as those to which cultured osteocytes are most receptive. If crack opening and shear displacements can rupture these cell processes, then an obvious question is what is the effect of a crack or ruptured cell process on the local fluid shear stresses and to what extent does this influence bone adaptation?

Chapter 7 References

Aarden, E. M., Burger, E. H. and Nijweide, P. J. (1994) Function of osteocytes in bone, *J Cell Biochem,* **55,** 287-299.

Adams, D. J., Spirt, A. A., Brown, T. D., Fritton, S. P., Rubin, C. T. and Brand, R. A. (1997) Testing the daily stress stimulus theory of bone adaptation with natural and experimentally controlled strain histories, *J Biomech,* **30,** 671-678.

Ahmed, Y. X. and Noor, K. (2000) Perturbation mapping method for sensitivity analysis of three-dimensional cracks near a free surface, *Comput. Methods Appl. Mech. Engrg.,* **189,** 613-624.

Akkus, O. and Rimnac, C. M. (2001) Cortical bone tissue resists fatigue fracture by deceleration and arrest of microcrack growth, *J Biomech,* **34,** 757-764.

Alberts, B., Bray, D., Lewis, J., Raff, M., Roberts, K. and Watson, J. D. (1994). Molecular biology of the Cell. New York, Garland Publishing.

Allen, M. R. and Bloomfield, S. A. (2003) Hindlimb unloading has a greater effect on cortical compared with cancellous bone in mature female rats, *J Appl Physiol,* **94,** 642-650.

Aloia, J. F., Vaswani, A., Delerme-Pagan, C. and Flaster, E. (1998) Discordance between ultrasound of the calcaneus and bone mineral density in black and white women, *Calcif Tissue Int,* **62,** 481-485.

Anderson, T. L. (1995). Fracture Mechanics Fundamentals and Applications. Florida, CRC Press.

Ang, K. C., Das De, S., Goh, J. C., Low, S. L. and Bose, K. (1997) Periprosthetic bone remodelling after cementless total hip replacement. A prospective comparison of two different implant designs, *J Bone Joint Surg Br,* **79,** 675-679.

Aniniwa, Y., Tanaka, K. and Zhang, L. (1996) Prediction of Fatigue Thresholds of Notched Components Based on Resistance-Curve Method, In: *Fatigue 96*, Vol. 1 (Ed, Nowack, H.) Emasbooks, Berlin, pp. 449-454

Ansys (2003) Chapter 11: Fracture Mechanics. In: *Theory reference manual* (version 7.1).

Arndt, A., Ekenman, I., Westblad, P. and Lundberg, A. (2002) Effects of fatigue and load variation on metatarsal deformation measured in vivo during barefoot walking, *J Biomech,* **35,** 621-628.

Ascenzi, A. and Bonucci, E. (1967) The tensile properties of single osteons, *Anat Rec,* **158,** 375-386.

Ascenzi, A., Bonucci, E. and Bocciarelli, D. S. (1967) An electron microscope study on primary periosteal bone, *J Ultrastruct Res,* **18,** 605-618.

Atkinson, K., Coutts, F. and Hassenkamp, A. (2003). Physiotherapy in Orthopaedics A Problem-solving Approach. London, Churchill Livinstone.

Bailey, A. J., Sims, T. J., Ebbesen, E. N., Mansell, J. P., Thomsen, J. S. and Mosekilde, L. (1999) Age-related changes in the biochemical properties of human cancellous bone collagen: relationship to bone strength, *Calcif Tissue Int,* **65,** 203-210.

Banerjee, D., Rho, H., Jackson, H. E. and Singh, R. N. (2002) Mechanics of load transfer from matrix to fiber under flexural loading in a glass matrix composite using microfluorescence spectroscopy, *Composites Science and Technology,* **62,** 1181-1186.

Bauer, T. W. and Schils, J. (1999) The pathology of total joint arthroplasty.II. Mechanisms of implant failure, *Skeletal Radiol,* **28,** 483-497.

Beaupre, G. S., Orr, T. E. and Carter, D. R. (1990) An approach for time-dependent bone modeling and remodeling--theoretical development, *J Orthop Res,* **8,** 651-661.

Beck, T. J., Ruff, C. B., Shaffer, R. A., Betsinger, K., Trone, D. W. and Brodine, S. K. (2000) Stress fracture in military recruits: gender differences in muscle and bone susceptibility factors, *Bone,* **27,** 437-444.

Becker, T. L., Connon, R. M. and Ritchie, R. O. (2001) Finite crack kinking and T-stress in functionally graded materials, *International Journal of Solids and Structures,* **38,** 5545-5563.

Belnap, J. D. and Shetty, D. K. (1998) Micromechanics of crack bridging in sapphire/epoxy composites, *Composite Science and Technology,* **58,** 1763-1773.

Bennell, K. L., Hart, P., Nattrass, C. and Wark, J. D. (1998) Acute and subacute changes in the ultrasound measurements of the calcaneus following intense exercise, *Calcif Tissue Int,* **63,** 505-509.

Bennett, J. A. and Young, R. J. (1998) The effect of fibre-matrix adhesion upon crack bridging in fibre reinforced composites, *Composites,* **Part A,** 1071-1081.

Bentolila, V., Boyce, T. M., Fyhrie, D. P., Drumb, R., Skerry, T. M. and Schaffler, M. B. (1998) Intracortical remodeling in adult rat long bones after fatigue loading, *Bone,* **23,** 275-281.

Bland, J. M. and Altman, D. G. (1986) Statistical methods for assessing agreement between two methods of clinical measurement, *Lancet,* **1,** 307-310.

Bonfield, W. and Datta, P. K. (1976) Fracture toughness of compact bone, *J Biomech,* **9,** 131-134.

Boyce, T. M., Fyhrie, D. P., Glotkowski, M. C., Radin, E. L. and Schaffler, M. B. (1998) Damage type and strain mode associations in human compact bone bending fatigue, *J Orthop Res,* **16,** 322-329.

Brown, T. D. (2000) Techniques for mechanical stimulation of cells in vitro: a review, *J Biomech,* **33,** 3-14.

Brunski, J. B. (1999) In vivo bone response to biomechanical loading at the bone/dental-implant interface, *Adv Dent Res,* **13,** 99-119.

Burger, E. H. and Klein-Nulend, J. (1999) Mechanotransduction in bone: role of the lacuno-canalicular network, *Faseb J,* **13 Suppl,** S101-112.

Burkitt, H. G., Young, B. and Heath, J. W. (2000). Wheater's Functional Histology. New York, Churchill-Livingstone.

Burr, D. B. (1997) Bone, exercise, and stress fractures, *Exerc Sport Sci Rev,* **25,** 171-194.

Burr, D. B. (2002a) Bone material properties and mineral matrix contributions to fracture risk or age in woman and men, *J Musculoskel Neuron Interact,* **2,** 201-204.

Burr, D. B. (2002b) Targeted and nontargeted remodeling, *Bone,* **30,** 2-4.

Burr, D. B. and Martin, R. B. (1993) Calculating the probability that microcracks initiate resorption spaces, *J Biomech,* **26,** 613-616.

Burr, D. B., Martin, R. B., Schaffler, M. B. and Radin, E. L. (1985) Bone remodeling in response to in vivo fatigue microdamage, *J Biomech,* **18,** 189-200.

Burr, D. B., Milgrom, C., Boyd, R. D., Higgins, W. L., Robin, G. and Radin, E. L. (1990) Experimental stress fractures of the tibia. Biological and mechanical aetiology in rabbits, *J Bone Joint Surg Br,* **72,** 370-375.

Burr, D. B., Robling, A. G. and Turner, C. H. (2002) Effects of biomechanical stress on bones in animals, *Bone,* **30,** 781-786.

Burr, D. B., Schaffler, M. B. and Frederickson, R. G. (1988) Composition of the cement line and its possible mechanical role as a local interface in human compact bone, *J Biomech,* **21,** 939-945.

Burr, D. B. and Stafford, T. (1990) Validity of the bulk-staining technique to separate artifactual from in vivo bone microdamage, *Clin Orthop,* 305-308.

Burr, D. B., Turner, C. H., Naick, P., Forwood, M. R., Ambrosius, W., Hasan, M. S. and Pidaparti, R. (1998) Does microdamage accumulation affect the mechanical properties of bone?, *J Biomech,* **31,** 337-345.

Caler, W. E. and Carter, D. R. (1989) Bone creep-fatigue damage accumulation, *J Biomech,* **22,** 625-635.

Caler, W. E., Carter, D. R. and Harris, W. H. (1981) Techniques for implementing an in vivo bone strain gage system, *J Biomech,* **14,** 503-507.

Carter, D. R. (1982) The relationship between in vivo strains and cortical bone remodeling, *Crit Rev Biomed Eng,* **8,** 1-28.

Carter, D. R. (1987) Mechanical loading history and skeletal biology, *J Biomech,* **20,** 1095-1109.

Carter, D. R. and Caler, W. E. (1985) A cumulative damage model for bone fracture, *J Orthop Res,* **3,** 84-90.

Carter, D. R., Caler, W. E., Spengler, D. M. and Frankel, V. H. (1981a) Fatigue behavior of adult cortical bone: the influence of mean strain and strain range, *Acta Orthop Scand,* **52,** 481-490.

Carter, D. R., Fyhrie, D. P. and Whalen, R. T. (1987) Trabecular bone density and loading history: regulation of connective tissue biology by mechanical energy, *J Biomech,* **20,** 785-794.

Carter, D. R. and Hayes, W. C. (1977a) Compact bone fatigue damage: a microscopic examination, *Clin Orthop,* 265-274.

Carter, D. R. and Hayes, W. C. (1977b) Compact bone fatigue damage--I. Residual strength and stiffness, *J Biomech,* **10,** 325-337.

Carter, D. R., Vasu, R. and Harris, W. H. (1981b) The plated femur: relationships between the changes in bone stresses and bone loss, *Acta Orthop Scand,* **52,** 241-248.

Carter, D. R., Vasu, R., Spengler, D. M. and Dueland, R. T. (1981c) Stress fields in the unplated and plated canine femur calculated from in vivo strain measurements, *J Biomech,* **14,** 63-70.

Castro, J. T. P., Giassone, A. and Kenedi, P. P. (1995) Fatigue Propagation of Superficial Cracks in Wet Welds, *Fracture, Fatigue and Life Prediction,*

Chambers, I. R., Fender, D., McCaskie, A. W., Reeves, B. C. and Gregg, P. J. (2001) Radiological features predictive of aseptic loosening in cemented Charnley femoral stems, *J Bone Joint Surg Br,* **83,** 838-842.

Chan, G. K. D., G. (2002) Age-Related Bone Loss: Old Bone, New Facts, *Gerontology,* **48,** 62-71.

Chapetti, M. D., Tagawa, T. and Miyata, T. (2001) Fatigue notch sensitivity of steel blunt-notched specimens, *Fatigue & Fracture of Engineering Materials & Structures,* **25,** 629-634.

Charnley, J. (1968) Total prosthetic replacement of the hip, *Triangle,* **8,** 211-216.

Chen, Y. Z. (1999) Stress intensity factors for curved and kinked cracks in plane extension, *Theoretical and Applied Fracture Mechanics,* **31,** 223-232.

Chen, Y. Z., Lin, X. Y. and Peng, Z. Q. (1997) Application of differential-integral equation to elliptical crack problem under shear load, *Theoretical and Applied Fracture Mechanics,* **27,** 63-78.

Chou, C. T. and Sun, C. T. (1980) Stress distributions along a short fibre in fibre reinforced plastics, *J Mater Sci,* **15,** 931-938.

Cohen, J. and Harris, W. H. (1958) The three-dimensional anatomy of Haversian systems, *J Bone Joint Surg,* **40A,** 419-434.

Corondan, G. and Haworth, W. L. (1986) A fractographic study of human long bone, *J Biomech,* **19,** 207-218.

Cowin, S. C. (2002) Mechanosensation and fluid transport in living bone, *J Musculoskel Neuron Interact,* **2,** 256-260.

Cowin, S. C., Moss-Salentijn, L. and Moss, M. L. (1991) Candidates for the mechanosensory system in bone, *J Biomech Eng,* **113,** 191-197.

Cullen, D. M., Smith, R. T. and Akhter, M. P. (2001) Bone-loading response varies with strain magnitude and cycle number, *J Appl Physiol,* **91,** 1971-1976.

Currey, J. D. (1970) The mechanical properties of bone, *Clin Orthop,* **73,** 209-231.

Currey, J. D. (2002). Bones: Structure and Mechanics. Woodstock, Oxfordshire, Princeton University Press.

Currey, J. D., Brear, K. and Zioupos, P. (1996) The effects of ageing and changes in mineral content in degrading the toughness of human femora, *J Biomech,* **29,** 257-260.

Daffner, R. H., Martinez, S. and Gehweiler, J. A. (1982) Stress fractures in runners, *Jama,* **247,** 1039-1041.

Dandy, D. j. a. E., D.J. (2003). Essential Orthopaedics and Trauma. London, Churchill Livingstone.

Denda, M. and Dong, Y. F. (1999) Analytical formulas for a 2-D crack tip singular boundary element for rectilinear cracks and crack growth analysis, *Engineering Analysis with Boundary Elements,* **23,** 35-49.

Doblare, M. and Garcia, J. M. (2001) Application of an anisotropic bone-remodelling model based on a damage-repair theory to the analysis of the proximal femur before and after total hip replacement, *J Biomech,* **34,** 1157-1170.

Donahue, S. W., Sharkey, N. A., Modanlou, K. A., Sequeira, L. N. and Martin, R. B. (2000) Bone strain and microcracks at stress fracture sites in human metatarsals, *Bone,* **27,** 827-833.

Dugdale, D. S. (1960) Yielding of steel sheets containing slits, *J. Mech. Phys. Solids,* **8,** 100-104.

Duncan, J. L., Ding, S. C. and Jiang, W. L. (1999) Moment-curvature measurement in thin sheet-part II:
yielding and kinking in aged steel sheet, *International Journal of Mechanical Sciences,* **41,** 261-267.

Duncan, R. L. and Turner, C. H. (1995) Mechanotransduction and the functional response of bone to mechanical strain, *Calcif Tissue Int,* **57,** 344-358.

Dunstan, C. R., Somers, N. M. and Evans, R. A. (1993) Osteocyte death and hip fracture, *Calcif Tissue Int,* **53 Suppl 1,** S113-116; discussion S116-117.

Ebeling, T., Hiltner, A. and Baer, E. (1997) Delamination failure of a woven glass fiber composite, *Journal of Composite Materials,* **31,** 1318-1333.

El Haddad, M. H., Dowling, N. E., Topper, T. H. and Smith, K. N. (1980) J Integral Application for Short Fatigue Cracks at Notches, *International Journal of Fracture,* **16,** 15-30.

Elmann-Larsen, B. and Schmitt, D. (2003) Staying in bed to benefit ESA's astronauts and Europe's citizens, *ESA Bull,* **113,** 34-39.

Eriksen, E. F. and Langdahl, B. (1995) Bone changes in metabolic bone disease, *Acta Orthop Scand Suppl,* **266,** 195-201.

Evans, F. G. and Riolo, M. L. (1970) Relations between the fatigue life and histology of adult human cortical bone, *J Bone Joint Surg Am,* **52,** 1579-1586.

Ewalds, H. L. and Wanhill, R. J. H. (1989). Fracture Mechanics. London, Delfse U.M.

Fazzalari, N. L., Forwood, M. R., Smith, K., Manthey, B. A. and Herreen, P. (1998) Assessment of cancellous bone quality in severe osteoarthrosis: bone mineral density, mechanics, and microdamage, *Bone,* **22,** 381-388.

Feng, Z., Rou, J., Han, S. and Ziv, I. (2000) Orientation and loading condition dependence of fracture toughness in cortical bone, *Materials Science and Engineering C,* **11,** 41-46.

Forwood, M. R. and Turner, C. H. (1995) Skeletal adaptations to mechanical usage: results from tibial loading studies in rats, *Bone,* **17,** 197S-205S.

Frank, J. D., Ryan, M., Kalscheur, V. L., Ruaux-Mason, C. P., Hozak, R. R. and Muir, P. (2002) Aging and accumulation of microdamage in canine bone, *Bone,* **30,** 201-206.

Fritton, S. P., McLeod, K. J. and Rubin, C. T. (2000) Quantifying the strain history of bone: spatial uniformity and self-similarity of low-magnitude strains, *J Biomech,* **33,** 317-325.

Frost, H. M. (1960) In *Henry Ford Hosp Bull*, pp. 25-35.

Frost, H. M. (1969) Tetracycline-based histological analysis of bone remodeling, *Calcif Tissue Res,* **3,** 211-237.

Frost, H. M. (1987) Bone "mass" and the "mechanostat": a proposal, *Anat Rec,* **219,** 1-9.

Frost, H. M. (1998) A brief review for orthopedic surgeons: fatigue damage (microdamage) in bone (its determinants and clinical implications), *J Orthop Sci,* **3,** 272-281.

Galileo, G. (1638) Discorsi e dimostrazioni matematiche, intorna a due nuove scienze attentanti alla meccanica ed a muovementi locali. (Eds, Crew, H. and deSalvio, A.) The University of Wisconsin Press, Madison, pp. 158-172.

Garcia, J. M., Martinez, M. A. and Doblare, M. (2001) An anisotropic internal-external bone adaptation model based on a combination of CAO and continuum damage mechanics technologies, *Comput Methods Biomech Biomed Engin,* **4,** 355-377.

Gibson, L. J. and Ashby, M. F. (1988). Cellular Solids - structures and properties. Oxford, Pergammon Press.

Gittes, F., Mickey, B., Nettleton, J. and Howard, J. (1993) Flexural rigidity of microtubules and actin filaments measured from thermal fluctuations in shape, *J Cell Biol,* **120,** 923-934.

Goergen, T. G., Venn-Watson, E. A., Rossman, D. J., Resnick, D. and Gerber, K. H. (1981) Tarsal navicular stress fractures in runners, *AJR Am J Roentgenol,* **136,** 201-203.

Goto, M. (1994) Statistical investigation of the behaviour of short cracks and fatigue life in carbon steels with different ferrite grain sizes, *Fatigue and Fracture of Engineering Materials and Structures,* **17,** 635-649.

Griffith, A. A. (1920) In *Phil. Trans. Roy. Soc.*London.

Gunston, F. H. (1971) Polycentric knee arthroplasty. Prosthetic simulation of normal knee movement, *J Bone Joint Surg Br,* **53,** 272-277.

Guo, X. E., Liang, L. C. and Goldstein, S. A. (1998a) Micromechanics of osteonal cortical bone fracture, *J Biomech Eng,* **120,** 112-117.

Guo, X. E., Liang, L. C. and Goldstein, S. A. (1998b) Micromechanics of osteonal cortical bone fracture, *J Biomech Eng,* **120,** 112-117.

Guo, X. E., McMahon, T. A., Keaveny, T. M., Hayes, W. C. and Gibson, L. J. (1994) Finite element modeling of damage accumulation in trabecular bone under cyclic loading, *J Biomech,* **27,** 145-155.

Guozhong, C., Kangda, Z. and Dongi, W. (1996) Analysis of embedded elliptical cracks in finite thickness plates under uniform tension., *Engineering Fracture Mechanics,* **54,** 579-588.

Haapasalo, H., Kontulainen, S., Sievanen, H., Kannus, P., Jarvinen, M. and Vuori, I. (2000) Exercise-induced bone gain is due to enlargement in bone size without a change in volumetric bone density: a peripheral quantitative computed tomography study of the upper arms of male tennis players, *Bone,* **27,** 351-357.

Hain, S. F. and Fogelman, I. (2002) Nuclear medicine studies in metabolic bone disease, *Semin Musculoskelet Radiol,* **6,** 323-329.

Hammouda, M. M. I., Fayed, A. S. and Sallam, H. E. M. (2003) Stress intensity factors of a shortly kinked slant central crack with frictional surfaces in uniaxially loaded plates, *International Journal of Fatigue,* **25,** 283-298.

Hardiman, D., Croke, D., Prendergast, P. and Lee, T. (2002) Morphological change in a disuse osteoporosis model in rats: hindlimb suspension, In: *Bioengineering in Ireland 8: Proceedings of the 8th Annual Conference of the Section of Bioengineering of the Royal Academy of Medicine in Ireland and the 16th Meeting of the Northern Ireland Biomedical Engineering Society*, (Eds, FitzPatrick, D., McCormack, B. and Dickson, G.) University College Dublin, pp. 60

Harmon, K. G. (2003) Lower extremity stress fractures, *Clin J Sport Med,* **13,** 344-350.

Harris, W. H. (1997) Early loosening of the femoral component at the cement-prosthesis interface after total hip replacement, *J Bone Joint Surg Am,* **79,** 313-314.

Hart, R. T., Davy, D. T. and Heiple, K. G. (1984a) A computational method for stress analysis of adaptive elastic materials with a view toward applications in strain-induced bone remodeling, *J Biomech Eng,* **106,** 342-350.

Hart, R. T., Davy, D. T. and Heiple, K. G. (1984b) Mathematical modeling and numerical solutions for functionally dependent bone remodeling, *Calcif Tissue Int,* **36 Suppl 1,** S104-109.

Havelin, L. I., Espehaug, B., Vollset, S. E. and Engesaeter, L. B. (1995) Early aseptic loosening of uncemented femoral components in primary total hip replacement. A review based on the Norwegian Arthroplasty Register, *J Bone Joint Surg Br,* **77,** 11-17.

Hayes, W. C. (1991) Biomechanics of cortical and trabecular bone: Implications for assesment of fracture risk., In: *Basic Orthopedic Biomechanics.* Raven Press, New York, pp. 93-142.

Hazelwood, S. J., Bruce Martin, R., Rashid, M. M. and Rodrigo, J. J. (2001) A mechanistic model for internal bone remodeling exhibits different dynamic responses in disuse and overload, *J Biomech,* **34,** 299-308.

Hazenberg, J. G., O'Brien, F. J., Lee, T. C. and Taylor, D. (2002) Microcrack growth and shape development in compact bone. In: *Computer Methods in*

Biomechanics and Biomedical Engineering(Eds, Middleton, N. G., Shrive and Jones, M. L.) Gordon & Breach, Amsterdam, pp. 410-415.

Healy, W. L., Iorio, R. and Lemos, M. J. (2001) Athletic activity after joint replacement, *Am J Sports Med,* **29,** 377-388.

Heaney, R. P. (2003) Is the paradigm shifting?, *Bone,* **33,** 457-465.

Horri, H. and Nemat-Nassar, S. (1986) Brittle failure in compression: splitting, faulting and brittle-ductile transition, *Philosophical transactions of the royal society of london,* **319,** 337-374.

Hoshaw, S. J., Cody, D. D., Saad, A. M. and Fyhrie, D. P. (1997) Decrease in canine proximal femoral ultimate strength and stiffness due to fatigue damage, *J Biomech,* **30,** 323-329.

Hsieh, Y. F., Robling, A. G., Ambrosius, W. T., Burr, D. B. and Turner, C. H. (2001) Mechanical loading of diaphyseal bone in vivo: the strain threshold for an osteogenic response varies with location, *J Bone Miner Res,* **16,** 2291-2297.

Hsieh, Y. F. and Silva, M. J. (2001) Effects of in vivo fatigue loading on the mechanical properties and osteogenetic response of the rat ulna, In: *47th Annual Meeting of the ORS*, San Fransisco, California, pp. 309

Hsieh, Y. F. and Turner, C. H. (2001) Effects of loading frequency on mechanically induced bone formation, *J Bone Miner Res,* **16,** 918-924.

Hsieh, Y. F., Wang, T. and Turner, C. H. (1999) Viscoelastic response of the rat loading model: implications for studies of strain-adaptive bone formation, *Bone,* **25,** 379-382.

Huang, J. H. and Liu, H., K. (1998) On a flat ellipsoidal inclusion or crack in three-dimensional anisotropic media, *Int. J. Engng. Sci.,* **36,** 143-155.

Huiskes, R. (2000) If bone is the answer, then what is the question?, *J Anat,* **197 (Pt 2),** 145-156.

Huiskes, R. and Hollister, S. J. (1993) From structure to process, from organ to cell: recent developments of FE-analysis in orthopaedic biomechanics, *J Biomech Eng,* **115,** 520-527.

Huiskes, R., Weinans, H., Grootenboer, H. J., Dalstra, M., Fudala, B. and Slooff, T. J. (1987) Adaptive bone-remodeling theory applied to prosthetic-design analysis, *J Biomech,* **20,** 1135-1150.

Hutchinson, J. W. and Suo, Z. (1991) Mixed-mode cracking in layered materials, *Adv. Appl. Mech.,* **29,** 63-191.

Ingber, D. E. (1993) Cellular tensegrity: defining new rules of biological design that govern the cytoskeleton, *J Cell Sci,* **104 (Pt 3),** 613-627.

Inoue, M., Tanaka, H., Moriwake, T., Oka, M., Sekiguchi, C. and Seino, Y. (2000) Altered biochemical markers of bone turnover in humans during 120 days of bed rest, *Bone,* **26,** 281-286.

Ireman, T., Ranvik, T. and Eriksson, I. (2000) On damage development in mechanically fastened composite laminates, *Composite Structures,* **49,** 151-171.

Irwin, G. R. (1948) Fracture Dynamics. In: *Fracture of Metals* American Society for Metals, Cleveland, pp. 147-166.

Irwin, G. R. (1956) Onset of Fast Crack Propagation in High Strength Steel and Aluminium Alloys, In: *Sagamore Research Conference Proceedings*, Vol. 2, pp. 289-305

Irwin, G. R. (1957) Analysis of stress and strains near the end of a crack traversing a plate, *J. of Applied Mechanics, A.S.M.E.,*

Irwin, G. R. (1960) Plastic Zone Near a crack and Fracture Toughness, In: *Sagamore Research Conference Procedings*, Vol. 4 Syracuse University, Racquette Lake, NY, pp. 463-478

Iwamoto, J. and Takeda, T. (2003) Stress fractures in athletes: review of 196 cases, *J Orthop Sci,* **8,** 273-278.

Iwamoto, J., Takeda, T., Ichimura, S., Tsukimura, Y. and Toyama, Y. (2000) Age-related changes in cortical bone in men: metacarpal bone mass measurement study, *J Orthop Sci,* **5,** 4-9.

Jacobs, C. R., Simo, J. C., Beaupre, G. S. and Carter, D. R. (1997) Adaptive bone remodeling incorporating simultaneous density and anisotropy considerations, *J Biomech,* **30,** 603-613.

Jande, S. S. (1971) Fine structural study of osteocytes and their surrounding bone matrix with respect to their age in young chicks, *J Ultrastruct Res,* **37,** 279-300.

Jande, S. S. and Belanger, L. F. (1971) Electron microscopy of osteocytes and the pericellular matrix in rat trabecular bone, *Calcif Tissue Res,* **6,** 280-289.

Janssen, M., Zuidema, J. and Wanhill, R. J. H. (2002). Fracture Mechanics. London, Delft University Press.

Jernkvist, L. O. (2001) Fracture of wood under mixed mode loading I. Dervation of fracture criteria, *Engineering Fracture Mechanics,* **68,** 549-563.

Jiang, X. and Goa, Q. (2001) Stress-transfer analysis for fibre/matrix interfaces in short-fibre-reinforced composites, *Composite Science and Technology,* **61,** 1359-1366.

Judex, S., Gross, T. S., Bray, R. C. and Zernicke, R. F. (1997) Adaptation of bone to physiological stimuli, *J Biomech,* **30,** 421-429.

Kagayama, M., Sasano, Y., Mizoguchi, I. and Takahashi, I. (1997) Confocal microscopy of cementocytes and their lacunae and canaliculi in rat molars, *Anat Embryol (Berl),* **195,** 491-496.

Kageyama, N., Kusuzaki, K., Yamashita, F., Hirasawa, Y. and Ashihara, T. (1991) Staining of bone canaliculi using decalcified bone tissues, *Nippon Seikeigeka Gakkai Zasshi,* **65,** 757-761.

Kamioka, H., Honjo, T. and Takano-Yamamoto, T. (2001) A three-dimensional distribution of osteocyte processes revealed by the combination of confocal laser scanning microscopy and differential interference contrast microscopy, *Bone,* **28,** 145-149.

Kamioka, H., Miki, Y., Sumitani, K., Tagami, K., Terai, K., Hosoi, K. and Kawata, T. (1995) Extracellular calcium causes the release of calcium from intracellular stores in chick osteocytes, *Biochem Biophys Res Commun,* **212,** 692-696.

Kamioka, H., Sumitani, K., Tagami, K., Miki, Y., Terai, K., Hakeda, Y., Kumegawa, M. and Kawata, T. (1994) Divalent cations elevate cytosolic calcium of chick osteocytes, *Biochem Biophys Res Commun,* **204,** 519-524.

Karlson, K. A. (1998) Rib stress fractures in elite rowers. A case series and proposed mechanism, *Am J Sports Med,* **26,** 516-519.

Katz, J. L., Yoon, H. S., Lipson, S., Maharidge, R., Meunier, A. and Christel, P. (1984) The effects of remodeling on the elastic properties of bone, *Calcif Tissue Int,* **36 Suppl 1,** S31-36.

Ker, R. F., Wang, X. T. and Pike, A. V. (2000) Fatigue quality of mammalian tendons, *J Exp Biol,* **203 Pt 8,** 1317-1327.

Kessler, M. R., Sottos, N. R. and White, S. R. (2003) Self-healing structural composite materials, *Composites,* **34,** 743-753.

Khosla, S., Melton, L. J., 3rd, Wermers, R. A., Crowson, C. S., O'Fallon, W. and Riggs, B. (1999) Primary hyperparathyroidism and the risk of fracture: a population-based study, *J Bone Miner Res,* **14,** 1700-1707.

Kim, H. W., Deng, Y., Miranda, P., Pajares, A., Kim, D. K., Kim, H. E. and Lawn, B. R. (2001) Effect of Flaw State on the Strength of Brittle Coatings on Soft Substrates, *J. Am. Ceram. Soc.,* **84,** 2377-2384.

Kinney, J. H., Balooch, M., Marshall, G. W. and Marshall, S. J. (1999) A micromechanics model of the elastic properties of human dentine, *Arch Oral Biol,* **44,** 813-822.

Kiratli, B. J., Smith, A. E., Nauenberg, T., Kallfelz, C. F. and Perkash, I. (2000) Bone mineral and geometric changes through the femur with immobilization due to spinal cord injury, *J Rehabil Res Dev,* **37,** 225-233.

Klein-Nulend, J., van der Plas, A., Semeins, C. M., Ajubi, N. E., Frangos, J. A., Nijweide, P. J. and Burger, E. H. (1995) Sensitivity of osteocytes to biomechanical stress in vitro, *Faseb J,* **9,** 441-445.

Knothe Tate, M. L., Knothe, U. and Niederer, P. (1998) Experimental elucidation of mechanical load-induced fluid flow and its potential role in bone metabolism and functional adaptation, *Am J Med Sci,* **316,** 189-195.

Knothe-Tate, M., Niederer, P. and Forwood, M. (1997) In vivo observation of load-induced fluid displacements using procion red and microperoxidase tracers in the rat tibia, *J. Bone Miner. Res.,* **12,** S341.

Kusuzaki, K., Kageyama, N., Shinjo, H., Murata, H., Takeshita, H., Ashihara, T. and Hirasawa, Y. (1995) A staining method for bone canaliculi, *Acta Orthop Scand,* **66,** 166-168.

Kusuzaki, K., Kageyama, N., Shinjo, H., Takeshita, H., Murata, H., Hashiguchi, S., Ashihara, T. and Hirasawa, Y. (2000) Development of bone canaliculi during bone repair, *Bone,* **27,** 655-659.

Laird, C. (1967) The influence of metallurgical structure on the mechanisms of fatigue crack propagation. In: *Fatigue Crack Propagation* American Society for Testing and Materials, Philadelphia, pp. 131-168.

Lakes, R. S., Nakamura, S., Behiri, J. C. and Bonfield, W. (1990) Fracture mechanics of bone with short cracks, *J Biomech,* **23,** 967-975.

Lang, S. B. (1970) Ultrasonic method for measuring elastic coefficients of bone and results on fresh and dried bovine bones, *IEEE Trans Biomed Eng,* **17,** 101-105.

Langdahl, B. L., Mortensen, L., Vesterby, A., Eriksen, E. F. and Charles, P. (1996) Bone histomorphometry in hypoparathyroid patients treated with vitamin D, *Bone,* **18,** 103-108.

Lankford, J. (1983) The Effects of Environment on the Growth of Small Fatigue Cracks, *Fatigue of Engineering Materials and Structures,* **6,** 15-32.

Lanyon, L. E. (1993) Osteocytes, strain detection, bone modeling and remodeling, *Calcif Tissue Int,* **53 Suppl 1,** S102-106; discussion S106-107.

Lanyon, L. E., Paul, I. L., Rubin, C. T., Thrasher, E. L., DeLaura, R., Rose, R. M. and Radin, E. L. (1981) In vivo strain measurements from bone and prosthesis following total hip replacement. An experimental study in sheep, *J Bone Joint Surg Am,* **63,** 989-1001.

Lanyon, L. E. and Rubin, C. T. (1984) Static vs dynamic loads as an influence on bone remodelling, *J Biomech,* **17,** 897-905.

Laupacis, A., Bourne, R., Rorabeck, C., Feeny, D., Wong, C., Tugwell, P., Leslie, K. and Bullas, R. (1993) The effect of elective total hip replacement on health-related quality of life, *J Bone Joint Surg Am,* **75,** 1619-1626.

Lee, H. W., Kang, S. W. and Park, J. U. (2001) Fatigue Strength Depending on Position of Transverse Cracks in FCAW Process, *Welding Journal,* **80,** supl-1.

Lee, K. C., Maxwell, A. and Lanyon, L. E. (2002a) Validation of a technique for studying functional adaptation of the mouse ulna in response to mechanical loading, *Bone,* **31,** 407-412.

Lee, T. C. (1995) *Functional Adaptation in Compact Bone*, University of Dublin., Dublin

Lee, T. C., Myers, E. R. and Hayes, W. C. (1998) Fluorescence-aided detection of microdamage in compact bone, *J Anat,* **193 (Pt 2),** 179-184.

Lee, T. C., O 'Brien, F. J. and Taylor, D. (2000) The nature of fatigue damage in bone, *International Journal of Fatigue,* **22,** 847-853.

Lee, T. C., Staines, A. and Taylor, D. (2002b) Bone adaptation to load: microdamage as a stimulus for bone remodelling, *J Anat,* **201,** 437-446.

Lee, T. C. and Taylor, D. (1999) Bone remodelling: should we cry Wolff?, *Ir J Med Sci,* **168,** 102-105.

Lee, T. C. and Taylor, D. (2004) Quantification of ovine bone adaptation to altered load: Morphometry, density, and surface strain, *European Journal of Morphology,* **In press**

Levenston, M. E. and Carter, D. R. (1998) An energy dissipation-based model for damage stimulated bone adaptation, *J Biomech,* **31,** 579-586.

Lin, G. Y. and Shetty, D. K. (2003) Transformation zones,crack shielding,and crack-growth resistance of Ce-TZP/alumina composite in mode II and combined mode II and mode I loading, *Engineering Fracture Mechanics,*

Liu, J. Z. and Wu, X. R. (1997) Analytical expressions for crack opening displacements of edge cracked specimens under a segment of uniform crack face pressure, *Engineering Fracture Mechanics,* **58,** 107-119.

Lodish, H., Berk, A., Zipursky, L., Matsudaira, P., Baltimore, D. and Darnell, J. (1998). Molecular Cell Biology. New York, Scientific American Books.

Major, N. M. and Helms, C. A. (1997) Pelvic stress injuries: the relationship between osteitis pubis (symphysis pubis stress injury) and sacroiliac abnormalities in athletes, *Skeletal Radiol,* **26,** 711-717.

Malchau, H., Herberts, P., Soderman, P. and AOden, A. (2000) Prognosis of Total Hip Replacement: Update and Validation of Results from the Swedish National Hip Arthroplasty Registry 1979-1998., In: *67th Annual Meeting of the American Academy of Orthopaedic Surgeons*, Orlando, USA, pp. 1-18

Malik, C. L., Stover, S. M., Martin, R. B. and Gibeling, J. C. (2003) Equine cortical bone exhibits rising R-curve fracture mechanics, *J Biomech,* **36,** 191-198.

Marotti, G., Ferretti, M., Muglia, M. A., Palumbo, C. and Palazzini, S. (1992) A quantitative evaluation of osteoblast-osteocyte relationships on growing endosteal surface of rabbit tibiae, *Bone,* **13,** 363-368.

Marsh, K. J., Smith, R. A. and Ritchie, R. O. (Eds.) (1991) *Fatigue Crack Measurement: Techniques and Applications,* EMAS, Warley, westmidlands, UK.

Martin, P. A. (2001) On wrinkled penny-shaped cracks, *Journal of the Mechanics and Physics of Solids,* **49,** 1481-1495.

Martin, R. B. (1992) A theory of fatigue damage accumulation and repair in cortical bone, *J Orthop Res,* **10,** 818-825.

Martin, R. B. (1995) Mathematical model for repair of fatigue damage and stress fracture in osteonal bone, *J Orthop Res,* **13,** 309-316.

Martin, R. B. (2000) Toward a unifying theory of bone remodeling, *Bone,* **26,** 1-6.

Martin, R. B. and Boardman, D. L. (1993) The effects of collagen fiber orientation, porosity, density, and mineralization on bovine cortical bone bending properties, *J Biomech,* **26,** 1047-1054.

Martin, R. B. and Burr, D. B. (1982) A hypothetical mechanism for the stimulation of osteonal remodelling by fatigue damage, *J Biomech,* **15,** 137-139.

Martin, R. B. and Burr, D. B. (Eds.) (1989) *Structure, Function, and Adaptation of Compact Bone,* Raven Press, New York.

Martin, R. B., Burr, D. B. and Sharkey, N. A. (1998). Skeletal Tissue Mechanics. Berlin, Springer Verlag.

Martin, R. B., Stover, S. M., Gibson, V. A., Gibeling, J. C. and Griffin, L. V. (1996) In vitro fatigue behavior of the equine third metacarpus: remodeling and microcrack damage analysis, *J Orthop Res,* **14,** 794-801.

Martin, R. H. (1997) Delamination characterization of woven glass/polyester composites., *Journal of Composite Technological Research,* **19,** 20-28.

Mason, D. J., Suva, L. J., Genever, P. G., Patton, A. J., Steuckle, S., Hillam, R. A. and Skerry, T. M. (1997) Mechanically regulated expression of a neural glutamate transporter in bone: a role for excitatory amino acids as osteotropic agents?, *Bone,* **20,** 199-205.

Mason, M. W., Skedros, J. G. and Bloebaum, R. D. (1995) Evidence of strain-mode-related cortical adaptation in the diaphysis of the horse radius, *Bone,* **17,** 229-237.

McDowell, D. L. (1997). Applications of Continuum Damage Mechanics to Fatigue and Fracture. West Conshohocken, American Society for Testing & Materials (ASTM).

McLeod, K. J. and Rubin, C. T. (1992) Sensitivity of bone remodeling response to the frequency of applied strain., *Trans.Orthop.Res.Soc.,* **17,** 533.

McLeod, K. J., Rubin, C. T., Otter, M. W. and Qin, Y. X. (1998) Skeletal cell stresses and bone adaptation, *Am J Med Sci,* **316,** 176-183.

Melvin, J. W. and Evans, F. G. (1973) Crack propagation in bone, In: *Biomechanics Symposium ASME*, New York, pp. 87-88

Micheli, L. J., Sohn, R. S. and Solomon, R. (1985) Stress fractures of the second metatarsal involving Lisfranc's joint in ballet dancers. A new overuse injury of the foot, *J Bone Joint Surg Am,* **67,** 1372-1375.

Mikuni-Takagaki, Y., Kakai, Y., Satoyoshi, M., Kawano, E., Suzuki, Y., Kawase, T. and Saito, S. (1995) Matrix mineralization and the differentiation of osteocyte-like cells in culture, *J Bone Miner Res,* **10,** 231-242.

Mikuni-Takagaki, Y., Suzuki, Y., Kawase, T. and Saito, S. (1996) Distinct responses of different populations of bone cells to mechanical stress, *Endocrinology,* **137,** 2028-2035.

Milgrom, C., Finestone, A., Levi, Y., Simkin, A., Ekenman, I., Mendelson, S., Millgram, M., Nyska, M., Benjuya, N. and Burr, D. (2000a) Do high impact exercises produce higher tibial strains than running?, *Br J Sports Med,* **34,** 195-199.

Milgrom, C., Finestone, A., Sharkey, N., Hamel, A., Mandes, V., Burr, D., Arndt, A. and Ekenman, I. (2002) Metatarsal strains are sufficient to cause fatigue fracture during cyclic overloading, *Foot Ankle Int,* **23,** 230-235.

Milgrom, C., Finestone, A., Simkin, A., Ekenman, I., Mendelson, S., Millgram, M., Nyska, M., Larsson, E. and Burr, D. (2000b) In-vivo strain measurements to evaluate the strengthening potential of exercises on the tibial bone, *J Bone Joint Surg Br,* **82,** 591-594.

Miller, E. H., Schneider, H. J., Bronson, J. L. and McLain, D. (1975) A new consideration in athletic injuries. The classical ballet dancer, *Clin Orthop,* 181-191.

Miller, K. J. (1987) The Behaviour of Short Fatigue Cracks and their Initiation, *Fatigue and Fracture of Engineering Materials and Structures,* **10,** 93-113.

Miller, K. J., Mohamed, H. J., Brown, M. W. and de los Riois, E. R. (1986) Barriers to short fatigue crack propagation at low stress amplitudes in a banded ferrite-pearlite structure. In: *Small Fatigue Cracks*(Eds, Ritchie, R. O. and Lankford, J.) Metallurgical Society, Warrendale, Pennsylvania, pp. 639-656.

Miller, M. A., Chin, J., Miller, S. C. and Fox, J. (1998) Disparate effects of mild, moderate, and severe secondary hyperparathyroidism on cancellous and cortical bone in rats with chronic renal insufficiency, *Bone,* **23,** 257-266.

Miranda, A. C. O., Meggiolaro, M. A., Castro, J. T. P., Martha, L. F. and Bittencourt, T. N. (2002) Fatigue Crack Propagation under Complex Loading in Arbitrary 2D Geometries. In: *Applications of Automation Technology in Fatigue and Fracture Testing and Analysis*, Vol. 4 (Eds, Braun, A. A., McKeighan, P. C., Nicolson, A. M. and Lohr, R. D.) American Society for Testing and Materials, West Conshohocken.

Mori, S. and Burr, D. B. (1993) Increased intracortical remodeling following fatigue damage, *Bone,* **14,** 103-109.

Mori, S., Harruff, R., Ambrosius, W. and Burr, D. B. (1997) Trabecular bone volume and microdamage accumulation in the femoral heads of women with and without femoral neck fractures, *Bone,* **21,** 521-526.

Mosley, J. R. and Lanyon, L. E. (1998) Strain rate as a controlling influence on adaptive modeling in response to dynamic loading of the ulna in growing male rats, *Bone,* **23,** 313-318.

Mosley, J. R. and Lanyon, L. E. (2002) Growth rate rather than gender determines the size of the adaptive response of the growing skeleton to mechanical strain, *Bone,* **30,** 314-319.

Mosley, J. R., March, B. M., Lynch, J. and Lanyon, L. E. (1997) Strain magnitude related changes in whole bone architecture in growing rats, *Bone,* **20,** 191-198.

Muir, P., Johnson, K. A. and Ruaux-Mason, C. P. (1999) In vivo matrix microdamage in a naturally occurring canine fatigue fracture, *Bone,* **25,** 571-576.

Mullender, M. G. and Huiskes, R. (1997) Osteocytes and bone lining cells: which are the best candidates for mechano-sensors in cancellous bone?, *Bone,* **20,** 527-532.

Mullender, M. G., Huiskes, R. and Weinans, H. (1994) A physiological approach to the simulation of bone remodeling as a self-organizational control process, *J Biomech,* **27,** 1389-1394.

Murakami, Y. (Ed.) (1987) *Stress Intensity Factors Handbook,* Pergamon Press, New York.

Murakami, Y., Takahashi, K. and Kusumoto, R. (2003) Threshold and growth mechanisms of fatigue cracks under mode II and III loadings, *Fatigue Fract. Engng. Mater. Strauct.,* **26,** 523-531.

Nakai, Y. and Hiwa, C. (2002) Effects of loading frequency and environment on delamination fatigue crack growth of CFRP, *International Journal of Fatigue,* **24,** 161-170.

Nemat-Nassar, S. and Horii, H. (1982) Compression-Induced Nonplanar CRack Extension with Application to Splitting, Exfoliation, and Rockburst, *Journal of Geophysical research,* **87,** 6805-6821.

Newman, J. A. (2000) *The Effects of Load Ratio on Threshold Fatigue Crack Growth of Aluminum Alloys*, Faculty of the Virginia Polytechnic Institute and State University, Blacksburg, Virginia

Nicolella, D. P., Nicholls, A. E., Lankford, J. and Davy, D. T. (2001) Machine vision photogrammetry: a technique for measurement of microstructural strain in cortical bone, *J Biomech,* **34,** 135-139.

Nijs, J., De Meirleir, K., Englebienne, P. and McGregor, N. (2003) Chronic fatigue syndrome: a risk factor for osteopenia?, *Med Hypotheses,* **60,** 65-68.

Noble, B. S., Peet, N., Stevens, H. Y., Brabbs, A., Mosley, J. R., Reilly, G. C., Reeve, J., Skerry, T. M. and Lanyon, L. E. (2003) Mechanical loading:

biphasic osteocyte survival and targeting of osteoclasts for bone destruction in rat cortical bone, *Am J Physiol Cell Physiol,* **284,** C934-943.

Noble, B. S. and Reeve, J. (2000) Osteocyte function, osteocyte death and bone fracture resistance, *Mol Cell Endocrinol,* **159,** 7-13.

Noble, B. S. and Stevens, H. Y. (2003) Techniques for the study of apoptosis in bone, *Methods Mol Med,* **80,** 225-236.

Norman, T. L., Nivargikar, S. V. and Burr, D. B. (1996) Resistance to crack growth in human cortical bone is greater in shear than in tension, *J Biomech,* **29,** 1023-1031.

Norman, T. L., Vashishth, D. and Burr, D. B. (1992) Effect of groove on bone fracture toughness, *J Biomech,* **25,** 1489-1492.

Norman, T. L., Vashishth, D. and Burr, D. B. (1995) Fracture toughness of human bone under tension, *J Biomech,* **28,** 309-320.

Norman, T. L. and Wang, Z. (1997) Microdamage of human cortical bone: incidence and morphology in long bones, *Bone,* **20,** 375-379.

Norman, T. L., Yeni, Y. N., Brown, C. U. and Wang, Z. (1998) Influence of microdamage on fracture toughness of the human femur and tibia, *Bone,* **23,** 303-306.

O'Brien, F. J., Taylor, D., Brennan, O. and Lee, T. C. (2002) The effect of bone microstructure on the initiation and growth of microcracks., In: *Transactions of 48th Meeting of the Orthopaedic Research Society*, Publ.ORS, Dallas, Texas, pp. 324

O'Brien, F. J., Taylor, D., Dickson, G. R. and Lee, T. C. (2000) Visualisation of three-dimensional microcracks in compact bone, *J Anat,* **197 Pt 3,** 413-420.

O'Brien, F. J., Taylor, D. and Lee, T. C. (2002) An improved labelling technique for monitoring microcrack growth in compact bone, *J Biomech,* **35,** 523-526.

O'Brien, F. J., Taylor, D. and Lee, T. C. (2003) Microcrack accumulation at different intervals during fatigue testing of compact bone, *J Biomech,* **36,** 973-980.

O'Brien, F. J. T., D. Brennan, O. Lee, T.C. (2002) The effect of bone microstructure on the initiation and growth of microcracks, In: *Transactions of 48th Meeting of the Orthopaedic Research Society*, Publ.ORS, Dallas, Texas, pp. 324

Orowan, E. (1948) Fracture strength of Solids, *Reports on Progress in Physics,* **8,** 185.

Otter, M. W., Palmieri, V. R., Wu, D. D., Seiz, K. G., MacGinitie, L. A. and Cochran, G. V. (1992) A comparative analysis of streaming potentials in vivo and in vitro, *J Orthop Res,* **10,** 710-719.

Owan, I., Burr, D. B., Turner, C. H., Qiu, J., Tu, Y., Onyia, J. E. and Duncan, R. L. (1997) Mechanotransduction in bone: osteoblasts are more responsive to fluid forces than mechanical strain, *Am J Physiol,* **273,** C810-815.

Palumbo, C. (1986) A three-dimensional ultrastructural study of osteoid-osteocytes in the tibia of chick embryos, *Cell Tissue Res,* **246,** 125-131.

Palumbo, C., Palazzini, S. and Marotti, G. (1990) Morphological study of intercellular junctions during osteocyte differentiation, *Bone,* **11,** 401-406.

Parfitt, A. M. (1977) The cellular basis of bone turnover and bone loss: a rebuttal of the osteocytic resorption--bone flow theory, *Clin Orthop*, 236-247.

Parfitt, A. M. (1984) The cellular basis of bone remodeling: the quantum concept reexamined in light of recent advances in the cell biology of bone, *Calcif Tissue Int,* **36 Suppl 1,** S37-45.

Parfitt, A. M. (2002) Targeted and nontargeted bone remodeling: relationship to basic multicellular unit origination and progression, *Bone,* **30,** 5-7.

Paris, P. C. and Erdogan, F. (1963) A Critical Analysis of Crack Propagation Laws, *Journal of Basic Engineering*, 528-534.

Pearson, S. (1975) Initiation of Fatigue Cracks in Commercial Aluminum Alloys and the Subsequent Propagation of Very Short Cracks, *Engineering Fracture Mechanics,* **7,** 235-247.

Pickard, A. C. (1985) *The application of 3-dimensional finite element methods to fracture mechanics and fatigue life predictions*,

Poe, C. C., Reeder, J. R. and Yaun, F. G. (2001) Fracture Behaviour of a stitched Warp-Knit Carbone Fabric Composite, Virginia NASA Langley Research Center

Pope, M. H. and Murphy, M. C. (1974) Fracture energy of bone in a shear mode, *Med Biol Eng,* **12,** 763-767.

Power, J., Loveridge, N., Rushton, N., Parker, M. and Reeve, J. (2002) Osteocyte density in aging subjects is enhanced in bone adjacent to remodeling haversian systems, *Bone,* **30,** 859-865.

Prendergast, P. J. (1997) Finite element models in tissue mechanics and orthopaedic implant design, *Clin Biomech (Bristol, Avon),* **12,** 343-366.

Prendergast, P. J. and Huiskes, R. (1996) Microdamage and osteocyte-lacuna strain in bone: a microstructural finite element analysis, *J Biomech Eng,* **118,** 240-246.

Prendergast, P. J. and Taylor, D. (1992) Design of intramedullary prostheses to prevent bone loss: predictions based on damage-stimulated remodelling, *J Biomed Eng,* **14,** 499-506.

Prendergast, P. J. and Taylor, D. (1994) Prediction of bone adaptation using damage accumulation, *J Biomech,* **27,** 1067-1076.

Qin, Y. X., Kaplan, T., Saldanha, A. and Rubin, C. (2003) Fluid pressure gradients, arising from oscillations in intramedullary pressure, is correlated with the formation of bone and inhibition of intracortical porosity, *J Biomech,* **36,** 1427-1437.

Qin, Y. X., McLeod, K. J., Guilak, F., Chiang, F. P. and Rubin, C. T. (1996) Correlation of bony ingrowth to the distribution of stress and strain parameters surrounding a porous-coated implant, *J Orthop Res,* **14,** 862-870.

Ramtani, S. and Zidi, M. (2001) A theoretical model of the effect of continuum damage on a bone adaptation model, *J Biomech,* **34,** 471-479.

Reilly, D. T. and Burstein, A. H. (1975) The elastic and ultimate properties of compact bone tissue, *J Biomech,* **8,** 393-405.

Reilly, G. C. (2000) Observations of microdamage around osteocyte lacunae in bone, *J Biomech,* **33,** 1131-1134.

Reilly, G. C. and Currey, J. D. (1999) The development of microcracking and failure in bone depends on the loading mode to which it is adapted, *J Exp Biol,* **202 (Pt 5),** 543-552.

Reilly, G. C. and Currey, J. D. (2000) The effects of damage and microcracking on the impact strength of bone, *J Biomech,* **33,** 337-343.

Reynaud, P., Dalmaz, A., Tallaron, C., Rouby, D. and Fantozzi, G. (1998) Apperent Siffening of Ceramic-matrix Composites Induced by Cyclic Fatigue, *Journal of the European Ceramic Society,* **18,** 1827-1833.

Rho, J. Y., Kuhn-Spearing, L. and Zioupos, P. (1998) Mechanical properties and the hierarchical structure of bone, *Med Eng Phys,* **20,** 92-102.

Rho, J. Y., Tsui, T. Y. and Pharr, G. M. (1997) Elastic properties of human cortical and trabecular lamellar bone measured by nanoindentation, *Biomaterials,* **18,** 1325-1330.

Rho, J. Y., Zioupos, P., Currey, J. D. and Pharr, G. M. (1999) Variations in the individual thick lamellar properties within osteons by nanoindentation, *Bone,* **25,** 295-300.

Rho, J. Y., Zioupos, P., Currey, J. D. and Pharr, G. M. (2002) Microstructural elasticity and regional heterogeneity in human femoral bone of various ages examined by nano-indentation, *J Biomech,* **35,** 189-198.

Rice, J. R. (1968) A Path Independent Integral and the Approximate Analysis of Strain Concentration by Notches and Cracks., *Journal of Applied Mechanics,* **35,** 379-386.

Ritchie, R. O. (1988) Mechanisms of fatigue crack propagation in metals, ceramics and composites: Role of crack-tip shielding., *Materials Science and Engineering,* **A103,** 15-28.

Ritchie, R. O. (1999) Mechanisms of fatigue-crack propagation in ductile and brittle solids, *International Journal of Fracture,* **100,** 55-83.

Robertson, D. M., Robertson, D. and Barret, C. R. (1978) Fracture toughness, critical crack length and plastic zone size in bone, *J Biomech,* **11,** 359-364.

Roesler, H. (1987) The history of some fundamental concepts in bone biomechanics, *J Biomech,* **20,** 1025-1034.

Roux, W. (1881). Der Kempf der Teile im Organismus. Leipzig, Engelmann.

Rubin, C., Xu, G. and Judex, S. (2001) The anabolic activity of bone tissue, suppressed by disuse, is normalized by brief exposure to extremely low-magnitude mechanical stimuli, *Faseb J,* **15,** 2225-2229.

Rubin, C. T. (1984) Skeletal strain and the functional significance of bone architecture, *Calcif Tissue Int,* **36 Suppl 1,** S11-18.

Rubin, C. T. and Lanyon, L. E. (1984) Regulation of bone formation by applied dynamic loads, *J Bone Joint Surg Am,* **66,** 397-402.

Rubin, C. T. and Lanyon, L. E. (1985) Regulation of bone mass by mechanical strain magnitude, *Calcif Tissue Int,* **37,** 411-417.

Rubin, C. T. and McLeod, K. J. (1994) Promotion of bony ingrowth by frequency-specific, low-amplitude mechanical strain, *Clin Orthop,* 165-174.

Ruff, C. B. (2000) Biomechanical analysis of archeological human skeletons. In: *Biological anthropology of the human skeleton*(Eds, Katzenberg, M. A. and Saunders, S. R.) Wiley-Liss Inc., New York, pp. 71-102.

Saha, T. K., Chatterjee, M. and Roy, A. (1999) Interaction between coplanar elliptic cracks-II shear loading, *International Journal of Solids and Structures,* **36,** 619-637.

Sanderlin, B. W. and Raspa, R. F. (2003) Common stress fractures, *Am Fam Physician,* **68,** 1527-1532.

Schaffler, M. B., Choi, K. and Milgrom, C. (1995a) Aging and matrix microdamage accumulation in human compact bone, *Bone,* **17,** 521-525.

Schaffler, M. B., Choi, K. and Milgrom, C. (1995b) Aging and matrix microdamage accumulation in human compact bone, *Bone,* **17,** 521-525.

Schaffler, M. B., Pitchford, W. C., Choi, K. and Riddle, J. M. (1994) Examination of compact bone microdamage using back-scattered electron microscopy, *Bone,* **15,** 483-488.

Schaffler, M. B. and Verborgt, O. (2000) Mechanisms of microdamage repair in bone, In: *12th Conference of the European Society of Biomechanics*, (Ed,

Prendergast, P. J., Lee, T.C., Carr, A.J.) Royal Academy of Medicine in Ireland, Dublin

Schneider, S. M., Amonette, W. E., Blazine, K., Bentley, J., SM, C. L., Loehr, J. A., Moore, A. D., Jr., Rapley, M., Mulder, E. R. and Smith, S. M. (2003) Training with the International Space Station Interim Resistive Exercise Device, *Med Sci Sports Exerc,* **35,** 1935-1945.

Scholz, C. H., Boitnott, G. and Nemat-Nassar, S. (1986) The Bridgeman Ring Paradox Revised, *Pure and Applied Geophysics,* **124,** 587-599.

Sciti, D., Guicciardi, S. and Bellosi, A. (2002) Microstructure and properties of Si3N4-MoSi2 composites, *Journal of Ceramic Processing Research,* **3,** 87-95.

Scott, J. M., Wells, G. M. and Phillips, D. C. (1980) Low temperature crack propagation in an epoxide resin, *Journal of Matererial Science,* **15,** 1436-1448.

Seif, M. A. and Dasari, N. B. (2001) Effect of combined loading on cracks in graphite/epoxy composites, *Composite Structures,* **52,** 539-544.

Seireg, A. and Gray, W. (1978) A feasibility study for the use of a silastic gage as an in vivo muscle force transducer, *J Bioeng,* **2,** 159-166.

Sevostianov, I. and Kachanov, M. (2000) Impact of the porous microstructure on the overall elastic properties of the osteonal cortical bone, *J Biomech,* **33,** 881-888.

Simkin, A. and Robin, G. (1974) Fracture formation in differing collagen fiber pattern of compact bone, *J Biomech,* **7,** 183-188.

Skerry, T. M., Suswillo, R., el Haj, A. J., Ali, N. N., Dodds, R. A. and Lanyon, L. E. (1990) Load-induced proteoglycan orientation in bone tissue in vivo and in vitro, *Calcif Tissue Int,* **46,** 318-326.

Smalt, R., Mitchell, F. T., Howard, R. L. and Chambers, T. J. (1997) Induction of NO and prostaglandin E2 in osteoblasts by wall-shear stress but not mechanical strain, *Am J Physiol,* **273,** E751-758.

Snijders, C. J., Nordin, M. and Frankel, V. H. (1995). Biomechanica van het spier-skeletstelsel. Utrecht, Uitgeverij Lemma BV.

Spector, D. L., Goldman, R. D. and Leinwand, L. A. (1998). Cells: a laboratory manual; Culture and Biochemical Analysis of Cells. New York, CSHL Press.

Stanford, C. M. and Brand, R. A. (1999) Toward an understanding of implant occlusion and strain adaptive bone modeling and remodeling, *J Prosthet Dent,* **81,** 553-561.

Steck, R., Niederer, P. and Tate, M. L. (2003) A finite element analysis for the prediction of load-induced fluid flow and mechanochemical transduction in bone, *J Theor Biol,* **220,** 249-259.

Steward, K. G. and Alvarez, W. (1991) Mobile-hinge kinking in layered rocks and models, *Journal of Structural Geology,* **13,** 243-259.

Suzuki, Y., Maekawa, Z., Hamada, H., Yokoyama, A., Sugihara, T. and Hojo, M. (1993) Influence of silane coupling agents on interlaminar fracture in glass fibre fabric reinforced unsaturated polyester laminates., *J Mater Sci,* **28,** 1725-1732.

Talreja, R. (1987). Fatigue of Composite Materials. Lancaster, Pennsylvania, USA, Technomic Publishing Company.

Tami, A. E., Nasser, P., Schaffler, M. B. and Knothe Tate, M. L. (2003) Noninvasive fatigue fracture model of the rat ulna, *J Orthop Res,* **21,** 1018-1024.

Tanabe, T. and Bonfield, W. (1999) Effect of initial crack length and specimen thickness on fracture toughness of compact bone, *JSME international Journal,* **42,** 532-538.

Tanabe, T., Tanner, K. E. and Bonfield, W. (1998) Effect of loading rate on fracture toughness of bovine cortical bone, In: *11th Confrence of the ESB*, Toulouse, France, pp. 121

Tanaka, K. and Akiniwa, Y. (1988) Resistance-curve method for predicting propagation threshold of short fatigue cracks at notches, *Engineering Fracture Mechanics,* **30,** 863-876.

Tanaka, K., Akiniwa, Y., Nakai, Y. and Wei, R. P. (1986) Modelling of small fatigue crack growth interacting with grain boundary., *Engineering Fracture Mechanics*, 803-819.

Tanno, M., Horiuchi, T., Nakajima, I., Maeda, S., Igarashi, M. and Yamada, H. (2001) Age-related changes in cortical and trabecular bone mineral status. A quantitative CT study in lumbar vertebrae, *Acta Radiol,* **42,** 15-19.

Taylor, D. (1986) Fatigue of Short Cracks: The Limitation of Fracture Mechanics. In: *The Behaviour of Short Fatigue Cracks*(Eds, Miller, K. J. and de los Riois, E. R.) EGF Publications, London, pp. 479-490.

Taylor, D. (1997) Bone maintenance and remodeling: a control system based on fatigue damage, *J Orthop Res,* **15,** 601-606.

Taylor, D. (1998a) Fatigue of bone and bones: an analysis based on stressed volume, *J Orthop Res,* **16,** 163-169.

Taylor, D. (1998b) Microcrack growth parameters for compact bone deduced from stiffness variations, *J Biomech,* **31,** 587-592.

Taylor, D. (2001) A mechanistic approach to critical-distance methods in notch fatigue, *Fatigue Fracture Engineering Material Structures,* **24,** 215-224.

Taylor, D. (2002) Modelling of fatigue crack growth at the microstructural level, *Computational Material Science,* **25,** 228-236.

Taylor, D., Casolari, E. and Bignardi, C. (2004) Predicting Stress Fractures Using a Probabilistic Model of Damage, Repair and Adaptation, *Journal of Orthopaedic Research,* In press.

Taylor, D. and Kuiper, J. H. (2001) The prediction of stress fractures using a 'stressed volume' concept, *J Orthop Res,* **19,** 919-926.

Taylor, D. and Lee, T. C. (1998) Measuring the shape and size of microcracks in bone, *J Biomech,* **31,** 1177-1180.

Taylor, D. and Lee, T. C. (2003) A crack growth model for the simulation of fatigue in bone, *International Journal of Fatigue,* **25,** 387-395.

Taylor, D., O 'Reilly, P., Vallet , L. and Lee, T. C. (2003a) The fatigue strength of compact bone in torsion, *Journal of Biomechanics,* **36,** 1103-1109.

Taylor, D., O'Brien, F., Prina-Mello, A., Ryan, C., O'Reilly, P. and Lee, T. C. (1999) Compression data on bovine bone confirms that a "stressed volume" principle explains the variability of fatigue strength results, *J Biomech,* **32,** 1199-1203.

Taylor, D., O'Reilly, P., Vallet, L. and Lee, T. C. (2003b) The fatigue strength of compact bone in torsion, *J Biomech,* **36,** 1103-1109.

Taylor, D. and Prendergast, P. J. (1997) A model for fatigue crack propagation and remodelling in compact bone, *Proc Inst Mech Eng [H],* **211,** 369-375.

Taylor, R. L., Flechtenmacher, J. and Dedrick, D. K. (1993) Variation of the Holmes method for histlogical staining of bone canaliculi, *Journal of Histotechnology,* **16,** 355-357.

Tew, S. R., Kwan, A. P., Hann, A., Thomson, B. M. and Archer, C. W. (2000) The reactions of articular cartilage to experimental wounding: role of apoptosis, *Arthritis Rheum,* **43,** 215-225.

Tomkinson, A., Reeve, J., Shaw, R. W. and Noble, B. S. (1997) The death of osteocytes via apoptosis accompanies estrogen withdrawal in human bone, *J Clin Endocrinol Metab,* **82,** 3128-3135.

Trebacz, H. (2001) Disuse-induced deterioration of bone strength is not stopped after free remobilization in young adult rats, *J Biomech,* **34,** 1631-1636.

Turner, C. H. (1999) Adaptation Of Bone To Mechanical Forces: The Role Of Cellular Accommodation, In: *ASME Summer Bioengineering Conference*, Vol. 42 ASME Technical Publishing, Montana, USA, pp. 493-494

Turner, C. H. and Forwood, M. R. (1994) On animal models for studying bone adaptation, *Calcif Tissue Int,* **55,** 316-317; author reply 318.

Turner, C. H. and Forwood, M. R. (1995) What role does the osteocyte network play in bone adaptation?, *Bone,* **16,** 283-285.

Turner, C. H., Forwood, M. R., Rho, J. Y. and Yoshikawa, T. (1994) Mechanical loading thresholds for lamellar and woven bone formation, *J Bone Miner Res,* **9,** 87-97.

Turner, C. H., Owan, I. and Takano, Y. (1995) Mechanotransduction in bone: role of strain rate, *Am J Physiol,* **269,** E438-442.

Turner, C. H., Rho, J., Takano, Y., Tsui, T. Y. and Pharr, G. M. (1999) The elastic properties of trabecular and cortical bone tissues are similar: results from two microscopic measurement techniques, *J Biomech,* **32,** 437-441.

Van Buskirk, W. C., Cowin, S. C. and Ward, R. N. (1981) Ultrasonic measurement of orthotropic elastic constants of bovine femoral bone, *J Biomech Eng,* **103,** 67-72.

van der Loos, C. M. (1999). Immunoenzyme Multipule Staining Methods. Oxford, BIOS Scientific Publishers Limted.

van der Meulen, M. C. and Huiskes, R. (2002) Why mechanobiology? A survey article, *J Biomech,* **35,** 401-414.

van der Meulen, M. C., Morey-Holton, E. R. and Carter, D. R. (1995) Hindlimb suspension diminishes femoral cross-sectional growth in the rat, *J Orthop Res,* **13,** 700-707.

Vashishth, D., Behiri, J. C. and Bonfield, W. (1997) Crack growth resistance in cortical bone: concept of microcrack toughening, *J Biomech,* **30,** 763-769.

Vashishth, D., Gibson, G., Kimura, J., Schaffler, M. B. and Fyhrie, D. P. (2002) Determination of bone volume by osteocyte population, *Anat Rec,* **267,** 292-295.

Vashishth, D., Tanner, K. E. and Bonfield, W. (2000a) Contribution, development and morphology of microcracking in cortical bone during crack propagation, *J Biomech,* **33,** 1169-1174.

Vashishth, D., Verborgt, O., Divine, G., Schaffler, M. B. and Fyhrie, D. P. (2000b) Decline in osteocyte lacunar density in human cortical bone is associated with accumulation of microcracks with age, *Bone,* **26,** 375-380.

Verborgt, O., Gibson, G. J. and Schaffler, M. B. (2000) Loss of osteocyte integrity in association with microdamage and bone remodeling after fatigue in vivo, *J Bone Miner Res,* **15,** 60-67.

Viceconti, M., Casali M., Massari B., Cristofolini, L., Bassini S. and Toni, A. (1996) The 'Standardized femur program'. Proposal for a reference geometry to be used for the creation of finite element models of the femur, *Journal of Biomechanics,* **29,** 1241.

Viceconti, M. and Seireg, A. (1990) A generalized procedure for predicting bone mass regulation by mechanical strain, *Calcif Tissue Int,* **47,** 296-301.

Vico, L., Chappard, D., Alexandre, C., Palle, S., Minaire, P., Riffat, G., Morukov, B. and Rakhmanov, S. (1987) Effects of a 120 day period of bed-rest on bone mass and bone cell activities in man: attempts at countermeasure, *Bone Miner,* **2,** 383-394.

Villee, C. A., Solomon, E. P., Martin, C. E., Berg, L. R. and Davis, P. W. (1989). Biology. San Fransisco, Saunders College Publishing.

Voet, D. and Voet, J. G. (1990). Biochemistry. New York, John Wiley & Sons Inc.

Wang, N., Butler, J. P. and Ingber, D. E. (1993) Mechanotransduction across the cell surface and through the cytoskeleton, *Science,* **260,** 1124-1127.

Wang, X., Bank, R. A., TeKoppele, J. M. and Agrawal, C. M. (2001) The role of collagen in determining bone mechanical properties, *J Orthop Res,* **19,** 1021-1026.

Wang, Y. and Hadfield, M. (2002) A study of line defect fatigue failure of ceramic rolling elements in rolling contact, *Wear,* **253,** 975-985.

Wang, Z. K. and Huang, S. H. (1995) Stress intensification near an elliptical crack border, *Theoretical and Applied Fracture Mechanics,* **22,** 229-237.

Weinans, H., Huiskes, R. and Grootenboer, H. J. (1992) The behavior of adaptive bone-remodeling simulation models, *J Biomech,* **25,** 1425-1441.

Weinbaum, S. (2001) The role of actin bundels in microvilli and cell processes in mechanotransduction, In: *ASME Bioengineering Conference*, ASME Technical Publishing, Utah, USA, pp. 771-712

Weinbaum, S., Cowin, S. C. and Zeng, Y. (1994) A model for the excitation of osteocytes by mechanical loading-induced bone fluid shear stresses, *J Biomech,* **27,** 339-360.

Wells, A. A. (1961) Unstable crack propagation in metals: cleavage and fast fracture., In: *Proc. Crack Propagation Symp.*, Vol. 1 Cranfield, UK., pp. paper 84

Wenzel, T. E., Schaffler, M. B. and Fyhrie, D. P. (1996) In vivo trabecular microcracks in human vertebral bone, *Bone,* **19,** 89-95.

Wharmby, A. W., Ellyin, F. and Wolodko, J. D. (2003) Observations on damage development in fibre reinforced polymer laminates under cyclic loading, *International Journal of Fatigue,* **25,** 437-446.

Wolff, J. (1892). Das Gesetz der Transformation der Knochen. Hirschwald.

Wright, T. M. and Hayes, W. C. (1976a) The fracture mechanics of fatigue crack propagation in compact bone, *J Biomed Mater Res,* **10,** 637-648.

Wright, T. M. and Hayes, W. C. (1976b) Tensile testing of bone over a wide range of strain rates: effects of strain rate, microstructure and density, *Med Biol Eng,* **14,** 671-680.

Yanagawa, T., Watanabe, H., Shinozaki, T., Ahmed, A. R., Shirakura, K. and Takagishi, K. (2001) The natural history of disappearing bone tumours and tumour-like conditions, *Clin Radiol,* **56,** 877-886.

Yeni, Y. N., Brown, C. U. and Norman, T. L. (1998) Influence of bone composition and apparent density on fracture toughness of the human femur and tibia, *Bone,* **22,** 79-84.

Yeni, Y. N., Brown, C. U., Wang, Z. and Norman, T. L. (1997) The influence of bone morphology on fracture toughness of the human femur and tibia, *Bone,* **21,** 453-459.

Yeni, Y. N. and Fyhrie, D. P. (2003) A rate-dependent microcrack-bridging model that can explain the strain rate dependency of cortical bone apparent yield strength, *J Biomech,* **36,** 1343-1353.

Yeni, Y. N. and Norman, T. L. (2000) Fracture toughness of human femoral neck: effect of microstructure, composition, and age, *Bone,* **26,** 499-504.

Yoshikawa, T., Mori, S., Santiesteban, A. J., Sun, T. C., Hafstad, E., Chen, J. and Burr, D. B. (1994) The effects of muscle fatigue on bone strain, *J Exp Biol,* **188,** 217-233.

You, J., Reilly, G. C., Zhen, X., Yellowley, C. E., Chen, Q., Donahue, H. J. and Jacobs, C. R. (2001) Osteopontin gene regulation by oscillatory fluid flow via intracellular calcium mobilization and activation of mitogen-activated protein kinase in MC3T3-E1 osteoblasts, *J Biol Chem,* **276,** 13365-13371.

You, J., Yellowley, C. E., Donahue, H. J., Zhang, Y., Chen, Q. and Jacobs, C. R. (2000) Substrate deformation levels associated with routine physical activity are less stimulatory to bone cells relative to loading-induced oscillatory fluid flow, *J Biomech Eng,* **122,** 387-393.

Ypey, D. L., Weidema, A. F., Hold, K. M., Van der Laarse, A., Ravesloot, J. H., Van Der Plas, A. and Nijweide, P. J. (1992) Voltage, calcium, and stretch activated

ionic channels and intracellular calcium in bone cells, *J Bone Miner Res,* **7 Suppl 2,** S377-387.

Yum, Y. j. and Hong, C. s. (1991) Stress intensity factors in finite orthotropic plates whith a crack under mixed mode deformation, *International Journal of Fracture,* **47,** 53-67.

Zhao, Y. X., Goa, Q. and Wang, J. N. (1999) Microstructural effects on the short crack behaviour of a stainless steel weld during low-cycle fatigue, *Fatigue of Engineering Materials and Structures,* **22,** 469-480.

Zioupos, P. (1999) On microcracks, microcracking, in-vivo, in vitro, in-situ and other issues, *J Biomech,* **32,** 209-211, 213-259.

Zioupos, P. (2001) Accumulation of in-vivo fatigue microdamage and its relation to biomechanical properties in ageing human cortical bone, *J Microsc,* **201,** 270-278.

Zioupos, P. and Currey, J. D. (1994) The extent of microcracking and the morphology of microscracks in damaged bone., *Journal of Materials Science,* **29,** 978-986.

Zioupos, P., Currey, J. D., Mirza, M. S. and Barton, D. C. (1995) Experimentally determined microcracking around a circular hole in a flat plate of bone: comparison with predicted stresses, *Philos Trans R Soc Lond B Biol Sci,* **347,** 383-396.

Zioupos, P., X, T. W. and Currey, J. D. (1996) The accumulation of fatigue microdamage in human cortical bone of two different ages in vitro, *Clin Biomech (Bristol, Avon),* **11,** 365-375.

Chapter 8 Appendices

Appendix 1 Design of the rig
Appendix 2 Computer programmes
Appendix 3 Raw data specimens and crack analysis
Appendix 4 Specimen geometry

Appendix 1 Design of the rig

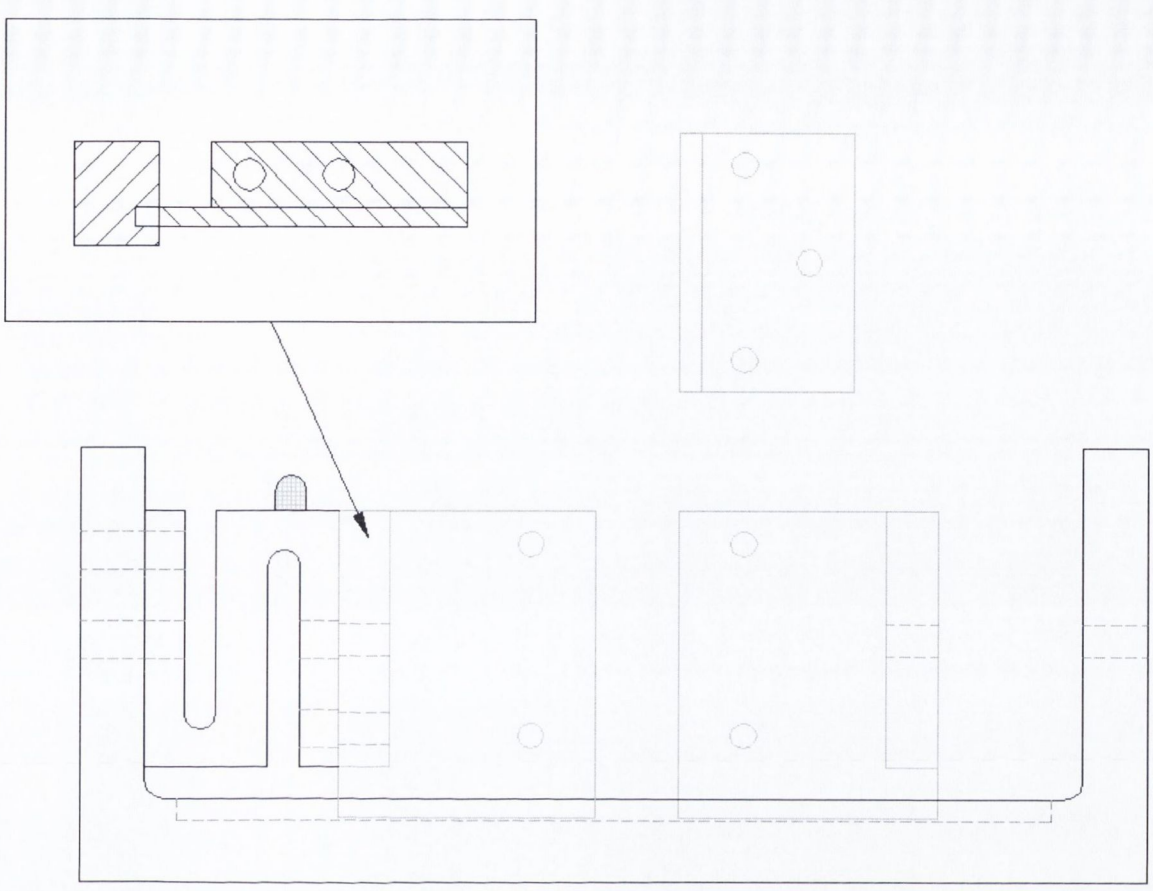

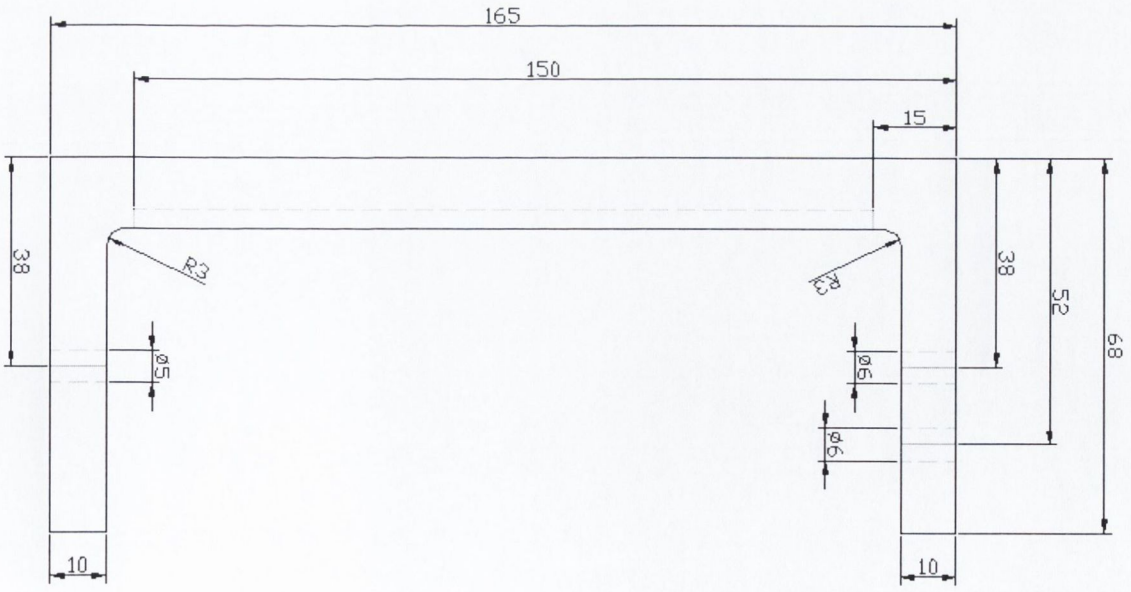
165
150
15
38
R3
R3
38
52
68
ø5
ø6
ø6
10
10

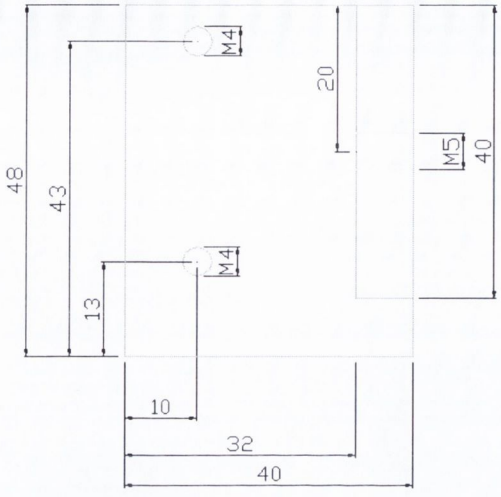

side view Nr. 2B

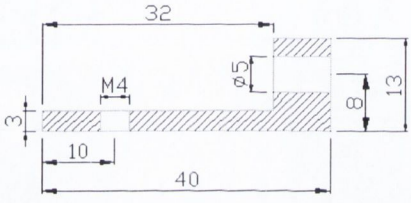

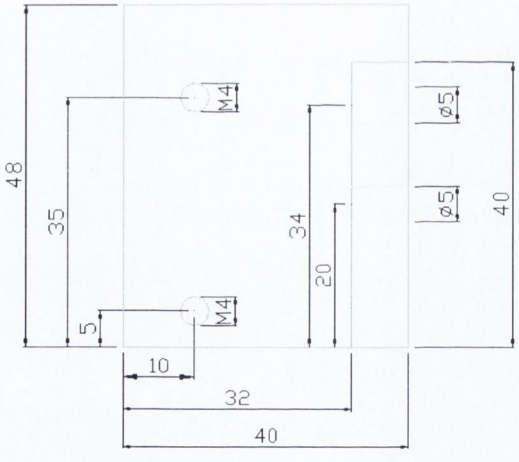

side view Nr. 2A

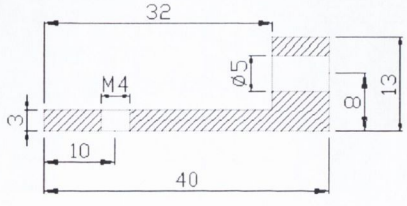

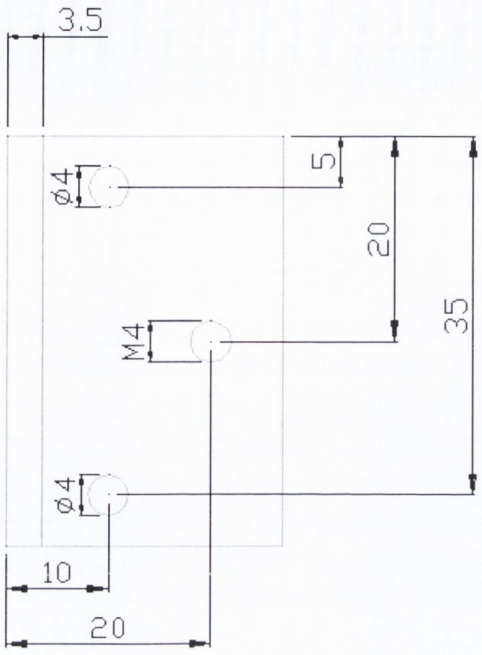
3.5
ø4
5
20
35
M4
ø4
10
20

Appendix 2 Computer programmes

CRGROW.f90 : Program written in order to predict cracks incorporating crack growth rates (Fortran90)

```
**************************************************************************
*******

program CRGROW

implicit none

real::hoek=1.13446,k,EI,Valb,Vala,KAI,KAII,KBI,KBII,KAtot,KBtot,pi=3.14159,a,
b,dagen,Tag
real::dadN,dbdN,Syield=115,life=6e3,young=17400,d1=15e-3,d2=250e-
3,n,rq,Aleng,Bleng
real:: rya, ryb, perim, volume, damagea, area, DA, xshear, zshear
real:: stre s=-5
integer, dimension(1):: i=1
a=5e-3
b=5e-3
n=1
rq=1
dagen=n/life

open (unit=11, file='resc0530.txt')
k=b/a
EI=1+(0.0538915*k)+(1.25750375*k**2)-
(1.49489655*k**3)+(1.074995681*k**4)-(0.3204405188*k**5)
Valb=stres*(sqrt(pi*b))/EI
Vala=stres*(b/a)*(sqrt(pi*a))/EI
KAI=Vala*cos(hoek)*cos(hoek)
KAII=Vala*cos(hoek)*sin(hoek)
KBI=Valb*cos(hoek)*cos(hoek)
KBII=Valb*cos(hoek)*sin(hoek)
if (stres<0) then
KAI=0
KBI=0
else
KAI=KAI
KBI=KBI
end if
KAtot=sqrt(KAI**2+KAII**2)
KBtot=sqrt(KBI**2+KBII**2)
dadN=(1.3e-5*(abs((KAtot/31.623)-
0.07)**4.5))+((0.013*(KAtot/31.623)**4.5)*((d2-a)/d2)**5)
```

```
dbdN=(1.3e-5*(abs((KAtot/31.623)-
0.19)**4.5))+((0.013*(KBtot/31.623)**4.5)*((d1-b)/d1)**5)

do while (dagen<100)
a=a+dadN
n=n+1
if (dbdN>0) then
b=b+dbdN
else
dbdN=0
end if
k=b/a
EI=1+(0.054*k)+(1.2575*k**2)-(1.495*k**3)+(1.075*k**4)-(0.32*k**5)
Valb=stres*(sqrt(pi*b))/EI
Vala=stres*(b/a)*(sqrt(pi*a))/EI
KAI=Vala*cos(hoek)*cos(hoek)
KAII=Vala*cos(hoek)*sin(hoek)
KBI=Valb*cos(hoek)*cos(hoek)
KBII=Valb*cos(hoek)*sin(hoek)
if (stres<0) then
KAI=0
KBI=0
else
KAI=KAI
KBI=KBI
end if
KAtot=sqrt(KAI**2+KAII**2)
KBtot=sqrt(KBI**2+KBII**2)
dadN=(1.3e-3*(abs((KAtot/31.623)-
0.07)**3.5))+((0.13*(KAtot/31.623)**3.5)*((d2-a)/d2)**5)
dbdN=(1.3e-5*(abs((KBtot/31.623)-
0.19)**4.5))+((0.13*(KBtot/31.623)**3.5)*((d1-b)/d1)**5)
Aleng=a*2000
Bleng=b*2000
dagen=n/life
rya=(1/pi)*(Katot/(0.25*Syield))**2
ryb=(1/pi)*(Kbtot/(0.25*Syield))**2
perim=(pi*sqrt(2*((a+rya)**2+(b+ryb)**2)))/(cos(hoek)*cos(hoek)*cos(hoek)*cos(
hoek))
volume=0.2618*perim*(rya**2+rya*ryb+ryb**2)
xshear=abs(-((0.1e-3/(0.765*(b/a)**0.1*(a/b)*(stres/young)*(1-0.39**2) *cos(hoek)
*sin(hoek)))**2) +b**2)**0.5
zshear=abs(-((0.1e-3/(0.765*(b/a)**0.1*(stres/young)*(1-0.39**2)*cos(hoek)
*sin(hoek)))**2) +a**2)**0.5
damagea=pi*xshear*zshear
area=pi*a*b
```

```
DA=damagea*100/area
Tag=life/rq
if (damagea>area) then
damagea=0
else
damagea=damagea
end if
if (Tag<1) then
write (11,*) Aleng, Bleng, volume,damagea
rq=1
else
rq=rq+1
end if

enddo

close(unit=11)

end program CRGROW
```

Composite approach using Denda: written in Matlab 5.1: file DendaNEW2.m

```
load thefinalcrackdata.txt;
M=thefinalcrackdata;
n=1;
res=[];
Q=[24880 8580 0; 8580 13700 0; 0 0 4140]; %stiffness matrix from
Sevostianov

%%%%%%%%%%%%%%%%%%%%%%%%%%%%%%%%%%%%%%%%%%%%%%%%%%%%%%%%%%%%%%%%%%%%%%%%%%%%%%%%
%%%%%%

while(n<431)                    %431 number of rows
Stress=M(n,6)/((M(n,7))*(M(n,9)));        %calculating the stress=>
F/width*thickness
hoek=M(n,5);                    %angle of the crack
if (hoek<=90);                  %we have to change the crack angle
here so
hoek=90-hoek;                   %that it is aligned perpendicular to
the load direction.
   else
      hoek=hoek-90;
   end
   hoek;
   tet2=hoek*pi/180;

%%%%%%%%%%%%%%%%%%%%%%%%%%%%%%%%%%%%%%%%%%%%%%%%%%%%%%%%%%%%%%%%%%%%%%%%%%%%%%%%
%%%%%%
   if hoek<45;
      Q=[13700 8580 0;8580 24880 0; 0 0 4140];
```

```
    else
       Q=[24880 8580 0;8580 13700 0; 0 0 4140];
    end

%%%
```

```
CTSD=2000*StSh*(sqrt((b/2)^2-a^2));

res=[res;CTOD CTSD];
n=n+1;
end
res;
save ('DendaNEWout2', 'res','-ascii');
```

Composite approach using Chen: written in Matlab 5.1: file ChenNEW.m

```
load thefinalcrackdata.txt;
M=thefinalcrackdata;
n=1;
res=[];
Q=[24880 8580 0;8580 13700 0;0 0 4140];%stiffenes matrix from
Sevostianov

%%%%%%%%%%%%%%%%%%%%%%%%%%%%%%%%%%%%%%%%%%%%%%%%%%%%%%%%%%%%%%%%%%%%%%%%%%%%
%%%%%%%

while(n<431)
      %431 number of rows
Stress=M(n,6)/((M(n,7))*(M(n,9)));        %calculating the stress=>
F/width*thickness
   hoek=M(n,5);                                                    %angle
of the crack
if (hoek<=90);
      %we have to change the crack angle here so
hoek=90-hoek;
      %that it is aligned perpendicular to the load direction.
else
    hoek=hoek-90;
end
hoek;
tet2=hoek*pi/180;

%%%%%%%%%%%%%%%%%%%%%%%%%%%%%%%%%%%%%%%%%%%%%%%%%%%%%%%%%%%%%%%%%%%%%%%%%%%%
%%%%%%%

if hoek<45;
    Q=[13700 8580 0;8580 24880 0; 0 0 4140];
else
    Q=[24880 8580 0;8580 13700 0; 0 0 4140];
end


%%%%%%%%%%%%%%%%%%%%%%%%%%%%%%%%%%%%%%%%%%%%%%%%%%%%%%%%%%%%%%%%%%%%%%%%%%%%
%%%%%%%
   nl=M(n,8);
      %the notch length
   a=M(n,2)/1000;
      %the crack length a in mm
   b=(nl+a*cos(tet2));
      %representative crack length
```

```
      b;
%%%
```

```
S=M(n,6)/((M(n,7))*(M(n,9)));                    %calculating the
stress=> (F/width)*thickness
   hoek=M(n,5);                                                %angle
of the crack
if (hoek<=90);
      %we have to change the crack angle here so
hoek=90-hoek;                                          %that it is
aligned perpendicular to the load direction.
   else
      hoek=hoek-90;
   end
   tet2=hoek*pi/180;
   nl=M(n,8);
      %the notch length
   a=M(n,2)/1000;                                              %the
crack length a in mm
   b=(nl+a*cos(tet2))/2;
   K=(S*sqrt(pi*b))/sqrt(1000);
   K2=(2/3)*K*sin(tet2/2)*cos(tet2/2);
   K1=1.12*(K*cos(tet2/2)*cos(tet2/2))*cos(tet2/1);

   if (M(n,10))<1.5;
      E=Et;
   else
      E=El;
   end

   CTOD=12*2000*(S/E)*a*cos(tet2/2)*cos(tet2/2);
   CTSD=12*2000*(S/E)*a*sin(tet2/2)*cos(tet2/2);
   erOP=M(n,3)/CTOD;
   erSH=M(n,4)/CTSD;
   res=[res;CTOD CTSD K1 K2 erOP erSH];

   n=n+1;
end
res;
save ('resallcrackdata', 'res','-ascii')
```

Using Chen: written in Matlab 5.1: file Chenall.m

```
load revspecdata.txt;
M=revspecdata;
n=1;
res=[];
Et=11700;                                              %stiffness in
transverse direction
El=20400;                                              %stiffness in
longitudinal direction
while(n<432)                                           %458 number of
rows
S=M(n,6)/((M(n,7))*(M(n,9)));       %calculating the stress=>
F/width*thickness
   hoek=M(n,5);                                    %angle of the crack
   if (hoek<=90);                                  %we have to change
the crack angle here so
```

```
hoek=90-hoek;                                          %that it is
aligned perpendicular to the load direction.
   else
      hoek=hoek-90;
   end
   tet2=hoek*pi/180;
   nl=M(n,8);                                          %the notch
length
   a=M(n,2)/1000;                                  %the crack length a
in mm
   b=(nl+a*cos(tet2));
   K=(S*sqrt(pi*b))/sqrt(1000);
   K1=K*cos(tet2/2)*cos(tet2/2);
   K2=K*sin(tet2/2)*cos(tet2/2);

   if (M(n,10))<1.5;
      E=Et;
   else
      E=El;
   end

   CTOD=2000*(4*S/Et)*(sqrt((b/2)^2-a^2))*cos(tet2/2)*cos(tet2/2);
   CTSD=2000*(4*S/Et)*(sqrt((b/2)^2-a^2))*sin(tet2/2)*cos(tet2/2);

   res=[res;CTOD CTSD K1 K2];

   n=n+1;
end
res;
save ('chenres', 'res','-ascii')
```

Using Denda: written in Matlab 5.1: file Nisitaniall.m

```
load revspecdata.txt;
M=revspecdata;
n=1;
res=[];
Et=11700;                                              %stiffness in
transverse direction
El=20400;                                              %stiffness in
longitudinal direction
while(n<432)                                           %432 number of
rows
S=M(n,6)/((M(n,7))*(M(n,9)));        %calculating the stress=>
F/width*thickness
hoek=M(n,5);                                           %angle of the
crack
if (hoek<=90);                                         %we have to
change the crack angle here so         hoek=90-hoek;
                        %that it is aligned perpendicular to the
load direction.
   else
      hoek=hoek-90;
   end
   tet2=hoek*pi/180;
```

```
   nl=M(n,8);                                          %the notch
length
   a=M(n,2)/1000;                                  %the crack length a
in mm
   c2=nl+(a*sin(tet2));
   if hoek<90
      b=nl+a;
   else
      b=c2/sin(tet2);
   end

   K=(S*sqrt(pi*b))/sqrt(1000);
   K1=K*cos(tet2/2)*cos(tet2/2);
   K2=K*sin(tet2/2)*cos(tet2/2);

   if (M(n,10))<1.5;
      E=Et;
   else
      E=El;
   end

   CTOD=2000*(3*S/Et)*(sqrt((b/2)^2-a^2))*cos(tet2/2)*cos(tet2/2);
   CTSD=2000*(3*S/Et)*(sqrt((b/2)^2-a^2))*sin(tet2/2)*cos(tet2/2);

   res=[res;CTOD CTSD K1 K2];

   n=n+1;
end
res;
save ('nisitanires', 'res','-ascii')
```

Appendix 3 Raw data of specimens and crack analysis

Longitudinal notches

Specimen	Filename	Length	Path	Open	Shear	Angle tip_tip	Force
D3s2	loadcel3005!030329104238	112.5	113.0	2.7	0.7	104.4	142.3
D3s2	loadcel3005!030329104258	158.9	161.1	3.7	1.0	111.8	142.6
D3s2	loadcel3005!030329104318	279.3	281.3	3.7	1.1	111.6	143.0
D3s2	loadcel3005!030329104338	367.0	389.7	5.6	1.8	109.1	143.7
D3s2	loadcel3005!030329104358	387.3	406.4	5.4	2.3	108.9	143.7
D3s2	loadcel3005!030329104418	395.4	412.7	5.5	2.1	109.4	144.0
D3s2	loadcel3005!030329104438	401.1	411.9	8.2	2.5	109.3	144.3
D3s2	loadcel3005!030329104458	400.4	412.2	8.4	1.9	109.1	144.6
D3s2	loadcel3005!030329104518	406.6	417.3	10.0	3.0	109.4	145.0
D3s2	loadcel3005!030329104538	411.6	426.5	9.2	2.2	109.7	145.6
D3s2	loadcel3005!030329104558	419.6	431.7	9.3	2.9	109.2	146.0
D3s2	loadcel3005!030329104618	394.9	432.7	10.2	2.9	109.7	146.3
D3s2	loadcel3005!030329104638	417.0	437.7	12.0	3.9	109.8	146.9
D3s2	loadcel3005!030329104658	419.4	439.5	13.0	3.8	109.9	147.3
D3s2	loadcel3005!030329104718	423.4	439.2	11.1	3.0	109.3	148.0
D3s2	loadcel3005!030329104738	423.4	439.3	13.8	4.3	109.5	148.2
D3s2	loadcel3005!030329104758	423.4	439.3	13.8	5.2	109.7	148.5
D3s2	loadcel3005!030329104818	437.9	453.9	13.0	3.9	109.8	149.3
D3s2	loadcel3005!030329104838	449.4	466.0	13.0	4.6	110.0	149.4
D3s2	loadcel3005!030329104858	454.4	474.4	13.9	3.8	110.1	150.4
D3s2	loadcel3005!030329104918	473.2	475.7	15.6	5.3	110.0	150.7
D3s3	loadcel3006!030329105629	144.8	187.3	1.7	1.2	104.4	81.6
D3s3	loadcel3006!030329105649	146.8	191.1	2.8	1.8	105.9	81.0
D3s3	loadcel3006!030329105709	174.4	219.1	3.6	2.2	105.0	81.1
D3s3	loadcel3006!030329105729	175.1	221.5	4.8	3.6	106.5	81.2
D3s3	loadcel3006!030329105749	190.9	231.3	5.5	3.9	104.7	81.5
D3s3	loadcel3006!030329105809	192.9	240.9	5.6	3.7	105.2	81.5
D3s3	loadcel3006!030329105829	308.6	364.0	4.5	3.0	96.7	81.8
D3s3	loadcel3006!030329105849	322.0	365.8	6.4	4.8	96.0	82.6
D3s3	loadcel3006!030329105909	697.0	726.9	6.8	4.2	92.8	82.8
D3s3	loadcel3006!030329105929	709.3	790.4	7.4	4.7	93.0	83.4

D3s4	loadcel3007!030329111745	299.0	324.7	5.6	2.7	85.4	73.0
D3s4	loadcel3007!030329111800	356.0	383.8	6.4	2.3	86.6	73.4
D3s4	loadcel3007!030329111815	394.3	407.5	5.4	2.3	86.1	73.6
D3s4	loadcel3007!030329111830	395.6	416.4	5.5	2.1	86.9	74.3
D3s4	loadcel3007!030329111845	412.1	426.5	6.3	3.3	86.9	74.5
D3s4	loadcel3007!030329111900	434.4	467.2	7.5	1.8	87.4	74.9
D3s4	loadcel3007!030329111915	438.6	470.9	7.5	1.7	88.6	75.3
D3s4	loadcel3007!030329111930	446.1	477.1	9.2	2.4	90.4	76.7
D3s4	loadcel3007!030329111945	469.3	494.5	9.3	2.8	90.8	77.7
D3s4	loadcel3007!030329112000	502.8	536.3	10.9	4.5	90.5	78.3
D3s4	loadcel3007!030329112015	824.3	894.8	9.9	2.7	96.0	79.2
D3s5	loadcel3009!030329113354	234.4	253.2	2.7	0.6	79.7	91.4
D3s5	loadcel3009!030329113409	363.9	408.1	3.7	0.9	81.0	92.2
D3s5	loadcel3009!030329113424	442.6	473.4	4.6	1.1	80.8	92.8
D3s5	loadcel3009!030329113439	445.6	474.9	5.6	0.9	98.0	93.7
D3s5	loadcel3009!030329113454	544.5	569.9	6.5	0.9	79.0	94.4
D3s5	loadcel3009!030329113509	559.1	592.2	7.3	1.6	78.7	95.2
D3s5	loadcel3009!030329113524	609.0	645.6	8.4	1.8	78.9	95.9
D3s6	loadcel3010!030329114626	675.8	727.4	3.6	1.3	101.1	73.3
D3s6	loadcel3010!030329114641	683.2	728.1	5.6	1.7	100.6	74.0
D3s6	loadcel3010!030329114656	688.3	744.3	5.4	1.7	100.4	75.0
D3s6	loadcel3010!030329114711	707.8	755.2	7.4	2.9	100.4	75.6
D3s6	loadcel3010!030329114726	815.6	883.2	6.4	2.3	99.0	75.9
D3s6	loadcel3010!030329114741	832.6	884.0	7.3	2.5	99.4	77.0
D3s6	loadcel3010!030329114756	849.4	908.2	9.3	2.7	98.7	77.3
D3s6	loadcel3010!030329114811	891.4	943.4	9.2	3.2	98.8	78.0

D3s7	loadcel3011!030329120013	120.2	120.2	2.7	1.1	102.8	89.0
D3s7	loadcel3011!030329120028	150.3	151.7	3.7	1.1	99.3	89.7
D3s7	loadcel3011!030329120043	163.6	164.5	4.7	1.8	99.1	90.5
D3s7	loadcel3011!030329120058	212.9	216.6	6.5	2.8	95.8	91.2
D3s7	loadcel3011!030329120113	508.9	522.3	6.4	1.4	96.1	91.7
D3s7	loadcel3011!030329120128	686.8	758.9	4.6	1.1	103.8	92.7
D3s7	loadcel3011!030329120143	733.2	801.3	5.5	1.3	103.7	93.1
D3s7	loadcel3011!030329120158	733.5	801.5	6.4	2.1	103.5	94.0
D3s7	loadcel3011!030329120213	735.5	801.7	6.5	1.9	103.9	94.4
D3s7	loadcel3011!030329120228	737.1	805.9	7.4	2.2	103.2	95.0
D3s7	loadcel3011!030329120243	739.4	807.9	7.4	2.0	103.3	95.4
D3s7	loadcel3011!030329120258	741.4	810.2	10.2	3.8	103.3	95.5
D3s7	loadcel3011!030329120313	742.5	832.9	9.3	2.9	103.0	96.5
D3s7	loadcel3011!030329120328	771.2	848.1	9.3	2.1	102.9	97.4
D3s7	loadcel3011!030329120343	771.6	848.2	9.1	2.6	102.7	97.9
D3s7	loadcel3011!030329120358	771.8	849.6	11.1	3.8	100.7	98.6
D3s7	loadcel3011!030329120413	822.1	902.3	11.1	3.2	101.1	99.5
D3s7	loadcel3011!030329120428	839.8	914.0	11.0	2.7	100.9	100.1
D5s1	loadcel5001!030407095007	169.5	173.7	4.6	0.5	89.4	99.9
D5s1	loadcel5001!030407095022	173.3	180.3	4.6	0.7	85.0	100.0
D5s1	loadcel5001!030407095037	254.0	254.0	5.5	0.7	84.0	100.1
D5s1	loadcel5001!030407095052	352.0	363.3	7.4	0.7	87.9	100.4
D5s1	loadcel5001!030407095108	363.2	373.9	6.4	1.0	87.6	100.6
D5s1	loadcel5001!030407095122	364.1	375.6	7.4	0.6	88.0	100.8
D5s1	loadcel5001!030407095137	364.2	375.9	7.4	0.7	86.3	101.6
D5s1	loadcel5001!030407095152	394.0	429.0	7.4	0.5	87.1	101.8
D5s1	loadcel5001!030407095207	424.5	435.9	8.4	0.4	87.1	102.2
D5s1	loadcel5001!030407095223	464.5	487.3	10.2	1.6	83.9	103.0
D5s1	loadcel5001!030407095238	603.4	646.4	11.2	1.2	89.7	103.6
D5s1	loadcel5001!030407095252	625.9	662.4	9.3	0.2	89.9	103.8
D5s1	loadcel5001!030407095307	632.3	667.4	10.2	0.2	89.4	104.2
D5s1	loadcel5001!030407095322	641.7	675.0	10.2	0.3	89.9	104.5
D5s1	loadcel5001!030407095338	643.6	680.9	12.1	1.0	89.1	105.2
D5s1	loadcel5001!030407095352	659.2	711.8	13.0	1.5	89.8	106.1
D5s1	loadcel5001!030407095407	681.6	724.3	13.0	0.6	89.8	106.2
D5s1	loadcel5001!030407095422	714.2	755.3	12.1	0.6	90.0	106.8
D5s1	loadcel5001!030407095438	721.6	761.7	11.2	0.0	91.5	107.3
D5s1	loadcel5001!030407095453	733.8	779.9	11.2	0.5	91.1	107.9
D5s1	loadcel5001!030407095507	769.4	823.2	12.1	0.8	91.1	108.1
D5s1	loadcel5001!030407095522	806.8	855.6	10.2	1.3	91.8	109.1
D5s1	loadcel5001!030407095537	819.3	859.1	11.2	0.5	92.5	109.8

D5s3	loadcel5004!030407102218	245.8	251.2	9.3	0.6	84.7	107.9
D5s3	loadcel5004!030407102234	254.3	264.3	7.4	0.5	84.1	108.3
D5s3	loadcel5004!030407102248	352.1	365.3	9.3	0.7	88.6	108.5
D5s3	loadcel5004!030407102303	364.3	381.9	8.4	0.2	88.7	108.7
D5s3	loadcel5004!030407102318	365.2	382.1	9.3	0.6	98.4	110.0
D5s3	loadcel5004!030407102333	370.0	383.0	11.1	0.8	88.2	110.3
D5s3	loadcel5004!030407102349	374.5	382.6	11.1	0.8	88.5	111.2
D5s3	loadcel5004!030407102404	374.5	382.6	10.2	0.4	85.1	111.8
D5s3	loadcel5004!030407102419	414.6	438.2	11.2	0.3	85.0	112.8
D5s3	loadcel5004!030407102433	414.6	438.2	10.2	0.4	85.4	113.9
D5s3	loadcel5004!030407102448	421.9	458.1	11.2	0.6	85.0	114.5
D5s3	loadcel5004!030407102504	421.9	458.1	11.2	0.5	84.6	114.8
D5s3	loadcel5004!030407102519	427.5	467.1	10.2	0.0	83.3	115.5
D5s3	loadcel5004!030407102533	460.2	490.0	12.1	0.6	83.4	116.0
D5s3	loadcel5004!030407102548	460.2	494.0	11.2	0.5	83.4	117.2
D5s3	loadcel5004!030407102603	500.5	526.8	12.1	0.0	83.3	117.5
D5s3	loadcel5004!030407102618	507.3	539.1	12.1	1.0	83.3	117.6
D5s3	loadcel5004!030407102634	515.7	542.5	14.0	0.7	83.4	117.8
D5s3	loadcel5004!030407102648	531.5	575.0	14.0	0.9	83.6	118.1
D5s3	loadcel5004!030407102703	562.4	607.0	14.0	0.7	81.6	119.4
D5s3	loadcel5004!030407102718	585.2	625.3	14.9	0.5	81.3	120.0
D5s3	loadcel5004!030407102733	594.5	625.5	14.9	0.5	80.6	120.1
D5s3	loadcel5004!030407102748	595.5	625.5	16.8	0.9	80.4	120.4
D5s3	loadcel5004!030407102803	599.7	626.3	16.7	1.5	80.4	120.9
D5s3	loadcel5004!030407102818	610.8	627.4	16.7	1.0	80.5	121.2
D5s3	loadcel5004!030407102833	628.7	670.8	17.6	2.5	80.4	121.5
D5s3	loadcel5004!030407102848	628.7	670.8	20.5	1.4	80.3	121.5
D5s3	loadcel5004!030407102903	640.0	670.9	23.3	0.8	80.4	121.5
D5s3	loadcel5004!030407102918	640.9	676.9	21.4	1.2	80.4	122.1
D5s3	loadcel5004!030407102933	647.2	691.1	19.5	0.8	80.8	122.4
D5s3	loadcel5004!030407102949	659.1	691.5	23.3	1.0	80.5	122.6
D5s3	loadcel5004!030407103003	672.0	700.9	25.0	1.8	80.4	122.8
D5s3	loadcel5004!030407103018	672.2	701.2	23.3	0.7	80.3	123.6
D5s3	loadcel5004!030407103033	672.2	701.2	25.1	1.0	80.3	123.9
D5s3	loadcel5004!030407103048	672.2	701.2	26.0	1.4	80.5	124.2
D5s3	loadcel5004!030407103103	679.6	702.8	27.9	2.1	80.8	125.1
D5s3	loadcel5004!030407103119	689.3	705.3	27.0	0.0	80.2	125.6

D5s5	loadcel5006!030407105148	242.6	253.6	6.5	1.9	73.9	102.1
D5s5	loadcel5006!030407105204	252.7	263.1	7.4	2.1	74.5	102.3
D5s5	loadcel5006!030407105218	255.4	266.2	9.2	2.4	74.1	102.6
D5s5	loadcel5006!030407105234	258.7	269.7	7.4	2.0	74.5	103.2
D5s5	loadcel5006!030407105249	316.7	366.7	8.3	2.1	71.6	103.6
D5s5	loadcel5006!030407105303	369.0	430.1	10.1	2.5	73.7	103.8
D5s5	loadcel5006!030407105318	394.3	445.7	11.2	2.9	74.4	104.8
D5s5	loadcel5006!030407105334	412.3	456.2	10.1	2.5	74.2	105.0
D5s5	loadcel5006!030407105349	414.4	469.7	11.2	2.8	72.5	105.4
D5s5	loadcel5006!030407105403	425.0	488.5	11.1	2.9	70.8	105.6
D5s5	loadcel5006!030407105418	497.9	545.7	12.0	3.3	70.8	106.0
D5s5	loadcel5006!030407105433	498.4	551.7	11.1	2.9	70.4	107.0
D5s5	loadcel5006!030407105448	565.4	628.7	14.9	3.7	72.3	107.4
D5s5	loadcel5006!030407105504	581.0	641.7	15.7	3.2	72.7	107.8
D5s5	loadcel5006!030407105518	585.7	647.1	16.9	4.2	72.6	108.5
D5s5	loadcel5006!030407105533	586.4	661.3	18.5	3.6	73.1	108.8
D5s5	loadcel5006!030407105548	586.4	661.5	20.4	5.0	73.1	110.1
D5s5	loadcel5006!030407105603	591.9	666.1	15.8	4.9	73.6	109.9
D5s5	loadcel5006!030407105618	618.9	676.2	19.2	4.5	73.8	110.2
D5s5	loadcel5006!030407105633	629.4	677.7	18.5	5.0	73.7	110.4
D5s5	loadcel5006!030407105648	642.5	690.8	19.5	4.9	73.7	111.3
D5s5	loadcel5006!030407105703	644.3	700.7	18.5	3.4	73.7	112.0
D5s5	loadcel5006!030407105719	644.7	705.1	18.6	4.9	73.7	112.2
D5s5	loadcel5006!030407105733	651.8	706.0	19.5	5.1	73.8	112.7
D5s5	loadcel5006!030407105748	675.5	715.6	18.5	5.9	73.8	113.7
D5s5	loadcel5006!030407105803	677.0	721.2	21.3	4.4	73.8	113.8
D5s5	loadcel5006!030407105818	698.4	753.2	22.3	3.7	74.1	114.1
D5s7	loadcel5008!030407111628	380.9	420.4	4.1	2.2	102.3	105.4
D5s7	loadcel5008!030407111643	497.8	533.7	2.9	1.5	100.7	105.7
D5s7	loadcel5008!030407111657	537.6	575.5	3.5	1.5	100.3	105.6
D5s7	loadcel5008!030407111712	542.9	593.9	3.7	1.2	99.5	105.9
D5s7	loadcel5008!030407111727	574.3	611.9	5.6	2.8	100.0	106.3
D5s7	loadcel5008!030407111742	578.2	639.2	5.6	2.7	99.8	106.7
D5s7	loadcel5008!030407111758	598.1	639.7	3.6	1.3	100.2	107.0
D5s7	loadcel5008!030407111813	601.6	639.8	6.3	3.2	99.9	107.7
D5s7	loadcel5008!030407111827	601.8	640.5	5.5	2.1	100.1	108.1
D5s7	loadcel5008!030407111842	603.7	644.4	6.5	2.8	100.9	108.5
D5s7	loadcel5008!030407111857	603.5	651.7	7.5	3.6	100.5	109.0
D5s7	loadcel5008!030407111913	609.0	655.5	8.2	3.4	101.5	109.8
D5s7	loadcel5008!030407111927	720.8	818.2	10.3	1.8	106.5	109.9
D5s7	loadcel5008!030407111942	732.6	820.9	10.2	1.4	106.5	110.0

D5s8	loadcel5009!030407112815	470.0	486.6	0.0	0.7	101.8	110.2
D5s8	loadcel5009!030407112829	595.5	620.7	3.7	0.9	104.3	111.3
D5s8	loadcel5009!030407112844	699.5	720.4	4.7	0.2	103.1	111.6
D5s8	loadcel5009!030407112859	710.7	738.9	6.5	0.8	103.2	112.0
D5s8	loadcel5009!030407112914	719.6	758.1	7.4	1.5	103.2	113.6
D5s8	loadcel5009!030407112929	725.8	759.9	10.2	0.0	103.2	114.6
D5s8	loadcel5009!030407112944	768.4	792.5	8.4	0.9	103.4	115.6
D5s8	loadcel5009!030407112959	803.9	825.4	8.4	0.4	102.9	116.4
D10S4	loadcel10004!030516031731	330.5	347.5	8.3	2.2	84.2	81.94
D10S4	loadcel10004!030516031746	375.1	390.8	8.3	2.3	86.1	83.00
D10S4	loadcel10004!030516031801	391.9	412.3	6.3	1.8	86.2	83.56
D10S4	loadcel10004!030516031816	400.6	425.9	6.5	2.1	86.2	83.68
D10S4	loadcel10004!030516031831	410.3	428.6	7.3	1.7	87.1	83.78
D10S4	loadcel10004!030516031846	446.6	467.9	6.4	1.5	87.2	83.70
D10S4	loadcel10004!030516031902	458.7	484.7	10.1	2.6	86.8	84.07
D10S4	loadcel10004!030516031917	490.8	519.5	8.3	2.3	88.4	85.16
D10S4	loadcel10004!030516031931	529.8	553.3	7.3	2.4	87.4	85.42
D10S4	loadcel10004!030516031947	542.9	563.6	9.2	3.0	89.6	85.59
D10S4	loadcel10004!030516032001	582.9	620.2	8.3	2.2	90.4	85.62
D10S4	loadcel10004!030516032017	599.6	627.8	11.1	3.0	91.0	85.95
D10S4	loadcel10004!030516032032	613.7	637.6	10.2	2.3	91.0	86.05
D10S4	loadcel10004!030516032047	667.2	704.89	10.1	2.7	94.2	86.00
D10S4	loadcel10004!030516032101	676.7	714.6	12.1	3.0	94.2	86.34
D10S4	loadcel10004!030516032116	684.3	736.6	8.6	2.0	93.6	87.66

D10S6	loadcel10006!030516035313	229.1	236.0	3.7	0.3	91.9	98.23
D10S6	loadcel10006!030516035329	275.6	286.4	4.6	0.4	89.6	98.59
D10S6	loadcel10006!030516035343	292.5	302.9	5.6	0.2	89.3	98.64
D10S6	loadcel10006!030516035358	295.2	303.6	6.5	0.7	89.0	99.04
D10S6	loadcel10006!030516035414	327.8	340.0	6.5	0.4	86.9	99.16
D10S6	loadcel10006!030516035429	327.9	339.96	5.6	0.1	86.9	99.23
D10S6	loadcel10006!030516035443	328.0	340.1	6.3	0.4	87.0	99.47
D10S6	loadcel10006!030516035458	328.2	341.0	7.4	0.7	86.9	99.77
D10S6	loadcel10006!030516035513	336.6	347.6	6.8	0.4	85.5	99.88
D10S6	loadcel10006!030516035528	353.4	365.1	8.8	0.6	85.8	100.46
D10S6	loadcel10006!030516035544	417.6	438.1	8.3	0.7	85.9	101.18
D10S6	loadcel10006!030516035558	417.5	438.2	8.4	0.6	86.2	101.45
D10S6	loadcel10006!030516035613	427.5	442.2	9.3	0.6	86.5	101.46
D10S6	loadcel10006!030516035628	459.6	478.3	6.5	0.3	85.1	101.69
D10S6	loadcel10006!030516035643	470.8	496.0	8.4	0.4	82.6	103.29
D10S6	loadcel10006!030516035658	470.4	498.89	10.2	0.4	82.9	103.79
D10S6	loadcel10006!030516035713	473.8	503.2	11.2	0.4	82.5	103.85
D10S6	loadcel10006!030516035728	475.0	508.7	10.2	0.4	79.2	104.90
D10S6	loadcel10006!030516035743	524.6	556.0	14.0	0.5	79.1	105.22
D10S6	loadcel10006!030516035758	529.0	560.9	13.0	0.6	78.9	105.42
D10S6	loadcel10006!030516035813	552.4	579.4	14.0	0.5	80.1	105.71
D10S6	loadcel10006!030516035829	567.0	593.0	12.1	0.7	80.5	105.99
D10S6	loadcel10006!030516035843	574.5	616.8	13.9	0.9	80.9	107.92
D10S6	loadcel10006!030516035858	578.0	642.6	12.1	0.4	81.5	108.34
D10S6	loadcel10006!030516035913	619.2	656.5	18.9	0.0	81.8	109.27
D10S6	loadcel10006!030516035929	641.3	682.76	13.0	0.6	81.5	109.81
D10S6	loadcel10006!030516035944	652.8	697.7	13.9	0.8	81.5	110.10
D10S6	loadcel10006!030516035958	674.2	721.0	13.0	0.0	81.8	110.32
D10S6	loadcel10006!030516040014	706.9	751.4	16.8	0.2	82.1	111.71
D10S6	loadcel10006!030516040028	736.9	783.4	17.7	0.0	80.4	112.20
D10S6	loadcel10006!030516040043	748.4	792.3	16.8	0.2	80.3	112.37

Transverse notches

Specimen	Filename	Length	Path	Open	Shear	Angle tip_tip	Force
D2s5	set5002!030327035732	285.7	306.1	1.8	1.5	150.6	320.5
D2s5	set5002!030327035802	320.0	371.2	1.9	2.3	140.1	321.2
D2s5	set5002!030327035832	334.6	379.2	3.1	3.0	138.8	321.7
D2s5	set5002!030327035902	337.2	387.1	3.7	3.3	137.5	322.4
D2s5	set5002!030327035932	433.1	492.7	3.5	3.9	140.2	323.0
D2s5	set5002!030327040002	454.2	512.6	4.2	3.7	143.3	323.5
D2s5	set5002!030327040033	507.9	600.8	3.6	3.4	146.4	323.9
D2s5	set5002!030327040103	515.9	602.9	5.7	4.9	146.2	324.1
D2s5	set5002!030327040133	598.3	682.2	4.4	4.5	145.2	324.4
D2s5	set5002!030327040202	652.0	745.4	4.0	4.4	145.9	324.7
D2s5	set5002!030327040232	664.4	758.4	4.0	3.5	145.7	325.2
D4s2	loadcel4002!030401032628	688.9	702.5	17.7	0.2	177.0	51.5
D4s2	loadcel4002!030401032643	919.7	939.2	15.8	0.3	177.4	51.5
D4s2	loadcel4002!030401032658	925.2	941.6	18.4	0.6	177.7	51.7
D4s2	loadcel4002!030401032713	929.9	952.3	20.5	0.0	177.6	52.0
D4s2	loadcel4002!030401032728	970.4	991.3	19.5	0.3	178.5	52.4
D4s2	loadcel4002!030401032743	1005.4	1037.3	21.4	0.9	177.4	52.8
D4s2	loadcel4002!030401032758	1060.6	1077.6	24.2	0.9	177.1	53.7
D4s2	loadcel4002!030401032813	1069.7	1079.7	23.3	0.6	177.0	55.1
D6s1	loadcel6001!030411103505	491.4	556.3	4.1	3.3	33.9	179.9
D6s1	loadcel6001!030411103520	552.1	643.2	4.9	4.4	32.3	181.2
D6s1	loadcel6001!030411103535	552.9	650.4	5.0	4.2	32.0	182.2
D6s1	loadcel6001!030411103551	564.2	651.4	7.5	6.4	31.8	183.9
D6s1	loadcel6001!030411103605	584.2	658.5	6.9	5.1	32.0	185.2
D6s1	loadcel6001!030411103620	696.5	754.5	7.4	5.6	31.3	186.4
D6s1	loadcel6001!030411103635	711.2	799.7	7.1	6.0	30.9	187.7
D6s1	loadcel6001!030411103651	721.3	815.9	8.1	6.9	31.5	188.9
D6s1	loadcel6001!030411103706	728.1	824.6	7.0	7.0	32.0	190.1
D6s1	loadcel6001!030411103720	735.4	830.1	8.1	6.7	31.0	191.2
D6s1	loadcel6001!030411103735	745.7	843.7	6.7	5.4	31.3	191.9
D6s1	loadcel6001!030411103750	749.4	856.6	7.8	6.1	31.1	193.4
D6s1	loadcel6001!030411103806	756.4	862.8	9.5	7.2	30.8	194.0
D6s1	loadcel6001!030411103820	757.9	869.7	8.6	7.2	31.5	195.2
D6s1	loadcel6001!030411103836	769.1	873.1	11.0	9.6	31.2	195.7
D6s1	loadcel6001!030411103851	795.6	888.9	11.2	10.2	31.9	196.5

D6s4	loadcel6004!030411112206	420.0	428.8	5.5	2.1	158.0	133.4
D6s4	loadcel6004!030411112221	553.3	558.5	8.5	2.6	158.0	134.5
D6s4	loadcel6004!030411112237	676.5	722.0	8.2	2.6	159.0	135.1
D6s4	loadcel6004!030411112251	680.0	750.9	9.3	2.7	153.8	135.8
D6s4	loadcel6004!030411112306	718.2	780.8	11.2	3.7	150.3	135.8
D6s4	loadcel6004!030411112322	762.2	868.3	11.0	3.3	146.0	136.0
D6s4	loadcel6004!030411112337	940.9	1128.9	11.0	3.5	139.0	137.5
D6s4	loadcel6004!030411112351	950.1	1184.5	15.7	5.2	139.0	137.8
D6s4	loadcel6004!030411112406	996.4	1215.4	15.0	3.4	139.3	137.6
D6s4	loadcel6004!030411112422	1280.5	1496.1	17.6	4.9	142.6	138.1
D6s4	loadcel6004!030411112436	1325.4	1543.7	18.5	6.0	143.0	139.0
D6s4	loadcel6004!030411112452	1344.8	1547.0	17.7	5.5	143.9	137.9
D6s5	loadcel6005!030411114757	578.3	621.5	1.3	1.3	46.2	215.0
D6s5	loadcel6005!030411114811	630.7	672.0	3.5	3.1	46.1	215.1
D6s5	loadcel6005!030411114826	800.0	873.8	3.7	2.9	45.8	215.0
D6s5	loadcel6005!030411114841	888.9	959.8	4.8	3.5	45.9	214.9
D6s5	loadcel6005!030411114856	1052.3	1126.8	7.4	5.7	43.9	214.7
D6s5	loadcel6005!030411114911	1064.9	1134.2	6.6	4.5	43.9	214.8
D6s5	loadcel6005!030411114927	1101.6	1192.6	9.2	6.7	44.6	215.0
D6s6	loadcel6006!030411120017	467.7	552.6	5.5	3.9	152.1	109.9
D6s6	loadcel6006!030411120032	522.8	614.0	5.6	2.7	151.6	110.2
D6s6	loadcel6006!030411120047	532.8	615.2	6.7	3.4	153.0	110.4
D6s6	loadcel6006!030411120102	540.6	621.2	7.2	5.0	146.3	110.5
D6s6	loadcel6006!030411120117	722.1	832.2	8.1	5.2	149.7	131.1
D6s6	loadcel6006!030411120132	816.8	934.6	8.4	4.7	148.1	130.8
D6s6	loadcel6006!030411120147	838.2	983.8	10.0	5.1	147.8	130.9
D6s6	loadcel6006!030411120202	930.1	1039.8	9.4	4.5	147.5	130.9
D6s6	loadcel6006!030411120217	1025.7	1148.1	10.0	6.9	148.8	131.1
D6s6	loadcel6006!030411120232	1049.0	1182.6	11.3	7.3	148.7	131.2
D6s6	loadcel6006!030411120247	1069.7	1216.3	11.7	6.7	148.4	131.1
D6s6	loadcel6006!030411120302	1158.1	1295.5	12.2	7.3	149.2	131.2
D6s6	loadcel6006!030411120318	1182.4	1320.2	11.8	7.1	149.3	131.2
D6s6	loadcel6006!030411120332	1226.6	1363.8	13.1	8.2	149.5	131.4
D6s6	loadcel6006!030411120347	1232.8	1351.3	14.3	9.1	149.4	131.2
D6s6	loadcel6006!030411120402	1259.7	1366.3	13.8	9.6	149.6	131.5

D6s8	loadcel6008!030411123522	847.3	900.0	10.9	6.1	164.4	178.1
D6s8	loadcel6008!030411123537	856.4	902.6	7.4	4.7	164.1	178.6
D6s8	loadcel6008!030411123552	857.8	911.3	9.4	5.5	164.0	178.9
D6s8	loadcel6008!030411123607	873.1	932.3	10.4	5.2	164.6	179.3
D6s8	loadcel6008!030411123622	915.5	990.9	9.2	4.9	164.2	179.8
D6s8	loadcel6008!030411123637	970.8	1030.6	10.2	7.5	162.8	180.1
D8s2	loadcel8002!030510025014	436.2	448.4	4.5	1.5	23.1	150.6
D8s2	loadcel8002!030510025030	604.3	627.6	5.4	1.7	29.4	151.3
D8s2	loadcel8002!030510025044	789.6	830.4	7.4	2.9	30.6	152.4
D8s2	loadcel8002!030510025059	824.4	867.2	6.4	2.1	31.5	153.6
D8s2	loadcel8002!030510025114	872.9	904.9	6.4	2.9	32.4	154.9
D8s2	loadcel8002!030510025129	983.9	1030.1	8.2	3.4	33.5	155.7
D8s2	loadcel8002!030510025144	1035.5	1083.8	9.1	2.6	33.9	155.8
D8s2	loadcel8002!030510025200	1146.3	1213.2	9.1	4.2	35.1	156.0
D8s2	loadcel8002!030510025214	1270.9	1341.2	11.2	4.5	36.0	157.0
D8s3	loadcel8003!030510030418	250.4	279.3	4.6	1.9	71.3	165.1
D8s3	loadcel8003!030510030433	304.2	331.1	3.6	2.0	66.8	166.3
D8s3	loadcel8003!030510030449	359.3	437.5	5.5	2.1	69.1	167.3
D8s3	loadcel8003!030510030504	422.2	512.5	6.5	2.8	64.1	168.5
D8s3	loadcel8003!030510030518	469.8	548.1	7.4	3.0	61.1	169.2
D8s3	loadcel8003!030510030533	524.4	627.9	8.5	4.4	66.1	169.8
D8s3	loadcel8003!030510030548	599.6	748.4	10.3	4.5	68.1	171.0
D8s3	loadcel8003!030510030603	734.0	869.6	9.2	3.9	64.2	171.6
D8s4	loadcel8004!030510031621	228.3	242.4	2.8	0.9	57.8	136.8
D8s4	loadcel8004!030510031635	228.5	242.5	2.8	0.9	57.9	137.9
D8s4	loadcel8004!030510031651	256.2	267.3	3.7	1.1	55.1	138.9
D8s4	loadcel8004!030510031706	274.0	287.9	4.5	2.2	56.8	140.0
D8s4	loadcel8004!030510031720	302.9	331.8	4.5	3.0	55.9	140.9
D8s4	loadcel8004!030510031735	345.9	369.1	4.5	3.0	57.6	141.6
D8s4	loadcel8004!030510031750	362.3	382.1	6.3	3.2	58.8	142.2
D8s4	loadcel8004!030510031805	464.8	491.5	7.2	2.6	58.1	143.6
D8s4	loadcel8004!030510031821	547.9	591.3	7.4	2.9	60.6	144.2

D8s5	loadcel8005!030510032814	284.4	305.9	4.4	3.2	39.4	125.7
D8s5	loadcel8005!030510032829	298.3	331.5	6.4	4.0	40.3	126.0
D8s5	loadcel8005!030510032843	413.4	448.6	5.6	3.7	35.6	127.3
D8s5	loadcel8005!030510032858	472.7	495.0	5.4	3.1	36.3	128.0
D8s5	loadcel8005!030510032913	558.9	595.5	7.5	4.5	34.7	129.1
D8s5	loadcel8005!030510032928	652.6	688.7	9.4	6.4	35.5	129.4
D8s5	loadcel8005!030510032944	715.0	750.7	11.2	7.5	35.6	129.8
D8s5	loadcel8005!030510032959	970.2	1007.4	11.2	7.4	34.3	129.8
D8s5	loadcel8005!030510033013	1106.8	1162.7	13.1	8.2	34.4	129.9
D9s2	loadcel9002!030512030114	190.4	264.0	1.9	0.8	36.6	126.8
D9s2	loadcel9002!030512030128	230.2	308.9	2.8	0.9	37.5	127.5
D9s2	loadcel9002!030512030143	256.6	332.6	5.5	2.2	37.0	128.0
D9s2	loadcel9002!030512030159	360.5	482.1	4.4	1.7	40.1	128.3
D9s2	loadcel9002!030512030214	433.8	593.9	5.6	1.9	39.4	129.2
D9s2	loadcel9002!030512030228	514.7	654.3	7.5	2.6	37.2	129.8
D9s2	loadcel9002!030512030243	603.2	778.7	8.2	2.6	36.8	129.3
D9s2	loadcel9002!030512030258	666.8	822.3	9.3	2.8	36.4	129.5
D9s2	loadcel9002!030512030313	781.7	986.3	11.2	3.6	35.7	129.7
D9s2	loadcel9002!030512030328	915.4	1098.6	11.1	3.2	35.5	131.1
D9s6	loadcel9006!030512050342	337.5	371.9	6.3	3.3	160.1	148.0
D9s6	loadcel9006!030512050358	362.2	381.8	6.3	2.5	160.5	148.6
D9s6	loadcel9006!030512050412	433.0	452.3	5.5	2.9	160.3	149.1
D9s6	loadcel9006!030512050427	598.0	622.5	6.7	3.3	159.9	150.5
D9s6	loadcel9006!030512050442	663.7	700.3	6.3	3.3	161.2	151.2
D9s6	loadcel9006!030512050458	673.7	717.8	6.3	3.2	160.6	152.1
D9s6	loadcel9006!030512050513	714.0	732.0	7.4	3.9	161.4	152.7
D9s6	loadcel9006!030512050527	714.0	732.1	8.4	3.8	161.4	154.0
D9s6	loadcel9006!030512050542	771.2	807.0	6.6	3.5	160.5	154.7
D9s6	loadcel9006!030512050557	819.0	855.9	8.4	4.7	160.2	155.7
D9s6	loadcel9006!030512050613	981.4	1008.3	7.1	3.7	160.3	156.8
D9s6	loadcel9006!030512050628	1021.8	1046.2	7.5	4.6	160.1	157.3
D9s6	loadcel9006!030512050642	1059.2	1110.9	11.2	5.5	160.1	158.3

D11s3	loadcel11003!030517105918	348.8	370.9	4.7	4.6	138.4	142.0
D11s3	loadcel11003!030517105933	353.4	371.0	2.7	2.9	137.8	142.5
D11s3	loadcel11003!030517105948	353.4	371.0	3.9	3.5	138.6	143.0
D11s3	loadcel11003!030517110004	356.8	373.4	4.6	4.7	138.3	144.2
D11s3	loadcel11003!030517110018	359.3	377.3	4.6	4.7	138.0	144.6
D11s3	loadcel11003!030517110033	382.1	399.8	3.6	3.8	138.2	144.9
D11s3	loadcel11003!030517110048	382.1	400.0	4.5	4.8	139.5	145.8
D11s3	loadcel11003!030517110103	392.4	416.5	4.6	4.7	140.0	146.3
D11s3	loadcel11003!030517110119	449.8	475.7	5.4	5.8	140.7	146.5
D11s5	loadcel11005!030517112230	215.5	263.7	4.5	1.6	52.4	142.0
D11s5	loadcel11005!030517112244	225.9	264.7	4.6	2.1	54.5	143.0
D11s5	loadcel11005!030517112259	230.4	287.2	7.2	3.4	54.8	144.3
D11s5	loadcel11005!030517112314	266.9	313.3	4.7	1.8	57.4	145.4
D11s5	loadcel11005!030517112329	302.4	344.8	6.5	3.8	61.0	146.8
D11s5	loadcel11005!030517112344	441.6	494.2	5.5	3.0	66.4	147.8
D11s5	loadcel11005!030517112359	726.4	784.7	11.2	0.0	68.0	153.0
D11s6	loadcel11006!030517114203	206.4	237.4	2.8	1.9	148.1	123.8
D11s6	loadcel11006!030517114217	222.2	254.1	4.7	3.7	150.4	123.9
D11s6	loadcel11006!030517114232	295.8	345.0	4.4	3.2	155.3	124.0
D11s6	loadcel11006!030517114248	315.3	354.4	4.7	4.6	154.1	124.3
D11s6	loadcel11006!030517114303	318.1	359.3	6.4	5.7	154.5	124.5
D11s6	loadcel11006!030517114317	337.0	385.0	7.3	6.7	152.5	124.8

D11s7	loadcel11007!030517115412	279.6	295.4	5.6	4.7	146.6	127.0
D11s7	loadcel11007!030517115427	315.8	325.4	6.5	4.7	146.0	127.4
D11s7	loadcel11007!030517115442	346.8	361.6	5.2	4.2	146.6	129.3
D11s7	loadcel11007!030517115457	349.7	362.5	7.5	5.5	146.9	129.4
D11s7	loadcel11007!030517115512	431.4	515.7	6.4	4.8	132.3	129.8
D11s7	loadcel11007!030517115527	448.4	569.9	6.6	4.6	133.9	130.3
D11s7	loadcel11007!030517115542	542.5	630.5	8.4	6.5	143.4	132.5
D11s7	loadcel11007!030517115557	547.1	631.7	8.7	6.1	142.3	132.6
D11s7	loadcel11007!030517115613	573.5	660.6	9.6	6.8	141.7	133.1
D11s7	loadcel11007!030517115627	599.6	699.4	9.2	7.3	142.4	133.7
D11s7	loadcel11007!030517115642	629.1	724.2	10.1	7.6	142.5	135.1
D11s7	loadcel11007!030517115658	649.4	735.2	10.3	8.2	142.4	135.5
D11s7	loadcel11007!030517115713	685.7	781.8	9.2	6.6	142.7	135.8
D11s7	loadcel11007!030517115727	719.2	800.8	10.2	7.5	140.3	137.1
D11s7	loadcel11007!030517115742	815.8	877.5	11.3	7.2	140.9	137.5
D11s7	loadcel11007!030517115757	826.1	878.1	9.3	7.5	140.6	137.8
D11s7	loadcel11007!030517115812	860.1	953.2	10.3	9.3	141.2	139.1
D11s7	loadcel11007!030517115827	891.7	973.3	11.3	8.2	142.0	139.6
D11s7	loadcel11007!030517115843	894.7	964.7	14.8	11.2	141.7	141.2
D11s7	loadcel11007!030517115858	1021.4	1118.9	14.2	9.9	144.0	141.9
D11s7	loadcel11007!030517115912	1034.4	1145.4	11.0	8.6	144.1	143.3
D11s7	loadcel11007!030517115927	1050.0	1164.9	14.4	10.9	143.8	143.9
D11s7	loadcel11007!030517115942	1081.4	1176.0	13.3	9.9	143.6	145.1
D11s7	loadcel11007!030517115958	1090.1	1196.0	12.0	9.4	143.5	146.2
D11s7	loadcel11007!030517120013	1091.1	1197.2	13.3	9.9	143.7	147.5

D11s9	loadcel11009!030517121504	279.2	302.4	2.9	1.6	139.1	122.1
D11s9	loadcel11009!030517121519	303.6	328.8	4.5	2.2	139.9	122.7
D11s9	loadcel11009!030517121534	306.7	336.2	5.6	2.7	140.5	123.1
D11s9	loadcel11009!030517121549	430.0	462.1	5.4	3.1	142.3	123.4
D11s9	loadcel11009!030517121605	477.5	520.8	8.5	5.5	142.0	123.5
D11s9	loadcel11009!030517121619	481.2	523.4	7.4	4.7	142.5	126.5
D11s9	loadcel11009!030517121634	506.5	541.3	7.4	4.8	142.7	126.8
D11s9	loadcel11009!030517121649	510.1	548.4	6.6	4.6	142.8	127.0
D11s9	loadcel11009!030517121704	511.4	556.6	7.6	5.3	142.6	127.1
D11s9	loadcel11009!030517121719	528.2	570.3	6.5	4.7	141.9	127.7
D11s9	loadcel11009!030517121735	540.1	571.6	8.5	6.4	142.3	129.4
D11s9	loadcel11009!030517121749	562.4	598.0	8.5	5.5	142.0	129.6
D11s9	loadcel11009!030517121804	577.4	614.8	9.4	9.3	143.6	129.9
D11s9	loadcel11009!030517121819	612.7	655.4	10.2	9.4	143.8	131.9
D11s9	loadcel11009!030517121834	817.2	884.0	10.1	7.6	141.5	132.0
D11s9	loadcel11009!030517121849	945.3	1031.0	9.3	6.6	143.7	132.4
D11s9	loadcel11009!030517121904	1006.9	1091.9	9.1	6.8	144.3	134.0
D11s9	loadcel11009!030517121919	1105.8	1210.9	13.7	9.7	146.0	134.0

Appendix 4 Specimen geometry